ABSTRACT

Title of Document: DESIGN AND ANALYSIS OF AN AUTOMATED ASSEMBLY PROCESS FOR MANUFACTURING PAINT BRUSH KNOTS

Aleksandr Borisovich Gorbashev, M.S. 2011
Mechanical Engineering

Directed By: Chandrasekhar Thamire
Department of Mechanical Engineering

Manufacturing process for paint brushes requires handling and assembling of flexible and delicate filaments and can be cumbersome in manual assembly processes. Common issues resulting from such manual assembly process include variations in filament density, deviations in filament straightness, and issues due to right and left handed bias in assembly operations, resulting in poor quality of the end products. Coupled with operator fatigue and health problems, these issues provide an excellent motivation for refining the process.

The primary objectives of this study were to develop an assembly system that will 1) increase product quality, and 2) improve the production rate. The secondary objective was to develop a set of design guidelines for handling flexible elements such as synthetic filaments within provided housings.

In order to develop the automated assembly process, needs analysis and product design specification exercises were performed first, followed by functional decomposition of the process at the first level. Designs for individual subsystems were developed next using functional decomposition at lower levels, concept generation, concept evaluation, feasibility testing, testing for design parameters, design through solid modeling, strength analysis, concept testing using physical prototypes and subsystem refinement.

In order to assess the response of filament assemblies when subjected to external loading and moving relative to the housings, experiments were designed and conducted. For a range of factors, tests were conducted to establish limits of pulling force required to displace filament bundles within the housings. Correlations relating filament motion to applied loading were developed for a variety of housing geometries and material types. Design guideline related to motion of filaments within housings was developed. In light of the testing performed, design guidelines for development of gripper-plates used for gripping of bulk filament bundles were also established. It is expected that these guidelines will be useful in the manufacturing automation industry, involving manufacture of toothbrushes, hair brushes and fiber-optic elements.

Upon successful completion of the feasibility tests, full-scale prototypes using the final concepts of subsystems were fabricated. Tests were conducted to determine the reliability of the process and quality of the brush knots. Results indicate that the quality of the brushes was much higher than the traditional hand-made brushes and that the productivity would nearly double. Upon delivery of the system to the company sponsoring this research, it is expected that the system developed would be able to produce up to 3 million brushes per year.

DESIGN AND ANALYSIS OF AN AUTOMATED ASSEMBLY PROCESS FOR MANUFACTURING PAINT-BRUSH KNOTS

By

Aleksandr Borisovich Gorbashev

Thesis submitted to the Faculty of the Graduate School of the
University of Maryland, College Park, in fulfillment
of the requirements for the degree of
Master of Science
2011

Advisory Committee:
Dr. Chandrasekhar Thamire, Chair
Dr. Santiago Solares
Dr. Kenneth Kiger

Dedication

This thesis is dedicated to my mother Irina Gorbasheva and my older brother Aleksey Gorbashev who have always been there for me. Both of them have given me the support I need to succeed in my academic career and in life. If it was not for them, I would not be who I am today.

Acknowledgements

First and foremost, I would like to thank Dr. Thamire with all my heart for everything that he has done for me. His kindness and understanding has no bounds, much like his work ethic. I want to thank him for giving me the opportunity to become a part of this research project. As a result I got the chance to learn within many aspects of science and also within myself. The relationships that I have established over the period of this research are some that I hope will never end, with people that I will never forget.

One of such relationships was with Chris Bunai. As an undergraduate student, Chris has already initiated research (on this project) when I came onboard. At the beginning, we did not have a dedicated lab space or tools, and needed to learn how to make things work with what we had. Chris was instrumental at this, no matter how hard the task, he never gave up. His wide imagination has always given him the drive to succeed while finding alternate solutions to problems at hand. From what I can read into him, I would say his motto was: "We don't have it? Can't afford it? Well then, I will make it myself!" During meetings, Chris often pitched ideas of machine designs that I thought were impossible to fabricate, yet he has proven me wrong. His work exemplified unique and intelligent ("outside-of-the-box") designs achieved through hard work and dedication; designs of machines that performed flawlessly when fabricated. Beginning this project from the ground up, we worked together, sharing a passion for machinery, tools and hands-on work. I guess what Chris does not know, is that I have learned a lot from him, including the aspects I just mentioned. I would say, that knowledge allowed me to succeed in this project. Thank you Chris!

With time, Chris graduated. After that, our lab went through extreme development as other graduate students filled our newly acquired laboratory room. With interests in so many different fields, Dr. Thamire enjoyed having a variety of projects from industrial design and manufacturing to bio-engineering and sustainable energy. Over the period of years I had the pleasure to meet a number of students; students that have become like family to me. In some shape or form, they have all contributed to my growth. Reflecting back at myself, I have learned something from each one of them. Furthermore, each of them was there when I needed them most. I am extremely grateful as I would like to acknowledge them individually and say thank you: Babak Eslami for his very intelligent but humble character, hard work, desire to learn and his support when I needed him as a friend and as a lab-mate; James Kromer for his "Let's get it done!" attitude and for pushing me forward; Andy Oles for his cool and understanding personality and lending me his (incredibly intelligent) helping hand; Erik Levin for his "project manager/IT" qualities, answering my nit-picky questions and leading the logistical aspect of this Sherwin Williams project; Esteban Echeveria for his support and kind intentions; Danica Gordon for her humorous, smiling and kind personality as well as her support during hard-times; Rabee Zuberi for being an overly relaxed, understanding, smooth and cool friend; Karim Najjar for his incredibly kind nature and thirst for knowledge as well as mental support.

I am grateful to have had all of you in my life! I admire you all. Thank you so much!

Table of Contents

Chapter 1: Introduction

1.1 Paint-Brush Applicator

Paint Brush Components. Paintbrushes are hand-held applicators used to apply paint, sealers or lacquers to objects or surfaces [1]. As shown in Figure 1.1, a typical paint brush consists of (1) filaments that may be made from synthetic material or animal hair, (2) a ferrule used to hold filaments, made from a metal or plastic, (3) a cardboard or wooden plug inside the ferrule to hold filaments and create a cavity for paint storage, (4) epoxy to lock the filaments in place, and (5) a handle that provides comfort and a good balance made from wood or plastic. In large size brushes, a metal insert is often also included inside the ferrule to help support filament structure but will not be discussed in this study.

Figure 1.1 Paint-Brush Components.

The first four components are typically pre-assembled together first and are referred to as a “knot” sample seen in Figure 1.2. The sample is processed until it is ready to be joined with the handle to complete the paint-brush applicator. Thousands of recipes of knots are manufactured annually as the types of components are varied. To promote the quality of finish while minimizing labor effort and time, the recipes are highly dependent on application requirements such as type of paint or varnish used. With professional users and home users in mind, the recipes can range from complex combinations to fine-tune the performance, to simple combinations for small and quick applications. Recipes are derived directly from the customer requirements and may often be altered to help satisfy the need of application. Factors such as filament type, brush tip form, brush trim and brush width are commonly the roots from which the recipes are defined.

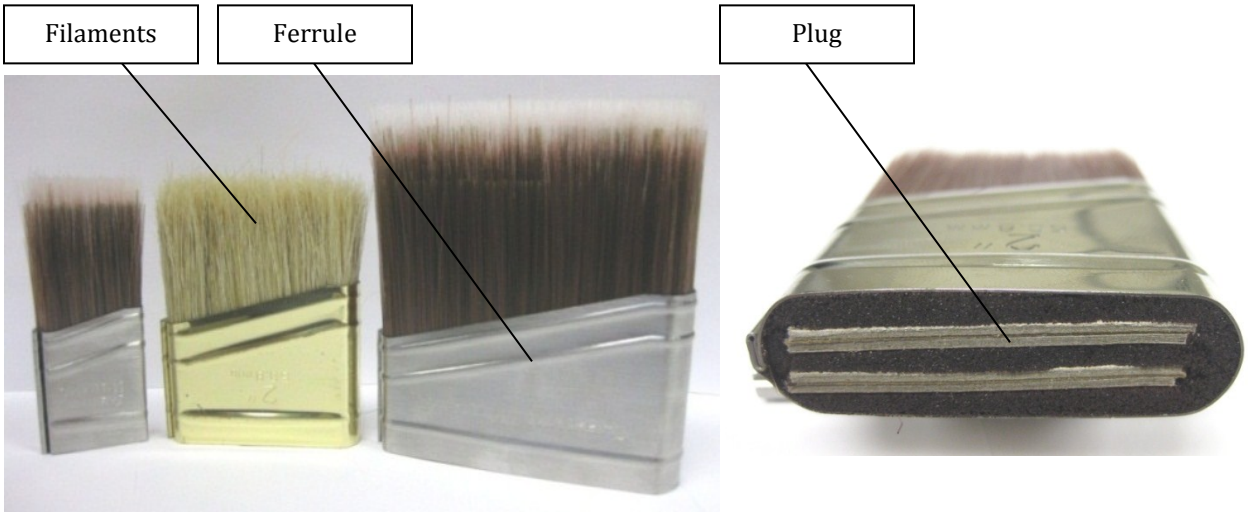

Figure 1.2 Knot Sample.

Filament Type. To achieve quality in paint distribution, water-based paints and oil-based lacquers require different material properties of filaments and are separated into categories of synthetic and natural hair types. Properties of synthetic filaments hold and release latex paint best to provide smoother paint finish while keeping their resiliency after repeated use. Innate "flagging" or splitting of filament tips (Figure 1.3) in natural type filament help to hold and create smooth release and finish of oil-based varnish.

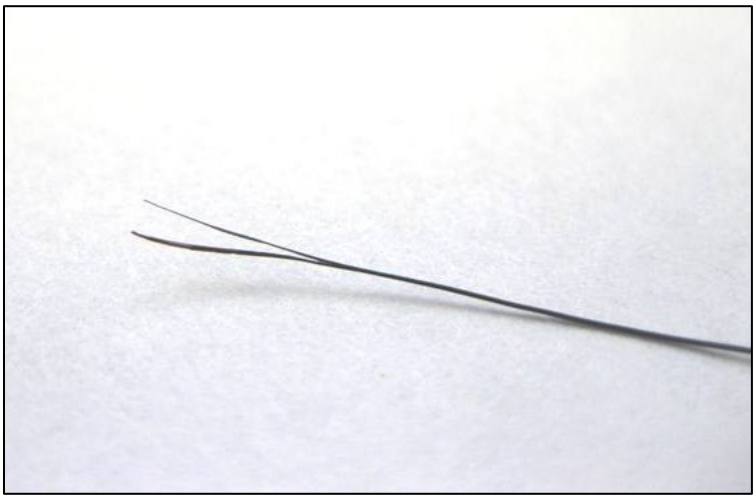

Figure 1.3 Natural Filament Flagging.

To further improve the efficiency of application, quality of finish and brush life, multiple types of synthetic and natural filaments are offered, such as nylon or polyester and white or black natural pig hair respectively (Figure 1.4). Nylon filaments offer longer lifespan with a higher stiffness over polyester type, creating it to be a more appropriate choice for use on rough or textured surface. However, polyester's softer qualities provide a smoother and finer finish for water-based paints. With oil based paints the fine quality of finish can depend on the type of hog or pig hair used for filaments. Most common types are white and black pig hair that are manufactured in China and are termed White China and Black China

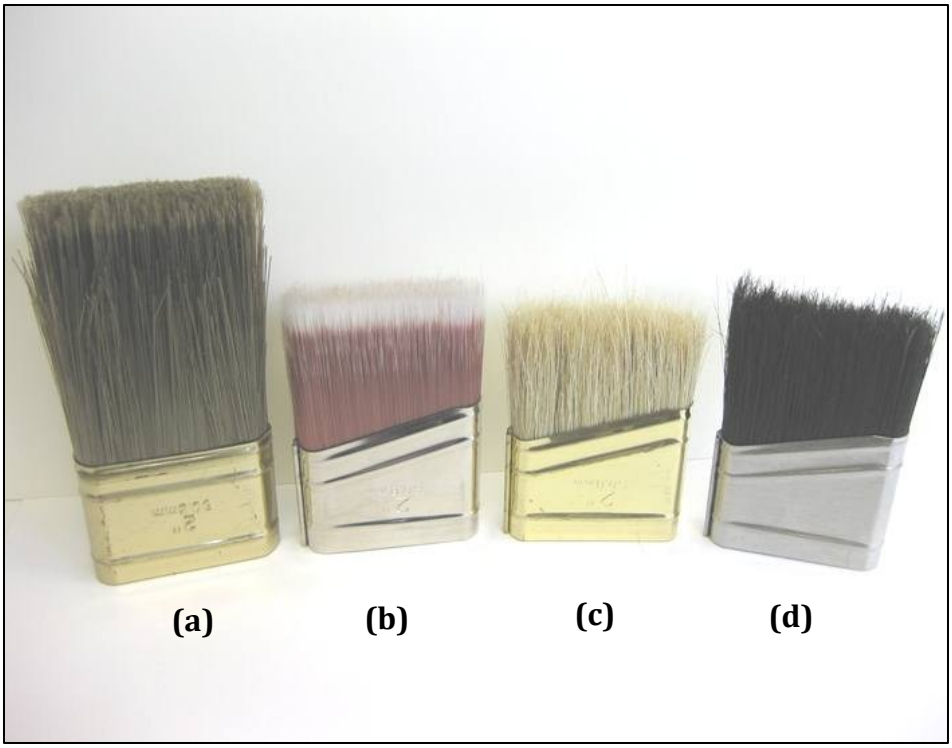

Figure 1.4 Filament Types: (a) Nylon; (b) Polyester; (c) White China Pig Hair; (d) Black China Pig Hair.

pig hair. Additional die coating added to White China changes filament properties to create Black China filaments. After the die coating, pig hair filaments become stiffer and thicker to work better with mostly oil-based paints. For other lacquers such as varnish, stain, or polyurethane, a finer surface finish is achieved with White China filaments due to its finer and softer filament texture.

Brush Trim and Tip Form. To fulfill workspace limitations and improve control, paint-brush applicators are offered in multiple types of trim and tip forms. Two common and most preferred types of trim are flat and angle trim applicators (Figure 1.5 (a, b)) with a flat tip form (Figure 1.5 (c)). Flat trim is used to apply paint on a large or small surface in a simple straight-line fashion without the need to manipulate the brush alignment for precision. More complex tasks require a more precise applicator. In such cases, angle trim

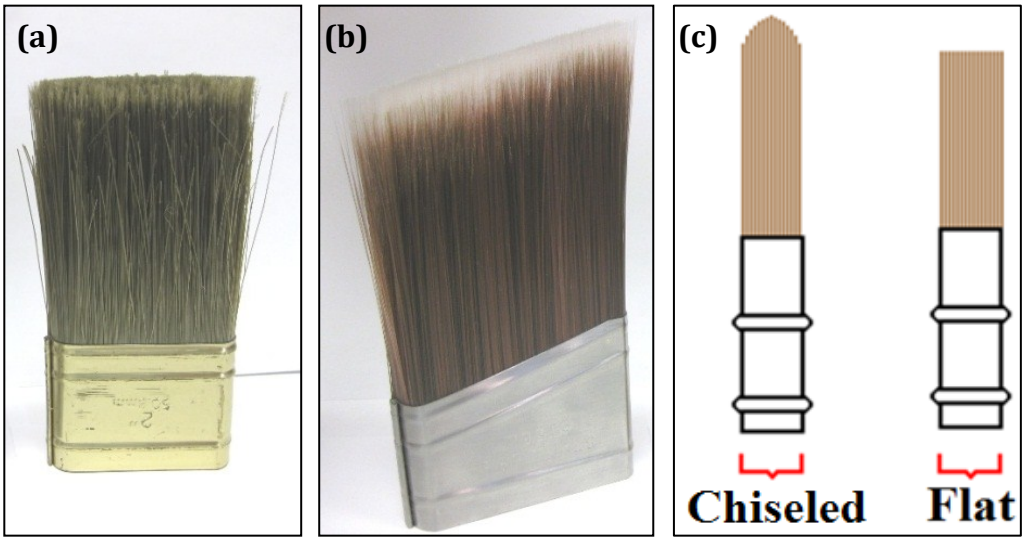

Figure 1.5 Brush Trim and Tip Forms:
(a) Flat Trim; (b) Angle Trim; (c) Chiseled and Flat Tip.

brushes are unique to help coat around complex shapes and inside hard to reach places. Angle trim (Figure 1.5 (b)) with an added chiseled tip is especially designed to improve brush control and end-user wrist alignment for cutting in a straight line at a wall and ceiling junction, filling in room corners and small cavities. With more functionality over the flat trim, angle trim brushes have become a more desired product by the customer while also having a reputation of a "higher-quality" and retained value.

Brush Width. To help save time and labor effort, brush width or "size" is offered in multiple forms. Relative to the type of surface or amount of area needed to be covered, sizes may vary from 1 to a 4-inch widths or larger for industrial applications. In most cases, manufacturing of paint-brush applicators is targeted such that sizes from 1 to 2-inches wide are used for window or other small trim, 3-inch for doors and cabinets and 4-inch for large, flat surface areas such as exterior walls and fences.

1.2 Manufacturing of Paint Brushes

Similar to other products, manufacturing and assembly processes for producing paint brushes can be automated, semi-automated, or manual [2]. At the current time, level of automation is based on the type of brush trim in production. Fully automated machines for flat trim brushes are available on the market; however, due to an additional processing necessary for the angle-trim brushes, world-wide manufacturing has been limited to a semi-automated fashion only. The list below shows the general steps for paint brush assembly, where manufacturing of paint brushes is performed through a combination of manual and automated assembly [1]:

1. Aligning and mixing the filaments;
2. Adjusting the system for brush size;
3. Picking and feeding the filaments into ferrules;
4. Inserting a plug;
5. Brush tip and trim forming and filament straightening;
6. Placing metal inserts, applying epoxy, and curing;
7. Finishing by removing loose hairs;
8. Inserting and securing handles, and
9. Packaging.

As described further, Steps #1-4 are performed by an automated knot assembly system, which assembles the knots necessary for manual processing in Step #5. Additional automated finishing equipment is used to finalize the paint-brush assembly in Steps #6-9.

1.2.1 Automated Knot Assembly

For most paint brush manufacturers, equipment used to perform automated knot assembly (Figure 1.6) has been in action since the 1960's [3]. With some modifications and incorporation of improved technological mechanisms of the 1990's, the automation of Steps # 1-4 is achieved through pure timing of mechanical and pneumatic devices. With operator loaded filaments and ferrule components (usually purchased as a pre-manufactured part based on the brush specifications), the machine follows the order of assembly described in this section.

Figure 1.6 Automated Knot Assembly Machine.

Due to a variety of brush specifications such as brush width, thickness and filament type, adjustment of physical sub-station devices are made first. Filament and ferrules are then loaded into machine feeders by a human operator. With some brushes requiring multiple lengths of filament to complete the brush recipe, the operator must feed in bundles of filaments separated by length. Aligning and mixing of filaments is performed by

the machine as a first step of the automated process. Filaments are then combed to straighten their alignment and to remove loose or curved hairs. Based on the brush size, a pre-defined amount of filament (which would define the knot filament density) is separated and inserted into the ferrule using a vibrating patter device to promote ease of insertion and filament alignment. With a prescribed length of filament ends exposed out of the ferrule bottom, the filament ends or “butts” are parted to insert a cardboard or wooden plug into the center of the ferrule. Exposed filaments along with the plug are then pushed flush with the ferrule bottom to complete the knot sample [4]. Figure 1.2 shows knots as delivered from the knot-making machine at the end of Step#4 of paint brush assembly process described previously.

Automated knot assembly is commonly followed for both, flat and angle trim brushes with minor differences in ferrule design. However, post processing is significantly different between the two types. To complete the process for a flat trim brush, one more sub-station device is normally added to the automated knot assembly system to displace filaments within the ferrule housings. After the cavity for epoxy and handle is created, the knot is sent from automated knot assembly system to an already existing automated epoxy filling and handle insertion machines to finalize the brush manufacturing. Contrary to the flat trim, angle trim knot requires a few more phases of manual processing before it can be completed to proceed to epoxy filling and handle insertion. Required phases for such manual processing are a part of Step #5 of paint brush assembly process and are described below.

1.2.2 Manual Processing

For the angle trim knots, assembled knots from the knot making machine are ejected onto a conveyor belt and delivered to a row of seated operators as shown in Figure 1.7. With up to five or more operators along the conveyor, knot processing is performed through manual hand operation. As a part of Step# 5, knots are processed with respect to multiple phases, (1) filament density assessment, (2) filament tip forming, (3) angle trim forming, and (4) filament straightening and combing.

Figure 1.7 Angle Trim Operator Processing.

Filament Density Assessment. Each knot recipe has a required number of filaments or filament density that must be present inside the ferrule in order to achieve a proper paint distribution. Filament density is in a form of mass, where a bundle of filaments is weighted to match the required standard for each recipe. The automated knot assembly machine is then adjusted to insert the amount of filaments required within each knot. During manual processing, the filament density is monitored manually as a result of inaccuracies associated with automated knot assembly machine. Filament density is checked by

squeezing the filaments and estimating the filament stiffness. Estimated stiffness is then compared to the control density for the knot in production. From the comparison, the operator is able to detect if density is sufficient. In non-sufficient cases, filament density is adjusted by removing or adding filaments manually within the knot.

Filament Tip Forming. After sufficient filament packing density is established, vibration tables are used to achieve the brush tip form. For a flat tip profile brush, a vibrating flat surface is used to settle filaments to the bottom of the ferrule to ensure that all ends or "butts" of filament are flush with the ferrule bottom. This is especially important for knots that require different lengths of filaments inside the ferrule, as the design of the knot recipe calls for all filament butt alignment to be flush with the ferrule bottom as a reference. For other knots requiring a chiseled tip form, rods of recipe specified diameter are mounted to the vibration table to settle the filament to a radial geometry of the rod. Settling is usually achieved by manually pushing filament out of the bottom of the ferrule to expose enough filament length to conform to a rod radius or simply to be flattened by the flat surface of the vibration table. After the exposed filaments are vibrated to settle, filaments are pulled up back into the ferrule as a bundle.

Angle Trim Forming. After filaments are settled and the tip form has been achieved, filaments are formed to create the angle trim. Angle trim forming or most commonly referred to as "gauging" is performed by physically displacing filaments from the bottom of the ferrule to create the angle trim. A metal gauging block (Figure 1.8(a)) of geometry specific to the knot recipe is inserted into the bottom of the knot (Figure 1.8(b)) to displace and form the filaments to the specifications of the gauging block as seen in Figure 1.8(c).

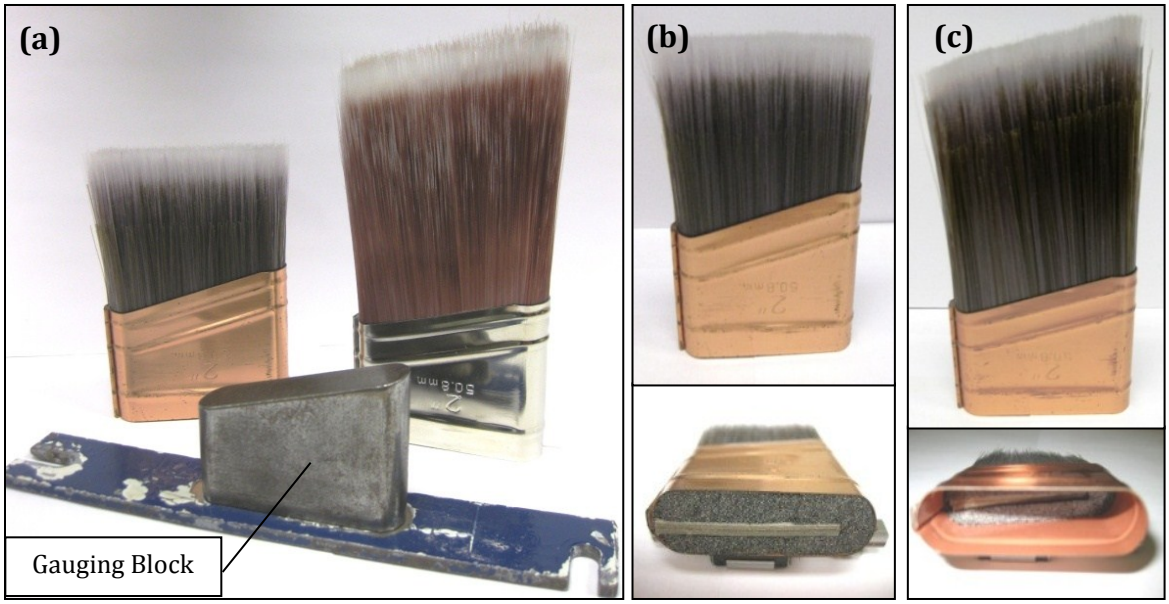

Figure 1.8 (a) Gauging Block; (b) Knot Sample prior to Angle Trim Forming; (c) Knot Sample after Angle Trim Forming.

Filament Straightening. Manual processing is completed by ensuring straight and parallel alignment of filaments within the knot. In each knot, existing filament alignment is assessed visually and then corrected through combing action. A hand comb is plunged into the filaments on a side of the knot and translated horizontally left or right to tilt the filament into a straight vertical alignment. After the process is repeated for both sides, filaments are combed out along the height of the knot to release overlapping or loose filaments.

1.2.3 Finishing Equipment

After manual processing, the paint-brush-applicator is finalized by securing filaments inside the ferrule of the knot with epoxy and mounting the handle. Similar to the knot making machine, epoxy filling and handle insertion actions are automated. The machines are pre-adjusted for the specifications of the knot. Manually processed knots are placed on an epoxy filling machine conveyor as they are picked up and aligned into the epoxy filling and curing oven tunnel upside down (cavity side of the ferrule pointing up). Inside the tunnel, the knot cavity is filled with epoxy just enough to leave space for insertion of the handle. After the curing time has elapsed, epoxy filled knots are manually transferred to the handle insertion machine. Pre-manufactured wooden or plastic injection molded handles are loaded into feeders of the machine by an operator as individual knot and handle set are assembled and locked together by nailing. The paint-brush applicator product is considered to be completed as it is hand packaged and shipped out.

To arrive at this final product, the described manufacturing process of Steps #1-9 on page#6 is performed individually for a single type of paint-brush recipe. Commonly, automated systems are adjusted for the desired knot specifications and run to produce the necessary knot quantity of a single knot type. To produce a knot of a different specification, systems are shut down, with the associated down time, and then re-adjusted to accommodate the required knot specifications.

1.3 Issues with Manual Processing

Multiple issues are associated with the current method of manual knot processing (Step#5), relating to knot product quality, processing time and operators' health. To help improve the process, manual operator processing can benefit from automation in light of the issues encountered below:

1. Inconsistency in filament density;
2. Inconsistencies in brush tip and angle trim forming;
3. Inconsistent straightness of the filaments;
4. Lowered quality and increased costs due to scrap;
5. Lower productivity compared to that from automated systems, and
6. Health-related issues of the personnel involved due to extended time in bending or other uncomfortable postures required for the process.

Issues noted above are hard to control due to the nature of human operation. The highlighted inconsistencies are also often magnified, as operator techniques differ significantly between operators and shifts of operators. Left-hand and right-hand bias during manual filament straightening is one of the examples of such inconsistencies. The inconsistency phenomenon is continued in attempts to control knot filament density and straightness through a sense of touch and visual assessment of filament straightness. Filament density, tip form, angle trim and filament straightness are all factors that define end-user satisfaction based on the product performance. Consequent lack of performance due to such inconsistencies results in lower popularity of company brand name, market share and financial profit.

Increased manufacturing costs and lack of knot quality are also evident during the process of angle trim forming through the use of the gauging block. Due to a floating tolerance in ferrule manufacturing, it is often found that filaments are left between the gauging block and ferrule walls and not fully displaced as seen in Figure 1.9. The not fully displaced filament, termed "dragback," often results in lack of quality and integrity of the knot during other phases of processing. Presence of dragback is considered to be a significant flaw with high potential for collapse of knot assembly and loss of product as well as additional cost due to filament scrap.

Figure 1.9 (Left) Dragback after Insertion of the Gauging Block; (Right) Dragback after Epoxy Filling and Curing.

Additional issues lay within the time required by each operator to process the knots. With manual operator processing as the only stage performed through human assembly among other automated stages of manufacturing, the process shows to be very restrictive for production. Performed by human labor, the processing is limited by capabilities of operators, where in some cases extended operating hours have led to significant operator health problems.

1.4 Motivation and Scope

In light of the described problems, the paint brush manufacturing process can highly benefit from automation, more specifically Step #5 - manual processing within the overall manufacturing process. The motivation is to eliminate the existing issues relating to manual assembly while improving the product quality and production rates with a goal to increase the client economic growth resulting from the execution of the project. Additional motivation arises from the world-wide need of innovation of an automated concept for the process of angle trim forming, which currently does not exist. Upon completion of the project, it is expected that through proper integration, the total manufacturing process can be converted to a stage of full automation from start to end in the future.

Automation of knot processing has multiple advantages; one of the most beneficial advantages is maximized quality of product at a level of machine consistency with higher production rates. Large sources of issues contributing to lack of quality such as human sense of touch may be eliminated completely with replacement of load sensors, leading to consistent and fine-tuned density values for each knot recipe. Mechanical precision in positioning, motion and timing can improve quality of filament tip forming and settling along with improved sharpness of angle trim geometry and precision of filament length-out.

To fulfill the need for automation, primary objectives of this research were to develop an assembly system to replace manual operator processing within brush manufacturing that will 1) increase product quality, and 2) improve the production rate while satisfying provided target specifications. For the sake of brevity and in light of the necessary innovation, the focus of this thesis was further directed to a design study of core

subsystems responsible for angle trim forming and filament straightening. Established secondary objectives were to develop a set of design guidelines related to gripping and translating of synthetic filaments within variable ferrule parameters for the benefit of scientific and industrial communities. As it was introduced previously, to create a cavity for epoxy and handle insertion, knot filament bundles needed to be gripped and displaced within the ferrule housing. As to our knowledge, no design guidelines currently exist for methods of gripping filament bundles or estimating the pulling force required to displace such bundles. As a result of this design study, the objectives were to (1) define a set of design guidelines for development of filament gripper-plates which can be used to sufficiently grip filament bundles without damage or loss of filaments, and (2) provide a design guideline to estimate pulling force required for displacement of filament bundles based on parameters of ferrule and filament bundle.

The following chapters were used to describe the design study associated with the development of the core subsystems as well the testing and analysis used to generate the design guidelines. Using an alternate industrial product development process, the study was described in the order of formulating system needs and specifications, functional decomposition and concept development, testing for design parameters, embodiment and system detail design, prototype fabrication and testing, and subsystem refinement. Following, resulting guidelines were introduced and discussed as well as additional work accomplished in order to arrive at final system design for automated knot processing.

Chapter 2: System Needs and Specifications

2.1 Design Process Followed

Typical machine or consumer product development involves a series of steps that are standardized to help guide and optimize the process. In this design case study, a more indirect approach for industrial system development was taken with focus on small quantity system manufacture. This process can be summarized, but not limited to:

1. Acquiring customer driven target specifications;
2. Functional decomposition of the proposed system;
3. Concept generation for individual subsystems;
4. Concept feasibility and testing;
5. Testing for design parameters;
6. Building and testing individual subsystem physical prototype;
7. System and detail design phases, involving system architecture, design of subsystem interfaces, motion analysis, part sizing, material selection, DFX, and other analyses;
8. Implementing modifications to generate finalized design as necessary;
9. Integrating final concept subsystems to produce the full system design, and
10. Preparing documentation necessary for manufacturing and operation of system.

Due to a large number of system functional requirements, further introduced in Section 3.1, the design study was performed through a morphological approach [5], [6]. Customer driven target specifications and system functional decomposition were established first. Then, the whole system was broken down into subsystems as Steps# 3-8 were followed for the discrete subsystem development. Upon completion of the subsystem design,

integration to generate the total process solution and complete the full system design was further performed as stated in Steps# 8-9.

2.2 Customer Driven Target Specifications

Paint-brush specifications were derived from end-user needs for desired product performance. Each brush was expected to produce a uniform and consistent paint distribution and at the required quality of application for different paints and surfaces used.

To accommodate the application and aesthetic requirements, brushes come in a wide range of attributes which define the brush recipe. Figure 2.1 and Table 2.1 summarize all attributes or specifications of knots that must be satisfied for the automated system in design [3]. For a selected brush recipe, the knot may vary in:

i) Brush width;
ii) Brush thickness;
iii) Trim type;
iv) Tip form;
v) Chiseled tip form diameter;
vi) Filament material type;
vii) Filament length;
viii) Length out;
ix) Filament packing density;
x) Ferrule type;
xi) Ferrule shape;
xii) Ferrule height, and
xiii) Ferrule material coating type.

Ferrules are manufactured out of stainless steel or plastic, while often varying from uncoated stainless steel ferrule to a ferrule plated with a chrome, copper or brass alloys. Inside the ferrule, filament must meet the required packing density, to meet the paint distribution requirement. Depending on the thickness of the knot, the radius of the chiseled

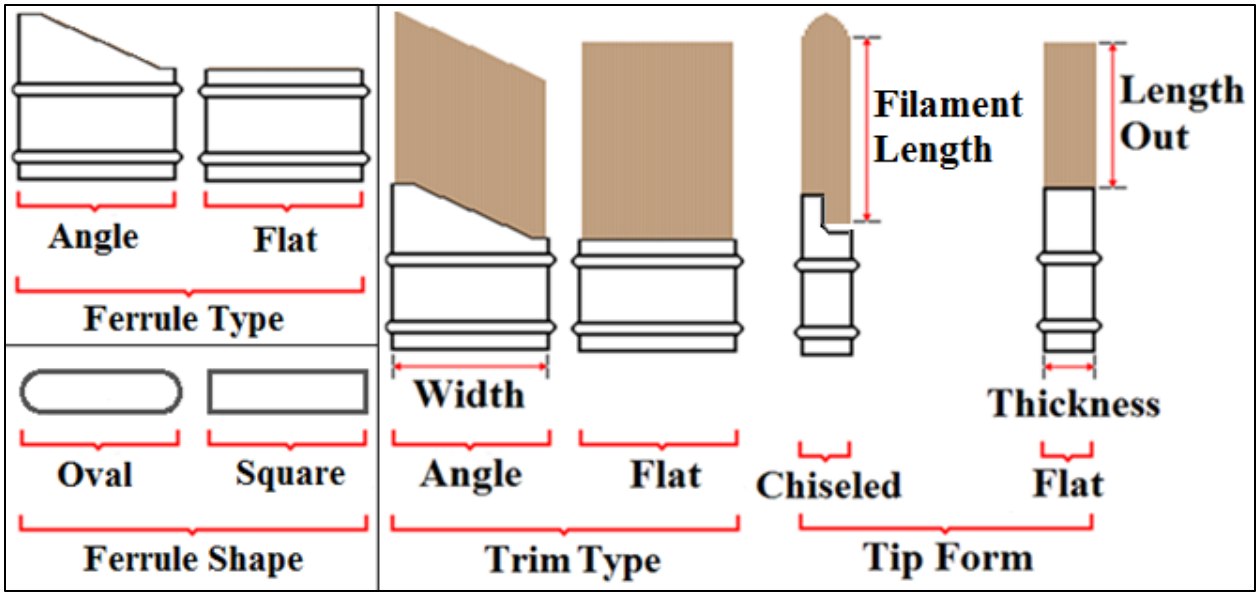

Figure 2.1 Visual Display of Knot Target Specifications.

Table 2.1 Numerical and Verbal Knot Target Specifications.

Brush Width (in.)	1, 1-1/2, 2, 2-1/2, 3
Brush Thickness (in.)	5/16, 3/8, 7/16, 1/2, 9/16, 5/8, 11/16, 3/4, 13/16, 7/8, 1
Trim Type	Angle or Flat
Tip Form	Chiseled or Flat
Chiseled Tip Form Diameter (in.)	3/8, 1/2, 5/8, 3/4, 11/16, 1
Filament Material Type	Nylon, Polyester, White China, Black China
Filament Length (in.)	1" to 3" brush = 2 to 4.25 inch range; To be Specified by Operator
Filament Length Out Value (in.)	1-7/8, 2, 2-1/8, 2-3/16, 2-3/8, 2-1/4, 2-7/16, 2-1/2, 2-9/16, 2-5/8, 2-11/16, 2-3/4,2-13/16, 2-7/8, 2 -15/16, 3, 3-3/16, 3-1/8, 3-1/4, 3-3/8, 3-1/2, 3-7/16, 3-11/16, 3-7/8
Filament Packing Density (grams)	1" to 3" brush = 7.5 to 92.1 gram range; To be Specified by Operator
Ferrule Type	Angle or Flat
Ferrule Shape	Oval or Square
Ferrule Height	Between 1-1/4 and 1-7/8
Ferrule Material Type	Plastic, Stainless Steel; Chrome, Copper or Brass Plated Steel

tip form is varied during the process of filament tip settling and forming through vibration. Different radii of vibration rods are used to generate the appropriate chiseled tip form. In similar terms, angle trim forming process requires the shaping of the angle or flat trim while displacing the filament from the bottom of the ferrule to a specified length-out value.

Target specifications were also present from the expected knot quality standards, expected production rate and physical space limitations. During the angle trim forming process, the trim profile was to conform to an angle of 15° with tolerance of ±1°, achieve specified length-out while also maintaining the chiseled tip form after filament settling. Consequently, the process of filament straightening was to conform to a straightness tolerance of ±3° from the vertical. To assist the discussion throughout the design study, it is important to highlight the concept of length-out (Figure 2.1), which is the measure of length of filaments protruding from the top of the ferrule after displacement of filaments from the ferrule bottom, or:

$$Lenght\ Out = Displacement\ Distance + Filament\ Length - Ferrule\ Height.$$

In order to achieve a correct value of length-out for a given knot recipe, displacement distance of the filament bundle will vary based on the filament length and ferrule height. With different lengths of filaments and heights of ferrules, the distance of filament displacement varies sufficiently, thus making it a challenge.

To continue, the system in design must also detect if the filament density of each knot is sufficient, settle filament to flat or chiseled tip form, create angle or flat trim form with a specified length-out value while maintaining the chiseled tip form (if necessary) and straighten and comb filament. The above steps must be sufficient to meet the production rate of 30 knots per minute while producing knot quality equal to or better than those

currently produced by hand, with only knots with accepted packing distribution allowed to pass through the system. In addition, the system must conform to the space limitations equal to the current length of the manual processing conveyor between knot making and epoxy curing machines with allowable length of 17 feet, width of no more than 10 feet and working table height of 2 feet and 5 inches.

Chapter 3: Functional Decomposition and Concept Development

3.1 Proposed System Functional Decomposition

The system for this research was functionally decomposed at the first level as seen in Figure 3.1. Based on the presented target specifications, the system in design was to meet primary functions of:

(1) Receive knots from the knot making machine;
(2) Assess filament density and warn an operator if insufficient;
(3) Input knots into the transfer system;
(4) Transfer knots between individual processes;
(5) Form flat or chiseled tip profile by settling filament through vibration;
(6) Displace filament to length-out value and shape flat or angle trim profile;
(7) Straighten and comb filaments, and
(8)Output finished knots for further assembly in epoxy filling and curing machines.

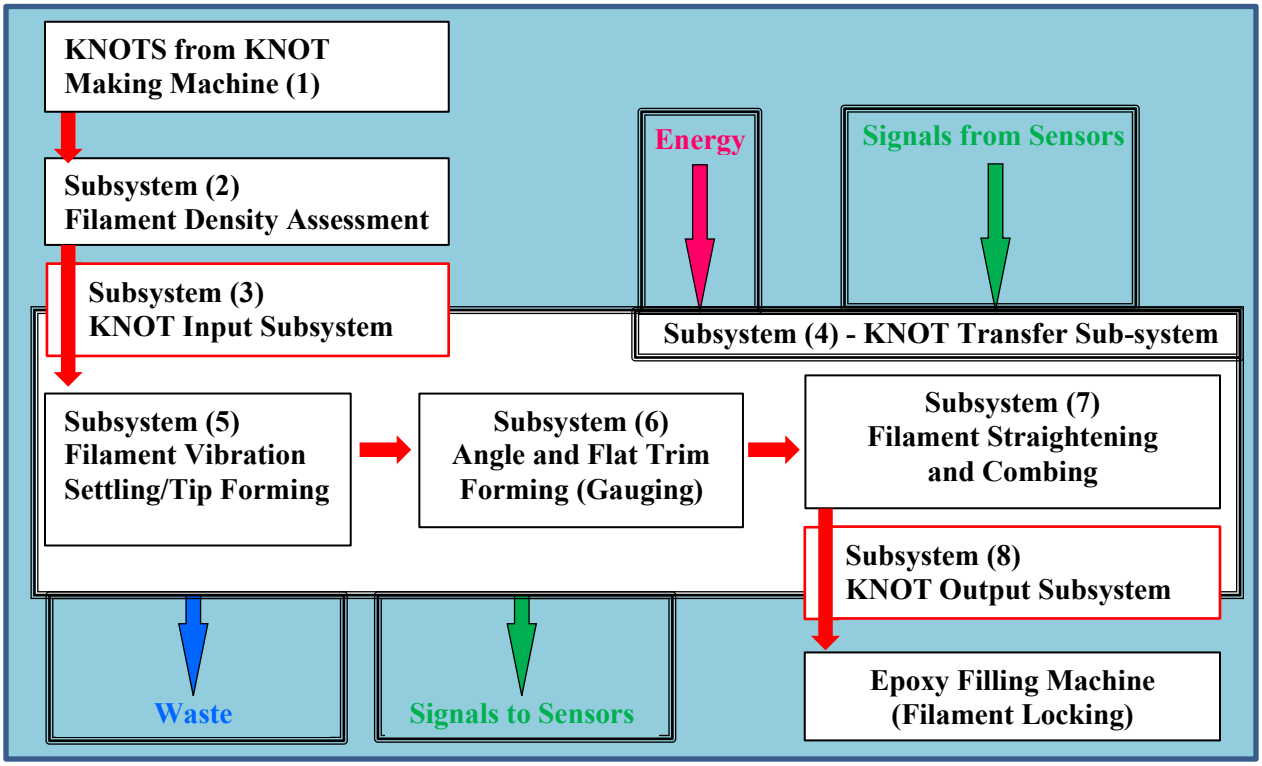

Figure 3.1 Knot Processing System Functional Decomposition.

Inputs into the system are materials (knots), energy (electrical and mechanical, including pneumatic), and tactile signals for operating or controlling the system. Outputs from the system again include materials and tactile signals. The materials here are knots that have been processed with satisfied target specifications, possible material waste, and tactile signals indicating the status or completion of the process.

In this system, subsystems are stationary and knots are moving from subsystem to subsystem. With reference to Figure 3.1, the system envisioned was comprised of a transfer system (Subsystem 4), which would transfer knots from subsystem to subsystem in the necessary order of the knot assembly. Knots from the knot making machine were to be inserted into a loading table as a part of filament density assessment subsystem (Subsystem 2). From the loading table, the knots were to be fed through the filament density subsystem, where each knot was to be analyzed for required filament density and forwarded to the input subsystem (Subsystem 3), if density was satisfactory. If the density requirement was not met, the knot was to be rejected by a warning to an overlooking operator, at which time the process was to be paused for knot removal. Accepted knots were to be further picked up and delivered into the transfer subsystem, which would translate the knot through subsystems (5), (6), and (7) until the knot processing was complete. Processed knots were to be removed from the transfer subsystem by an output subsystem (Subsystem 8) to be placed on a conveyor to further continue onto existing epoxy filling and curing.

The above process summarizes the expected order of automated system processing decomposed at the first level. Secondly, designs for individual subsystems were developed using functional decomposition at lower levels along with concept development and

feasibility testing. As noted previously, the design study within this thesis further demonstrates the morphological design approach taken for core subsystems of angle trim forming and filament straightening. However, the full system design decomposed in Figure 3.1 has also been performed and was introduced in Chapter 8.

3.2 Concept Development of Core Subsystems

This section highlights concept development and proof-of-concept testing of subsystems of angle trim forming and filament straightening. For the specified subsystems, concept generation was performed through an indirect approach based on functional requirements of individual subsystems. Concepts for different subsystems were generated mainly through brainstorming with influence of existing resources including other manufacturing systems and literature. Through intuition, top concepts were selected and tested by use of fabricated proof-of-concept models. From concept performance during proof-of-concept testing, best concepts were chosen for further physical prototype development and testing.

3.2.1 Creating Angle Trim

As an individual subsystem, angle trim forming was to achieve three primary functions:

(1) Displace filaments from ferrule bottom to a specified length-out value;
(2) Create angle or flat trim profile, and
(3) Maintain chiseled or flat tip form.

With consideration of the functional requirements and target specifications described, concept generation yielded three concepts of angle trim forming further described in the form of proof-of-concept models. When tested, models were evaluated using relaxed standards of knot quality for the amount of dragback present, total knot integrity, stability of plug and quality of 15° angle trim. To elaborate, criteria must be met to insure that after

trim forming, no dragback was present, knot integrity was conserved, plug stability within filaments was maintained (without plugs falling out) and filaments were not lost.

Concept One. One of the main concepts examined was an automation of the current angle trim forming process. As shown in Figure 3.2, the current process involves displacing filaments using a gauging block of size and angle specifications to conform filaments to the desired filament length-out and trim. The metal gauging block is simply inserted into the ferrule housing to form filaments to the shape of the block. To match different knot specifications of width, thickness, ferrule type, ferrule shape, trim type, tip form and length-out value, different gauging blocks are used.

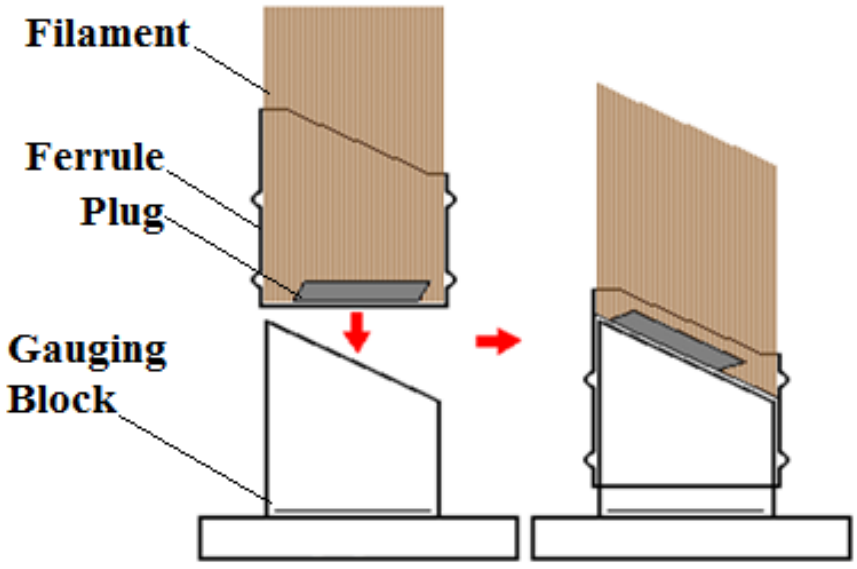

Figure 3.2 Manual Method of Knot Angle Trim Forming.

Feasibility model of the concept was developed in attempt to improve the process through automation to eliminate imprecisions associated with hand centering and positioning of the gauging block. Figure 3.3 shows the model where the knot and gauging block were matched to produce the required knot attributes. Angle trim forming was performed with the gauging block held stationary through a support structure while the knot is placed over top of the gauge. To allow precise location, the knot was secured though a support structure placed on a linear slide. To displace the filament, the linear slide was translated to achieve the desired result. The required trim of the knot was attained with signs of improvement over hand gauging; however, quality of the knots produced was low. Filament dragback was evident within knots, producing a poor, rounded 15° angle trim form, possibly due to wear of the gauging block. The integrity of the knot as well as the plug stability were found to be sufficient, however it was believed that the process can be improved further.

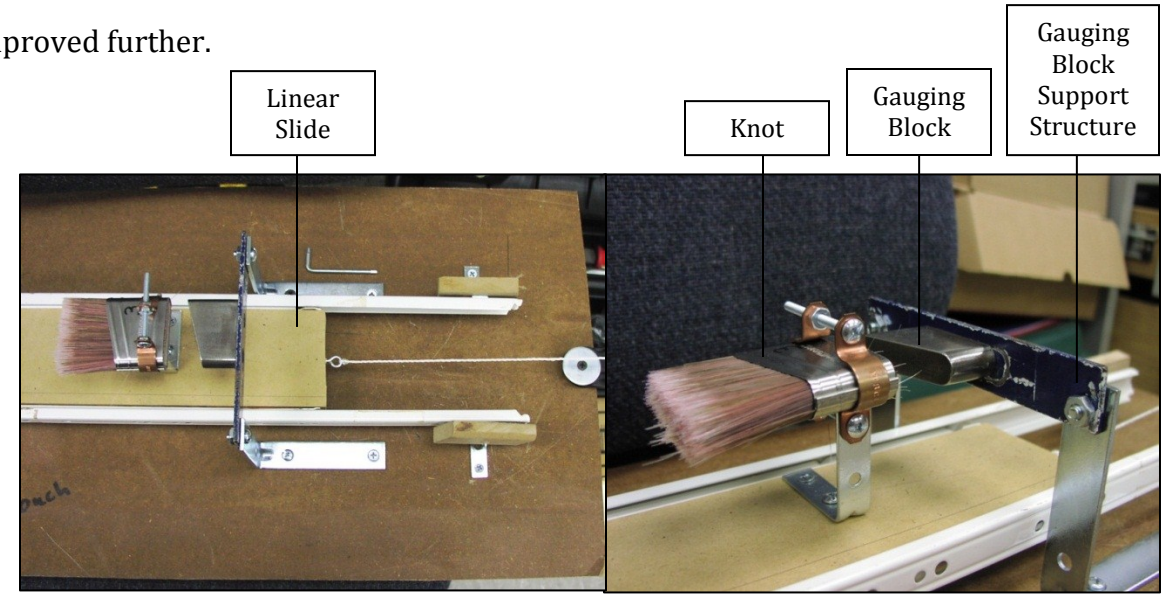

Figure 3.3 First Proof of Concept Model - Angle Trim Forming, Automation of Manual Angle Trim Forming Process: (Left) Testing Setup as shown from the Top; (Right) Testing Setup as shown from the Side.

Concept Two. To reduce dragback and improve angle trim form, an improved concept was tested as seen in Figure 3.4 and 3.5. The concept involved a two stage process of (1) gripping the filament bundle and pulling it to a specified length-out value without assistance of the gauging block, and (2) translating the angle tip of the gauging block to displace the filaments to create angle trim form. To insure proper gripping of filaments, gripper jaw plates were designed to ensure that squeezing force required was sufficient for various knot sizes without damage or loss of filaments due to gripping.

The concept model was constructed such that the knot was held stationary through a support structure during the process. Primary and secondary linear slides were built to achieve each stage of the process, where the secondary slide was mounted on top of the primary. The gripper jaws were located on the primary slide to pull the filament when actuated through a linear solenoid actuator to achieve the first stage of the process. During the first stage, the gauging block followed the filament displaced through pulling.

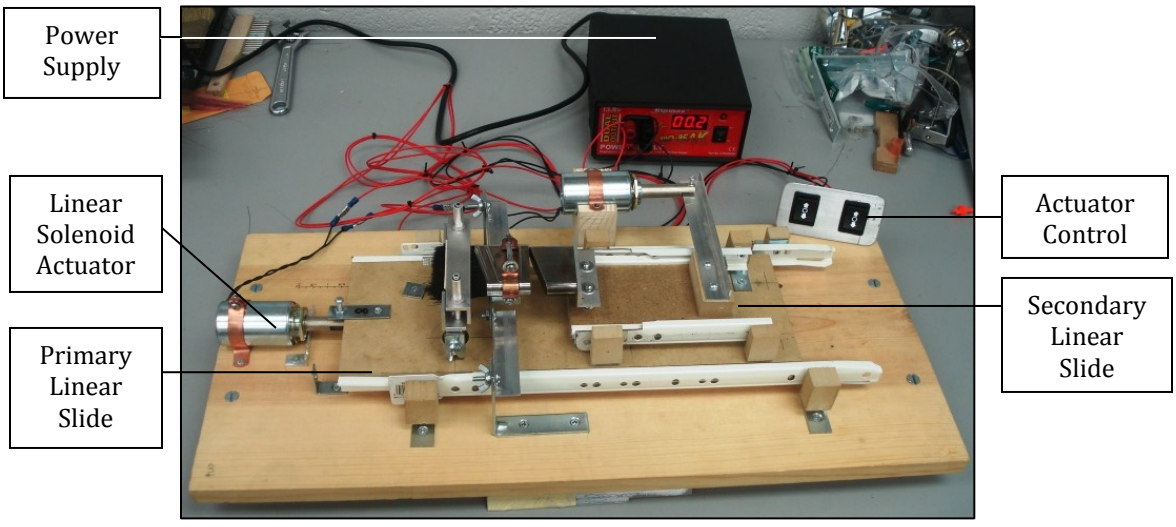

Figure 3.4 Second Proof of Concept Model - Angle Trim Forming, Two Stage Automated Angle Trim Forming; (Testing Setup as shown from the Side).

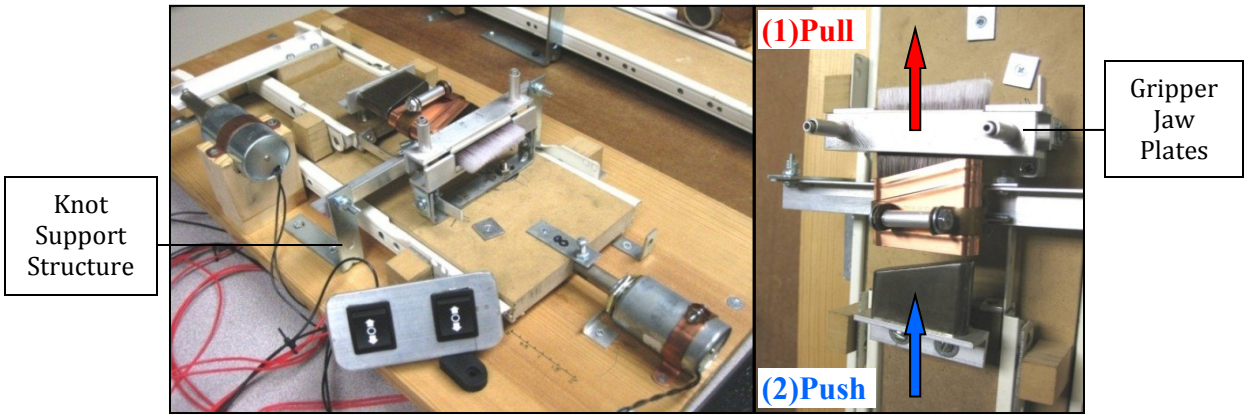

**Figure 3.5 Second Proof of Concept Model - Angle Trim Forming,
Two Stage Automated Angle Trim Forming:
(Left) Testing Setup as shown from the Side;
(Right)Testing Setup as shown from the Top:
Gripping and Pulling Filament to Length-Out (1), and
Pushing with Gauging Block to Create Angle Trim (2).**

To create the angle trim, the gripper jaws were released as the secondary slide was actuated to displace the filament to an angle profile using the tip of the gauging block.

While this concept has improved the shape and quality of the angle distribution, some dragback could still be seen and indicated that further refinement was necessary. From further investigation, it was found that dragback behavior was inevitable when using a gauging block. Due to an existing floating tolerance during ferrule manufacturing, variance in thickness and width of ferrule housings allow filaments to slide past the gauging block, leaving filaments behind. Although the resulting knot demonstrated satisfactory criteria of knot integrity, stability of plugs and quality of 15° angle trim, additional refinement was performed to investigate elimination of dragback completely.

Concept Three. To eliminate dragback, concept refinement was necessary without a gauging block. This concept was prepared and tested[1], which involved a similar two stage process of (1) gripping the filaments and pulling to a specified length-out value, and (2) rotating the gripped filaments to cause the angle trim profile (Figure 3.6). As an alternate of the previous concept, Figure 3.7 shows the model where the knot was held by a support structure while primary and secondary stages were translated through linear solenoid actuators to achieve each stage of the process. Gripper jaws were modified to allow the necessary 15° rotation, with rotation occurring at a vertex through a pivot bearing built within the primary stage. After actuation of the primary stage to pull filaments to a specified length-out value, rotation was engaged by converting translational motion of the secondary slide to rotational motion through a sliding pin bar connection.

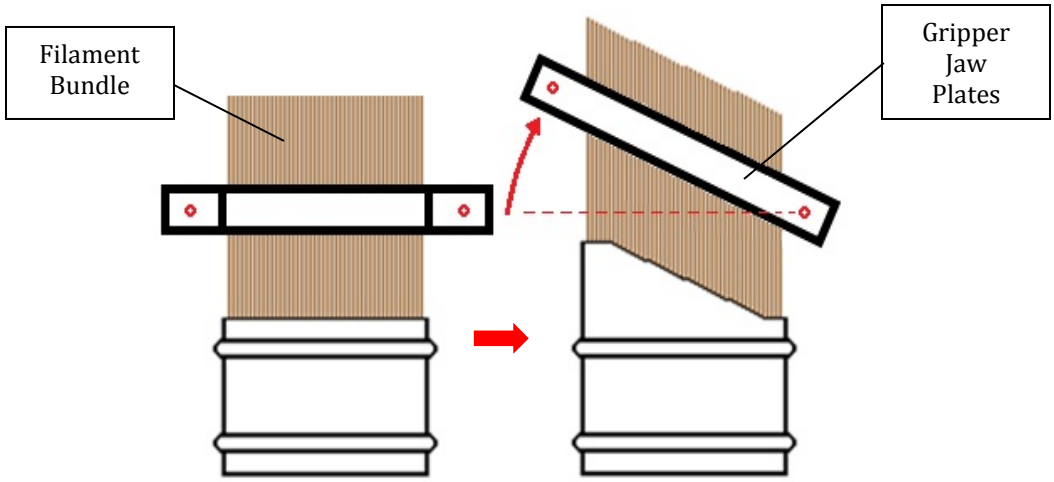

Figure 3.6 Notion of Gripping and Rotating Filaments to Achieve Angle Trim Profile: (Left) Filaments are Gripped by Gripper Jaw Plates; (Right) Gripper Jaw Plates are Rotated to Create the Angle Trim.

[1] Developed with Chris Bunai, Undergraduate Research Assistant

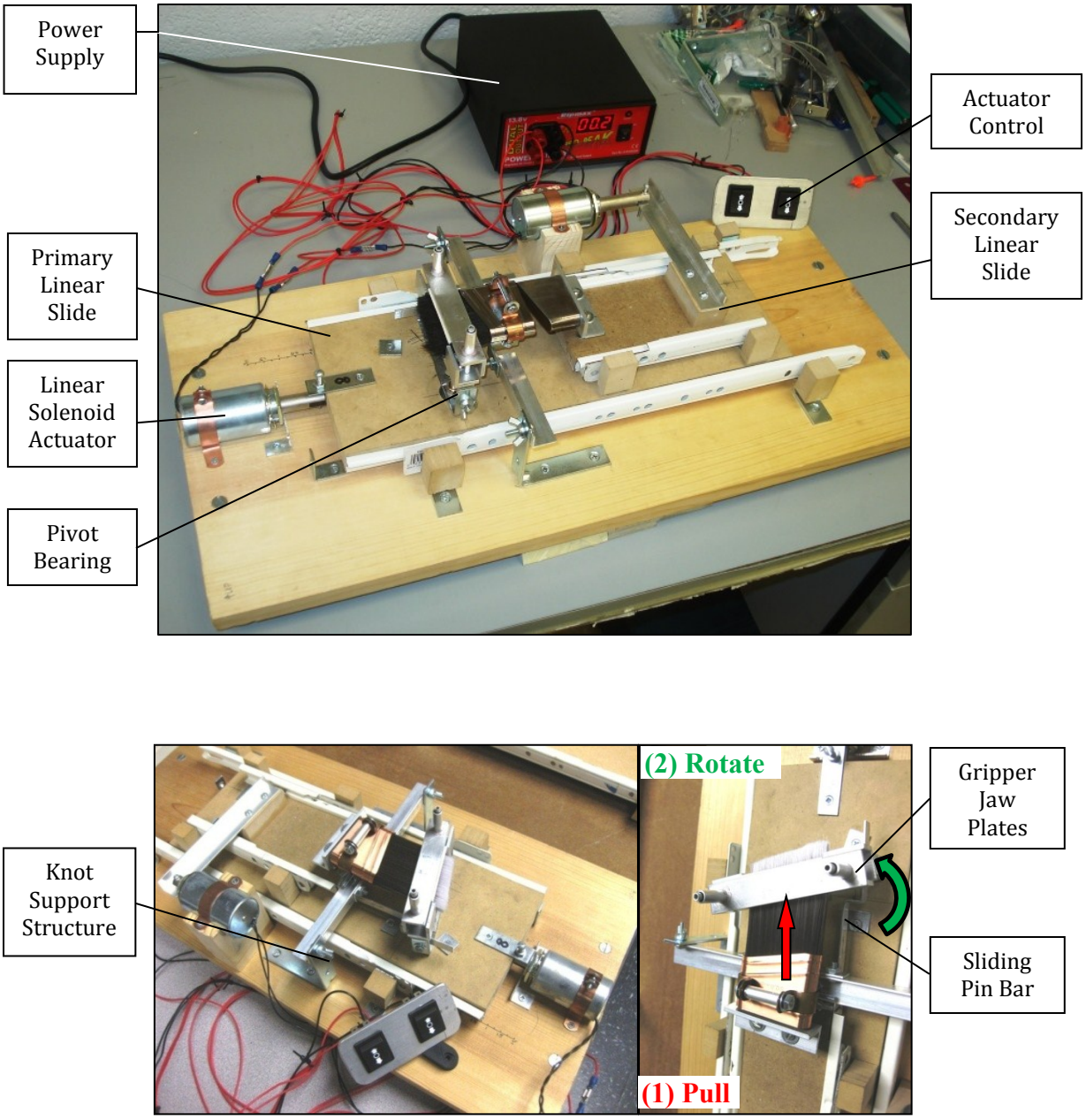

Figure 3.7 Third Proof of Concept Model - Angle Trim Forming, Involving Two Stage Automated Angle Trim Forming (No Gauging Block): (Top) Testing Setup as shown from the Side; (Bottom)Testing Setup as shown from the Top: Gripping and Pulling Filaments to Length-Out (1), and Rotating Filaments to Create Angle Trim (2).

Tests performed using this concept revealed that no dragback was present within the knots shaped. No loss of filaments was evident with knot integrity and plug stability being at its best. The angle trim profile showed significant improvement with sharp linear characteristics of the 15° angle trim tip. With satisfaction of the feasibility testing criteria, this third concept of angle trim forming was selected for further evaluation through testing of physical prototype models. The concept of (1) gripping the filaments and pulling to a specified length-out value, and (2) rotating the gripped filaments to cause the angle trim profile, demonstrates the aspect of innovation necessary for this process of angle trim forming.

3.2.2 Straightening of Filaments

Filament straightening and combing subsystem was to achieve two primary functions: (1) to straighten filament alignment on each side of the knot, that has been gauged to a specified length-out value and trim profile, and (2) comb the filament to untangle and remove loose filaments. The proof-of-concept criterion for filament straightening was to produce filament alignment within straightness tolerance of ±3° from the vertical as shown in Figure 3.8. Additional criteria also used to evaluate performance of feasibility models were to make sure that knot integrity was conserved, filaments are not lost and stability of plug within filaments was maintained after the straightening and combing process.

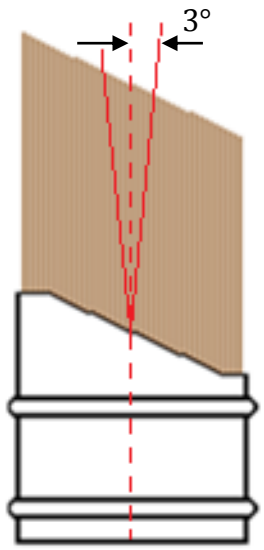

Figure 3.8 Required Filament Straightness Tolerance.

Proof of Concept Model. Through an informal concept generation and selection process, notions of multiple concepts were combined to produce a single concept for feasibility testing. Proof-of-concept model was built to test functionality as seen in Figure 3.9 and 3.10. The concept involved testing of filament straightening on a single side of a knot, where if successful, the process would be adjusted to simultaneously satisfy both sides with an addition of combing action. For straightening to occur, the knot was held stationary by a support structure, as a comb apparatus was inserted into the side of the knot and translated to tilt filaments into alignment. To better understand effect of comb insertion height and depth, location of comb apparatus was made adjustable through a set-screw and slot combination within the comb support structure (Figure 3.10). To translate the comb, the comb apparatus was secured to a linear bearing slide, allowing translational motion of the comb regulated by an electric actuator.

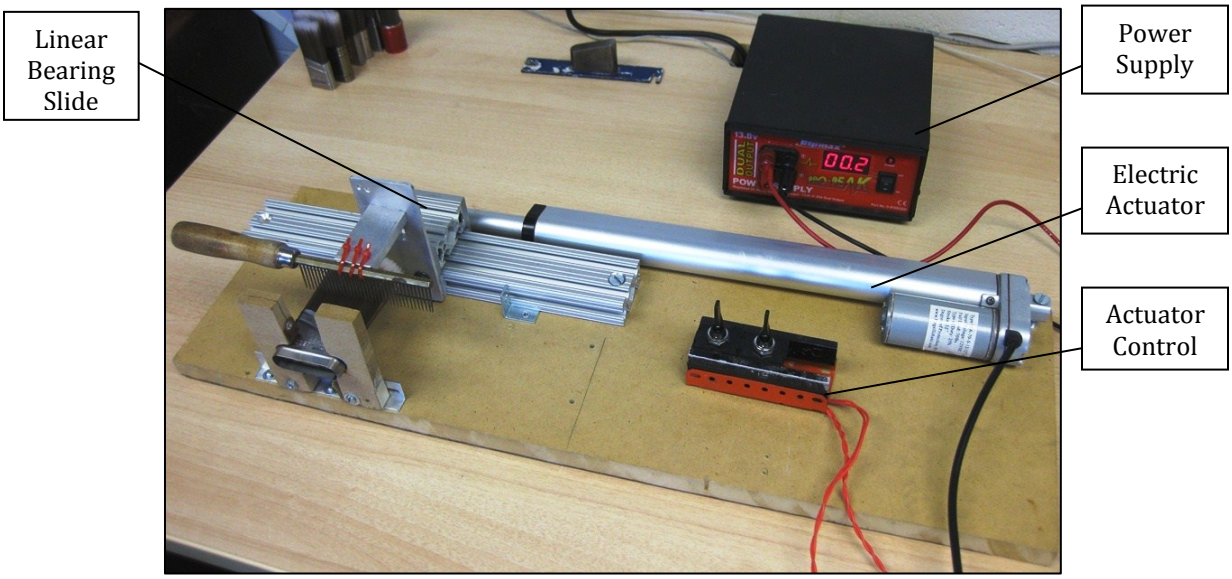

Figure 3.9 Proof of Concept Model for Straightening of Filaments. (Testing Setup as Shown From the Top)

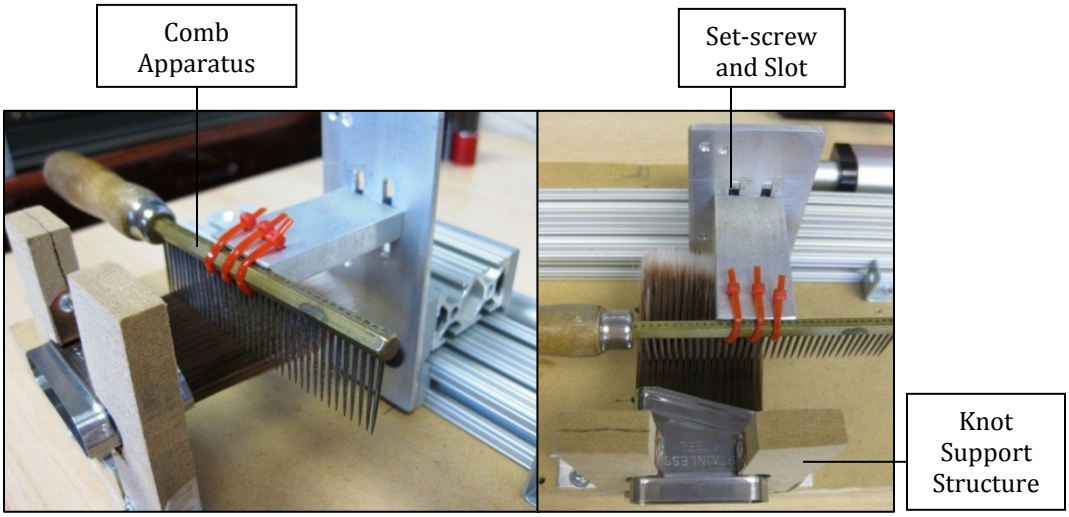

Figure 3.10 Comb Insertion Mechanism: (Left) Mechanism as Shown from the Side; (Right) Mechanism as Shown from the Top.

The knot was locked in place as the comb was inserted into the filaments for a prescribed depth. Testing was performed by regulating comb insertion depth, insertion height and distance of comb translation parameters for different type knots (Figure 3.11). Insertion of the comb was set at prescribed height from the top of the ferrule as the comb was translated to tilt filament into a straight vertical alignment. With testing performed for multiple knot specifications, the concept showed that required straightness with ±3° tolerance can be achieved and was a function of comb insertion depth, insertion height and distance of comb translation parameters. Assuming proper settings for the parameters, this concept showed straightness requirements can be met with conserved knot integrity, no loss of filaments and proper stability of the filament plug. With satisfactory testing results, this concept of filament straightening was selected for further evaluation through testing of physical prototype models.

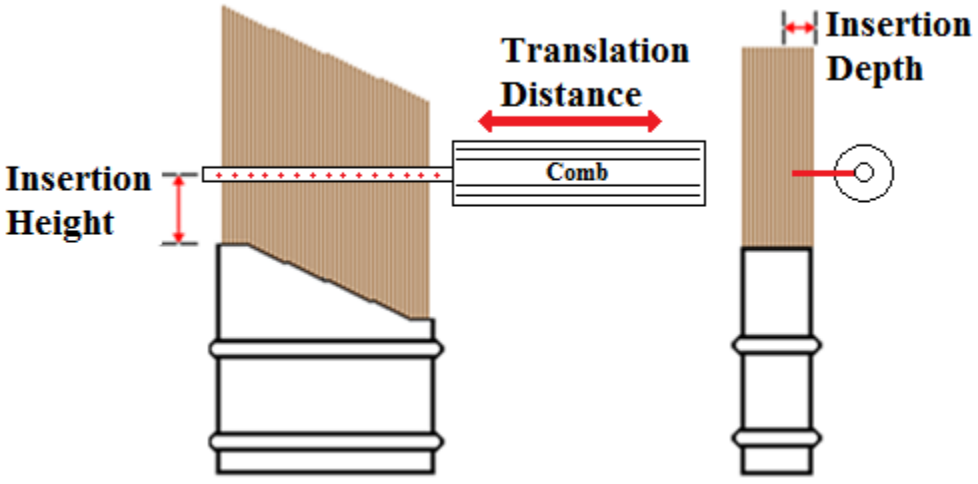

Figure 3.11 Comb Insertion: Insertion Height, Insertion Depth and Translation Distance Parameters.
(Regulated to Perform Straightening of Filament Alignment)

3.2.3 Results from Proof of Concept Model Testing

As a result from proof of concept model testing, top concepts for creating angle trim and filament straightening were established. Concepts for both subsystems demonstrate that through further development, desired quality of knots could be achieved within speciation. From three concepts tested for the process of creating the angle trim, a new, innovative method was established. In order to eliminate dragback completely, it was necessary to perform angle trim forming without the gauging block. Evaluation criteria of no dragback, conserved knot integrity and plug stability were all satisfied with pure actions of (1) gripping filaments, (2) pulling to achieve required displacement to length-out value, and (3) rotating filaments to create the angle trim. This method has demonstrated exceptional results as well as sharp, linear characteristics of the 15° angle trim tip. Furthermore, if proven to be sufficient through further development, this method of creating angle trim would eliminate the problems in relevance to the use of gauging block, such as the cost of gauging block manufacturing as well as ferrule and gauging block tolerance effects on knot quality or dragback. Likewise, this process eliminates the need of a gauging block for flat trim knots (also used to displace filaments within flat trim knots), where function of (3) rotating filaments to create the angle trim, can be excluded.

In similar terms, concept model for straightening of filaments displayed that the desired filament straightness could be achieved within the specification tolerance of ±3° while eliminating filament loss and maintaining knot integrity as well as original plug stability. The model demonstrated that the desired quality of filament straightness could be achieved for different knot recipes through adjustment of comb operation parameters of insertion depth, insertion height and horizontal translation.

To determine the quality of performance for the top concepts, process evaluation was performed through full-scale prototype models. However, before development of prototypes could occur in stages of detail design, testing for design parameters needed to be addressed. For the concept of creating the angle trim, for example, such design parameters would be the force required to displace filament bundles within ferrule housing or the compression force required to efficiently grip associated bundles without loss or damage of filaments. Series of tests were performed to establish different design parameters associated with development of the subsystems described in this study, however for the sake of brevity one of such tests is introduced.

The following chapter exhibits the design for parameter testing process further used to analyze the pulling force required to displace filaments as a function of filament packing density for varying factors of the ferrule, plug and filament bundle combination. The process shown is an example of testing necessary to establish design parameters for the following stages of embodiment and detail design of full scale prototype models.

Chapter 4: Testing for Design Parameters

As established through the proof of concept model, angle trim forming process of paint brush knots requires manipulation of different filament types within ferrule housings of different shapes, material coatings and sizes. Filaments would need to be gripped, displaced vertically from the ferrule housings to achieve a proper length-out value and rotated to create the angle trim. It was expected that force required for displacement of filaments through housings would vary sufficiently based on factors of the ferrule and plug as well as the filament packing density. Unfortunately, to our knowledge no established guidelines exist to estimate the required pulling force to achieve the desired displacement. To further proceed to stages of embodiment and system detail design, it was necessary to establish an understanding of the pulling force to cause displacement of filaments within varying factors of ferrule housing as a function of filament packing density.

This chapter demonstrates the testing process used to establish preliminary characterization of the pulling force, or in equivalence, the force required to overcome friction between filament bundle and ferrule. Described scope of testing involved experimentation with a specific set of factors, mainly to represent the most common type of knots manufactured and seen as 80% of annual production for the Sherwin Williams Company [3]. The associated testing factors, experimental setup as well as sequence of experimentation and experimental results are introduced below.

4.1 Testing Factors

Within the current practice of paint brush knot assembly, the amount of filaments used in each knot is dependent on the ferrule width and thickness to achieve the proper paint distribution [3]. For each combination of ferrule width and thickness, a plug size is matched for the desired knot recipe. Depending on the knot recipe at hand, upper and lower bounds for filament packing density are devised as acceptable amount to be placed inside each knot. For the testing performed, it was of interest to establish a preliminary understanding of the pulling force required to displace filaments at the low, medium and high limits of these bounds. Testing factors characterizing the knot recipe were selected to be assembled into knots and evaluated. With a large possible range of knot recipes, testing was performed using knot components of the most common manufactured type, using a single type of nylon synthetic filament of a discrete length. In-house fabricated circular ferrule housing was also added to the experimentation in order to generalize the testing performed for possible global applications in the future. Furthermore, the experimentation performed here was used to explore the dependence of pulling force on ferrule material type, size and shape.

Testing Factors. Testing factors were selected to be held constant for control of the experiment as well as varied for the sake of result comparison. Constant factor of silver tip nylon synthetic filaments of discrete length and density was used, where filaments would be packed into ferrule housings and tested. Factors selected to be varied within the experiment were ferrule material coating type, ferrule size, ferrule shape and filament packing density. Seven ferrule housings were chosen to be assembled into knots to perform

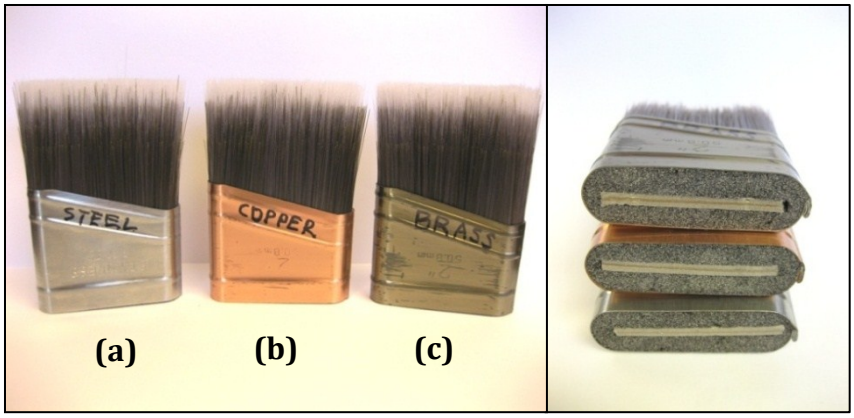

Figure 4.1 Knots Packed using 2" Oval Ferrule Housings;
(Left) Material Coating Type: (a) Stainless Steel; (b) Copper; (c) Brass.

the testing. Three 2" wide oval shape ferrule housings of 9/16" thickness were varied in ferrule coating material type (Figure 4.1). Identical in specification, the ferrule housings had different coating materials such as: stainless steel, copper and brass which had the same plug size as per specification of the factory. Additional three square shape stainless steel ferrules of 2", 1.5" and 1" width and 9/16", 7/16", 5/16" thickness respectively were also used to vary the factors of ferrule size (Figure 4.2). Again, plug sizes were of the required specification for the given square ferrule dimensions, with 2" wide square ferrule plug being of the same size as 2" oval ferrules.

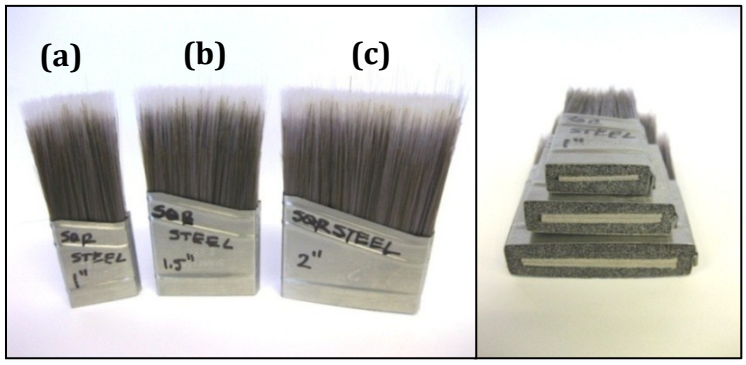

Figure 4.2 Knots Packed using Stainless Steel Square Ferrule Housings;
Ferrule Size: (a) 1" Width; (b) 1.5" Width; (c) 2" Width.

To provide a basis of comparison between 2" oval, 2" square and circular stainless steel ferrules, dimensions of the circular ferrule and wooden plug manufactured were prepared to roughly resemble volume available for packing of filaments between the ferrule and plug of 2" oval and 2" square ferrules. Figure 4.3 displays housings tested in oval, square and circular shapes.

Figure 4.3 Knots Packed using different Stainless Steel Ferrule Shapes; Ferrule Shape: (a) Oval; (b) Square; (c) Circular.

The ferrules, not fabricated in-house, were with rolled beads at the bottom and top of the ferrules as shown in Figure 4.3. The circular shape fabricated ferrule did not have beads. As previously stated, it was of interest to establish a preliminary understanding of maximum force required to displace filaments at the low, medium and high ranges of filament packing densities. The value of each range was provided by the sponsor, where filament packing density is a measure of filament bundle mass to be packed into a specific combination of the ferrule and plug. As shown in Equation 4.1, volume packing fraction is the ratio of volume of filament as a bundle (V_F) to the volume available for packing of filaments between the ferrule inner walls and plug (V_A). With an established value of

$$V_P(\%) = \frac{V_F}{V_A} \times 100;\ \frac{V_F = Volume\ of\ Filament\ Bundle}{V_A = Volume\ Available\ For\ Packing}$$

(Equation 4.1)

volume packing fraction for each range, knots were assembled and tested using the consistent low, medium and high volume fractions for each type of knot.

Figures 4.1-4.3 demonstrate an example of knots that were hand assembled for testing using the knot assembly process specified by the sponsor. In order to control the volume packing fraction, variables shown in Tables 4.1-4.2 were recorded at the time of knot assembly. The experimental setup, knot assembly and sequence of experimentation are described in the forgoing sections.

Table 4.1 Constant Testing Variables Recorded.

Testing Variables	Definition
L_F	Filament Length
ρ_F	Filament Density

Table 4.2 Changing Testing Variables Recorded.

Testing Variables	Definition
W_P	Plug Width
H_P	Plug Height
T_P	Plug Thickness
F_W	Ferrule Width
T_F	Ferrule Thickness
t_F	Ferrule Wall Thickness
m_F	Mass of Filament Bundle
V_P	Volume Packing Fraction
R_F	Inner Radius of Circular Ferrule
R_P	Outer Radius of Circular Plug

4.2 Experimental Setup

To perform testing of knots, a test apparatus was built to displace filaments within ferrule housings. Figure 4.4 shows the setup as a unit, with Figures 4.5-4.7 provided for a more detailed view to assist in further description. Basic operation of the experimental setup involved holding of the ferrule housing stationary, as the filament bundle was gripped and pulled to be displaced within the ferrule. Pulling of the filament bundle was performed using a force gauge, where the pulling force required to displace the filament bundle and displacement of the force gauge was recorded. A combination of a lead-screw-mechanism and a drive-motor were used to control the displacement increment of the force gauge, resulting in displacement of the filament bundle. For the purpose of experimental accuracy, testing was performed along a single axis of travel with motion of required components achieved through low friction precision linear bearings.

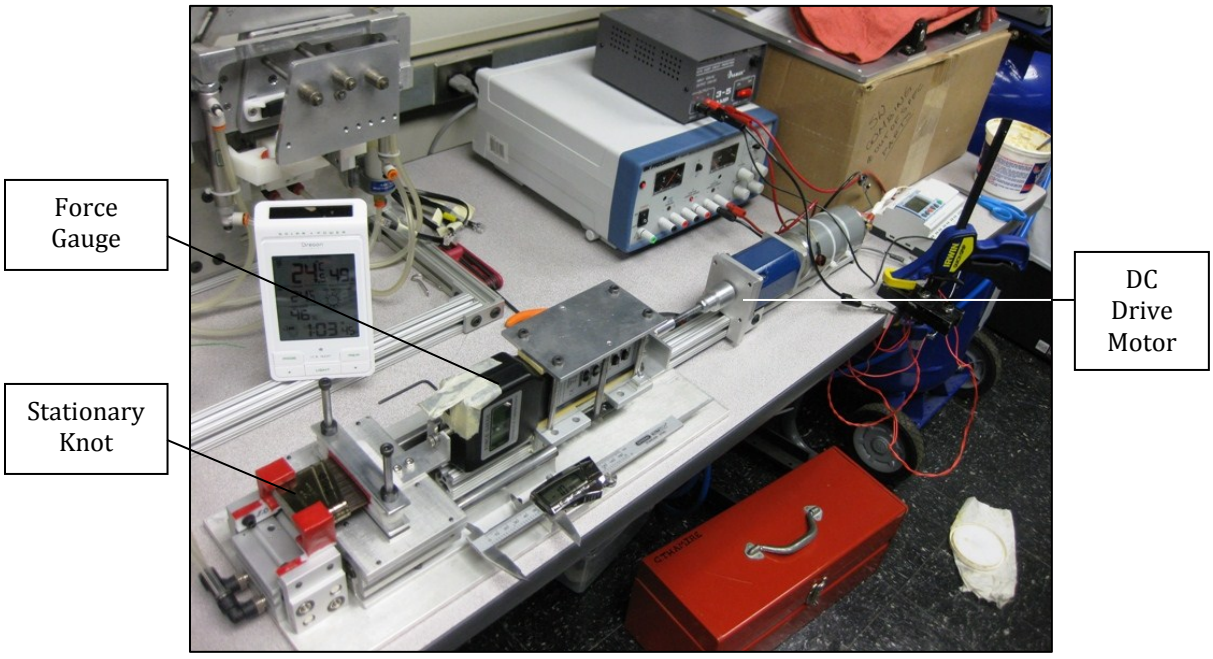

Figure 4.4 Pulling Force Measurement Experimental Setup.

The following description is performed with reference to Figure 4.5. Fabricated experimental apparatus was designed to hold the knot stationary in a horizontal alignment by a pneumatic gripper, equipped with gripper fingers designed to hold the required shape and size of ferrule. Air pressure of the pneumatic gripper was chosen to provide the required holding force without deforming the ferrule in compression. Gripper fingers were developed and manufactured through ABS plastic rapid prototyping to encompass radial portions of the sides of the knot. To protect the ferrule surface and to provide adequate friction, gripper fingers were also coated with vinyl material. Similarly designed filament gripper plates, coated with PTFE material for improved friction, were used to clamp the filament bundle uniformly without causing flaring or damage of the filaments.

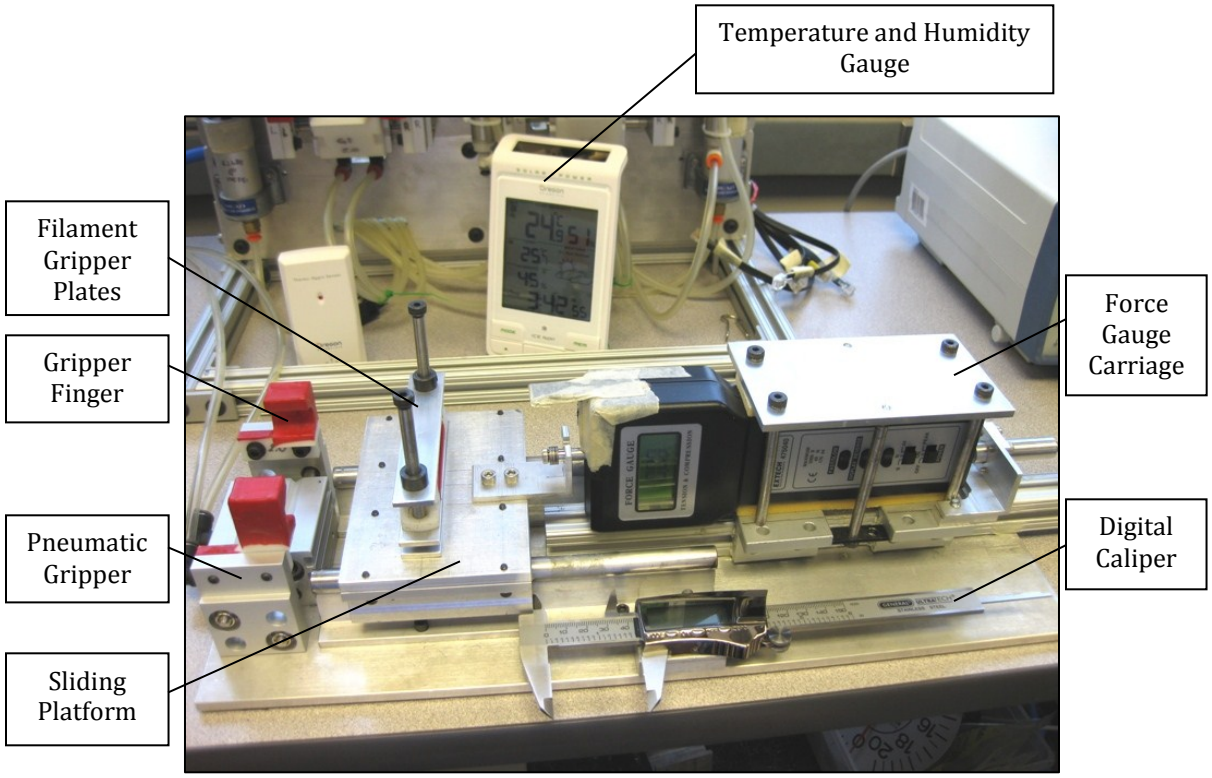

Figure 4.5 Pulling Force Measurement Experimental Setup. (Front Portion of the Setup Shown)

For displacement of clamped filament bundle, the filament gripper plates were secured to a sliding platform on precision linear bearings (Figure 4.5). To move the filament bundle within the ferrule housing, the sliding platform is drawn by a force gauge carriage, at which the force required to displace the filaments is recorded (Figure 4.5). With a condition of no slipping between filament bundle and filament gripper plates, the displacement of filament bundle is measured through a digital caliper connected to the sliding platform and recorded.

The described experimental setup offers the ability to measure both, static friction force required to displace the filament bundle at an incremental displacement and kinetic friction associated with dynamic translation of filaments at a constant velocity. Regulation of filament bundle displacement is performed using a combination of a lead-screw mechanism, geared-DC-motor and a programmable relay output (Figure 4.6). Using the rotational motion of the lead screw, matched with a female thread on the force gauge carriage, the carriage is drawn to displace the sliding platform. With a standard screw

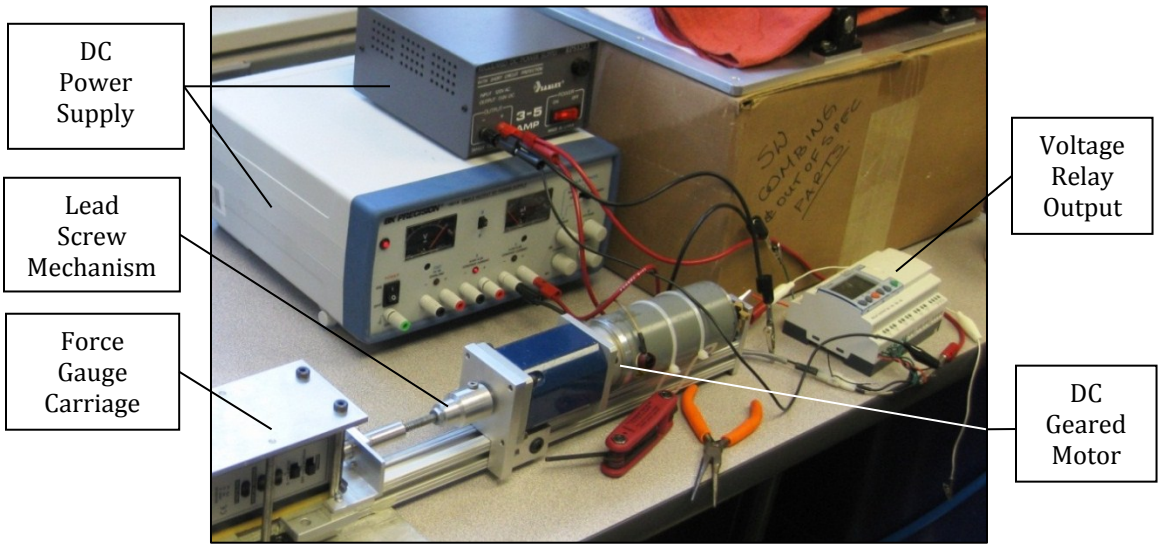

Figure 4.6 Pulling Force Measurement Experimental Setup.
(Back Portion of the Setup Shown)

size of ¼-20, the controlled rotational motion of the screw is converted into translational motion of the force gauge carriage. The motor was mounted to remain stationary and chosen to generate high torque and low RPM. The motor is driven through a programmable voltage relay output, where a time increment of voltage pulse was regulated to provide rotation of the lead-screw for the desired incremental displacement.

Due to a possible effect of humidity and temperature on lubricity of filaments during experimentation, a hydrometer/temperature gauge was added to the testing setup for monitoring of humidity and temperature (Figure 4.5). To test all knots described, the experimental setup was fine-tuned to displace filaments within the ferrule housings at a displacement increment of 1.5mm from the flush alignment of the filaments and the ferrule bottom (Figure 4.7). During testing, measurements of force required to overcome static friction were made at an increment of 1.5mm from the ferrule bottom to the maximum displacement of 20mm (maximum displacement as which the knot integrity is conserved). For the same displacement distance, the knot was repacked and the test was repeated where the bundle was displaced at a continuous rate of 8mm/sec. For the run performed, measurements of force required to overcome kinetic friction were also recorded.

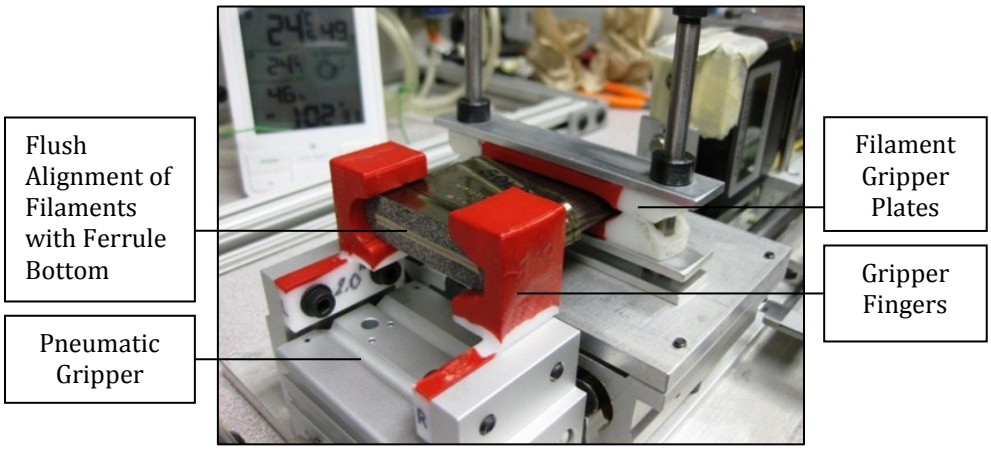

Figure 4.7 Alignment of Filaments with Ferrule Bottom.

4.3 Sequence of Experimentation

This section describes the sequence of steps performed for testing of a single knot sample from preparation and assembly of a knot to calibration and sequence of experimental testing performed using the setup described.

Preparation of a Knot Sample. Individual knot samples for testing previously introduced were prepared through manual assembly as per specifications of the company sponsoring this research. For assembly to occur, silver-tip nylon synthetic filament bundles of known length were weighed on a digital scale to match the requirement of the associated range of filament packing density. The mass of filament bundle was then recorded along with measurements of ferrule width, ferrule thickness, ferrule wall thickness, plug width, plug thickness and plug length. Using a provided density of the nylon filaments, mass of the filament bundles was converted into volume to calculate the associated volume packing fraction. Following, filaments were packed into ferrules with uniform filament distribution through-out the knot. The prescribed plug was inserted to support the filament bundle within the ferrule housing. Further processing of the knot was then performed using a vibratory table to settle all filaments to a flush arrangement with respect to the bottom of the ferrule (Figure 4.7), as hand straightening and combing of filaments was also performed to insure proper filament alignment. After this procedure, the knot was ready for testing.

Calibration. Prior to testing, calibration of the setup was performed to correct for counteracting friction force associated with motion of the sliding platform and digital caliper. To perform the calibration, the sliding platform, caliper ruler and force gauge carriage were placed at the top of their travel to resemble gripping of filaments. The

programmable relay output was turned on to displace the sliding platform and caliper ruler using the force gauge carriage while simulating incremental filament bundle displacement. Measurements of peak force required to overcome static friction to displace the sliding platform and caliper ruler were recorded at each displacement of 1.5 mm. The mean of the recorded static force measurements was used to serve as a calibration value, which would be subtracted from the force values gained during testing.

Sequence of Experimentation. For the experimentation to occur, all subsystems were first reset for proper alignment as the sliding platform and force gauge carriage were brought up to the top of their travel for adequate clamping of filament bundle. At this time, gripper fingers resembling the ferrule in testing were also installed onto the pneumatic gripper. The knot was inserted and secured by closing the gripper fingers as also shown in Figures 4.7. While making sure that the alignment of the filaments remains flush with the back of the ferrule (Figure 4.7), filaments were clamped by filament gripper plates (Figure 4.8). To clamp the filament bundle, filament gripper plates were made to open and close by sliding on precision cut shoulder bolts (Figure 4.8), where locking of gripper plates occurred through hand compression while tightening the set screws on locking collars of the shoulder bolts.

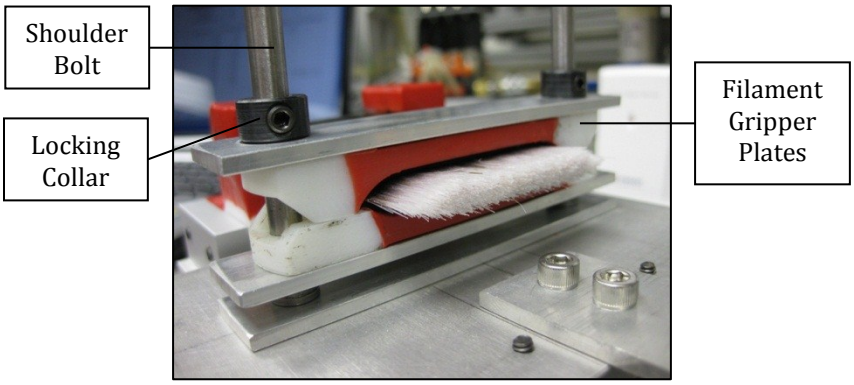

Figure 4.8 Clamping of Filaments by Filament Gripper Plates.

The test setup was ready to perform displacement of the filament bundle as the knot, sliding platform and force gauge carriage alignment was checked. To estimate the forces associated with static friction, the digital caliper and force gauge were zeroed while the run temperature and humidity were also recorded. To initiate the experimental run, the relay output program was turned on, as the lead screw rotated to displace the force gauge and pull the sliding platform to displace the filament bundle. For all knots tested, the filaments were displaced at 1.5mm increment with a two second break in between. After each displacement of 1.5 millimeters, the force required to overcome static friction was recorded along with the associated displacement. To complete the testing, a series of static force and displacement measurements were made until a maximum displacement of 20 millimeters was reached.

To measure the forces associated with kinetic friction, the setup is reset as described previously while the knot is also re-assembled to settle the filaments and plug back to original alignment. The knot is reinserted and held in place by the pneumatic gripper while the filaments are also clamped. The digital caliper and force gauge are zeroed. A direct voltage source is provided to the motor to displace the filament bundle at a constant rate of 8mm/second. With the displacement of the filaments occurring at the provided rate, the force values associated with kinetic friction are recorded up to the limit of twenty millimeters. For the run performed, the recorded force values are then averaged.

To perform additional testing, setup was reset as the sliding platform and force gauge carriage were brought up to the top of their travel for adequate clamping of filament bundle.

4.4 Experimental Results

Using the described testing approach, experimental data was gathered to establish the range of forces required to displace filament bundles for a range of experimental factors described. As an additional benefit during testing, ferrule housings were used to further explore if the displacement force values have a dependency on ferrule material type, ferrule size and ferrule shape. Results from the tests are provided in this section, where for clarity, discussion was firstly performed with respect to knots varying in material coating, secondly knots varying in ferrule size, and finally knots varying in shape.

To further understand if the suggested dependency exists on varying factors of ferrule housings, additional statistical analysis was performed. Results from testing were analyzed using ANOVA, Tukey-Kramer to compare the means of low, medium and high volume fractions for each knot to show that a statistical difference between means exists. To support the discussion, resulting box-plots were provided along with Student-t pairwise difference confidence intervals between means. Further, ANOVA, Tukey-Kramer as well as Student-t analysis were performed as a function of volume packing fraction between changing knot factors, such as ferrule material type, ferrule size and shape. For example, the means for low volume fractions for stainless steel, copper and brass ferrules were compared to asses if a statistical difference exists. The same procedure was also performed for comparison of means achieved within medium and high volume packing fractions. Possible existing statistical difference between means would suggest that a factor of ferrule coating material type is responsible for the difference in friction force experienced between the ferrule housing and filament bundle.

Result Trend Behavior. Results provided in a graph form of the forgoing sections characterize the required value of force (Y-Axis, Newtons) necessary to break static friction with respect to the associated displacement of filament bundle (X-Axis, mm) from the bottom of the ferrule. A trend was evident for knots tested within ferrule housings containing rolled beads (Figure 4.9), where a peak value of static friction force is achieved within the range of 6 to 10mm of displacement. An example plot shown in Figure 4.10 demonstrates characterization of the static friction force experienced by the filament bundle as a function of displacement for different volume packing fractions using 2" wide and 9/16" thick oval ferrule of stainless steel material.

Figure 4.9 Location of Top and Bottom Beads.

The plot demonstrates the peak behavior consistent for all ferrules manufactured by sponsor and having beads regardless of material type, size or shape of the ferrule housing. The behavior is a result of changing surface geometry due to a bottom rolled bead, performed during ferrule manufacturing for structural support of ferrule. The bead is of a round geometry of roughly 4mm diameter. From the response, it can be seen that a higher friction force is experienced due to changing geometry of ferrule wall surface at the location of the bead. It is speculated that the peak force trend seen is a result of translation

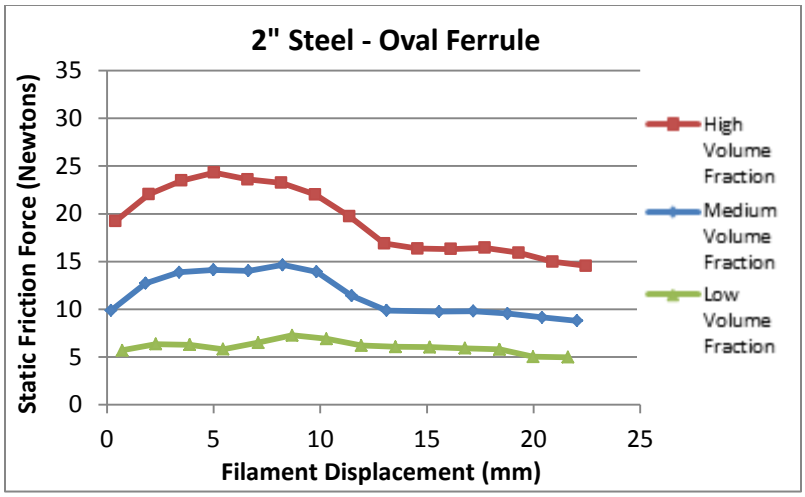

Figure 4.10 Static Friction Force Distribution in 2" (9/16" Thick) Stainless Steel Oval Ferrule.

of the plug through the rolled bead surface, where an increased pressure from the presence of the plug generates a higher friction force to overpass the bead curvature. With less interaction of filaments and ferrule wall surface, the static force distribution decreases as demonstrated by the resulting plots.

The described behavior was consistent for all ferrules having rolled beads. However, the manufactured ferrule housing of circular shape added to the experimentation did not have beads, thus eliminating the peak behavior seen here. The circular ferrule was added to the testing process to explore the resulting force distribution as well as help generalize the comparison made between shapes of ferrules. As a word of caution, testing and analysis of data to suggest possible force dependence on ferrule material type, shape and size was performed to establish a preliminary notion and would require further experimentation. Furthermore, resulting experimental data discussed was achieved using the best tools of knowledge and equipment at hand and does not take into the account the material surface finish of the ferrule housings.

4.4.1 Variation of Ferrule Material Coating

To analyze the friction force with respect to changing ferrule material type, three knots samples of 2" width and 9/16" thickness of oval shape were tested. For experiment control, all three knots were composed of the same experimental factors of ferrule size, ferrule shape and plug size while tested for low, medium and high volume packing fractions. The ferrule material type was the only difference between the experimental knots.

Figures 4.11, 4.12 and 4.13 display the resulting force distributions associated with breaking static friction (Y-Axis) at the matching displacement of filament bundle (X-Axis) for 2" oval ferrules of stainless steel, copper and brass material housings respectively. The data points represented by the plots were used to form the comparison through statistical analysis. For all three types of ferrule housings, ANOVA Tukey-Kramer statistical analysis was performed to establish a comparison of mean force averaged for low, medium and high volume packing fractions of each knot. The comparison showed that a significant statistical difference exists between means. Comparison of means for the knots tested yielded a p-value of $p= 1.26x10^{-16}$ using a stainless steel ferrule, $p= 9.45x10^{-25}$ using copper ferrule and $p= 1.51x10^{-15}$ for brass ferrule housing. Established comparison p-values were for volume packing fraction of low, medium and high of 46.4%, 48.1% and 49.8% for stainless steel ferrule housing, 47.2%, 48.9%, and 50.5% for copper housing and 46.6%, 48.4% and 50.5% for brass material housing respectively. Results from statistical analysis can be seen in Tables 4.3 and 4.4. Table 4.3 demonstrates mean force values achieved within 95% confidence interval as a function of ferrule housing material type and volume packing fraction.

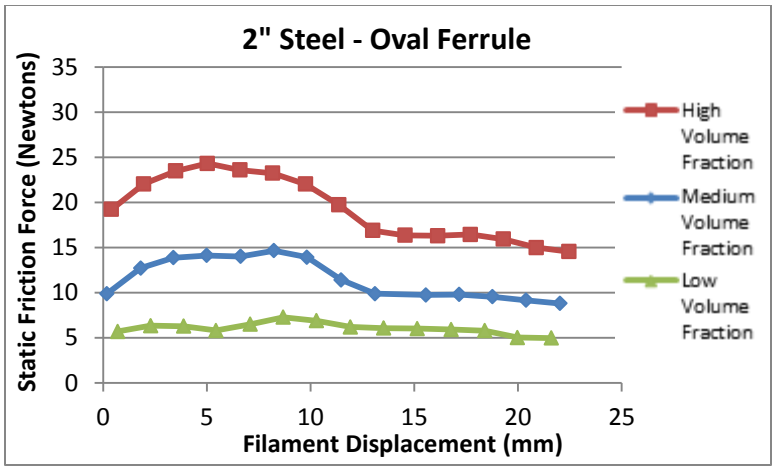

Figure 4.11 Static Friction Force Distribution in 2" Oval Stainless Steel Ferrule.

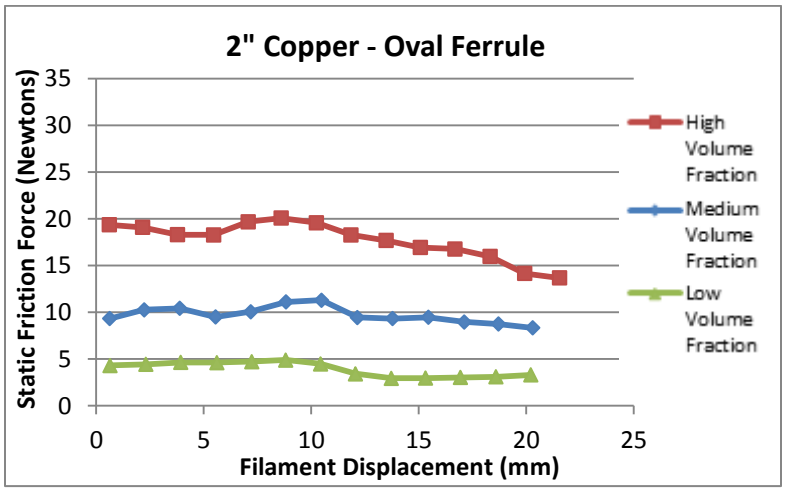

Figure 4.12 Static Friction Force Distribution in 2" Oval Copper Ferrule.

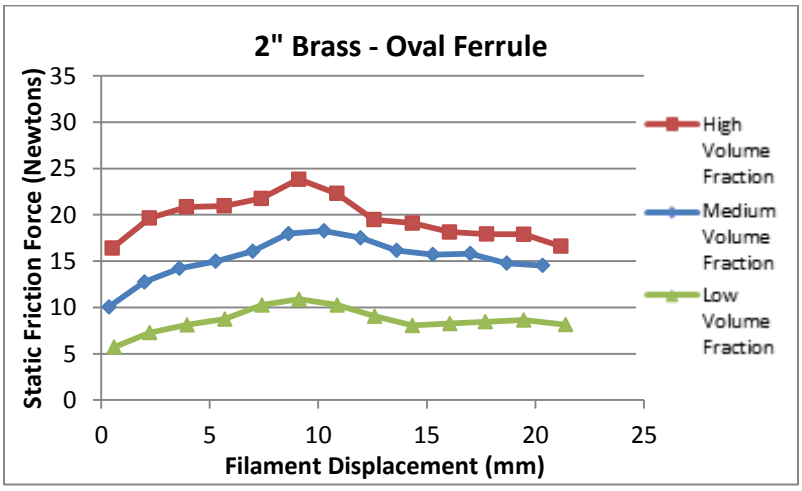

Figure 4.13 Static Friction Force Distribution in 2" Oval Brass Ferrule.

Table 4.3 Comparison of Means as a Function of Ferrule Material Type and Volume Packing Fraction. (2" Oval Shape Ferrules)

	Low		Medium		High	
	μ_1	95% CI	μ_2	95% CI	μ_3	95% CI
Steel	6.06	{5.70,6.42}	11.54	{10.26,12.82}	19.27	{17.31,21.23}
Copper	3.91	{3.44,4.39}	9.71	{9.18,10.24}	17.67	{16.54,18.85}
Brass	8.61	{7.79,9.42}	15.29	{13.95,16.62}	19.61	{18.25,20.97}

Table 4.4 Pairwise Difference Between Means of Volume Packing Fraction as a Function of Ferrule Material Type. (2" Oval Shape Ferrules)

	$\mu_1 - \mu_2$	95%CI	$\mu_1 - \mu_3$	95%CI	$\mu_2 - \mu_3$	95%CI
Steel	-5.47	{-7.75,-3.20}	-13.21	{-15.44,-10.97}	-7.73	{-9.97,-5.49}
Copper	-5.79	{-7.10,-4.49}	-13.78	{-15.06,-12.50}	-7.99	{-9.26,-6.70}
Brass	-6.68	{-8.58,-4.78}	-11.00	{-12.89,-9.10}	-4.32	{-6.22,-2.42}

Established statistical difference in means can also be seen in the pairwise difference between means shown in Table 4.4 as well as in box-plot form found in Appendix-A.

Combination of ANOVA, Tukey-Kramer and Student-t analyses were further performed to see if the means of the same volume packing fractions differ as a function of ferrule coating material type. To elaborate, the static friction force distribution achieved for low packing fraction of 2" stainless steel housing was compared to the static force distribution of low packing fraction of 2" copper and 2" brass housings. The same was performed between high and medium volume fraction distributions. As a result, a statistically significant difference with 95% confidence was found between the force distribution for volume packing fraction of low ($p=6.06\times10^{-14}$) and medium ($p=1.39\times10^{-8}$) ranges between the ferrule housing types and a difference within 84% confidence interval for high volume fraction ($p=0.16$). Table 4.5 and associated box-plots found in Appendix-A display the

Table 4.5 Pairwise Difference Between Means of Ferrule Type as a Function of Volume Packing Fraction. (2" Oval Shape Ferrules)

	μ_{Cu}- μ_{St}	95%CI	μ_{Cu} - μ_{Br}	95%CI	μ_{St}- μ_{Br}	95%CI
Low	-2.15	{-3.05,-1.24}	-4.69	{-5.61,-3.77}	-2.54	{-3.45,-1.64}
Medium	-1.95	{-3.70,-0.19}	-5.57	{-7.32,-3.81}	-3.62	{-5.40,-1.83}
High	p= 0.16 (Statistically Different within 84% CI)					

pairwise difference between means in table and box-plot forms respectively. Resulting statistical analysis suggests that ferrule housing material coating does provide a statistically significant effect on the pulling force required to displace the filament bundle within the ranges of volume packing fractions tested. Figure 4.14 displays the mean values of static friction force as a function of ferrule housing material type and volume packing fraction. As the figure demonstrates, the highest mean of pulling force is associated with brass material and lowest with copper material coating. From the results, it is evident that the highest coefficient of friction, assuming the same material surface finish, was associated with brass coated ferrules, the second highest with stainless steel and the lowest for copper coated ferrules.

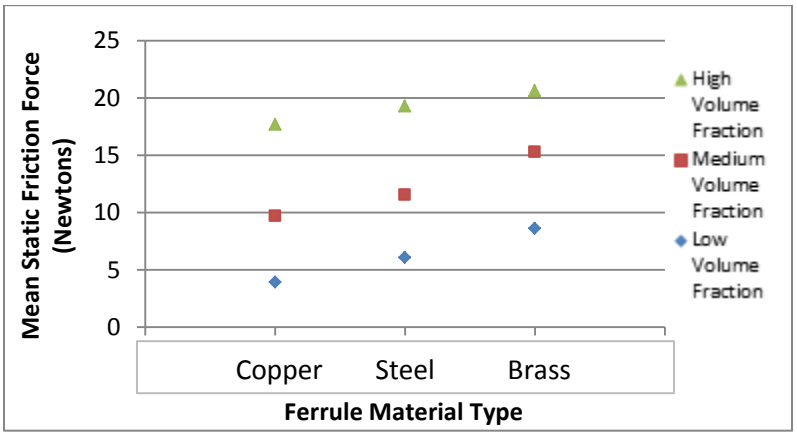

Figure 4.14 Mean Static Friction Force as a Function of Ferrule Material Type and Volume Packing Fraction.

4.4.2 Variation of Ferrule Size

Similar procedure was performed using statistical analysis techniques to explore the possible friction force dependence on the size of the ferrule housings. Square shape ferrules of 2", 1.5" and 1" width and 9/16", 7/16" and 5/16" thickness respectively were used to assimilate the static force distribution between varying ferrule sizes. Housings of 2", 1.5" and 1" width were prepared for testing with a combination of plug and volume packing fraction suitable for the ferrule size. For the purpose of further comparison between ferrule shapes, the 2" wide square ferrule housing was prepared with the same size plug as the 2" oval shape stainless steel ferrule. Supporting volume packing fraction of low, medium and high ranges were devised to closely resemble volume packing fractions for the 2" oval and circular stainless steel ferrules.

Figures 4.15-4.17 demonstrate the force distribution plots gathered from the testing performed. For the knots tested and analyzed, the volume packing fraction of low, medium and high were of 43.2%, 46.4% and 49.6% for 2" wide ferrule housing, 42.9%, 45.3%, and 47.5% for 1.5" wide ferrule and 44.2%, 45.2% and 46.1% for 1" wide ferrule respectively. Results from ANOVA Tukey-Kramer demonstrated that each ferrule size had a mean static force value significantly different with respect to the low, medium and high volume packing fractions with $p=8.07\times10^{-20}$, $p=2.85\times10^{-5}$ and $p=1.91\times10^{-4}$ for 2" wide, 1.5" wide and 1" wide square ferrules respectively. Achieved means of static friction force within 95% confidence interval are displayed as a function of ferrule size and volume packing fractions in Table 4.6 along with the pairwise difference between means shown in Table 4.7. Supporting box-plots exemplifying visual spread of the data and can be seen in Appendix-B.

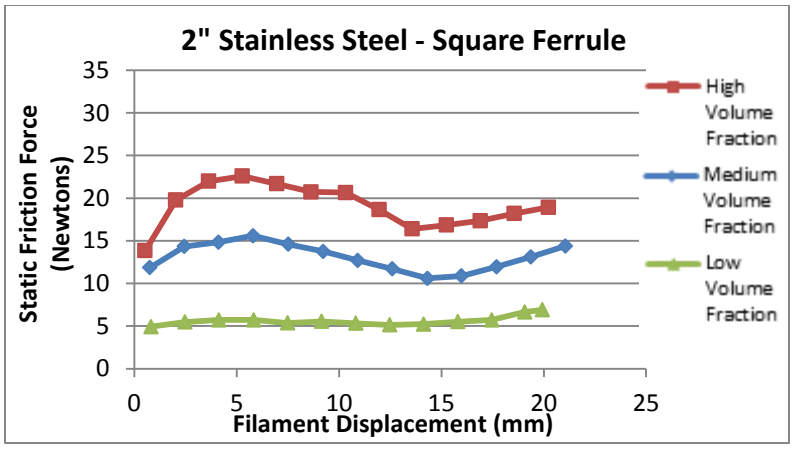

Figure 4.15 Static Friction Force Distribution in 2" Wide (9/16" Thick) Square Stainless Steel Ferrule.

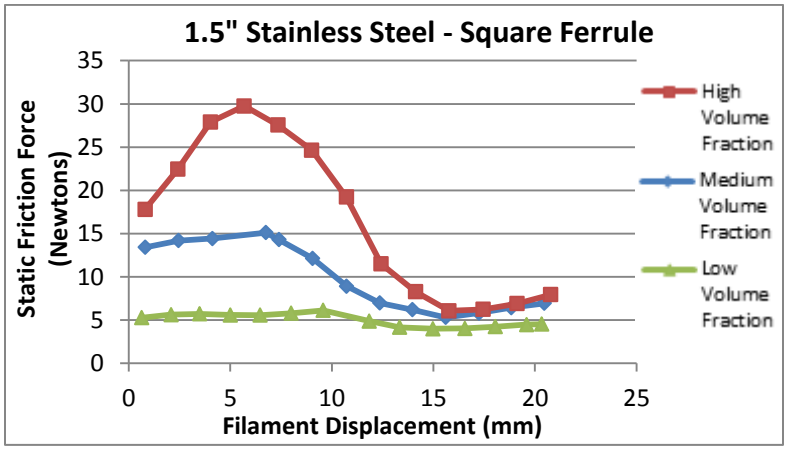

Figure 4.16 Static Friction Force Distribution in 1.5" Wide (7/16" Thick) Square Stainless Steel Ferrule.

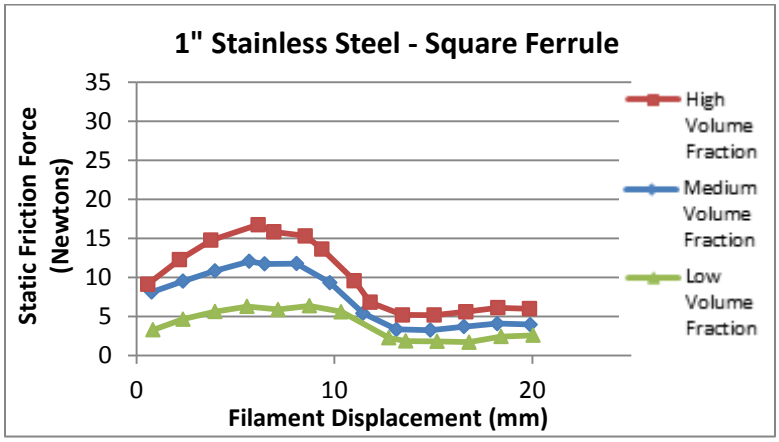

Figure 4. 17 Static Friction Force Distribution in 1" Wide (5/16" Thick) Square Stainless Steel Ferrule.

Table 4.6 Comparison of Means as a Function of Stainless Steel Square Size Ferrules and Volume Packing Fraction.

	Low		Medium		High	
	μ_1	95% CI	μ_2	95% CI	μ_3	95% CI
2”	5.63	{5.29,5.97}	13.09	{12.12,14.07}	19.05	{17.52,20.58}
1.5”	4.99	{4.56,5.43}	10.00	{7.63,12.38}	16.63	{11.08,22.18}
1”	3.87	{2.74,5.01}	7.47	{5.30,9.64}	10.15	{7.59,12.72}

Table 4.7 Pairwise Difference Between Means of Volume Packing Fraction as a Function of Stainless Steel Square Size Ferrules.

	$\mu_1 - \mu_2$	95%CI	$\mu_1 - \mu_3$	95%CI	$\mu_2 - \mu_3$	95%CI
2”	-7.47	{-9.16,-5.77}	-13.42	{-15.11,-11.73}	-5.95	{-7.64,-4.26}
1.5”	-5.01	{-10.37,0.35}	-11.63	{-16.99,-6.27}	-6.62	{-12.08,-1.16}
1”	-3.59	{-6.95,-0.24}	-6.28	{-9.577,-2.99}	-2.68	{-5.97,0.61}

Comparison of static force distribution with respect to ferrule size through statistical testing also yielded a significant difference within 95% confidence interval between volume packing fractions of low (p= 0.0024), medium ($p=3.46x10^{-4}$) and high (p=0.003) between 2”, 1.5” and 1” ferrules. With the pairwise difference between means of ferrule sizes highlighted in Table 4.8 and supporting box-plots found in Appendix-B, it can be suggested that static force value is a function of ferrule size.

Table 4. 8 Pairwise Difference Between Means of Ferrule Size as a function of Volume Packing Fraction.

	$\mu_{1”} - \mu_{1.5”}$	95%CI	$\mu_{1”} - \mu_{2”}$	95%CI	$\mu_{1.5”} - \mu_{2”}$	95%CI
Low	-1.12	{-2.25,0.01}	-1.75	{-2.91,-0.60}	-0.63	{-1.76,0.49}
Medium	-2.53	{-5.61,0.54}	-5.62	{-8.69,-2.55}	-3.09	{-6.16,-0.01}
High	-6.84	{-13.04,-0.63}	-9.26	{-15.46,-3.05}	-2.42	{-8.36,3.52}

Figure 4.18 displays the mean values of static friction force as a function of ferrule size and volume packing fraction. As shown in figure, experimental data suggests that the highest means of pulling force are associated with the largest ferrule housing of 2" width and the lowest with 1" wide ferrule.

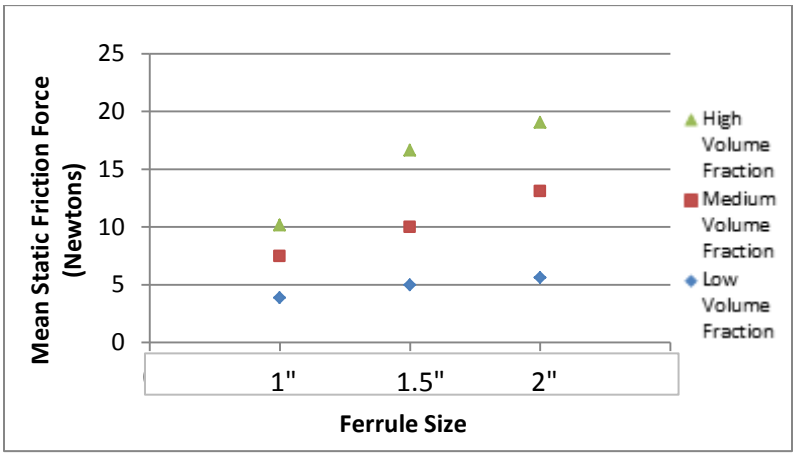

Figure 4.18 Mean Static Friction Force as a Function of Ferrule Size and Volume Packing Fraction.

4.4.3 Variation of Ferrule Shape

In order to widen the scope of testing, additional circular housing and plug were manufactured in-house. Shown in Figure 4.19, the housing was machined using stainless steel material to create properties of inner diameter, length and surface finish adequate for comparison with 2" wide oval and 2" wide square stainless steel ferrules. A supporting plug, made of wood, was also fabricated to match the ferrule housing with properties of height and outer diameter chosen to generate volume available for packing of filaments between ferrule walls and plug to approximately match the volume also found in 2" oval and 2" square housings.

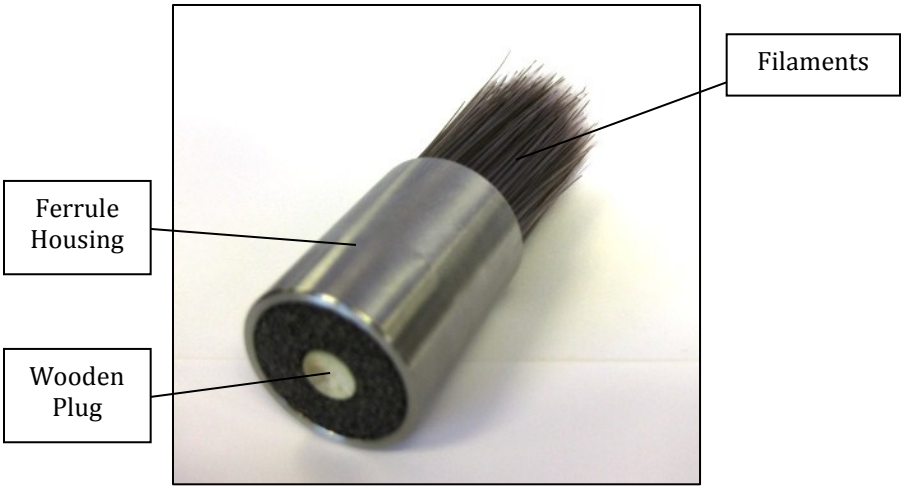

Figure 4.19 Circular Ferrule Housing.

Testing of circular ferrule was performed to help generalize the application, however as noted previously no beads were present. It is understood that the mean force values may be different due to the peak behavior; however results from testing of the circular ferrule housing are provided to explore the friction force behavior, as well as for a general comparison. Testing results using circular ferrule can be seen in Figure 4.20 along with the results from 2" oval (Figure 4.21) and 2" square (Figure 4.22) ferrules previously tested.

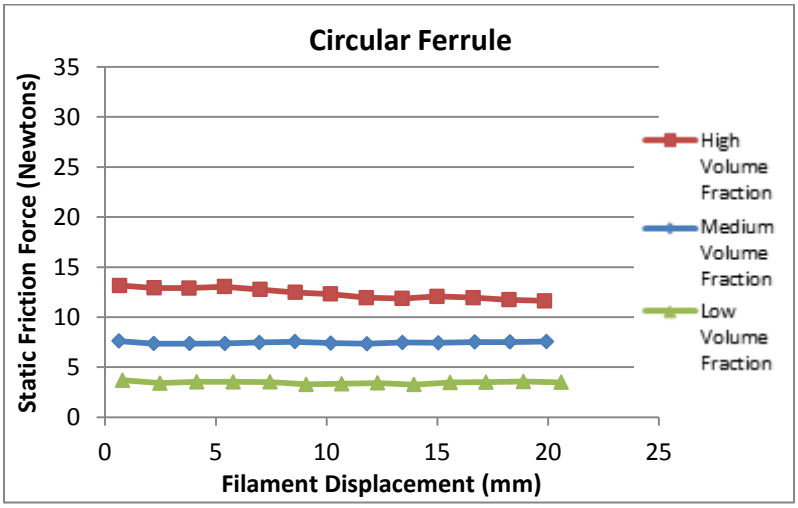

Figure 4. 20 Static Friction Force Distribution in Circular Stainless Steel Ferrule.

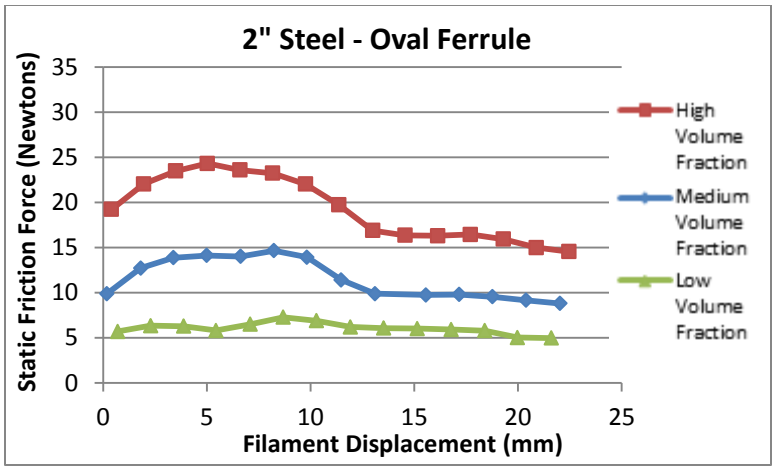

Figure 4.21 Static Friction Force Distribution in 2" Oval Stainless Steel Ferrule.

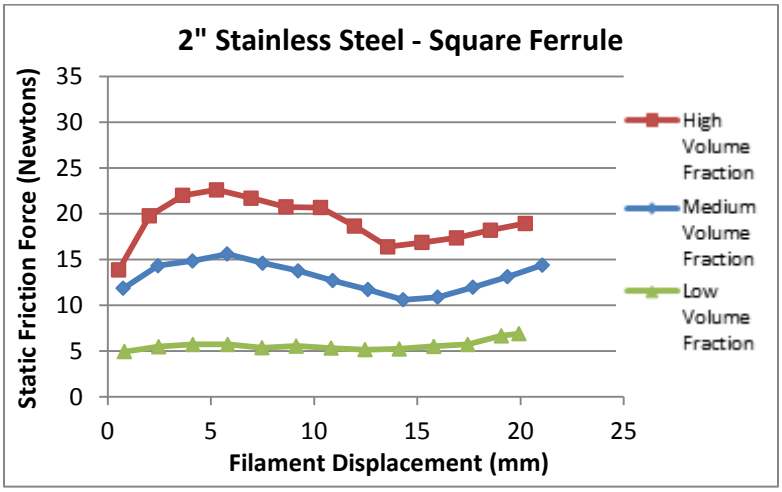

Figure 4.22 Static Friction Force Distribution in 2" Square Stainless Steel Ferrule.

As expected, a significant difference in friction force behavior can be seen for the circular ferrule housing (Figure 4.20). Due to the absence of the rolled beads, the force values attained within the circular housing do not display a peak in static force distribution; instead more expected friction force characteristics are evident. With consistent surface geometry, filament bundle and ferrule walls experience a consistent decrease in interaction of surface areas of as a function of displacement. In result, the

distribution displays the expected trend-line of decreasing static friction force as a function of filament bundle displacement.

Although evident from Figure 4.20, results from ANOVA Tukey-Kramer confirmed that circular ferrule static friction force means are significantly different (Table 4.9) between low, medium and high volume fractions with $p=2.92x10^{-39}$ for the circular ferrule. Shown in previous sections, consistent difference between volume fraction means was also found for 2" oval ferrule housing of stainless steel ($p=1.26x10^{-16}$) and 2" square ($p=8.07x10^{-20}$) ferrule housing of stainless steel. For the three varying ferrule shapes, the volume packing fractions of low, medium and high of 46.4%, 48.1% and 49.8% for the 2" oval ferrule housing, of 43.2%, 46.4% and 49.6% for the 2" square ferrule housing and 46.6%, 47.5% and 48.4% for the circular ferrule housing respectively. Results from statistical analysis for each ferrule housing material type can be seen in Tables 4.9-4.10 as well as in box-plot form of Appendix-C. Achieved mean static friction force as function of

Table 4.9 Comparison of Means as a Function of Ferrule Shape and Volume Packing Fraction.

	Low		Medium		High	
	μ_1	95% CI	μ_2	95% CI	μ_3	95% CI
2" Oval	6.06	{5.70,6.42}	11.54	{10.26,12.82}	19.27	{17.31,21.23}
2" Square	5.63	{5.29,5.97}	13.09	{12.12,14.07}	19.05	{17.52,20.58}
Circular	3.46	{3.39,3.53}	7.45	{7.39,7.50}	12.36	{12.04,12.69}

Table 4.10 Pairwise Difference Between Means of Volume Packing Fraction as a Function of Ferrule Shape.

	μ_1- μ_2	95%CI	μ_1- μ_3	95%CI	μ_2- μ_3	95%CI
2" Oval	-7.72	{-9.94,-5.50}	-15.46	{-17.64,-13.27}	-7.73	{-9.95,-5.51}
2" Square	-7.47	{-9.16,-5.77}	-13.42	{-15.11,-11.73}	-5.95	{-7.64,-4.26}
Circular	-3.99	{-4.30,-3.68}	-8.90	{-9.21,-8.59}	-4.91	{-5.22,-4.60}

ferrule shape and volume packing fraction are displayed in Table 4.9, with significant pairwise difference between means highlighted in Table 4.10.

Assuming the same surface finish for the inner walls of the selected ferrules, it was evident that the static friction force means for each volume packing fraction type using a circular ferrule are significantly lower to those found in 2" wide square and 2" wide oval ferrules. With 95% confidence, statistical analysis showed that a significant difference exists between mean values of static friction (Table 4.11) found for the three ferrule types as function of volume packing fractions of low ($p=4.74 \times 10^{-16}$), medium ($p=2.19 \times 10^{-10}$) and high ($p=1.22 \times 10^{-8}$) between circular, 2"oval and 2" square shape ferrules respectively. Supporting data can be seen in Table 4.11 and box-plots found in Appendix-C.

Table 4.11 Pairwise Difference Between Means of Ferrule Shape as a Function of Volume Packing Fraction.

	$\mu_{2O}-\mu_{2S}$	95%CI	$\mu_{2O}-\mu_{C}$	95%CI	$\mu_{2S}-\mu_{C}$	95%CI
Low	0.44	{-0.03,0.89}	2.61	{2.14,3.07}	2.17	{1.69,2.64}
Medium	-1.55	{-3.06,-0.04}	4.09	{2.58,5.60}	5.64	{4.11,7.18}
High	0.23	{-2.17,2.63}	6.91	{4.51,9.31}	6.68	{4.20,9.16}

Considering the type of comparison being made here, the results suggest that ferrule housing shape could provide an affect on the pulling force required to displace the filament bundle within the ranges of volume packing fractions tested. Figure 4.23 shows the compilation of mean values of static friction force a function of ferrule housing shape and volume packing fraction and. The results suggest that the square shape ferrule housing would require the maximum amount of force to displace a filament bundle, medium for oval shape housing and minimum for circular shape.

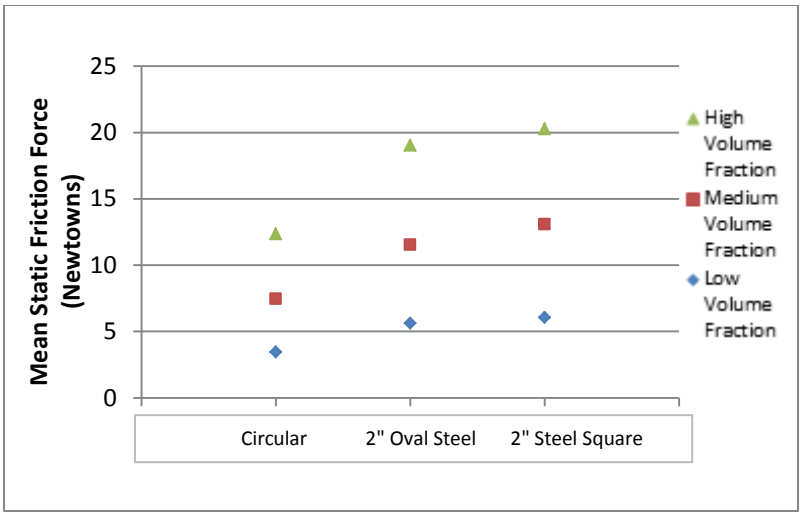

Figure 4.23 Mean Static Friction Force as a Function of Ferrule Shape and Volume Packing Fraction.

4.5 Discussion of Results

The experimental data collected suggests that force required to displace filaments from ferrule housings could be dependent on the ferrule housing material coating type, ferrule size and ferrule shape. However to establish a more accurate answer, more testing would be necessary with consideration of other factors that may contribute to the friction force such as the surface finish of housings. Again, it is important to establish that this was a preliminary exploration of the static friction force distribution within ferrule housings.

With the comparison performed through statistical analysis using ANOVA Tukey-Kramer and Student-t processes, it was found that the most common ferrules of stainless steel, copper and brass material types show the highest friction force values for brass coating, the lowest for copper and medium for stainless steel. In similar terms, the force values were also found to be the highest for the largest of the three ferrules tested within 2", 1.5" and 1" size. The provided statistical results show that the 2" square ferrule of stainless steel material type would require the highest pulling force, with 1.5" ferrule as the

second highest and the lowest for 1” ferrule. Analysis performed with respect to shape of ferrule housing also displayed that a significant difference between pulling force is present. With tests performed for individual ferrule housing shapes of oval, square and circular, all were found to be statistically different between each other. Most complex shape of square form between the ferrules tested was found to generate the highest force necessary to displace the filament bundle, with second highest for the oval shape. When considered, the results summarized here follow the expected outcome.

Results from testing also demonstrated the range of peak forces required for further subsystem prototype design stages. For the testing process performed, a maximum value of force required to overcome static friction was found to be 29.75 Newtons. This value would be used further in stages of embodiment and detail of angle trim forming full-scale prototype. The established magnitude of the maximum force found through testing would lead the appropriate component selection to provide the force necessary to displace the filament bundle and associated prototype subassemblies.

In the case of dynamic filament bundle displacement, it can assumed that the friction force would be lower; however, because the initial friction force is not equal to the peak force experienced during displacement, the value of the maximum force is used as the worst case design tactic for design of prototype. Additional testing would also be conducted for other existing specifications of knots not tested here.

Chapter 5: Embodiment and Detail Design

In order to evaluate the performance of the top chosen concepts from proof of concept testing, semi-automated physical prototype models for angle trim forming and filament straightening subsystems were designed and fabricated. This chapter describes the detail design stages of full scale prototype model development.

Models were developed through a combination of hand sketch design and hand calculations with solid modeling and analysis also performed through 3D Computer Aided Design (CAD) using Pro-Engineer software. Prototypes were intended to explore best suitable design for core subsystems to offer ease of subsystem refinement and integration in the future. Design objectives were to establish modular subsystem architecture and knot interface with minimal subsystem footprint while satisfying all specified target specifications, functional requirements and design criteria. Appropriate component design and selection was performed to meet the criteria of Design For X (DFX), or:

1. Design For Manufacture;
2. Design For Assembly;
3. Design For Maintenance, and
4. Design For Cost.

To make sure target specifications, functional requirements and DFX are satisfied, motion analysis as well as stress and deflection analysis were also performed using Pro-Engineer solid modeling software.

Prior to further elaboration it is important at this time to highlight that specifications of each component chosen or designed often show themselves to be extensively detailed, but nonetheless considered. In this chapter as well as chapter of

subsystem refinement, such specifications are not introduced for the sake of brevity. However, a record of all components and associated assemblies exists and can be available upon request. Examples of such records in the form of bill of materials, engineering drawings, pneumatic diagrams and assembly drawings are introduced further in Chapter 6.

5.1 Design Elements

To build automation systems in a modular way, it is often desired to use readily available, off-the-shelf components. This approach has many benefits, including ease of replacement of defective and worn-out parts, cost savings, shorter design times and more rapid implementation of the machine. A simple combination of pneumatic components, linear motion bearings, quick connect slotted aluminum extrusion profiles, sensors and programmable electronic controllers can often generate fairly complex, low cost, precise and efficient automated systems [7]. This catalog approach was taken to further develop the prototype models. Pneumatic components, linear and rotational motion hardware, custom fabricated components, structural support components, electronic control and programming were used to mechanize and automate actions necessary to satisfy the prototype functional requirements.

To create the most efficient design process using the catalog design approach, components and their specifications were researched first. Necessary components were selected and modeled using Pro-Engineer 3D CAD solid modeling software. As an alternative fabrication space, components were then assembled to model the full system prototype. Selection of components was performed such that for physical fabrication to occur, necessary components would be purchased, purchased and altered or custom fabricated to match the design specifications as well as provide necessary static and

dynamic performance checked through analysis available within solid modeling software. With variety of components and their distributors, prototype design stages were performed with a goal to minimize cost, time for assembly and time for maintenance. For this reason, component selection was performed from the most reputable automation component manufacturers of SMC Pneumatics, Clippard Minimatic, Omega, 80/20 Inc. as well as most popular industrial supply distributors of McMaster-Carr, MSC Direct, Grainger and Motion Industries. For further elaboration, different types of components are described below.

Pneumatic Components. Use of pneumatic components offers a number of benefits, almost always preferred by the automation industry. Compressed air is sustainable, cost efficient and safe. With a wide selection of modular components, use of pneumatics also offers fast system design time with ease of assembly and maintenance, while offering high cycle rates, repeatability with high precision and reliability. For the systems in design, commonly available pneumatic components such as actuator air cylinders and gripper mechanism were used to provide the required process actuation or motion (Figure 5.1). Round type cylinder actuators manufactured by Clippard Minimatic were of most utilized

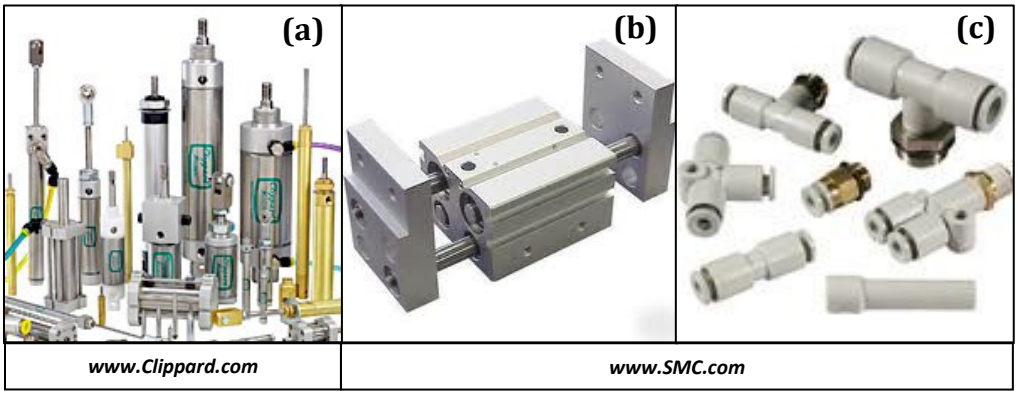

Figure 5.1 Pneumatic Components:
(a) Round Actuator Air Cylinders; (b) Pneumatic Gripper; (d) Fittings.

type, with a few exceptions of SMC Pneumatic and linear motion slide integrated actuators. Depending on the application, the actuators were selected based on the required rating of force, distance of actuation (stroke), and available mounting position to name a few. Fittings as well as flow control valves were used to offer control and necessary fine-tuning of speed of actuation. Furthermore, selection of standardized fittings, manifolds and Y-Union flow separators were used to offer ease of design of pneumatic circuits and distribution of air pressure to perform simultaneous motion of actuators when needed. Additional pneumatic components of electronic controlled solenoid valves were used to distribute and air flow to control cylinder actuation through electronic signal.

Motion Hardware. Using the provided actuation of pneumatic systems, linear and rotational motion requirements were achieved using a variety of readily available motion hardware, such as the ones shown in Figure 5.2. Most linear motion components were a combination of a precision cut or extruded guiding shafts or guide-rails and ball bearing filled pillow blocks to offer smooth and precise linear motion as well as ease of replacement and mounting. Specifications of guiding shafts and rails as well as associated

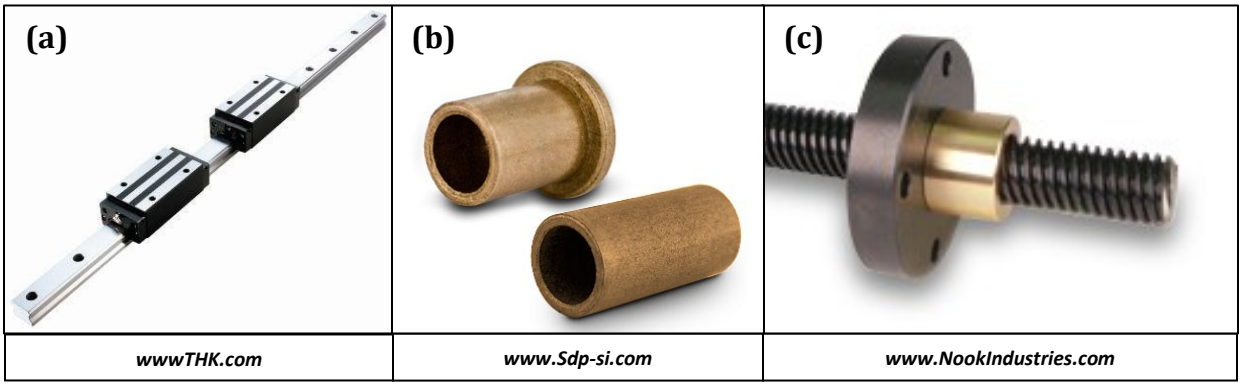

Figure 5.2 Motion Hardware Components:
(a) Guide-rail with Ball Bearing Filled Pillow Blocks; (b) Bronze Sleeve Bearings;
(c) ACME Screw and Nut.

bearing pillow blocks were selected to properly match the required loading requirements. In some cases, for ease of maintenance and limitations due to space, solid type bearings such as plastic UHMW-PE self-lubricating low friction bearings and PTFE oil impregnated bronze sleeve bearings were used to offer motion on flat or circular surface geometry. When ease of automated adjustment or precision of component location was necessary, precision ACME threaded rods and nuts were used to effectively convert rotary motion into smooth, precise linear motion. As a standardized type of transversal threading, ACME design threaded rods and nuts are machined with high precision to offer extended precision in component location. Use of shaft, guide-rail or ACME threaded-rod along with a bearing surface to achieve linear motion also offers ease of mounting, where shaft or rail mounts are offered to precisely mount the necessary hardware. For the shafts requiring rotational motion, thrust bearings and radial ball bearings were used to accommodate loads in axial and radial directions as well as provide smooth, low friction rotational motion.

Custom Fabricated Parts. In order to better meet the design requirements, some components would be custom fabricated. Using 3D CAD solid modeling techniques, components were designed and analyzed using Finite Element Analysis (FEA) Mechanica package integrated into Pro-Engineer design software. Analysis performed was used to check the selection of material necessary to satisfy the desired limits of stress and deflection of components. After the design has been established, engineering drawings were created to manufacture the part using manual or Computer Numerically Controlled (CNC) machining. In some cases, components would also be manufactured through rapid prototyping techniques using ABS plastic.

Design and fabrication would commonly be performed for components not available for purchase that require a specific design to satisfy the design requirements. As an example, most fabricated components were subassembly mounting support plates, jaw plates, shaft mounts and brackets to name a few. For the purpose of prototype fabrication, most components requiring machining would be of 6061 alloy aluminum, or cold rolled steel to offer quick fabrication time.

Structural Support Components. To offer ease of component mounting and adjustment, the supporting architecture was developed using 80/20 Inc. industrial erector set. As a widely popular alternative to fabrication and design of automation machinery, 80/20 offers a wide selection of components that can be fastened together to accommodate most industrial applications without the need of expensive fabrication equipment.

T-slotted aluminum extrusions, joining brackets, different methods of fastening as well as dynamic modules are offered in a variety of shapes and sizes to match the desired design application (Figure 5.3). Offered in a number of metric and fractional forms, T-slot aluminum extrusion beams were used to create the necessary prototype frame work. Extrusions could be machined down to the length required and then connected using a

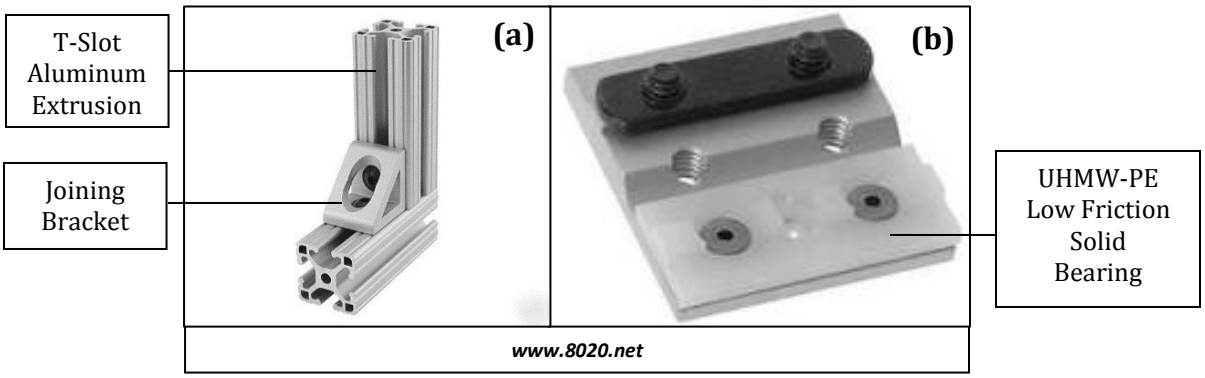

Figure 5.3 80/20 Components:
(a) T-Slot Extrusion and Joining Bracket; (b) Linear Bearing Bracket.

combination of a screw, T-nut and supporting brackets. For ease of adjustment, the T-nut is able to slide within the T-slot of the profile while also creating a sufficient fastening force when tightened with a screw and locked in place. In some cases, available high cycle UHMW-PE low friction linear solid bearings were also used to create the motion of necessary components or sub-assemblies of components. In such an example, the aluminum extrusions function as linear-guide rails (notion previously introduced in *Motion Hardware* section above) for the low friction linear bearings.

5.2 Prototype Architecture and Knot Interface

Using described design elements, stages of detail design were used to explore the most efficient prototype architecture and knot interface designs. From examination, it was found that the best quality of the knot was produced as all necessary actions were performed around stationary vertical position of the knot (Figure 5.4). Furthermore, to better meet the goal production rate of 30 knots/min, it was of interest to explore processing of multiple knots within each subsystem. Subsystem architecture and knot interface design needed to be established such that it was modular for all subsystems while offering ease of future integration with other subsystems, assembly and maintenance. Established notions for prototype architecture and knot interface are introduced below.

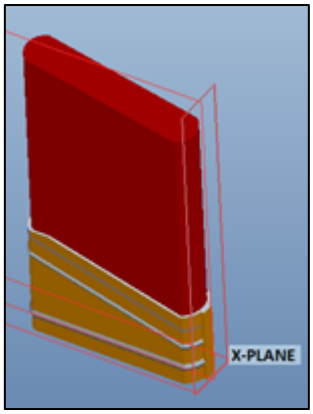

Figure 5.4 Vertical Position of the Knot: X-Plane Shows the Mounting Surface (Bottom of Ferrule).

Prototype Architecture. In order to achieve the desired criteria, multiple designs of prototype architecture and knot interface combinations were examined. Figure 5.5 shows the prototype architecture found to be most applicable with structural support and mounting provided through combination of 80/20 components in the form of "Inverse-T" design and a vertical mounting plate.

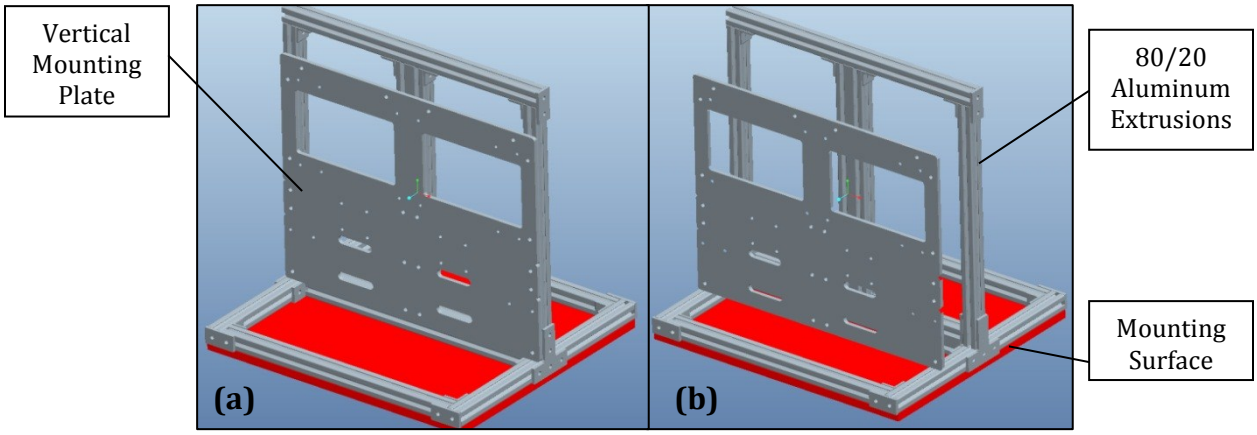

Figure 5.5 "Inverse-T" Subsystem Prototype Architecture: (a) Mounting Plate Fastened; (b) Mounting Plate Removed (for maintenance).

To create a simple yet rigid support structure, 80/20 1"x1" and 1"x2" T-slot aluminum extrusions were to be assembled through supporting 80/20 fasteners, brackets and plating to create "Inverse-T" prototype architecture. The shape of the structure provides two benefits, flat square base for mounting of subsystem at the bottom, where the red plate delineates a mounting surface (Figure 5.5), and vertical structural support for process performance. Using the support of the vertical extrusions, a vertical mounting plate was envisioned to house the necessary component subassemblies.

The vertical mounting plate was to be attached to the vertical beam extrusions through screw fasteners, where to offer ease of assembly and maintenance, the vertical mounting plate and attached components could be removed without disturbing the

mounting and alignment of the subsystem "Inverse-T" structure as shown in Figure 5.5(b). Concept of removable vertical mounting plate also offers modularity, where the architecture design can remain uniform for all subsystems with different assemblies on the mounting plate. Furthermore, Figure 5.5 demonstrates the prototype architecture that if considered as a unit could easily be adjusted when mounted or relocated if necessary. This can also help to better accommodate future integration other subsystems.

Knot Interface. Prototypes were envisioned to accommodate two knots at one time to better meet the required production rate while offering time for process performance and transfer of knots between subsystems. Although manual insertion of the knots would be necessary for prototype testing, prototype models were developed to mimic secure input, location and restraining of knots in a vertical alignment, performed later by the transfer subsystem. Assuming simultaneous input of a pair of knots, location of the knots would occur at the uniform height and position within the uniform architecture of all subsystems. Using manual input, two gripper subassemblies fastened to the vertical

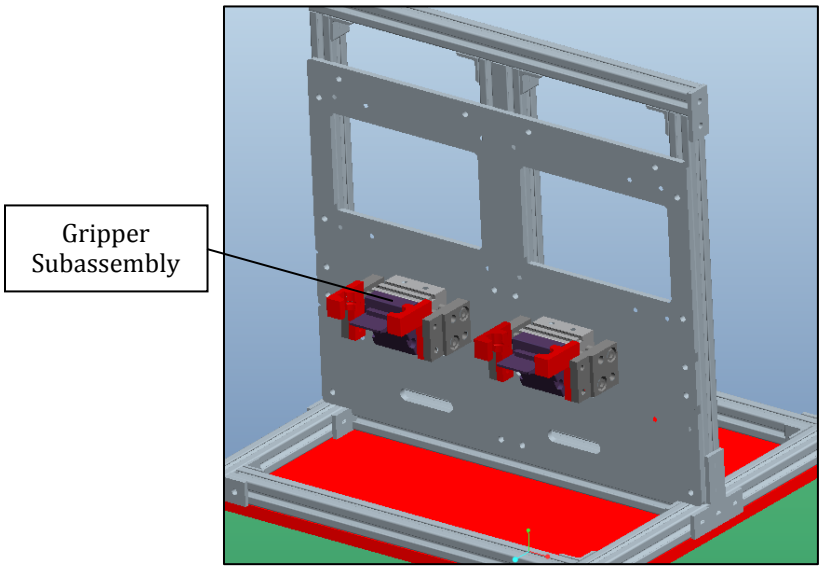

Figure 5.6 Subsystem Architercture and Knot Interface.

mounting plate (Figure 5.6), would simulate location and restraining of knots for process performance.

From manual calculations and supporting proof-of-concept model evaluation, the location of the knot was found to be critical for the process of angle trim forming. In order to create the desired quality of the angle trim form, the edge of the knot would have to be precisely aligned with the pivot axis of the filament gripper jaws. To achieve the desired precision, gripper subassembly (Figure 5.7) were designed to precisely align and hold the knot through a combination of a pneumatic gripper, alignment platform and gripper fingers. SMC parallel jaw pneumatic gripper was chosen to symmetrically grip the knot from both sides to hold it in place when closed. To simulate input, each knot would be placed on an alignment platform between the gripper fingers. Gripper piston bore was selected to provide the required holding force without deforming the ferrule excessively in compression while accommodating 1" to 3" widths of knots. If necessary, the holding force could also be regulated through the amount of pressure provided to the gripper.

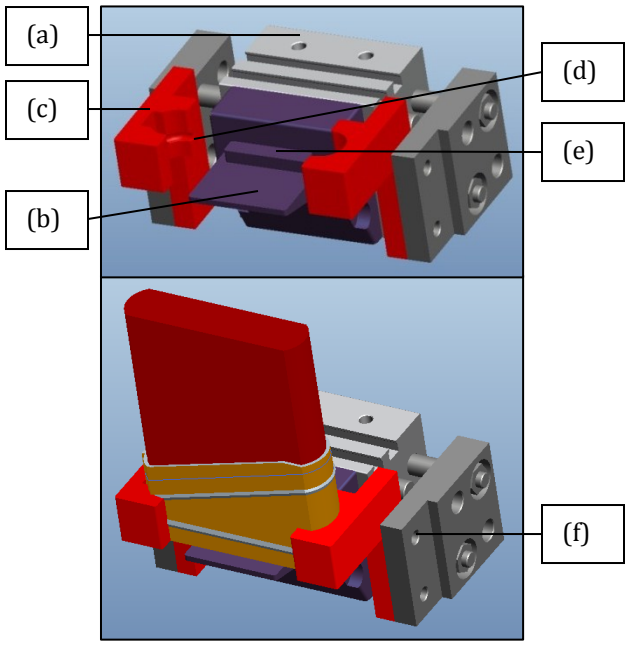

Figure 5.7 Gripper Subassembly
(Top) Gripper Subassembly;
(Bottom) Vertical Positioning of Knot;
(a) SMC Pneumatic Gripper;
(b) Alignment Platform;
(c) Gripper Finger;
(d) Bead Slot;
(e) Alignment Step;
(f) Mounting Thread.

Gripper fingers were designed so as to encompass radial portions on the sides of the knot, and include a slot at the bottom to hold the bottom bead of the knot (Figure 5.7). The alignment platform has a step in the rear, which, along with the grooves designed in the gripper fingers, helps to properly locate the knot with respect to the gripper and other subassemblies. Fastening of the gripper fingers as well as the alignment platform would occur through the provided mounting thread on the gripper jaws. For the testing of prototype models, gripper fingers and alignment platform were designed to accommodate oval shape ferrules of 2" width and thickness of 9/16" consisting of silver-tip nylon filaments and 2.5" width of 5/8" thickness consisting of nylon and white pig hair filament blend.

To hold the knot in the vertical position, gripper subassemblies would be mounted to a vertical mounting plate, spaced apart at a distance. Figure 5.6 demonstrates an example of a subsystem architecture and knot interface envisioned to be used uniformly between subsystems. Through further design refinement, the sizing of the extrusion structure and mounting plate would be established as well as the optimal distance between knots. In similar terms, location of knots with respect to the prototype architecture would need to be uniform, with defined X, Y and Z location for each knot. These aspects of refinement would need to be determined with consideration of the knot transfer subsystem, acceptable speed of transfer and spacing between subsystems.

The following detail design sections for angle trim forming and filaments straightening prototypes demonstrate the discussed knot architecture and knot interface design.

5.3 Angle Trim Forming Prototype Design

As demonstrated by the proof of concept model, the angle trim forming subsystem was required to perform multiple functions. Using the achieved prototype architecture and knot interface, for angle or flat trim forming to occur as per specification, (1) knots were to be received, positioned and held in a vertical position, (2) filaments were to be gripped and displaced to a specified length-out value, (3) flat trim: filaments were to be released; angle trim: filaments were to be rotated to create the 15° angle trim profile within ±1° tolerance, and (4) the knots were to be released from the subsystem for the next process. In order to achieve the functions described, physical prototype of angle trim forming was designed through Pro-Engineer solid modeling as seen in Figure 5.8.

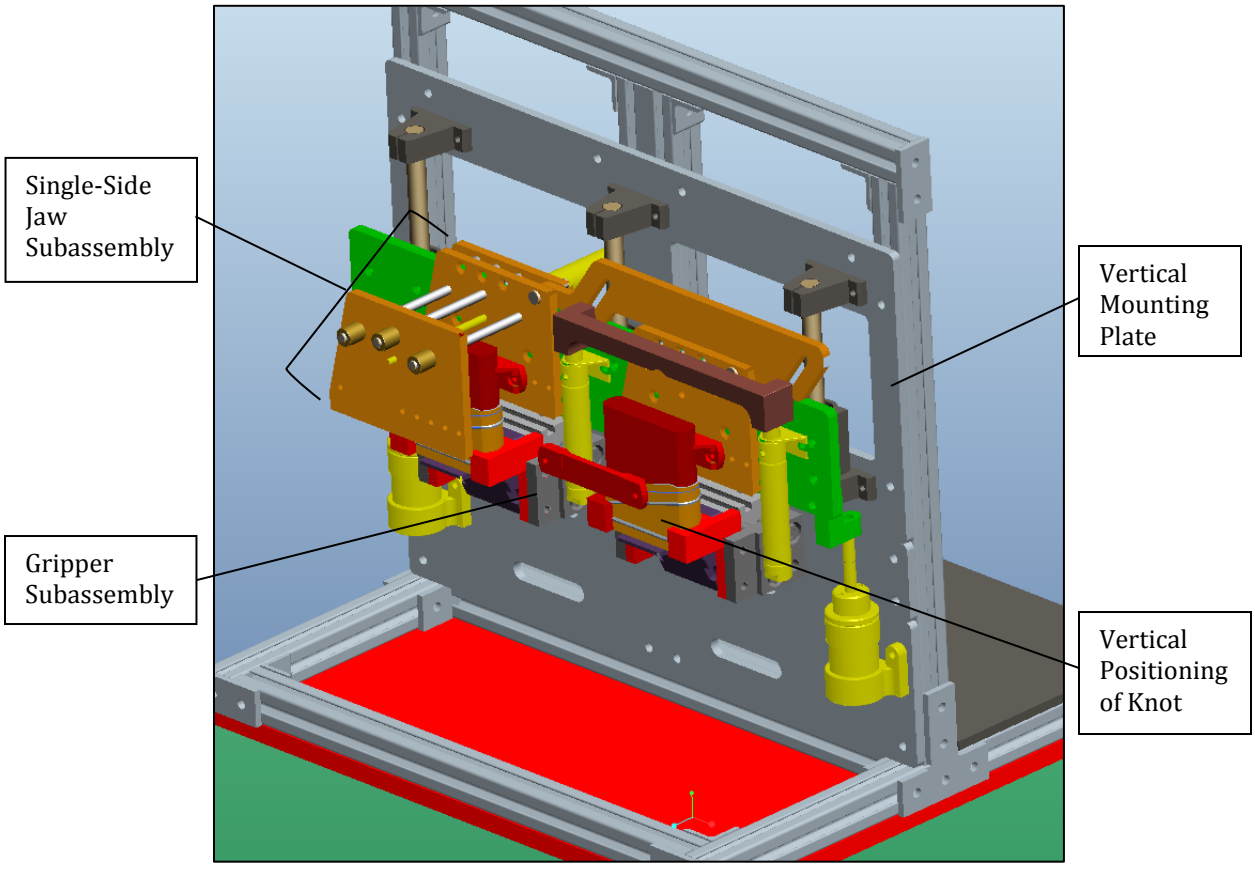

Figure 5.8 Angle & Flat Trim Forming Prototype (Pro-Engineer 3D Model).

In form shown, all required actions are performed around the knot held securely in a vertical position (Figure 5.8) using the previously described gripper subassemblies fastened to the vertical mounting plate. Location of the knots occurs such that they are placed between single-side actuated jaws, where one jaw is stationary and other is used to clamp the filaments. Knots are placed with sufficient space for gripping of filaments as well proper alignment of the ferrule edge with the pivot axis of the jaws. The jaws are a part of a filament-jaw-assembly (Figure 5.9), designed to create the previously described motions of vertical translation to length-out and 15° rotation of the filaments to create the angle trim form. To create the flat trim, the rotational motion could be disregarded.

Filament Jaw Assembly. The design structure of the assembly was established where a rotation plate was used to house two gripper jaw subassemblies to grip filaments and a bar-link subassembly to simultaneously rotate both gripper jaw subassemblies to 15°.

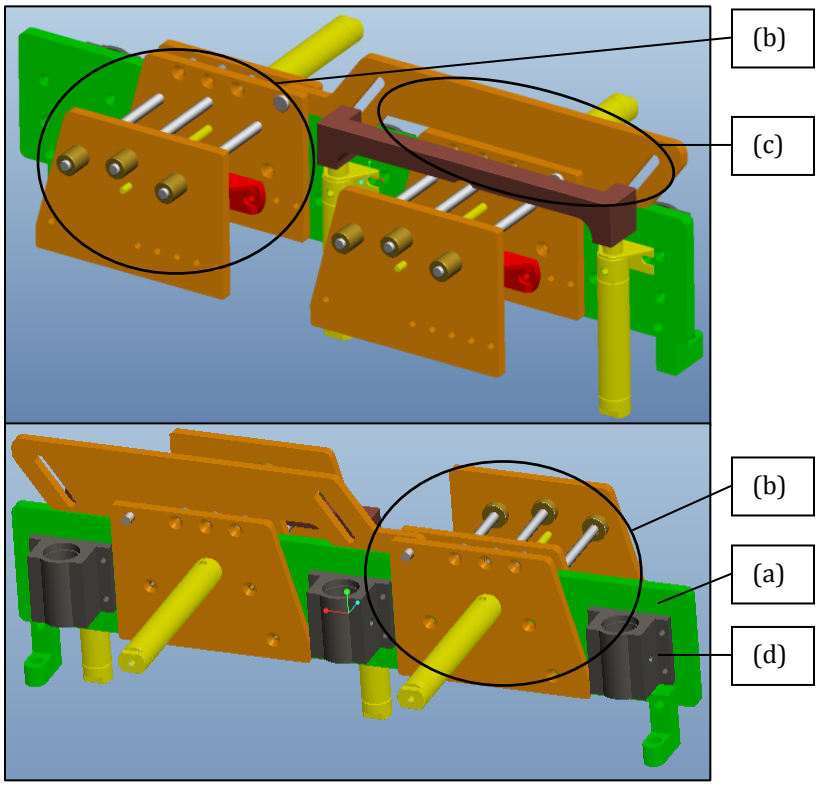

Figure 5.9 Filament Jaw Assembly:
(Top) Shown from Front;
(Bottom) Shown from Back;
(a) Rotation Plate;
(b) Jaw Subassembly;
(c) Bar Link Subassembly;
(d) Pillow Block Ball Bearing.

To create precise vertical travel of the filament jaw assembly, three pillow block bearings were mounted symmetrically to the rotation plate (Figure 5.9(d)). The bearings were made to match precision stainless steel shafts secured to the vertical mounting plate (Figure 5.10(a)). Vertical translation was achieved through pneumatic actuators (rated at 20 pounds of force) of regulated stroke length to allow for variability in length-out displacement value (Figure 5.10(b)). Selection of the bore of the actuator and its force rating was based on calculations of weight of the filament jaw assembly and the defined maximum force of filament displacement from design for parameter testing. A factor of 1.5 was also used to accommodate filament displacement for larger size knots if necessary.

Figure 5.10 shows the angle trim forming prototype without the filament jaw assembly, where the established prototype architecture is used to house the precision stainless steel shafts and pneumatic actuators. Design of the gripper-jaw and bar-link subassemblies are described below.

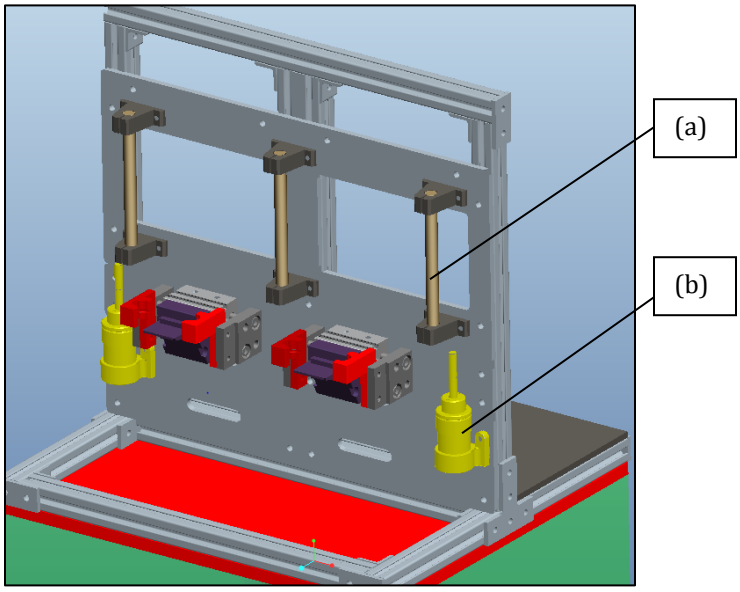

Figure 5.10 Angle Trim Forming Prototype:
(Filament Jaw Assembly Hidden)
(a) Precision Stainless Steel Shafts;
(b) Pneumatic Actuators with Variable Stroke (20 lbf Rating).

Gripper Jaw Subassembly. Gripper jaw subassemblies were designed to create a single-sided closing action necessary for gripping of filaments. Figure 5.11 shows a pair of such subassemblies, which were designed to be fully symmetrical in design to offer modularity (satisfaction of DFX). A single jaw subassembly is composed of three jaw plates. Jaw plates A and B act as mounting and support plates while plate-C (hidden for elaboration purposes) was used as a single acting dynamic jaw to compress filament bundles. In order to create an efficient method of filament bundle gripping without filament loss or damage, plates C and B were equipped with filament gripper plates described further. Closing action of the jaw plate-C was to be performed through a pneumatic actuator, which was nose-mounted on the back of the jaw plate-A as shown in Figure 5.11(Bottom). To close the jaw, the actuator rod pulls jaw plate-C against jaw plate-B. To guide the motion of the jaw plate-C, precision ground stainless steel shafts were mounted to plate-B, allowing precise and low friction motion of the jaw plates through PTFE oil impregnated bronze sleeve bearings press-fit into jaw plat-C.

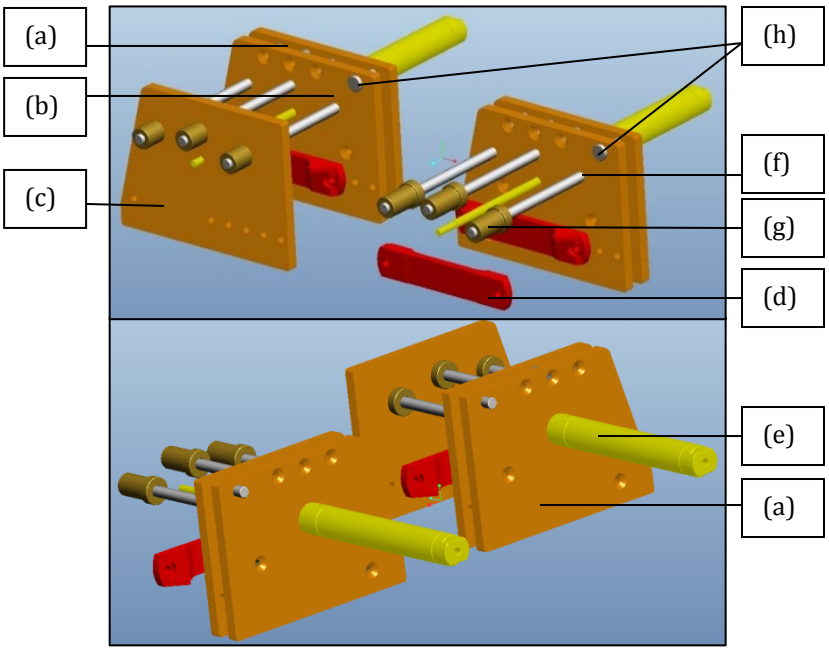

Figure 5.11 Pair of Gripper Jaw Subassemblies:
(Top) Shown from Front;
(Bottom) Shown from Back;
(a) Jaw Plate-A;
(b) Jaw Plate-B;
(c) Jaw Plate-C;
(d) Filament Gripper Plate;
(e) Nose Mounted Pneumatic Actuator;
(f) Precision Stainless Steel Shaft;
(g) Bronze Sleeve Bearing;
(h) Clevis-pin Connection Pivot Points.

The actuator was selected to provide an adequate force range which can be adjusted through the pressure provided. With varying filament types, pressure could be regulated to assure that clamping force was adequate to provide the necessary friction force to grip filaments without causing damage to the filaments. Shown in Figure 5.11 are also pivot points achieved through a clearance-hole and clevis-pin combination for connection to the bar-link subassembly described further.

Figure 5.12 (Top) shows an established filament gripper plate design mounted on jaw plates B and C to grip filament bundles. Many different concepts were examined with combinations of geometries and materials to properly grip filaments. Resulting form of a gripper plate was designed to encompass the filament bundle with sufficient gripping surface, preventing filament flaring under compression through side-walls (Figure 5.12(b)) and offer ease of mounting and replacement through symmetrical, recessed mounting holes. Additional considerations were symmetry of the plate design to cut down on manufacturing cost (satisfaction of DFX) and time, where a duplicate of a single plate can generate a pair of gripper plates to symmetrically grip the filament bundle.

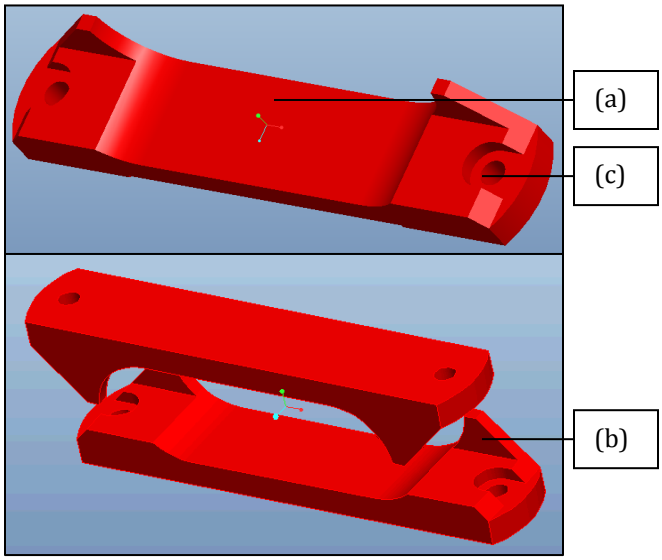

Figure 5.12 Filament Gripper Plates:
(Top) Single Gripper Plate;
(Bottom) Pair of Gripper Plates
(Method of Gripping Filament Bundle);
(a) Contact Gripping Surface;
(b) Side-walls (To Prevent Flaring);
(c) Recessed Fastener Mounting Holes.

Figure 5.12 (Bottom), demonstrates the proposed method of filament bundle gripping, where the plates are offset to fully encompass the filament bundle. For a different type of knot, different filament gripper plates would be installed by the operator in the future to accommodate different widths of knots through quick release fasteners. To allow ease of gripper plate replacement, jaw plates C and B would include pre-established mounting holes for all sizes of gripper plates.

Connection of the gripper jaw subassemblies to the rotation plate was performed to allow rotational motion. Figure 5.13 demonstrates the method of connection, where jaw plates B and C are hidden for one of the subassemblies. When assembled, the jaw plates are restricted to the plane of the rotation plate, with only freedom to rotate the required 15°. Mounting to the rotational plate occurs through a radial pivot bearing, to precisely identify the rotation vertex, and a series of precision collars to guide the motion of the gripper jaw subassembly. Fastening of the pivot bearing occurs through a press-fit connection, where the mounting hole and bearing tolerances are calculated to create an interference-fit.

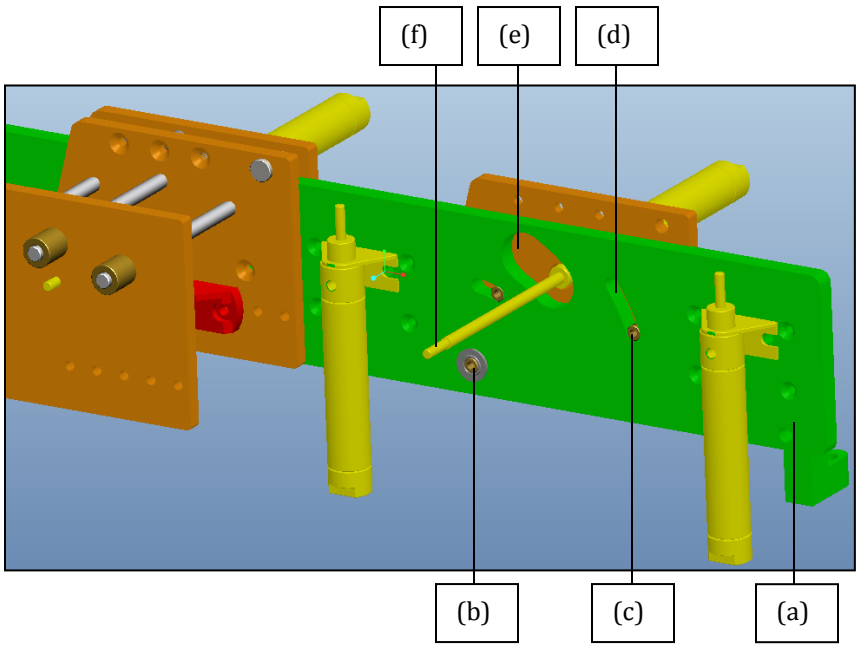

Figure 5.13 Mounting of Jaw Subassemblies:
(a) Rotation Plate;
(b) Radial Pivot Bearing;
(c) Precision Collars;
(d) Radial Motion Grooves;
(e) Radial Clearance Grooves;
(f) Actuator Shaft.

Radial motion grooves inside the main rotation plate were designed precisely to allow sliding motion of the precision cut collars for the prescribed 15°. Again, tolerances of the precision collars and motion grooves were calculated to allow smooth, precise radial motion. Jaw plate A and B sandwich the collars and the pivot bearing, locked in place through a set of screw fasteners. Additional clearance radial grooves were also added to allow clearance for the shaft of the actuator used to actuate the motion of jaw plate-C.

Bar Link Subassembly. In order to perform simultaneous rotation of jaw mechanisms, a bar link subassembly was used. Shown in Figure 5.14(Left), the bar link subassembly is composed of a lever plate, a C-bar and two pneumatic actuators. To perform simultaneous rotation, the gripper jaw subassemblies were connected together using a lever plate, resembling a 3-bar link mechanism with four pivot points (Figure 5.14 (Right)). To create a more compact solution as well ease of maintenance, the lever plate was made to fit between top parts of plate A and B, with two pivot connections

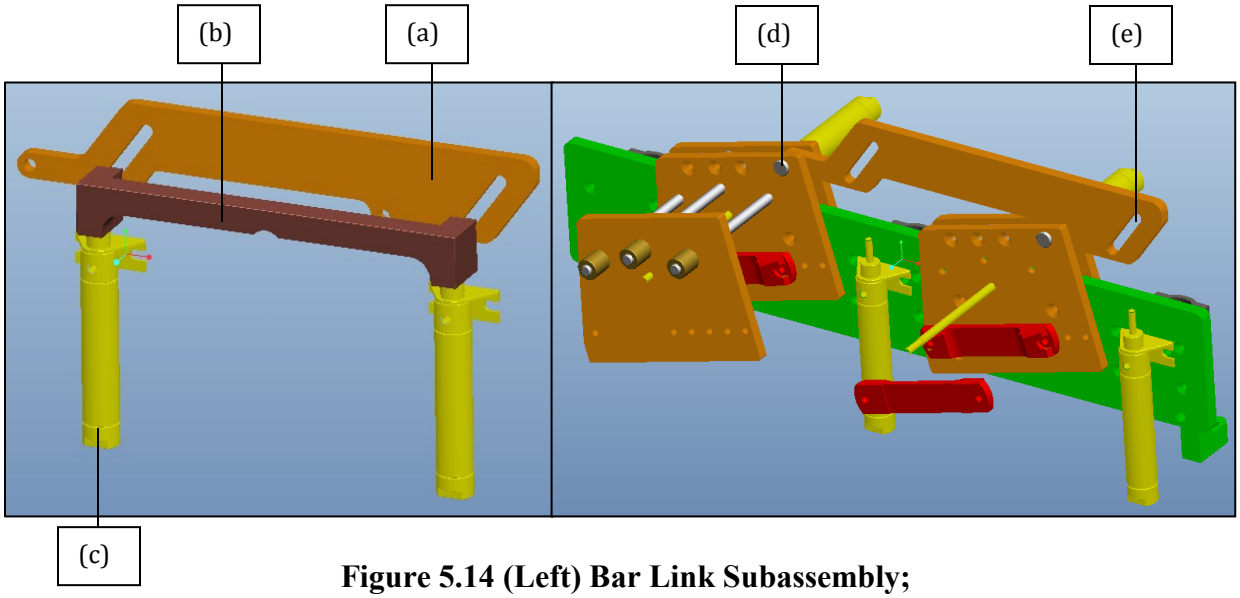

Figure 5.14 (Left) Bar Link Subassembly;
(Right) Rotation using Bar Link Subassembly (C-bar hidden);
(a) Lever Plate; (b) C-bar; (c) Pneumatic Actuator; (d) Clevis-pin; (e) Motion Grooves.

occurring through a clearance-hole and clevis-pin combination as introduced previously. Additional two pivot points were radial pivot bearings connecting the jaw subassemblies to the rotation plate.

Due to space limitations and to minimize weight of the filament jaw assembly, the rotational motion was achieved by converting the vertical actuation motion of two pneumatic actuators to rotational motion. Close tolerance motion grooves (Figure 5.14(e)) in the level plate were designed to convert the vertical actuator stroke of 1.5" to exact rotational motion of 15^{o} to create an angular profile at the edge of the filaments within specified tolerance.

With actuators securely mounted to the rotation plate, connecting C-bar (Figure 5.14(b)) was used to provide a connection between tips of actuators to create symmetrical vertical motion for precision shoulder bolts used to slide within the grooves. Upon actuation, sliding action of precision shoulder bolts displace the lever plate in an arching motion, causing the required 15^{o} rotational motion of the gripper jaw subassemblies as shown in Figure 5.14(Right).

Final Form. Figure 5.15 below shows the design of the angle trim forming prototype in its finalized form with established prototype architecture, knot interface and filament jaw assembly. Figure 5.15(a) demonstrates the benefit of modular architecture design and satisfaction of design for maintenance and assembly criteria, where a vertical mounting plate is removed with the associated components (for maintenance purposes). The back view in Figure 5.15(c) also demonstrates a location of a control plate which would be used to store pneumatic and electronic control components, making it easily available for adjustment and maintenance. With all the necessary control and pneumatic systems stored

on the control plate, it is expected that each subsystem as a unit can be easily re-positioned or removed without complications.

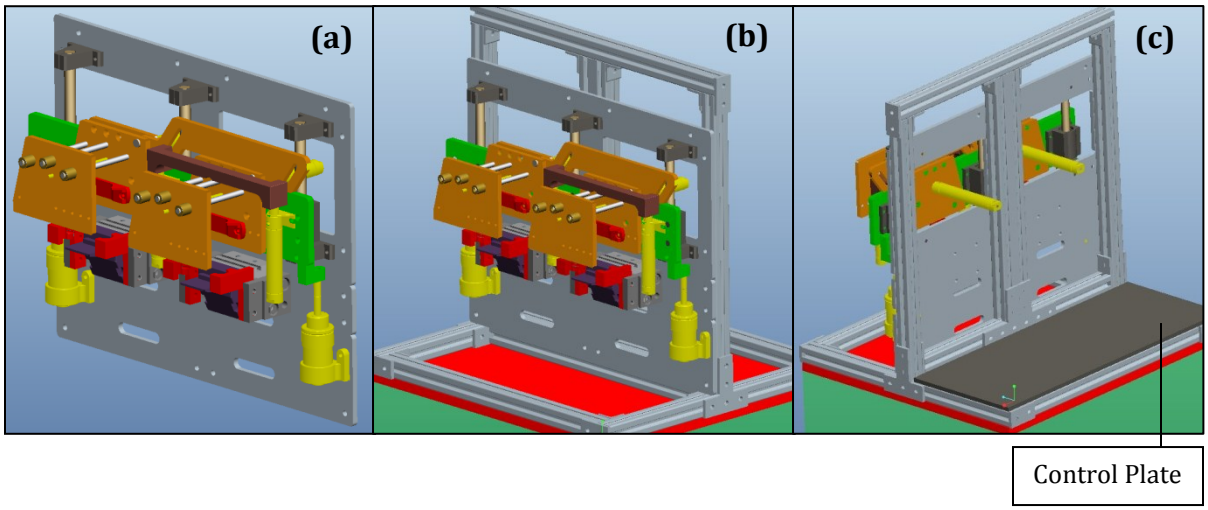

Figure 5.15 Final Form of Angle Trim Forming Prototype:
(a) Vertical Mounting Plate Removed; (b) Front View; (c) Back View.

5.4 Filament Straightening Prototype Design

Likewise, for filament straightening and combing to occur as per specification, (1) knots were to be received after angle trim forming, positioned and held in a vertical position, (2) filament alignment was to be straightened to a vertical alignment within the specified tolerance of ±3°, (3) filaments were to be combed out to loosen tangled filaments, and (4) the knots were to be released from the system for the next process. Figure 5.16 below shows the physical prototype of filament straightening designed to achieve the functions described.

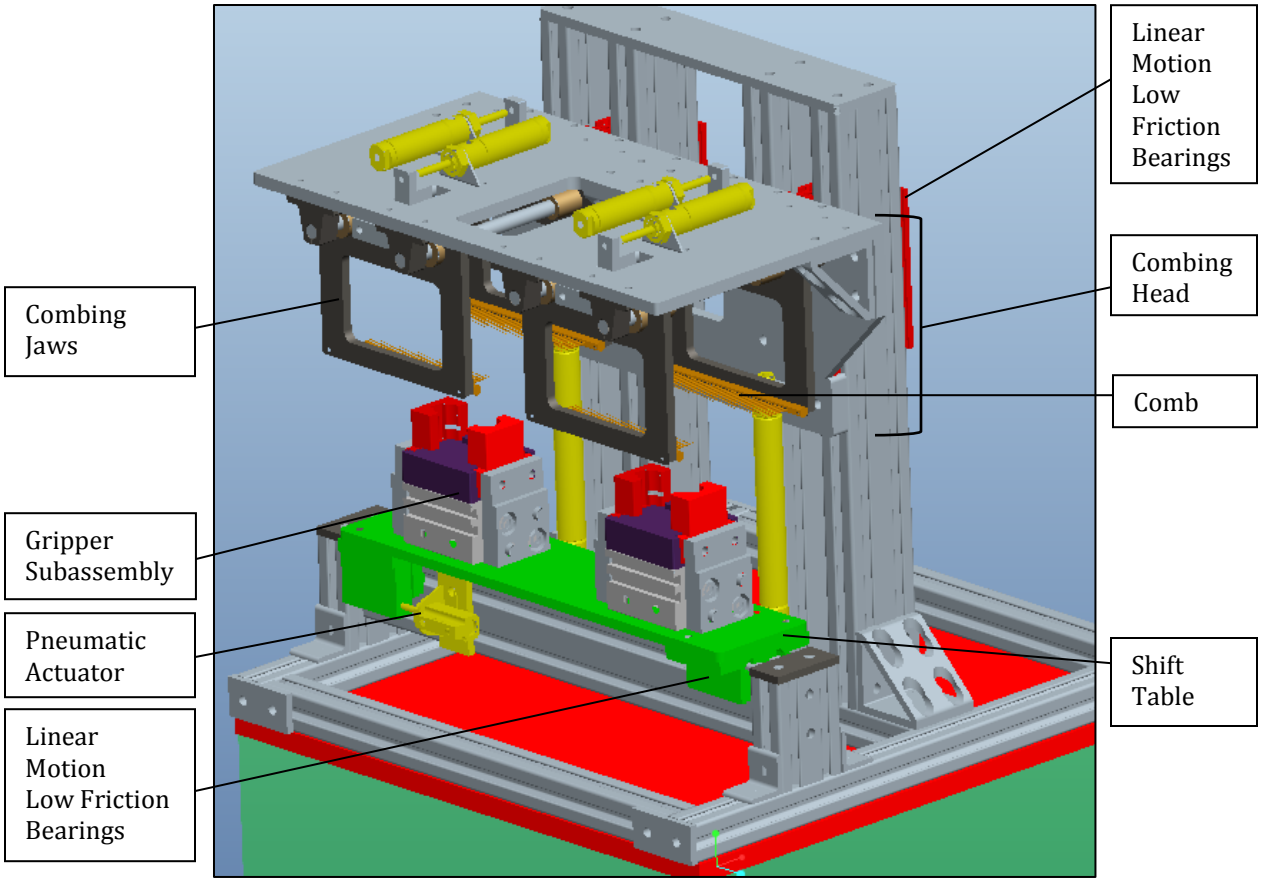

Figure 5.16 Filament Straightening and Combing Prototype (Pro-Engineer 3D Model).

As established before, all required actions are performed around the knot held securely in a vertical position. Previously described gripper subassemblies (Figure 5.16) perform location and holding of the knot in a vertical alignment to mimic input by the transfer subsystem. Location of the knot within each gripper subassembly is established to match the location of knots within angle trim forming prototype relative to the uniform architecture of both prototypes. This would aid in the future subsystem integration with a knot transfer subsystem responsible for transfer and location of knots for each process. Upon input, the knot is located between the parallel-motion combing jaws containing combs (Figure 5.16). To straighten the alignment of filaments, combs are inserted into the

sides of the knot symmetrically at a specified depth and height and then horizontally translated for a specified distance to tilt filaments into place. Following, the filaments are combed using a vertical motion of the combs. The jaws containing combs are a part of a combing head assembly designed to perform motions just described.

Figure 5.16, demonstrates the prototype architecture design previously discussed in a form of "Inverse-T" architecture. However, it is important to note that in order to meet the functional requirements for testing in a shorter time and lower cost a vertical mounting plate was not used. Instead, vertical beam extrusions served the function of linear-motion guide rails with a combination of 80/20 low friction linear bearings to achieve vertical motion of the combing head. Furthermore, the function of tilting of filaments into alignment was performed through a relative motion between the knot and comb. In order to avoid high manufacturing cost for miniature linear bearings to create motion of small combs within the combing jaws, the knot is translated relative to a stationary comb instead. The shift table subassembly used to translate the knots is described below.

Shift Table Subassembly. Translation of the knot is performed through a shift table (Figure 5.17(a) shown below) which houses the gripper subassemblies. Figure 5.17 shows the modifications of the prototype architecture and knot interface performed for the purpose of this prototype. Associated alignment platform and gripper fingers
(Figure 5.17(c, d)) were redesigned to properly locate the center of the knot with the center of the combing jaws. Again, translational motion of the shift table is achieved through a combination of aluminum extrusions (Figure 5.17(g)) and low friction bearings (Figure 5.17(f)). To achieve the alignment of filaments within the desired tolerance,

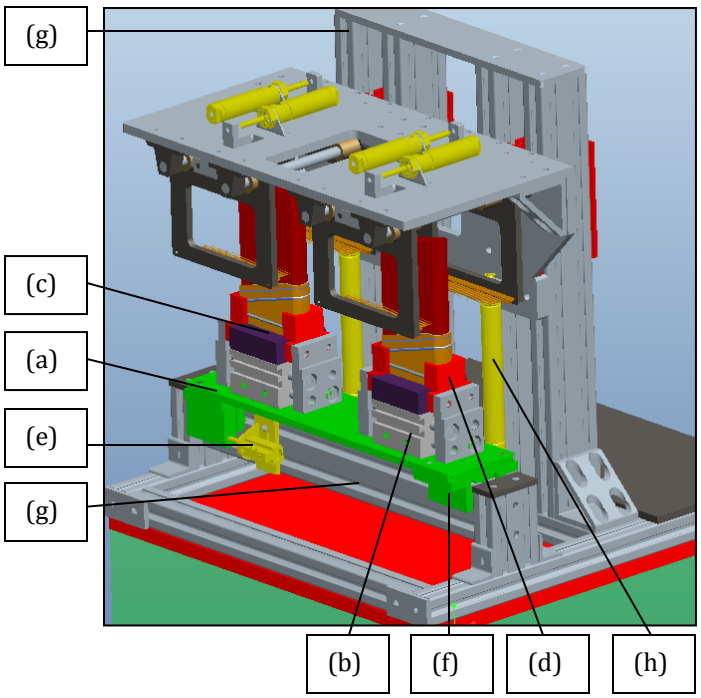

Figure 5.17 Modified Prototype Architecture and Knot Interface:
(a) Shift Table;
(b) Vertical Alignment of Gripper Subassemblies;
(c) Modified Alignment Platform;
(d) Modified Gripper Fingers;
(e) Adjustable Stroke Pneumatic Actuator;
(f) Linear Motion Low Friction Bearings;
(g) Extrusions as Linear Motion Guide-rails;
(h) Pneumatic Actuators for Combing Head Vertical Motion.

horizontal translation distance is regulated through an adjustable stoke pneumatic actuator (Figure 5.17(e)).

Symmetrical insertion of combs at a prescribed depth and height, as well as vertical combing motion is performed by a combing head assembly. Design of the combing head assembly is described below.

Combing Head Assembly. As it was established, the shift table subassembly is used to perform the function of translating knots relative a pair of stationary combs to tilt filaments into place. Additional functions of inserting combs at a prescribed depth and height, as well as combing, are performed by the combing head assembly. After knot input, combing jaws are closed symmetrically to insert the combs, the knot is translated to tilt filaments into place (function of the shift table), and the filaments are combed through vertical motion of the combing head.

Figure 5.18(i) shows the design of the combing head assembly. The combing head design was established where two combing jaw subassemblies (Figure 5.18(i-a)) are housed in an L-frame (Figure 5.18(i-b)) with supporting pneumatic and linear motion components. Low friction linear bearings (Figure 5.18(i-c)) mounted to the L-frame are used to create precise vertical motion of the combing head on vertical extrusions of

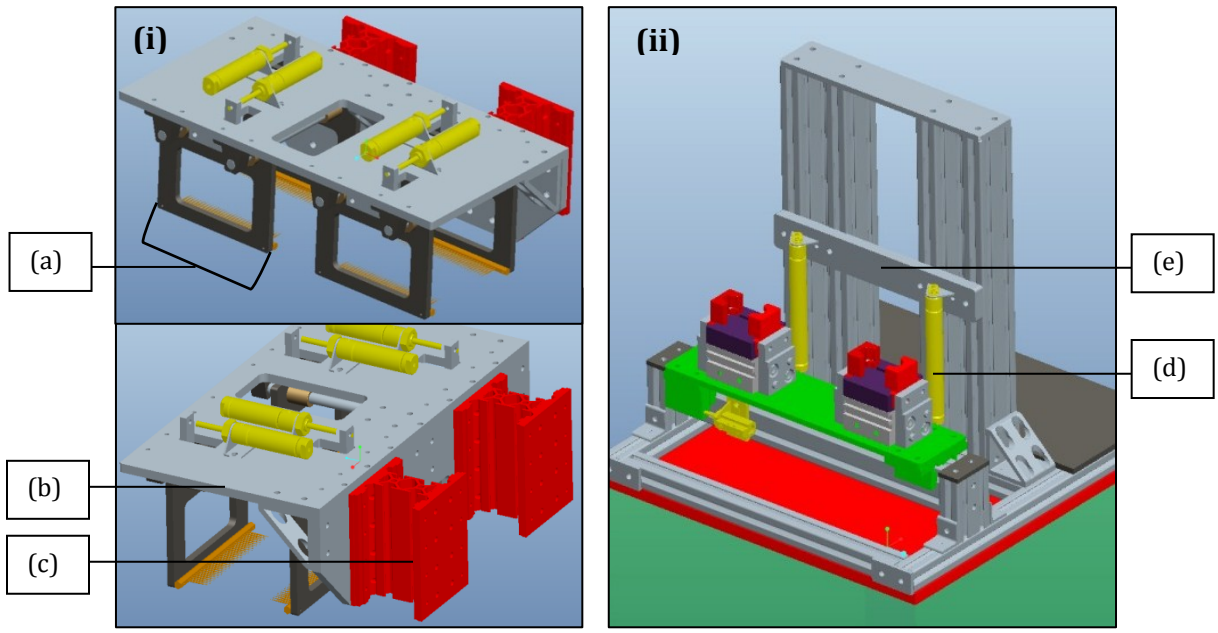

Figure 5.18 (i) Combing Head Assembly: (Top) Front View, Bottom (Back View); (ii) Filament Straightening Prototype Architecture (Combing Head Assembly Hidden). (a) Combing Jaw Subassembly; (b) L-frame; (c) Linear Bearings; (d) Pneumatic Actuator; (e) Vertical Adjustment Plate.

the prototype architecture shown in Figure 5.18(ii). To perform vertical translation, pneumatic actuators of constant stroke were selected to accommodate the required height of combing (Figure 5.18(ii-d)). The actuators are mounted on a vertical adjustment plate (Figure 5.18(ii-e)), which can be regulated in vertical position relative to the knot. With a solid connection of actuator rods to the combing head, height of comb insertion into the knot is regulated by the vertical position of the vertical adjustment plate. Likewise to

satisfy DFX, the combing head can be easily taken off the vertical extrusion for maintenance much like shown in Figure 5.18(i,ii).

L-frame and Combing Jaw Subassemblies. The combing jaw subassemblies were designed to create symmetrical motion of comb jaws such that combs are inserted on both sides of the knot. Figure 5.19(Top) shows a pair of such subassemblies which are uniform in design. Each combing jaw subassembly is composed of two jaw plates containing combs, bronze sleeve bearings, a pair of precision stainless steel shafts and associated shaft mounts, and two lever tabs. Combs, designed to be modular, were modified from existing hand combs to mount to the combing jaw plates.

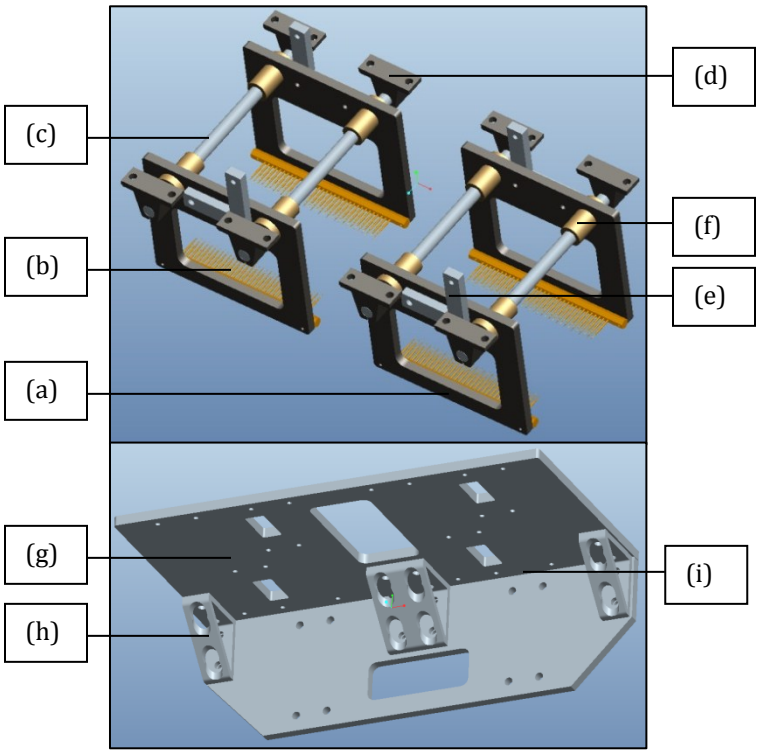

Figure 5.19
(Top) Pair of Combing Jaw Subassemblies;
(Bottom) L-frame.
(a) Jaw Plate;
(b) Comb;
(c) Precision Shaft;
(d) Shaft Mount;
(e) Lever Tab;
(f) Bronze Sleeve Bearing;
(g) L-frame Top Plate;
(h) 80/20 Gusset;
(i) Connecting Seam.

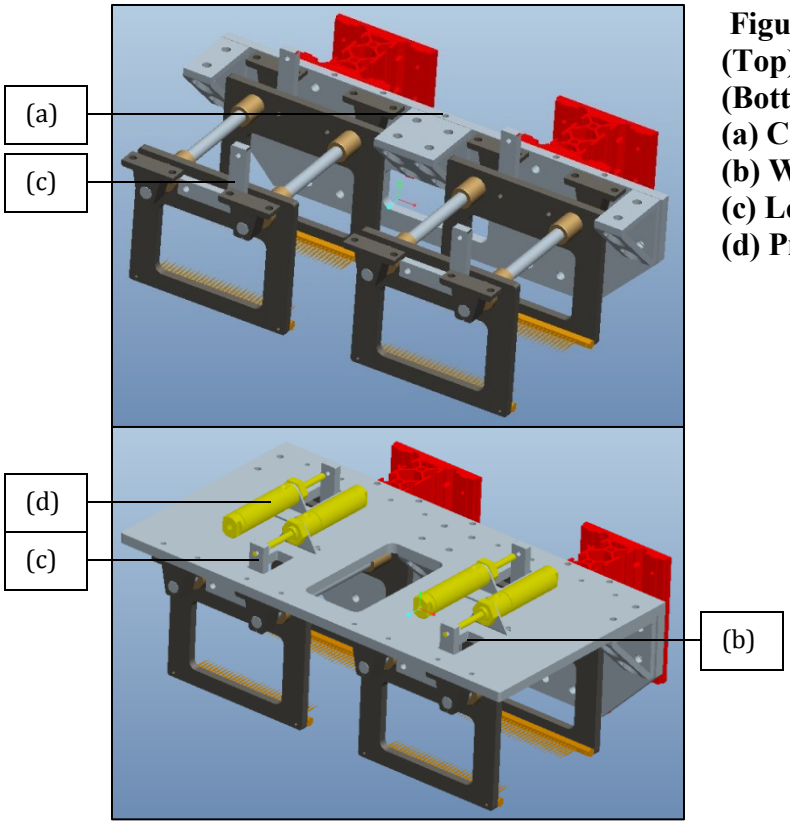

Figure 5.20 Combing Head Assembly:
(Top) Shown with Top Plate Hidden;
(Bottom) Assembled Combing Head;
(a) Connecting Seem;
(b) Window;
(c) Lever Tab;
(d) Pneumatic Actuator.

The plates are also uniform in design, where to offer precise and reliable method of motion, PTFE bronze oil impregnated sleeve bearings (Figure 5.19) were press-fit with the plates to slide on precision shafts. Mounting of the subassemblies occurs through shaft mounts onto the top plate of the L-frame (Figure 5.19(g)). Figure 5.20(Top) demonstrates the resulting assembly with top plate hidden. The L-frame design has been formed to offer ease of maintenance, where two plates are joined through fasteners at a connecting seam (Figure 5.19(i) and Figure 5.20(a)) as well as gussets provided by 80/20 (Figure 5.19(h)). If desired, the top plate of the L-frame can be removed with combing jaw subassemblies and pneumatics intact. Within the top plate are windows (Figure 5.20(b)), designed to accept the sliding motion of a lever-tab (Figure 5.20(c)) connecting the jaw plates to pneumatic actuators (Figure 5.20(d)). One pneumatic actuator is dedicated to actuate the motion of a

single combing jaw. In order to select the desired depth of knot insertion, adjustments can be made at the connection of the actuator rod to the lever-tab.

Final Form. Figure 5.21 shows the filament straightening prototype in its finalized form. As noted previously, the prototype architecture and knot interface have been modified, however the functional requirements of the prototype as well as the knot interface requirements were met. As highlighted in the description, the filament straightening prototype is good example of a modular design with satisfaction of DFX criteria. With already modular prototype architecture, ease of maintenance and assembly is offered through simplicity of component removal such as the combing head assembly. For example, the combing head offers the option of separating the plates of the L-frame with combing jaw subassemblies and associated pneumatics intact for ease of access to perform maintenance. The modular design of the combing jaw subassembly is a good example of satisfaction of DFX, with uniform design for multiple components such as jaw plates and combs as well as minimized types of fasteners used. As introduced previously, Figure 5.21 also shows the control plate used to house pneumatic and electronic control components to better aid in system maintenance.

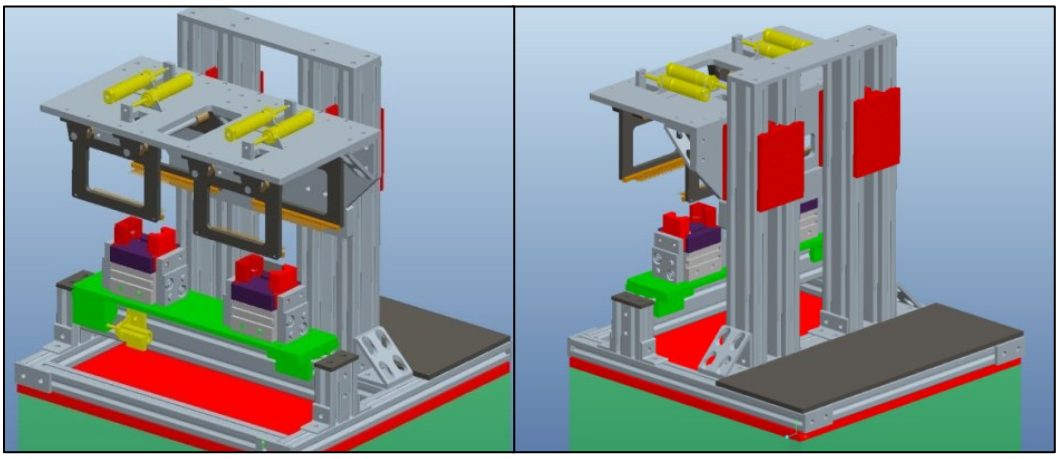

Figure 5.21 Final Form of Filament Straightening Prototype.

Chapter 6: Prototype Fabrication and Testing

From the stages of design performed through solid modeling, prototype models were fabricated and tested in order to evaluate the performance of established concepts for angle trim forming and filament straightening. This chapter further introduces the process of physical prototype model fabrication and testing accomplished.

6.1 Prototype Fabrication

This section describes the fabrication process in the order of which it was performed, where the bill of materials was compiled first, engineering drawings, assembly drawings and pneumatic diagrams were created second and the process of assembly was performed last.

Bill of Materials (BOM). In order to assist in fabrication, a bill of materials was compiled, which is a list of components necessary for prototype assembly and important information pertinent to such components. As described previously, most design elements would require direct ordering from a supplier, ordering and alteration or custom fabrication. The bill of materials helps to keep track of such relevant and other useful information. Appendix-D demonstrates an example of a bill of materials formed, where individual lists were formed for subassemblies and then further divided into categories of required hardware components, pneumatic components and electronic components. To better communicate the required information, each BOM would support required reference information for assembly, description of the component and ordering information. In order to properly reference the component among assembly documentation, each component was given an item number, part number and specified engineering drawing number (if alteration or fabrication was necessary). Additional description was also provided to assist

in assembly, where the use of the component, design element component type and additional comments were provided if necessary. To complete the BOM, required ordering information was also specified such as ordering quantity, supplier part number and associated prices. Compiled BOM was then used to procure the necessary components for alteration and assembly.

Engineering Drawings. To manufacture or alter required components, engineering drawings were created. In order to properly communicate the required component design, engineering drawings were used to specify critical manufacturing information to meet the DFX and other criteria. Appendix-E demonstrates an example of engineering drawings, which communicate instances of critical information such as dimension tolerances to achieve sliding motion or interference type fit for joining of components. Additional details, commonly specify type of fastener thread to be created and at what thread engagement. If flat type fastener is to be used, the radius and angle of countersink was also to be specified. Common specifications were also established for clearance type and blind holes. To complete the drawing, drawing number, part name, material type and necessary quantity for fabrication were also specified. In some cases, comments were added to reference to other components and their tolerances.

Assembly Drawings and Pneumatic Diagrams. Manufactured components were used to assemble the required prototype. Steps of assembly were documented using assembly drawings. Appendix-F shows an assembly drawing which helps to visually communicate the steps of required assembly along with specified part number. To create ease of assembly, design through solid modeling has been performed to meet DFA criteria, resulting in building of subassemblies as modules to be later incorporated into larger

assemblies. Appendix-G also shows and example of a pneumatic diagram, also documented to display pneumatic system design, component type and pressure routing design. Appendices D through G demonstrate an example of bill of materials, engineering drawings, engineering drawings as well as assembly and pneumatic diagrams needed to manufacture a single filament jaw subassembly seen as a part of the angle trim forming subsystem. The documentation shown in these appendices is an example of documentation provided to the sponsor of this research upon project completion.

Prototype Assembly. Documentation above was used to guide the fabrication process of full scale prototype models. As already introduced, components were ordered, ordered and altered or custom fabricated as per requirement of bill of materials and engineering drawings. Resulting components were then assembled using the provided assembly and pneumatic diagrams. Furthermore, for the purpose of further testing, prototype models were made to interface with control modules to simulate automated method of knot processing. Figure 6.1 on the following page shows the physical prototype models resulting from the fabrication process described here. However, for the sake of brevity the general fabrication process is introduced where further examples shown pertain to the prototype of angle trim forming. As it can be seen in Figure 6.1, the fabricated models demonstrate all the design aspects just described in the chapter of embodiment and detail design.

Prototype Architecture and Gripper Interface. To fabricate the supporting "Inverse-T" structure of the prototype models seen in Figure 6.1, 8020 aluminum extrusions (Figure 6.1(a)) were cut down using manual machining to establish the lengths required. Individual sections of the lengths where then joined using a combination of 8020 aluminum

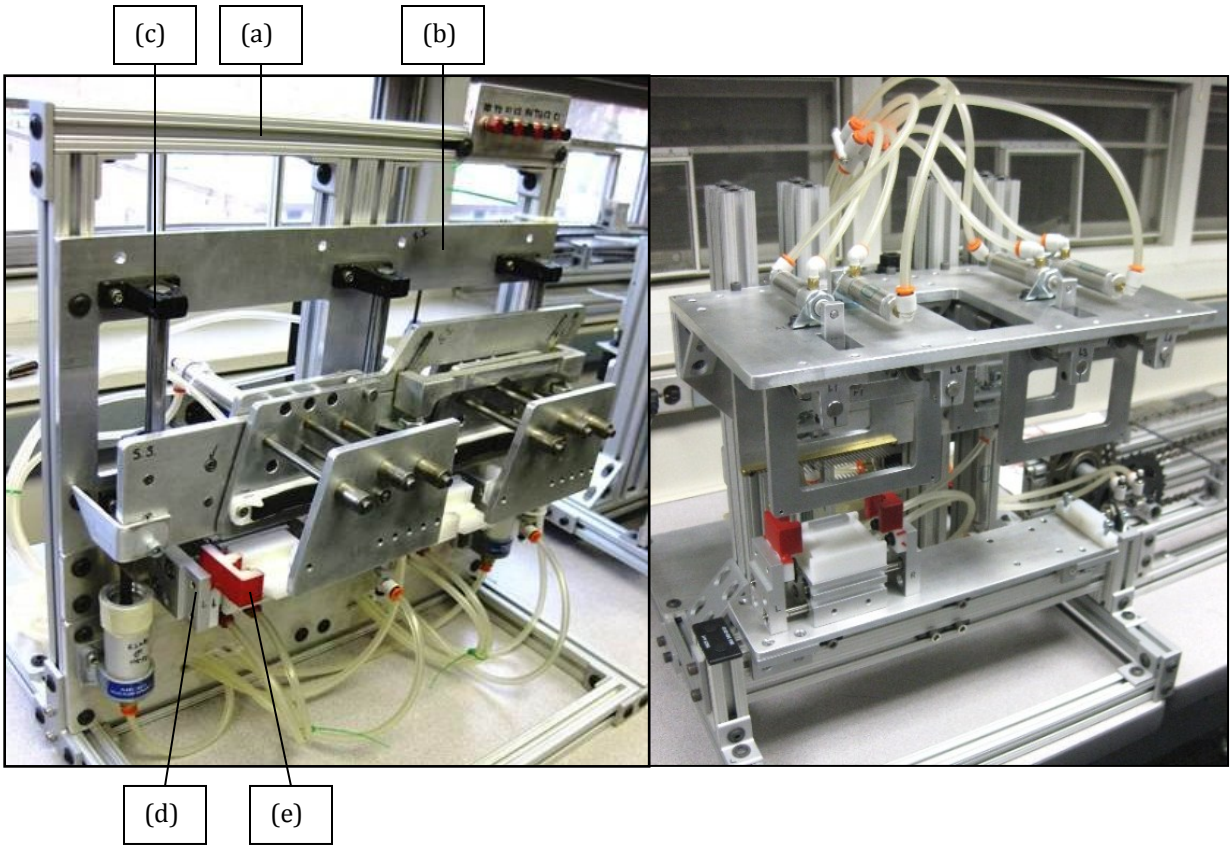

Figure 6.1 Fabricated Physical Prototype Models:
(Left) Angle Trim Forming Prototype;
(Right) Filament Straightening Prototype;
(a) 8020 Aluminum Extrusion; (b) Vertical Mounting Plate; (c) Precision Shafts;
(d) SMC Pneumatic Gripper; (e) Gripper Fingers.

brackets, T-Nut and screw methods of fastening. A vertical mounting plate (Figure 6.1(b)) was CNC machined as per specifications of the design, to offer mounting of precision shafts (Figure 6.1(c)) for vertical motion of filament jaw assembly; and then attached to the vertical beams of the supporting aluminum extrusion structure.

In order to simulate input and holding of knots performed by a transfer subsystem, gripper sub-assemblies were assembled. SMC Pneumatic Grippers (Figure 6.1(d)) were ordered which would provide holding of knots for knot processing. In order to properly interface between the SMC gripper jaws, gripper fingers (Figure 6.1(e)) were fabricated to match the specification of the knots later used for testing. Figure 6.2(Left) below shows an

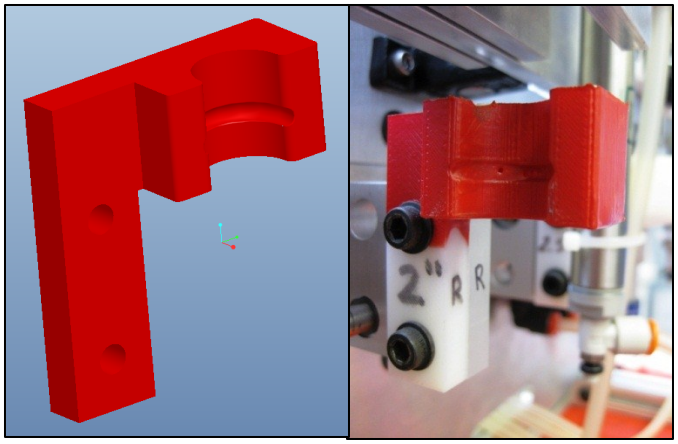

Figure 6.2 Gripper Finger Design:
(Left) Shown as Modeled through Pro-Engineer 3D CAD;
(Right) Shown as Fabricated though ABS Plastic Rapid Prototyping and Vinyl Coated.

example of a gripper finger as modeled in Pro-Engineer and Figure 6.2(Right) shows the gripper finger after it has been fabricated through ABS plastic rapid prototyping and then coated with vinyl to promote friction. Figure 6.3 shows an example of a complete gripper subassembly which includes a pair of gripper fingers, an alignment platform, also rapid prototyped, and the pneumatic gripper itself.

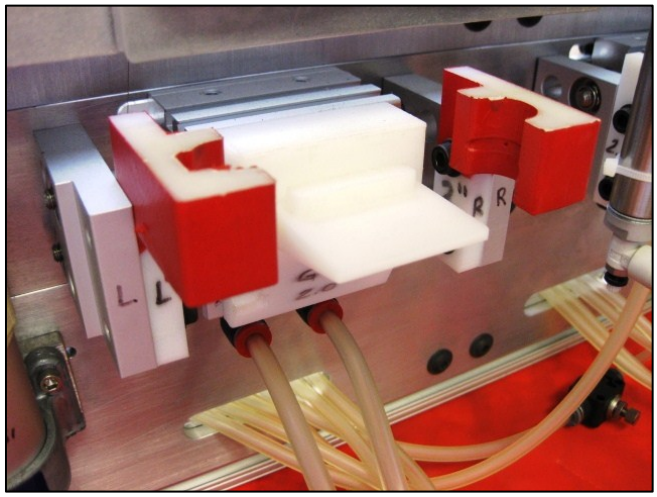

Figure 6.3 Complete Gripper Subassembly.

Building of SubAssemblies. Using individually ordered or manufactured components, subassemblies were assembled next and then integrated into assemblies. Figure 6.4 shows the bristle jaw assembly in its assembled form. Like most assemblies, a major component such as the rotation plate would house other components and subassemblies. For example, to complete this assembly, subassemblies of filament gripper jaws would be put together first (example of documental used for manufacture and assembly seen in Appendices D through G) and then integrated into the major component of rotational plate. The rotation plate is an example of a component manufactured through

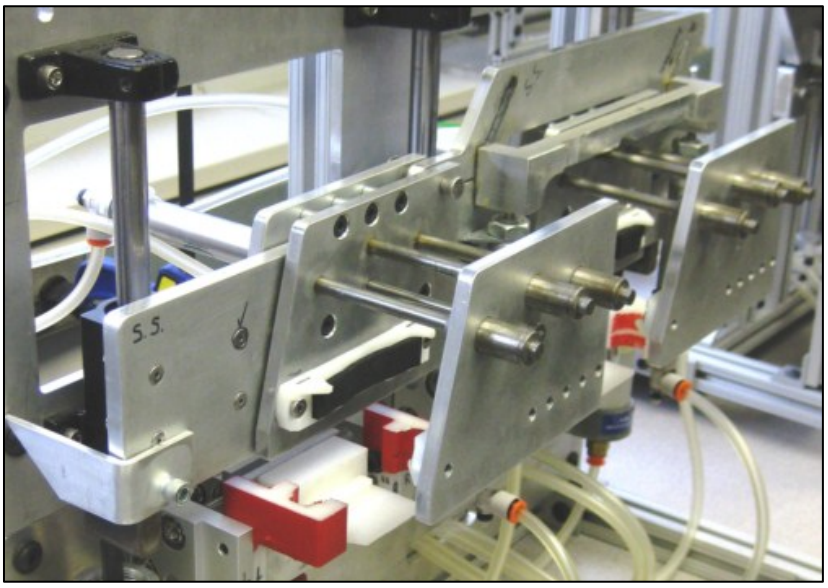

Figure 6.4 Filament Jaw Assembly (Shown as Fabricated).

CNC machining to achieve complex geometry for the radial motion grooves and their tight tolerances for smooth motion of collars. Further assembly would occur around the rotational plate, as other components and subassemblies would be attached through specified methods of fastening and interference fit connections. Such components would include motion hardware such as radial bearings, pillow block bearings, as well as

pneumatic hardware. To complete the fabrication for the angle trim forming prototype, filament jaw assembly would be placed on precision shafts and mounted to the vertical mounting plate (Figure 6.1). Likewise, gripper subassemblies would be attached to the mounting plate to properly locate the knot with respect to the filament jaws. Mounting of pneumatic actuators to the vertical mounting plate, responsible for vertical actuation of the filament jaw assembly would follow as a finishing touch.

Preparation and Fine-Tuning. To prepare the prototype for testing, associated pneumatic and electronic control routing was performed. To help fine-tune the motion of pneumatic components, flow control valves were installed. Through additional pneumatic hardware such as Y-Unions, manifolds and electronic control valves, pneumatic routing was established to allow control of pneumatic components (Figure 6.5), some in synchronous motion. As a part of the stages of prototype testing in a semi-automated fashion, electronic control programming was also explored through LabView-Lego NXT programmable modules and electronic-controlled solenoid pneumatic valves.

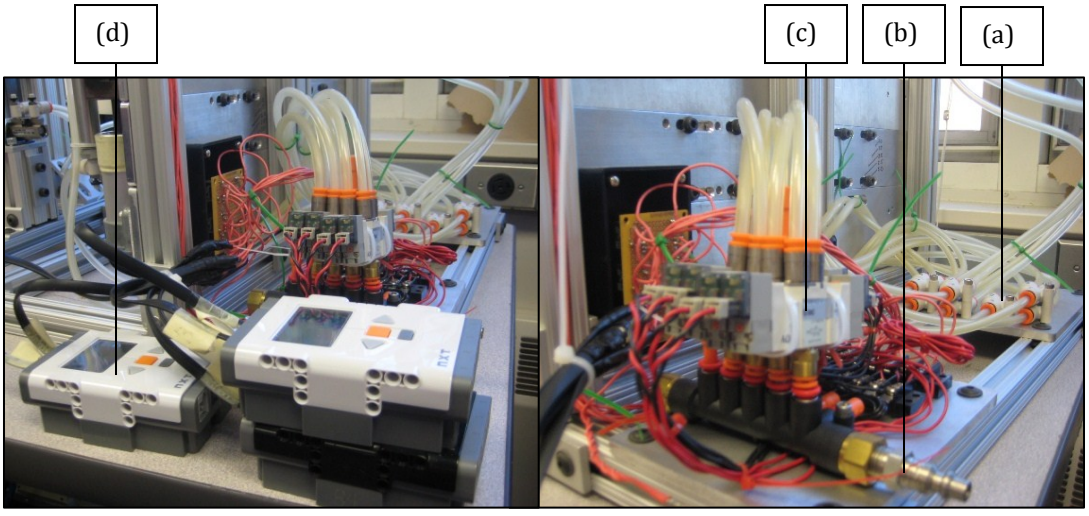

Figure 6.5 Pneumatic Components and Electronic Control Setup:
(a) Y-Union Fittings and Pneumatic Routing; (b) Pneumatic Manifold;
(c) Electronic-controlled Solenoid Pneumatic Valves; (d) LabView-Lego NXT Module.

Figure 6.5 shows a pneumatic manifold which distributes the air flow at the desired pressure to electronically controlled solenoid valves. Using LabView software, the NXT modules were programmed to simulate semi-automated processing, where through a voltage pulse, the electronic solenoid valves would distribute airflow in a sequence of required operation. In the form shown, the knots would be input manually as the rest of the process would be automated.

6.2 Prototype Testing

To evaluate the performance of angle trim forming and filament straightening prototypes, testing was performed with two distinct knot recipes. Knots selected were of oval shape ferrule and angle trim type, with a nominal size of 2" width and thickness of 9/16" consisting of silver-tip nylon filaments and 2.5" width of 5/8" thickness consisting of nylon and white pig hair natural filament blend as shown in Figure 6.6.

Figure 6.6 Knot Samples Tested:
(Left) 2" Knot with Silver Tip Nylon Synthetic Filaments;
(Right) 2.5" Knot with Nylon and White Pig Hair Natural Filament Blend.

Ten knot samples of each kind were received from sponsor as assembled by the factory. The samples were then settled in the laboratory using a vibration table and then tested in the order of knot processing, where the samples were treated to create the angel trim form and then straighten filaments. For the sake of comparison, for each process, five knots were processed by hand, and another five using the semi-automated prototypes. Sections below describe the sequence of testing and associated results for each process.

6.2.1 Testing of Angle Trim Forming Prototype

For each size brush, five knot samples were shaped by hand, using a gauging block, as currently performed by manual operation; and five were shaped using the prototype developed. All knots were weighed prior to gauging and reviewed for uniform-filament distribution. Figure 6.7 shows additional views of the full scale prototype. On the following page, Figure 6.8 demonstrates the sequence of angle trim prototype operation during testing.

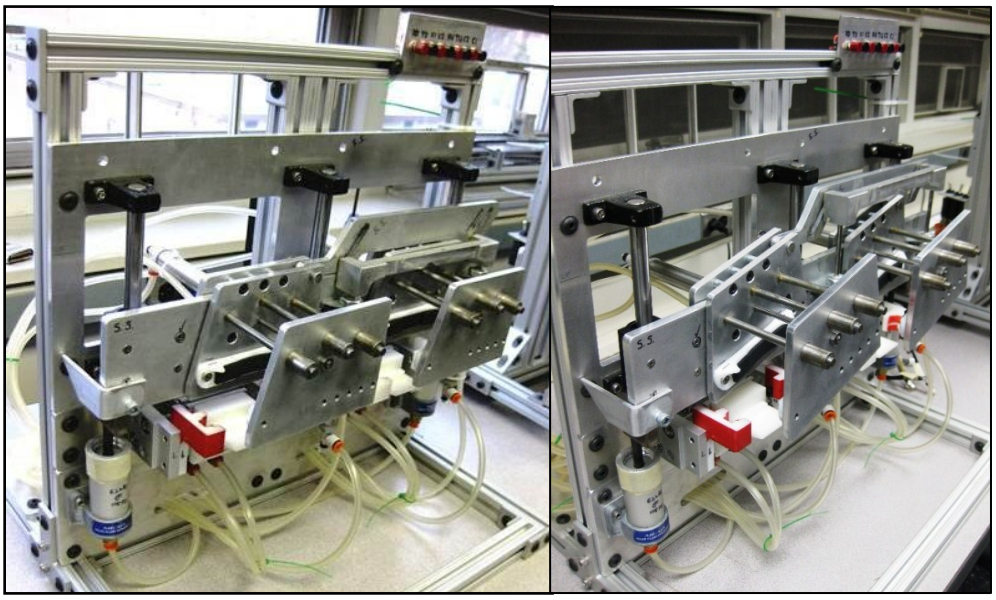

Figure 6.7 Angle Trim Forming Fabricated Physical Prototype.

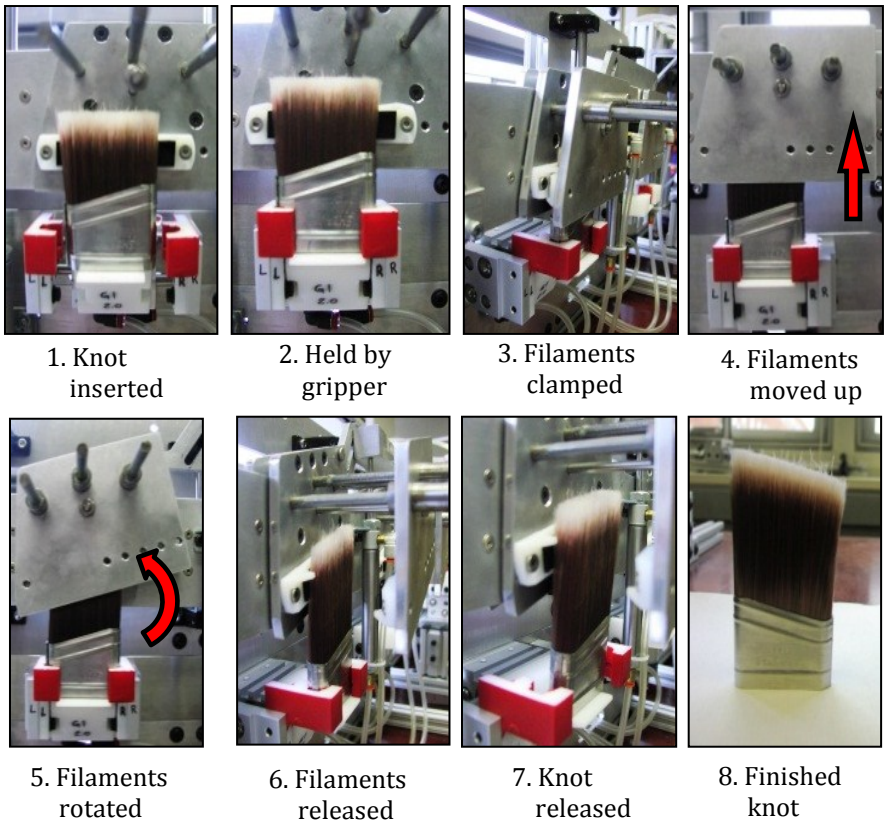

Figure 6.8 Angle Trim Forming Prototype 1-8: Sequence of Operation.

To simulate semi-automated processing, each knot was manually placed on an alignment platform between the gripper fingers Figure 6.8 (step 1). The NXT modules were turned on to run the designed program as rest of the process, Figure 6.8 (step 2- step 7) was performed though automated actuation of pneumatic components.

Results from Testing. Seven knot characteristics were measured or evaluated for each knot to asses resulting quality. Characteristics assessed were, (1) precision of the 15° trim (±1° tolerance), (2) quality of angle trim linearity, (3) quality of knot in terms of dragback present, (4) stability of plug inside the knot, (5) total knot integrity, (6) precision of length-out value, and (7) time of process. Through visual assessment, the precision of the

15° trim, quality of angle trim linearity, amount of dragback present, stability of plug and total knot integrity were recorded using a rank scale of 0 to 5 with 5 being the best. A score of 5 thus indicates no dragback present in the knot or a perfect angular distribution of the filament. Time to gauge the knot was recorded using a stop watch in seconds, while the length out value was measured using a digital caliper in inches. Length-out value was measured in three places of the knot and then averaged and recorded for each run. The precision of the angle trim was determined by using a template manufactured through computer aided design to resemble the knot specifications as seen in Figure 6.9(a). To compare the angle trim distribution, the knot was centered on the template with the angle profile trim aligned against the edge as pictured in Figure 6.9(b). With a very tight tolerance of ±1°, knots not following the template were expected to be outside of the tolerance range (commonly receiving a rank less then 4 – or not acceptable). Displayed result in Figure 6.9(b) demonstrates an example of a knot assessed visually receiving a ranking of 5 for both angle trim precision and angle trim linearity.

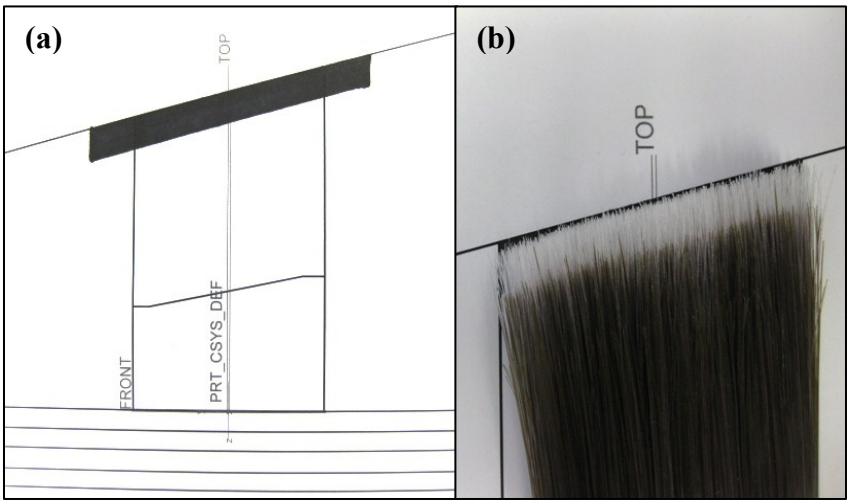

Figure 6.9 (a) Angle Trim Profile Template;
(b) Example of Angle Trim Profile Visual Assessment:
Precision of 15° Angle Trim – Rank 5;
Angle Trim Linearity – Rank 5.

Results from the test (Tables 6.1-6.4) show that the prototype's performance was significantly better than that of the hand-operated process for both types of brushes. Six of the seven test criteria showed a significant improvement for the 2" inch knot ($p << 0.05$), and four of the seven for a 2.5" knot ($p << 0.05$). Both types of brushes received a mean rank of 5 for precision of the angle trim using the prototype with no dragback present, while hand assembly of the 2" knot received a $\mu = 2.60$; 95% CI: {1.92,3.28}, and 2.5" knot received a $\mu = 1.80$; 95% CI: {1.24, 2.35} with presence of dragback.

Table 6.1 2" Silver Tip Nylon Synthetic Knot;
Angle Trim Forming Criteria Results.

	Hand Operation		Prototype Operation			
	Mean	95% CI	Mean	95% CI	Comparison P-Value	$\mu_2 - \mu_1$
15° Angle Trim (±1°) (Rank)	3.40	{2.72,4.08}	5	{5,5}	0.0079	1.60
Angle Trim Linearity (Rank)	2.80	{1.76,3.84}	5	{5,5}	0.0079	2.20
Dragback (Rank)	2.60	{1.92,3.28}	5	{5,5}	0.0079	2.40
Plug Stability (Rank)	5.00	{5,5}	5	{5,5}	1	0
Knot Integrity (Rank)	3.00	{1.48,4.52}	5	{5,5}	0.0079	2.00
Time (sec)	3.52	{3.35,3.70}	2.02	{1.87,2.18}	0.0079	-1.5

Table 6.2 2.5" White Pig Hair & Natural Filament Blend Knot;
Angle Trim Forming Criteria Results.

	Hand Operation		Prototype Operation			
	Mean	95% CI	Mean	95% CI	Comparison P-Value	$\mu_2 - \mu_1$
15° Angle Trim (±1°) (Rank)	3.20	{2.16,4.24}	5	{5,5}	0.0079	1.80
Angle Trim Linearity (Rank)	3.20	{2.16,4.24}	5	{5,5}	0.0079	1.80
Dragback (Rank)	1.80	{1.24,2.35}	5	{5,5}	0.0079	3.20
Plug Stability (Rank)	5.00	{5,5}	5	{5,5}	1	0
Knot Integrity (Rank)	5.00	{5,5}	5	{5,5}	1	0
Time (sec)	3.65	{3.50,3.79}	2.03	{1.93,2.14}	0.0079	-1.62

A significant improvement in time to form the knot was also evident as both types of knots received a μ = 2.02; 95% CI: {1.87,2.18} and a μ = 2.03; 95% CI: {1.93,2.14} for the time required by the prototype for 2" and 2.5" inch knot respectively. Time required by hand operation were recorded to be μ = 3.52; 95% CI: {3.35,3.70} and μ = 3.65; 95% CI: {3.50, 3.79} for 2" and 2.5" inch knot respectively. Angle trim forming operation through the prototype showed a mean rank of 5 for angle trim linearity, plug stability and knot integrity for both types of knots over hand operation.

As expected, precision of the length-out value also showed a statistically different performance ($p << 0.05$) between the two methods of operation for both types of knots. The comparison is displayed below in Tables 6.3 and 6.4 along with the specification value of length-out used for testing. No statistical difference was observed in plug stability for both types of knots due with an equal rank of 5 for hand and prototype angle trim forming. Both types of knots preserved the stability of the plugs without any visible sign of plug displacement or falling out.

Table 6.3 2" Silver Tip Nylon Synthetic Knot;
Length-Out Value Results.

		Hand Operation		Prototype Operation			
	Specification (in)	Mean	95% CI	Mean	95% CI	Comparison P-Value	$\mu_2 - \mu_1$
Length-Out Value (in)	2.85	2.79	{2.69,2.89}	2.86	{2.84,2.86}	0.0079	-0.07

Table 6.4 2.5" White Pig Hair & Natural Filament Blend Knot;
Length-Out Value Results.

		Hand Operation		Prototype Operation			
	Specification (in)	Mean	95% CI	Mean	95% CI	Comparison P-Value	$\mu_2 - \mu_1$
Length-Out Value (in)	2.6875	2.60	{2.57,2.62}	2.66	{2.64,2.68}	0.0079	-0.27

Although the plug stability did not differ between hand and prototype operation, a sign of prototype system reliability needs to be highlighted; where the stability of the plug was conserved without any support of the gauging block from the bottom during displacement of filaments to create the length-out specification. Furthermore, the action of filament rotation to create the angle trim form also did not falter the stability of the plug.

Example of angle trim formed knots can be seen in Figure 6.10, where images (a) and (b) display knots formed by hand, and (c) and (d) display knots formed by prototype. A significant difference in quality can be seen between the hand and prototype methods of operation, especially in the precision and linearity of the angle trim.

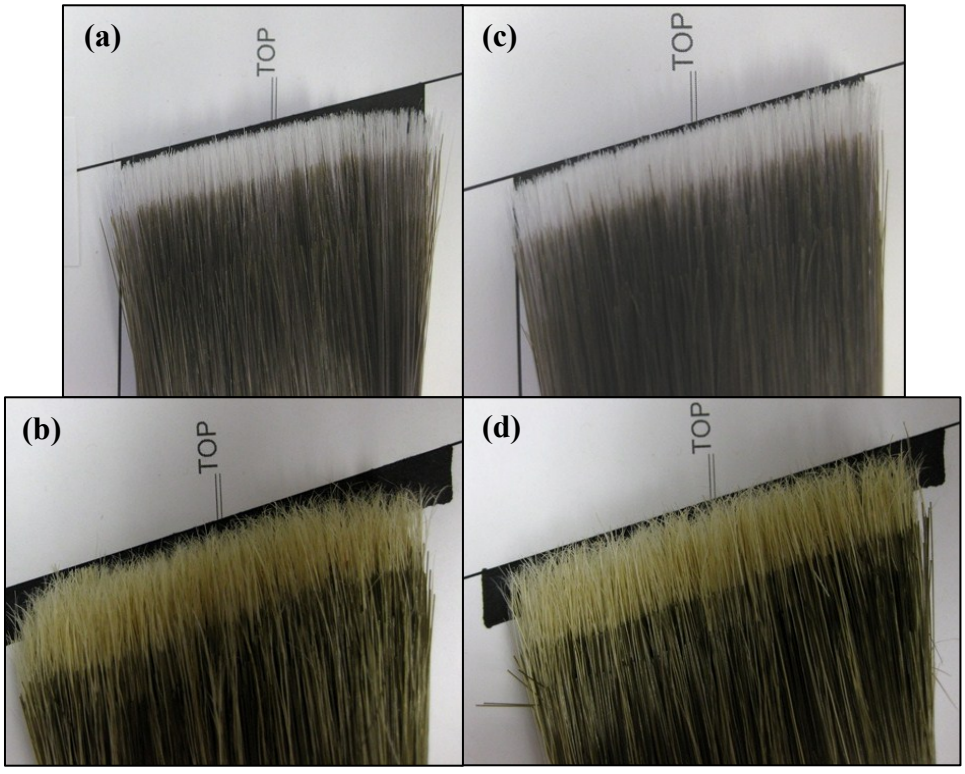

Figure 6.10 Angle Trim Formed Knots:
(a) 2" Silver Tip Synthetic-Hand Operation;
(b) 2.5" White Pig Hair-Hand Operation;
(c) 2" Silver Tip Synthetic-Prototype Operation;
(d) 2.5" White Pig Hair-Prototype Operation.

Figure 6.10(a) displays a knot formed by hand, receiving a rank of 2 for knot integrity, 3 for angle trim linearity and 4 for trim angle precision. Common signs of loss of knot integrity can be seen in filaments on the right side of the knot, deviating from the overall filament bundle. Due to dragback, loss of sharpness or linearity of filament angle trim tip can also be noted, with rounded behavior of angle trim. Figures 6.10(c, d) display knots formed by the prototype, receiving a rank of 5 for knot integrity, trim linearity and trim angle precision with sings of filament bundle stability, sharpness of angle trim linearity and precision of the 15° tip achieved within tolerance.

6.2.2 Testing of Filament Straightening Prototype

Knot samples used to evaluate the performance of the angle trim forming process were further used to support the evaluation of the filament straightening process. Already formed through hand and prototype operation for the angle trim, knots were further processed for straightening of filament alignment. Figure 6.11 shows the physical prototype in its fabricated form.

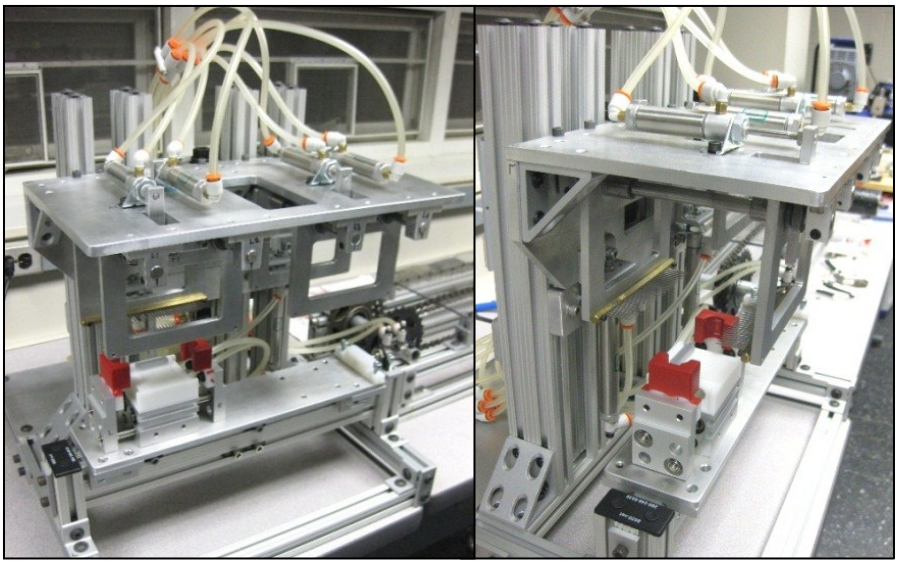

Figure 6.11 Filament Straightening and Combing Fabricated Physical Prototype.

For each size knot, five knot samples were straightened and combed by hand using a hand comb and five were straightened and combed using the prototype. For operation of knot prototype, each knot was manually placed on an alignment platform between the combing jaws Figure 6.12(step 1) as rest of the process Figure 6.12(step 2- step 7) was performed though automated actuation of pneumatic components.

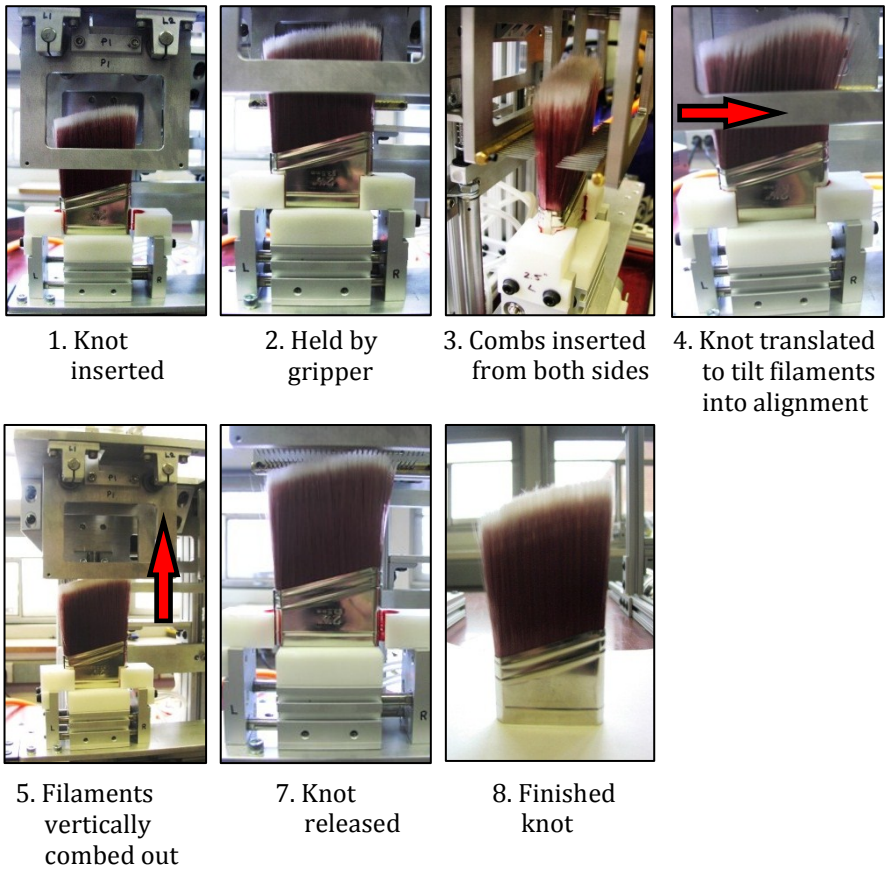

Figure 6.12 Filament Straightening and Combing Prototype 1-8: Sequence of Operation.

Results from Testing. Four knot characteristics were measured or evaluated for each knot. Characteristics assessed were (1) precision of the filament straightness (±3° tolerance from vertical), (2) stability of plug inside the knot, (3) total knot integrity, and (4) time of straightening and combing process.

Precision of straightness measurement was determined visually using a transparent template with highlighted ±3° tolerance bounds (Figure 6.13). Sequence of measurement using a 2" nylon synthetic knot is shown in Figure 6.14 (a-c), where three measurements on each side of the knot were made to estimate straightness on the left (Figure 6.14(a)), in the middle (Figure 6.14(b)) and on the right (Figure 6.14(c)) of the knot. For each measurement made, a pass or fail ranking of 1 or 0 was given if the straightness was within or outside of tolerance bounds respectively. Generated ranks of the filament straightness were then averaged to resemble the knot associated straightness.

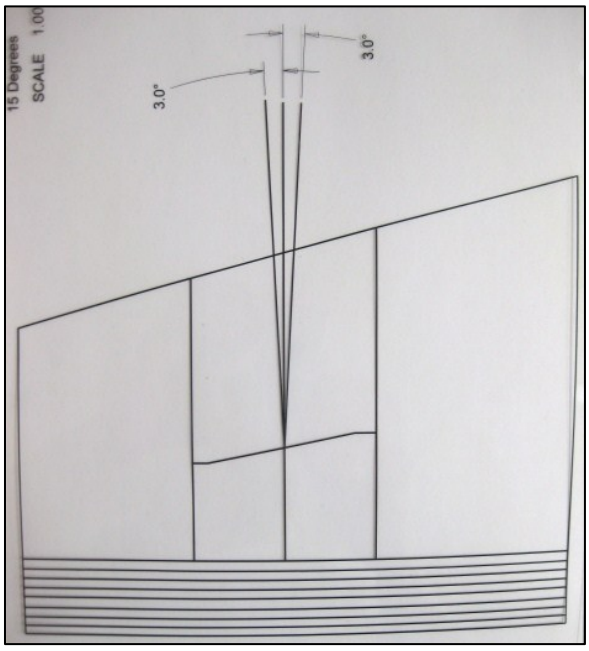

Figure 6.13 Transparent Template Used for Assessment of Filament Straightness.

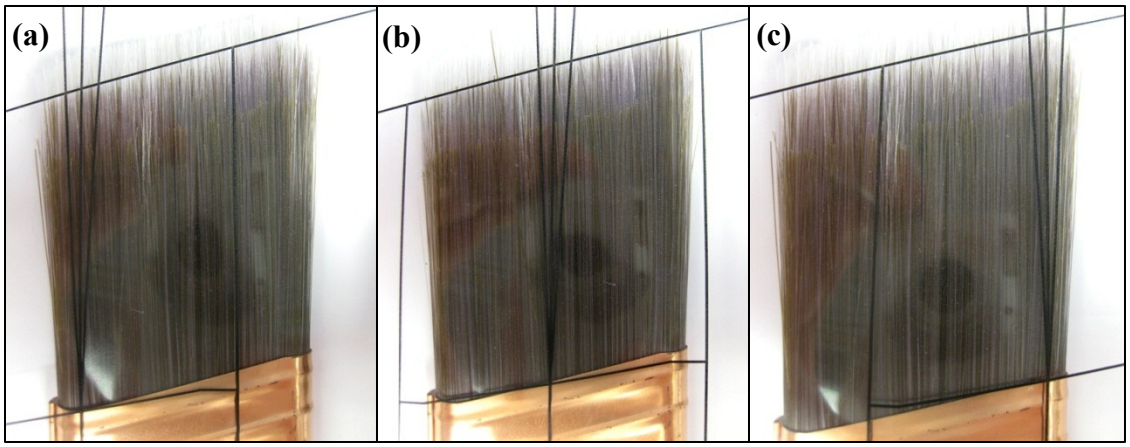

Figure 6.14 Sequence of Straightness Measurement along the Width of the Knot: (a) Left Side; (b) Middle; (c) Right Side.

Stability of the plug and knot integrity were further analyzed and ranked on a scale of 0 to 5 (5 being the best), also performed through visual assessment. Time was measured in seconds, using a stop watch from the time the knot was received into the hand or inserted into the prototype alignment platform to the time of process completion.

From testing performed, straightening prototype showed improvements over hand gauging (Table 6.5-6.6). For both types of knots, significant improvement was recorded for criteria of straightness and time ($p << 0.05$). Time required to perform straightening and combing was dramatically decreased through the use of the prototype; for the 2" and 2.5"

Table 6.5 2" Silver Tip Nylon Synthetic Knot; Filament Straightening Results.

	Hand Operation		Prototype Operation			
	Mean	95% CI	Mean	95% CI	Comparison P-Value	$\mu_2 - \mu_1$
Filament Straightness (±3°) (Rank)	0.80	{0.71,0.89}	1	{1.00,1.00}	0.0079	0.2
Plug Stability (Rank)	5	{5.00,5.00}	5	{5.00,5.00}	1	0
Knot Integrity (Rank)	4.2	{3.16,4.94}	5	{5.00,5.00}	0.1667	0.8
Time (sec)	33.46	{30.62,36.30}	4.49	{4.06,4.91}	0.0079	-28.97

Table 6.6 2.5" White Pig Hair & Natural Filament Blend Knot; Filament Straightening Results.

	Hand Operation		Prototype Operation			
	Mean	95% CI	Mean	95% CI	Comparison P-Value	$\mu_2 - \mu_1$
Filament Straightness (±3°) (Rank)	0.7	{0.53,0.87}	0.9	{0.78,0.98}	0.0079	0.2
Plug Stability (Rank)	4.8	{4.24,4.95}	5	{5.00,5.00}	1	0.2
Knot Integrity (Rank)	5	{5.00,5.00}	5	{5.00,5.00}	1	0
Time (sec)	34.68	{32.68,36.69}	4.58	{4.25,4.91}	0.0079	-30.10

knot respectively, μ = 4.49; 95% CI: {4.06, 4.91} and μ = 4.58; 95% CI: {4.25, 4.91} in seconds for straightening performed by prototype and μ = 33.46; 95% CI: {30.62, 36.30} and μ = 34.68; 95% CI: {32.68, 36.69} in seconds for straightening performed by hand. Statistically significant improvement in straightness was also evident with μ = 1 and μ = 0.9; 95% CI: {0.78, 0.98} for filament straightness performed by the prototype for 2" and 2.5" inch knot respectively. Hand operation, however, resulted in μ = 0.80; 95% CI: {0.71, 0.89} and μ = 0.7; 95% CI: {0.53, 0.87} for straightness achieved with 2" and 2.5" inch knot respectively. Other criteria for both types of knots, such as stability of plug and integrity of knot did not show statistically significant difference while exemplifying acceptable ranking for both.

Evident time difference with time required to straighten and comb the knot between hand and prototype methods can be attributed to the intricacy of manual straightening process. With straightening process occurring individually on each side of the knot, the knot is usually held and visually assessed for filament straightness first. The comb is then inserted into the knot and translated horizontally to tilt filaments into alignment. As the comb is withdrawn, the side of the knot is re-assessed and process is repeated

continually until the filaments are considered to be aligned. The filaments are then combed out, as this sequence is also repeated for the other side of knot. Consumption of time occurs in the need to re-assess the filament straightness and tilt filaments multiple times for each side of the knot individually, where using the prototype both sides are straightened at the same time. Testing additionally revealed that knots formed through manual operation of angle trim forming did not have consistent filament alignment, thus requiring additional assessment prior to filament straightening. With the operation of angle trim forming occurring using the prototype, misalignment of filaments after the trim forming process was consistent for all knots tested. As a result, straightening of filaments as performed by the prototype could occur with a single attempt assuming proper settings of comb insertion height, comb insertion depth and translation distance.

Nonetheless, both full scale physical prototypes exhibited a significantly higher performance in processing of knots in comparison to manual operation. The established concepts of process performance demonstrated that the desired quality of knots can be achieved with the benefits of reliability, consistency and precision associated with automated systems. The testing performed also demonstrated that a pair of knots can be processed under five seconds, which is sufficient to achieve the desired production rate of 30 knots/min pending further refinement.

The next chapter introduces the stages of refinement performed for the subsystems of angle trim forming and filament straightening to arrive at final subsystem design models.

Chapter 7: Subsystem Refinement

Now, the prototypes require further refinements in order to satisfy all process target specifications previously described, including all specifications of knots.

To follow current method of manufacturing, the system in design would need to be preset to run a production of one type of knot recipe for a discrete amount of time. After which, the system would be stopped, adjusted, and run to produce another type of knot recipe. To advance the degree of subsystem automation, eliminate operator error during subsystem adjustment and minimize the down time, refinement was performed to provide automated methods of adjustment for changing knot specifications. Implemented modifications were performed through 3D-CAD solid modeling using design techniques demonstrated in stages of prototype design, with consideration of previously described DFX criteria to arrive at a final subsystem design models. Using generated final design, motion analysis as well as stress and deflection analyses were performed to simulate and evaluate the final design model operation. Upon completion of the subsystem design, documentation necessary for manufacturing and operation were prepared.

Refinement introduced in this chapter, was performed with simultaneous design of a knot transfer subsystem (described in Chapter 8), responsible for safe transfer of knots between subsystem processes. Knots were expected to be transferred along a single plane of motion between all subsystems to be properly located between symmetrical jaw mechanisms of individual subsystems. Figure 7.1 below shows a pair of knots, which were expected to travel along the Y-Plane of motion (shown in figure) in the direction of the depicted arrows. With motion occurring in a single plate, knots were also expected to travel along a uniform height between subsystems. Furthermore, to properly locate the knots

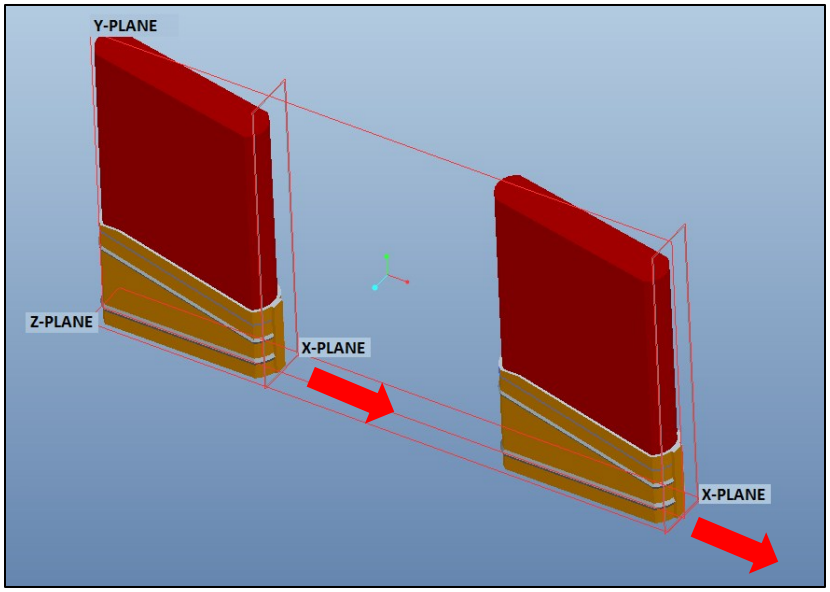

Figure 7.1 Expected Knot Transfer and Knot Reference Planes.

along the plane of motion, the X-Plane depicted in Figure 7.1 was established as a reference for all knots. To help elaborate, to perform angle trim forming, a knot would enter between filament gripper jaws (Y-Plane of motion) at a uniform height, and stop such that the edge of the knot depicted by the X-Plane would align with the pivot vertex of the filament gripper jaws. As introduced before, to achieve the desired quality of angle trim form, the edge of the ferrule (depicted by X-Plane in Figure 7.1) must be aligned with the pivot vertex.

7.1 Refinement of Angle Trim Forming Subsystem

To accept production of all knot specifications, refinement from angle trim forming prototype was necessary to accommodate adjustments in:

(1) Gripping of filament bundles of different sizes of knots (1-3 Inch width);

(2) Displacement of filament bundles for different specifications of length-out, and

(3) Gripping of filaments for different settings of height, due to variations of ferrule height and filament length.

Figure 7.2 shows the final concept of angle trim forming subsystem that has been refined to accommodate the parameters just discussed. In order to meet such requirements, the filament jaw assembly was modified to interact with additional assembly of vertical adjustment. The figure also demonstrates an updated and final form of prototype architecture. The discussion below introduces the modifications that have been made to the filament jaw assembly as well the design of newly added assemblies necessary to perform automated adjustments of length-out and filament gripping height.

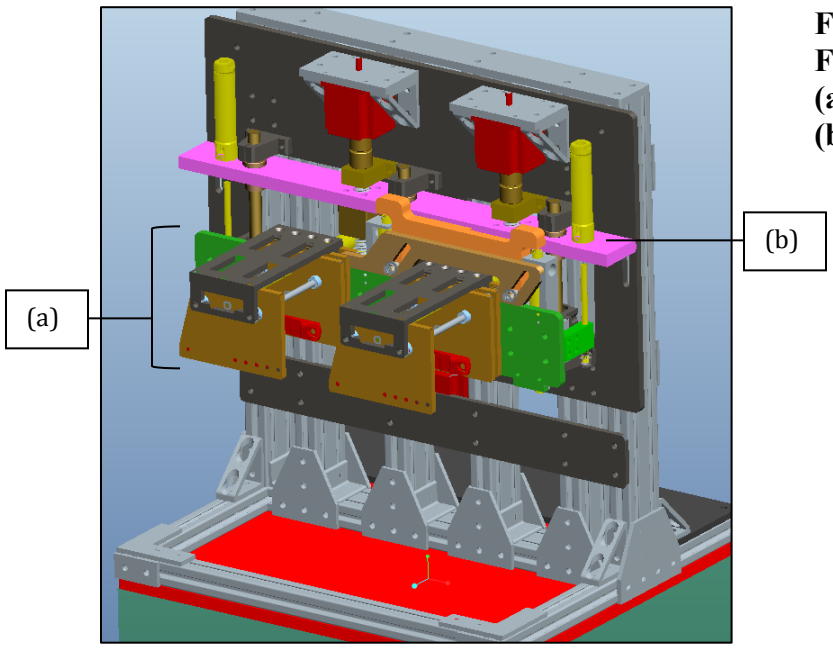

Figure 7.2 Angle & Flat Trim Forming Final Design Model: (a) Filament Jaw Assembly; (b) Vertical Adjustment Assembly.

Refined Filament Jaw Assembly. Figure 7.3 on the following page shows the refined filament jaw assembly, where the structure of the assembly has remained the same with some modifications performed within the rotation plate as well as jaw and bar-link subassemblies. The functional requirements of the rotating plate have remained the same, as the modifications made were only to accommodate changes of the jaw and bar-link subassemblies. With respect to DFX and space limitations, mounting of the bar link

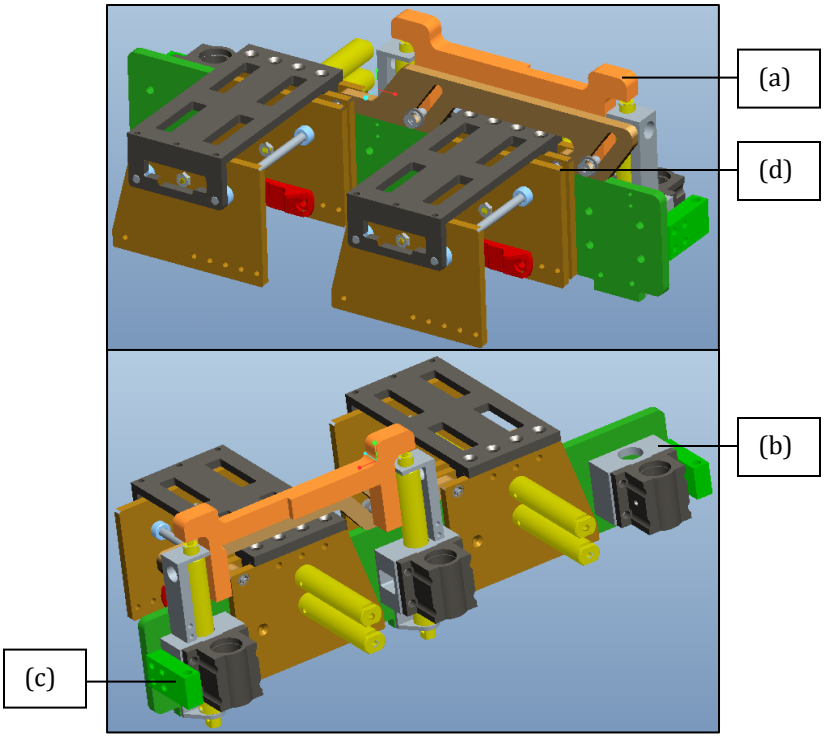

Figure 7.3 Refined Filament Jaw Assembly:
(a) Modified C-bar;
(b) Spacer;
(c) Side-Tab;
(d) Clevis Pin and Radial Bearing Connection.

subassembly has been relocated to the back of the rotation plate with a modified C-bar as shown in Figure 7.3. Spacers were added to the rotation plate to accommodate the pneumatic actuators of the bar link subassembly as well as pillow blocks necessary for vertical translation. With three symmetrically placed pillow blocks, two side spacers were also made to accommodate side-tabs (for adjustment of length-out travel described further).

Conversion of actuator vertical stroke to rotational motion within bar-link subassembly is achieved the same way, where for added reliability pivoting connection of the lever plate and jaw plates occurs through a combination of press-fit radial bearings and removable clevis-pins, making it easy to remove for maintenance (Figure 7.3(d) and Figure 7.4(a)). It is expected that the motion grooves within the lever and rotation plate would be heat treated to harden the groove surface for reliability. Individual jaw subassemblies have been modified to create symmetrical gripping of filament bundles to satisfy input of knots

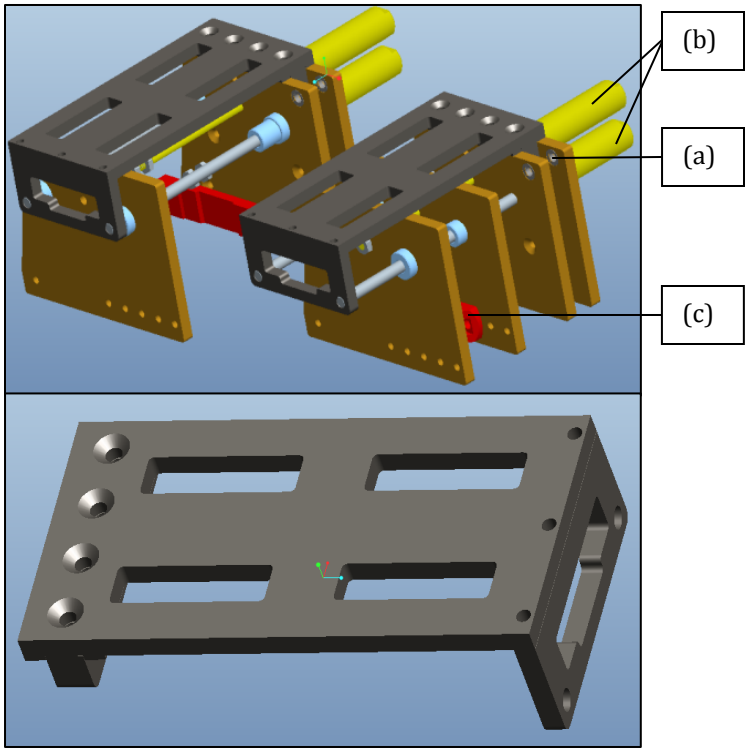

Figure 7.4
(Top) Refined Jaw Subassemblies;
(Bottom) Shaft Support Subassembly;
(a) Clevis Pin and Radial Bearing Connection;
(b) Pneumatic Actuators;
(c) Filament Gripper Plates.

long a single plane of motion. To clamp filaments, jaw plate-D was added to compliment motion of jaw plate-C, both equipped with filament gripper plates (Figure 7.4(c)). Figure 7.4(Top) shows an example of both jaw plates closed symmetrically with established mounting holes for different size gripper plates. As described in prototype design, gripper plates were made to be modular as different gripper plates would be switched-out for different widths of knot. Closing action of both jaw plates was performed by an addition of a pneumatic actuator, also nose mounted to jaw plate-A (Figure 7.4(b)). To close the plates, top mounted actuator pulls the jaw plate-D, while the bottom mounted actuator pushes the jaw plate-C. To eliminate loading and deformation of precision shafts used to guide jaw plate motion, a shaft support subassembly was added (Figure 7.4 (Bottom)). Composed of three individual pieces, the mounting of the shaft support subassembly occurs at the top and in between jaw plates A and B as well as at the tip of the precision shafts as shown in Figure 7.4(Top).

The shaft support subassembly is a good example of a major component design which would result in improved system reliability. To eliminate deformation or bending of precision shafts, top plate of the shaft support subassembly was designed to take the required loading. Figure 7.5 shows an example of deformation and stress analysis performed for major components in design through FEA Pro-Engineer Mechanica software. To create the analysis of the plate, constraints signifying mounting locations and applied loading were imposed. For the example shown in Figure 7.5, a force of 40lbs was applied at the tip of the shaft support (made of 304 Stainless Steel) to simulate worst-case scenario of loading. Figure 7.5(Left) demonstrates the deformation in units of an inch, where maximum deformation achieved was 8.43×10^{-3} inches depicted by the brightest color of red. Furthermore, Figure 7.5(Right) shows the Von-Mises stress in units of Psi, where the maximum magnitude of stress occurs at the brightest color of blue at 2.68×10^{3} Psi. From the results achieved here, the design was found to be acceptable.

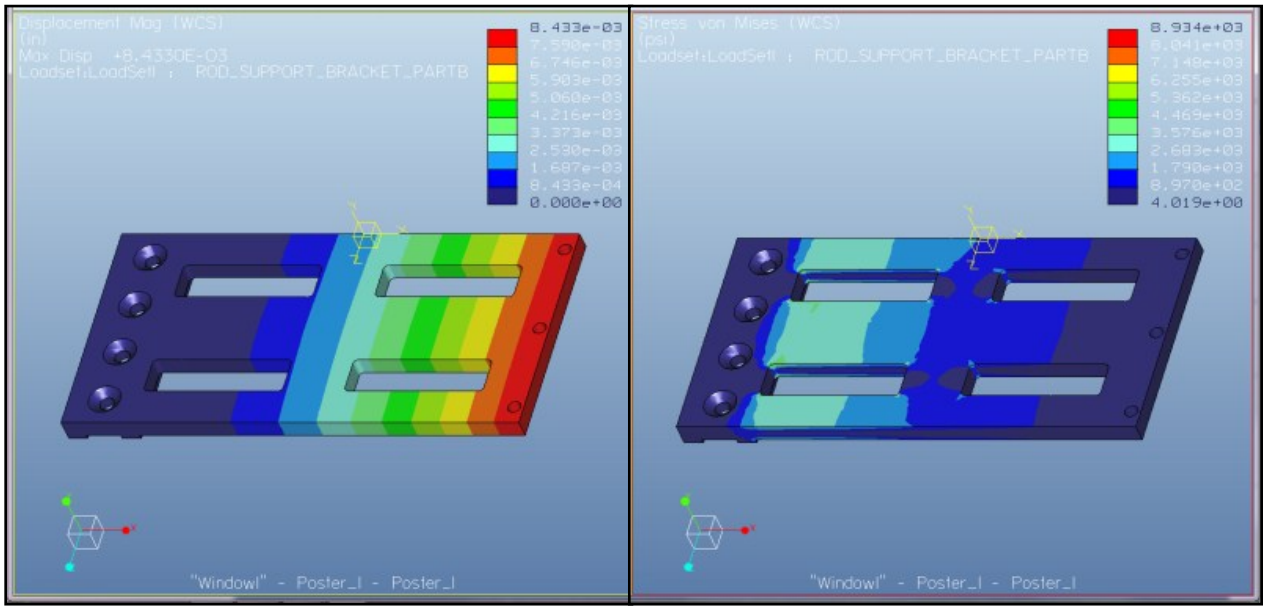

Figure 7.5 FEA Analysis Result for Top Plate of Shaft Support Subassembly: (Left) Deformation in Units of an Inch – Max=8.43×10^{-3} inches; (Right) Von-Mises Stress in units of Psi – Max=2.68×10^{3} Psi.

With a yield stress of 304 Stainless Steel being on the order of 34,800 Psi, the magnitude of Von-Mises stress was insignificant. However, the material of 304 Stainless Steel remained as a chosen option to eliminate deformation over $1x10^{-2}$ inches.

Adjustment of Length-Out. In order to displace filaments vertically, the filament jaw subassembly must translate within different vertical increments to satisfy different length-out values. To eliminate complexity, decrease cost and improve reliability, adjustment of vertical translation for length-out was performed through a purely mechanical method. A concept of "relative location" of the vertical adjustment subassembly to the filament jaw assembly is used to allow automated adjustment of length-out. Shown in Figure 7.6(Left), is the vertical adjustment subassembly consisting of an adjustment plate (Figure 7.6(a)), two pneumatic actuators (Figure 7.6(b)), sleeve bearings (Figure 7.6(c)) and ACME nuts (Figure 7.6(d)). With a set distance of stroke, the pneumatic actuators are responsible for a

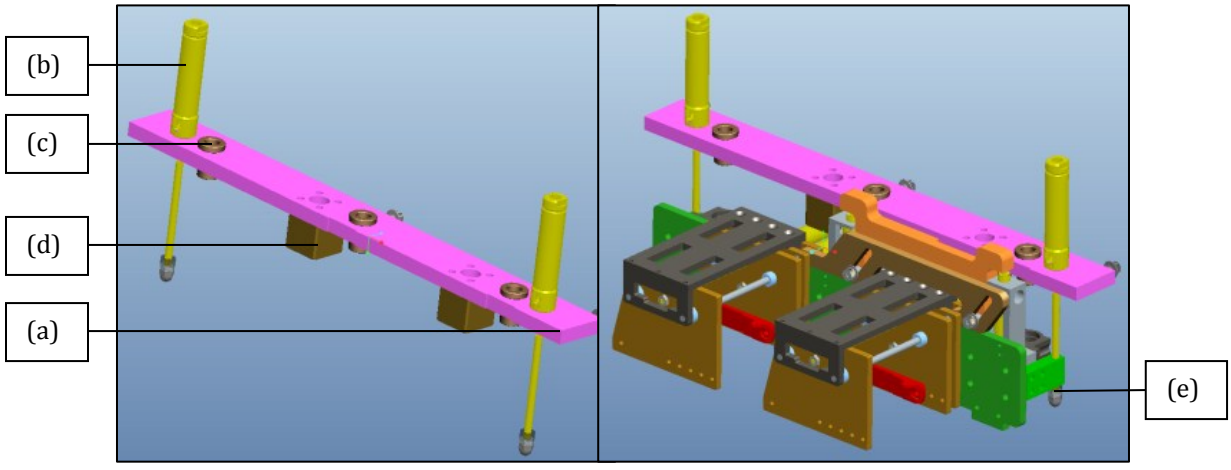

**Figure 7.6 (Left) Vertical Adjustment Subassembly;
(Right) Filament Jaw Assembly and Vertical Adjustment Subassembly Together;
(a) Adjustment Plate; (b) Pneumatic Actuator; (c) Sleeve Bearing; (d) ACME Nut;
(e) Actuator Rod Tip and Side Tab Contact.**

vertical displacement of the filament jaw assembly assuming stationary position of the vertical adjustment plate. To allow adjustment of vertical displacement, the contact distance between the actuator rod tips and the side-tabs of the filament jaw assembly is varied (Figure 7.6(e)) through different increments of location of the vertical adjustment subassembly relative to the filament jaw assembly. The vertical adjustment plate is guided vertically through PTFE bronze sleeve bearings press-fit into the vertical adjustment plate, sliding on the same precision rods as the filament jaw assembly. Figure 7.7(Left) shows a mounting plate with vertical adjustment subassembly, precision rods and ACME threaded rods with filament jaw assembly hidden. The relative placement of the adjustment plate is performed through a pair of ACME rods, where rotational motion driven by stepper motors is converted to vertical motion of the adjustment plate using ACME nuts. Mounting of the ACME rods is performed through rod-mounts, designed to contain a thrust bearing. Through the use of the stepper motors and electronic control, setting of the length-out value can be adjusted automatically based on the knot in production.

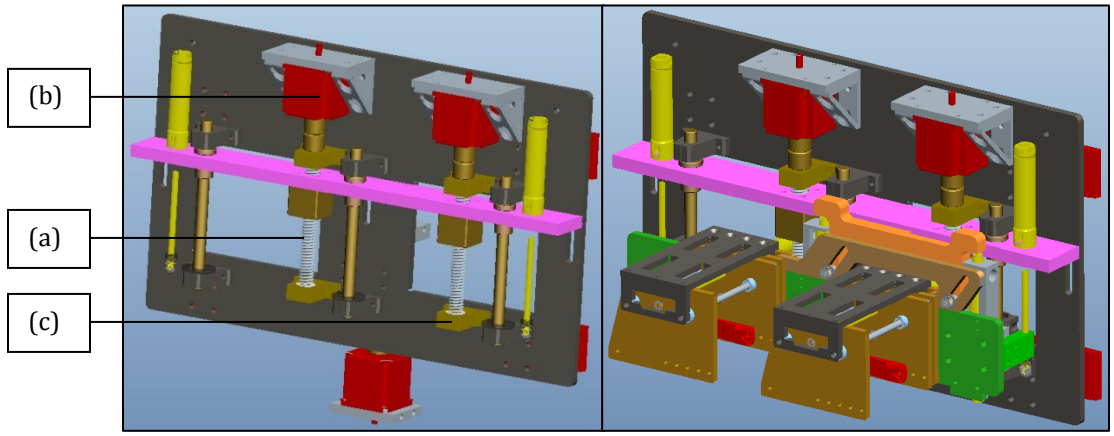

Figure 7.7 (Left) Vertical Mounting Plate (Filament Jaw Assembly Hidden); (Right) Assembled Mounting Plate with all Assemblies and Subassemblies Intact; (a) ACME Rod; (b) Stepper Motor; (c) ACME Rod Mount.

Adjustment of Filament Gripping Height. In Figure 7.7(Right), a combination of the previously described subassemblies is displayed on vertical mounting plate, highlighting the previously discussed design for assembly criteria. However, in the form shown, the mounting plate was made to be dynamic and not stationary. In order to grip filaments at different heights from the top of the ferrule, the combination of subassemblies in Figure 7.7(Right) is able to translate vertically through a combination of low friction 8020 linear bearings (Figure 7.8(c)) and associated vertical extrusions of the prototype architecture (Figure 7.8(d)). Figure 7.8(Left) demonstrates the back of the mounting plate with the low friction bearings and matching prototype architecture shown in Figure 7.8(Right). The vertical location of the mounting plate relative the prototype architecture can be regulated to set the required height of filament gripping. As shown in Figure 7.8(Left), the height adjustment is performed using an ACME adjustment mechanism and stepper motor, establishing a relative location of the vertical mounting plate and the prototype architecture shown in Figure 7.8(Right).

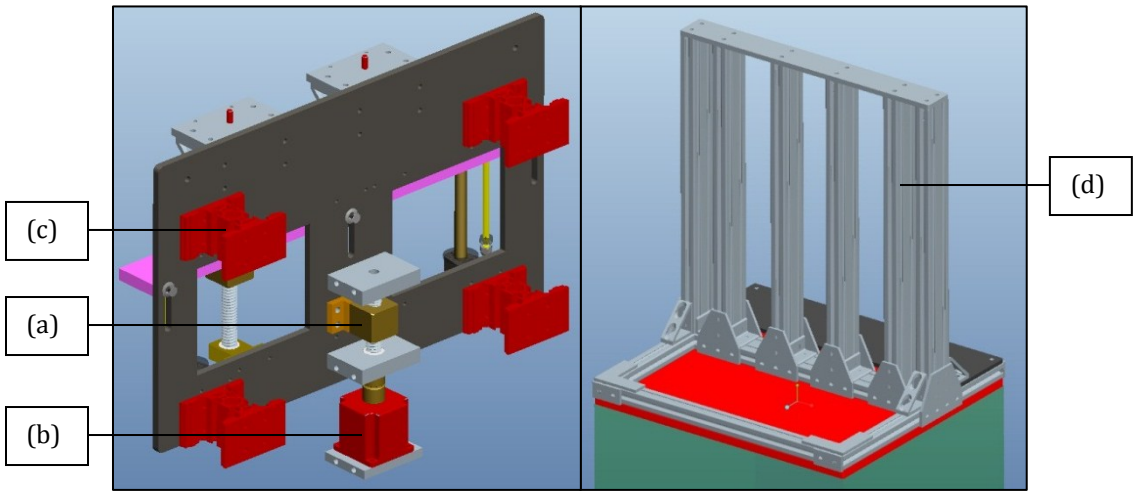

Figure 7.8 (Left) Back of Vertical Mounting Plate Assembly;
(Right) Prototype Architecture;
(a) ACME Adjustment Mechanism; (b) Stepper Motor;
(c) Low Friction Linear Bearings; (d) Vertical Extrusion as Linear Guide Rail.

Final Form. Figure 7.9 shows the angle trim forming final subsystem design model with automated methods of adjustment for settings of length-out and height of filament gripping to accommodate all target knot specifications. In order to perform knot processing, desired settings based on knot specifications can be input for automated adjustment through an electronic control. If a change in width is required, filament gripper plates would be switched out through quick release fasteners.

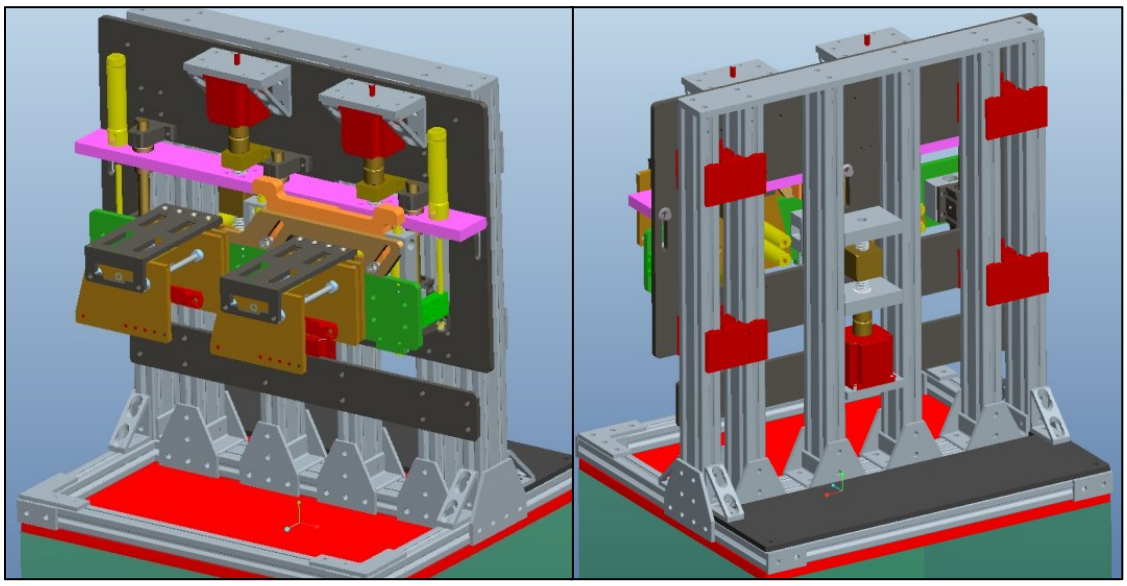

Figure 7.9 Final Design Model of Angle Trim Forming Subsystem:
(Left) Front View;
(Right) Back View.

7.2 Refinement of Filament Straightening Subsystem

Similarly, refinement of the combing subsystem was also necessary to adjust for changing knot specifications. To achieve straightening of filaments within tolerance for a specific knot recipe, the system would have to be preset for height of comb insertion, depth of insertion and distance of horizontal translation. To meet these requirements, the subsystem must accommodate different adjustments in:

(1) Height of comb insertion (from the top of the ferrule);

(2) Depth of comb insertion, and

(3) Distance of horizontal translation of comb.

In Figure 7.10, the final concept of filament straightening subsystem is shown as refined. The refinements from stages of prototype were minor, with modifications made to improve reliability of the combing head along with automated method of adjustment of height of comb insertion. Due to space limitations and imposed high cost, additional adjustments of comb insertion depth and distance of comb translation were made to require adjustment

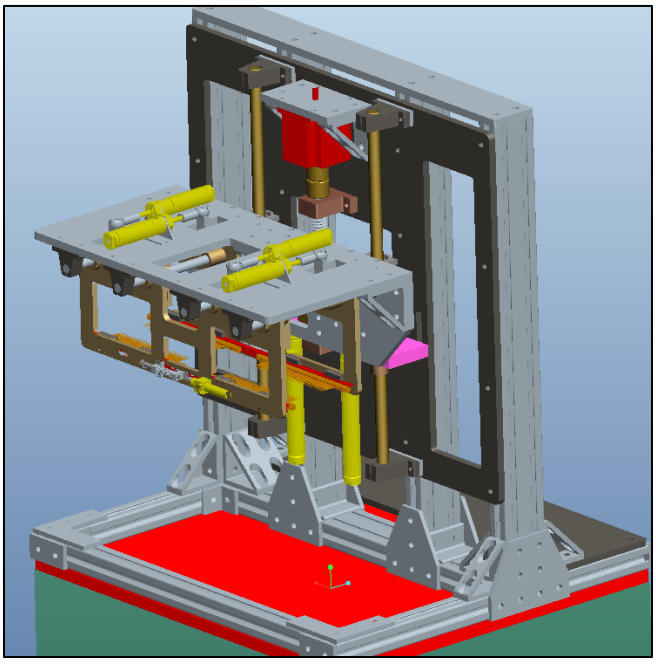

Figure 7.10 Filament Straightening and Combing Final Design Model

by an operator. However, the refinement performed was used to enforce simplicity and quickness of such adjustments. The following discussion is performed with respect to the modifications made to the combing head assembly as well as modifications performed to allow automated adjustment of height of comb insertion.

Combing Head Assembly. With a well-established design in stages of prototype, the combing head required minor modifications. Figure 7.11 shows the combing head in its refined form. To improve reliability as well for the purpose of vertical adjustment discussed further, pillow block ball bearings (Figure 7.11(a)) were added to combine with precision shafts provided by the vertical mounting plate to allow precise vertical motion of the combing head. Brackets shown in Figure7.11(b) were also added to offer ease of connection of combing head to the actuators which displace the assembly vertically. With a pivoting rod-end unit (Figure 7.11(c)) on such actuators, the brackets were designed to establish a clevis-pin and c-clip connection to offer easy and quick disconnection upon removal of combing head assembly. Likewise, to allow ease of adjustment in setting of comb insertion depth, pivot-rod ends have also been added to actuators responsible for motion of combing jaws (Figure 7.11(c)). The rod ends, offer ease of adjustment from the

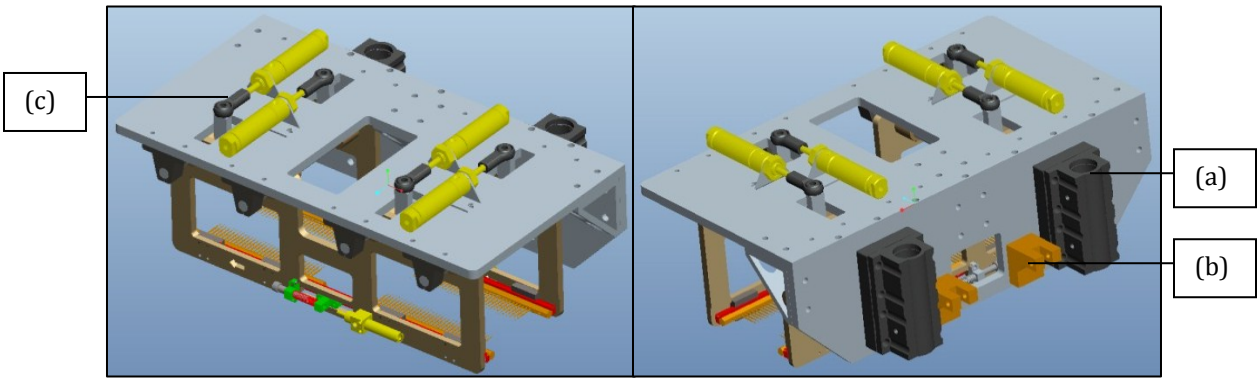

Figure 7.11 Refined Combing Head Assembly:
(Left) Front View; (Right) Back View;
(a) Pillow Block Ball Bearing; (b) Actuator Connecting Bracket; (c) Pivot-Rod End.

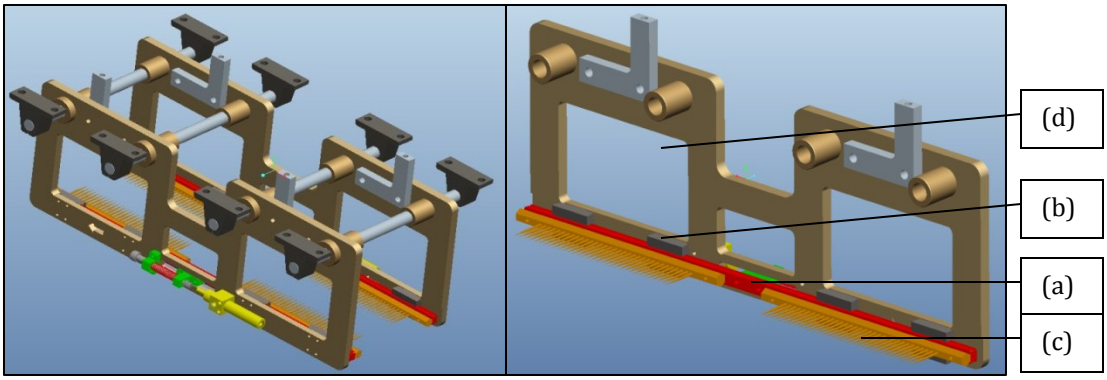

Figure 7.12 Refined Combing Jaw Plates:
(Left) Combing Jaw Subassembly; (Right) Single Combing Jaw Plate;
(a) Linear Guide Rail; (b) Ball Bearing Pillow Block;
(c) Comb; (d) Removed Material (Window).

top of the head. In order to provide motion of the combs within combing jaw assemblies, the combing jaw plates have been redesigned as shown in Figure 7.12(Right). Opposite side jaw plates have been connected, to allow motion of combs thought a combination of miniature linear guide-rails (Figure 7.12(a)) and ball bearing pillow blocks (Figure 7.12(b)). Miniature ball bearing pillow blocks were mounted to the jaw plate, as the guide-rail was able to slide within the pillow blocks. Combs (Figure 7.12(c)) were mounted to the guide rail to allow motion with controlled amount of displacement. To minimize weight and provide strength of individual jaw plates, material was removed as seen by the windows within the jaw plates (Figure 7.12(d)). Other aspects of the combing jaw subassembly have remained the same (as Figure 7.12 demonstrates). To adjust the amount of comb displacement, each combing jaw plate was equipped with an adjustment mechanism. Shown in Figure 7.13 (on the following page) is the comb translation adjustment mechanism on one of the combing jaw plates, where a guide bracket is connected to the comb guide-rail through a window of the jaw plate, to be actuated by the pneumatic actuator.

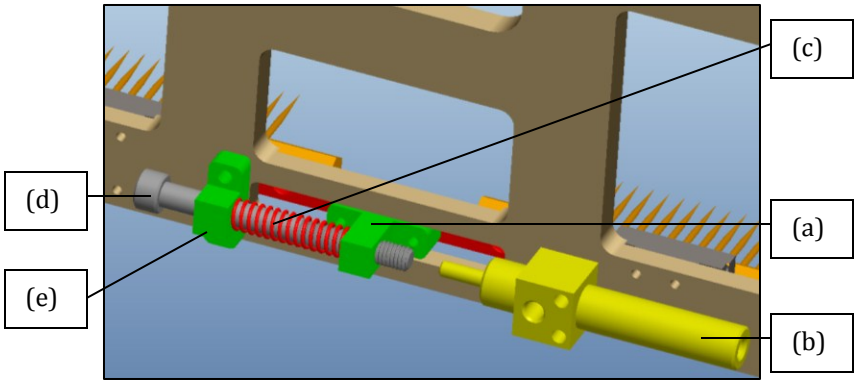

Figure 7.13 Comb Translation Adjustment Mechanism:
(a) Guide Bracket;
(b) Pneumatic Actuator;
(c) Spring;
(d) Lead Screw;
(e) Stopper Bracket.

With constant stroke of an actuator, the distance of comb translation is regulated through a spring loaded adjustment mechanism consisting of a spring, lead screw and a stopper bracket. Travel adjustment is expected to be performed manually by turning the screw to regulate interference distance between the actuator and the screw. If the actuator tip and lead screw are touching, the comb travel will be at full stoke of the actuator. However, if an offset distance between them exists, the comb travel would be shorter by that offset distance upon actuation. The actuator stroke, length of the lead screw and travel of the linear guide-rail have all been selected to accommodate all required settings of comb translation distance to satisfy all knot target specifications.

Adjustment of Comb Insertion Height. As noted previously, the combing head can travel vertically on precision shafts mounted on the vertical mounting plate (Figure 7.14-Combing Head Assembly Hidden). To create adjustment of comb insertion height with respect to the stationary knot, the comb insertion height setting was made to be regulated through a vertical adjustment plate subassembly. Very similar to a subassembly in the angle trim forming subsystem, the subassembly consists of a vertical adjustment plate (Figure 7.14(a)), two pneumatic actuators (Figure 7.14(b)), ACME nut (Figure 7.14 (c)), and bronze sleeve bearings (Figure 7.14(d)). Connection of the adjustment plate to the

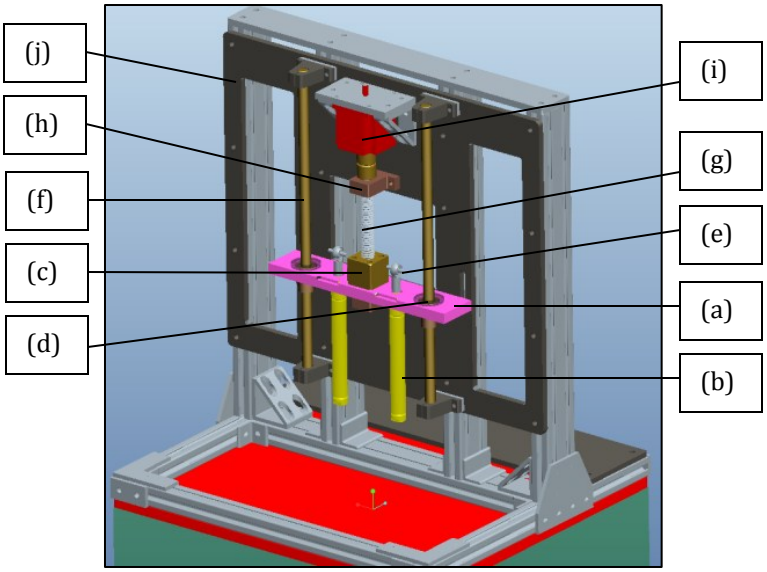

Figure 7.14 Subsystem Architecture (Combing Head Hidden):
(a) Vertical Adjustment Plate;
(b) Pneumatic Actuator;
(c) ACME Nut;
(d) Bronze Sleeve Bearing;
(e) Pivot Rod-End;
(f) Precision Shaft;
(g) ACME Rod;
(h) ACME Rod Mount;
(i) Stepper Motor;
(j) Vertical Mounting Plate.

combing head occurs through pivot rod-ends (Figure 7.14(e)) on the tips of the actuators and actuator connecting brackets previously described in Figure 7.11(b). Through the sleeve bearings, the adjustment plate was designed to slide on precision shafts (Figure 7.11(f) - mounted on the vertical mounting plate) also used for vertical motion of the combing head assembly. Vertical position of the adjustment plate defines the vertical position of the combing head, or the height at which the comb insertion is performed. Through an ACME threaded rod (Figure 7.14(g)) and rod mounts, the height of the vertical adjustment plate can be regulated by converting rotational motion of the ACME rod to vertical translational motion of the ACME nut mounted to the vertical adjustment plate. Using a stepper motor (Figure 7.14(i)), the height can be preset through electronic control to define the comb insertion height with respect to the top of the ferrule. Once the combs have been inserted into the sides of the knot and translated, combing action is performed by translating the combing head assembly using pneumatic actuators imbedded in the vertical adjustment plate. The vertical mounting plate (Figure 7.14(j)), which houses the main subassemblies of the subsystem, is mounted to the vertical support structure. In this

subsystem, the vertical mounting plate is fastened against the subsystem architecture with no need for motion.

Final Form. Shown in Figure 7.15 is the established final form of the filament straightening and combing subsystem. In comparison to the angle trim forming final design model, uniformity of subsystem architecture can be seen. For both subsystems, sizing of the architecture was established were it is uniform. Such uniform design has shown itself as key to proper subsystem integration to generate the total automated system design. The total system design is discussed in the next chapter.

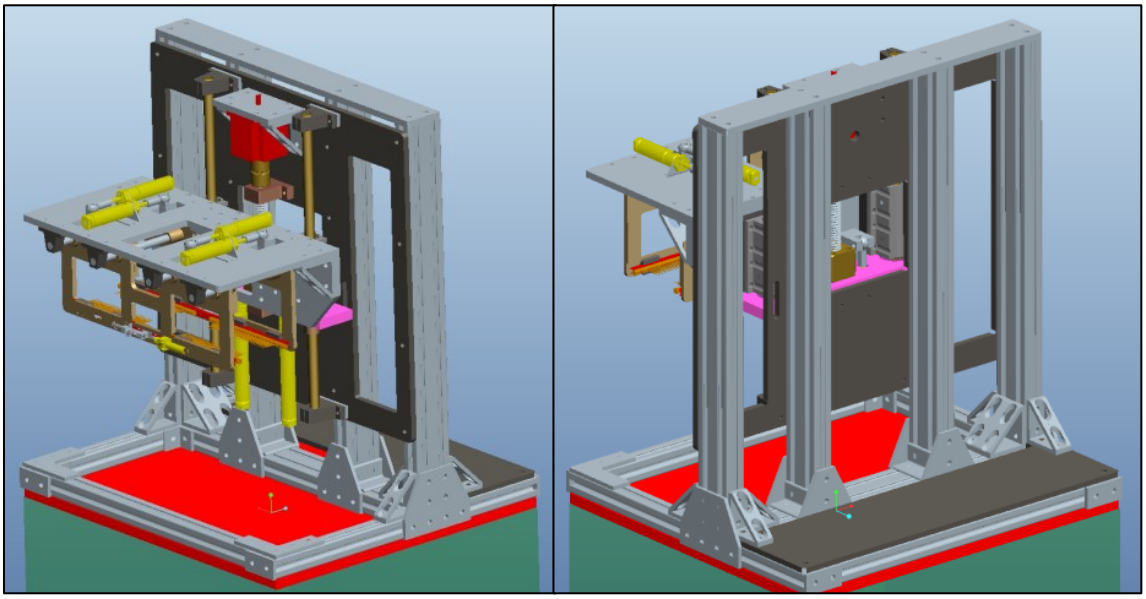

Figure 7.15 Final Design Model of Filament Straightening and Combing Subsystem: (Left) Front View; (Right) Back View.

Chapter 8: Discussion

This design study described the development of angle trim forming and filament straightening subsystems used to replace human operation with a goal of eliminating process and operator health problems. To arrive at final design concepts for each subsystem, the development process was described in detail. In the final form shown in the previous chapter of Subsystem Refinement, the subsystems are able to accept all paint brush knot specifications with automated methods for forming of angle trim and straightening of filaments.

This chapter further discusses the key elements of the design study introduced in this thesis, including the summary of the development process to arrive at the final design models. Furthermore, the chapter proposes a set of design guidelines as an outcome of this study with hope to be of benefit to the industrial and scientific communities. In order to satisfy all requirements associated with manufacturing of knots in an automated fashion, additional subsystems that have been developed are also discussed.

8.1 Summary of Design Study

As already established, angle-trim paint brush manufacturing worldwide is currently performed through only semi-automated methods of assembly, where a large portion of paint-brush-applicator processing is performed through human operation. Some issues resulting from such manual processing include inconsistencies in filament density, filament straightness and shape of angle trim form, resulting in poor quality of end products.

To eliminate process problems associated with inconsistency in product quality and productivity, as well as operator health problems, design of an assembly system was performed. To satisfy the requirement of innovation of core subsystems, focus of the design

study was placed on subsystems of angle trim forming and filament straightening, where final designs for each have been established. The modified product development process was followed during the development of the assembly system, where target specifications of the system were defined first, followed by functional decomposition of the overall system at the first level. With morphological design approach, the modified product development process was applied to development of individual core subsystems in the following order: formulating system needs and specifications, determining the functional decomposition and concept development, testing for design parameters, designing the embodiment and system details, fabricating and testing prototype, and refining the subsystem.

Target Specifications. Established initial target specifications were provided from the sponsor based on the customer required product performance. The subsystems developed were made able to accommodate all of such specifications, resulting in hundreds of different knot types. Possible knot specifications were different filament material types, trim, tip form, thickness, width, ferrule type, ferrule shape, ferrule material type and other specifications provided in Chapter 2.

Core Subsystem Concept Development. With target specifications and functional requirements in mind, core subsystems were taken through concept generation and selection stages. Based on the top concepts, proof-of-concept models were developed and tested. For the angle trim forming process, three concepts were tested to satisfy functions of (1) displacing filament bundle with respect to the ferrule housing to establish the length-out value and (2) creating the angle or flat trim profile. The three concepts were: (1) to automate the current method of filament forming through insertion of gauging block, (2) to

grip and displace filaments while forming the angle trim using the tip of a gauging block, and (3) to grip, displace and rotate filaments to achieve the required angle trim form. Concept 3, gripping and rotating of filaments, showed excellent results with no dragback of filaments as well as improved knot integrity, stability of plug and quality of the angle trim profile specification of 15°.

In similar terms, a single proof-of-concept testing model showed that straightening of filaments can be achieved through functions of (1) inserting a comb into filaments on a side of a knot, followed by (2) horizontally translating the comb to tilt filaments into alignment. Testing revealed that alignment of filaments for different knot recipes can be achieved through a distinct setting for depth of comb insertion, height of comb insertion (measured from the top of the ferrule) and horizontal translation distance of the comb. With the established setting for each parameter of the required knot recipe, quality was found to result in the required filament straightness specification of ±3° tolerance from vertical, conserved knot integrity and proper plug stability.

Testing for Design Parameters. In order to continue to the stages of physical prototype design, testing for design parameters was performed for the selected concept of angle trim forming. Among the different design parameters requiring testing, the focus within this design study was to establish an understanding of the pulling force required to displace filament bundles within ferrule housings to create the angle trim.

The scope of testing involved experimentation with a specific range of factors, mainly to represent the most common types of knots manufactured and seen as 80% of annual production for the Sherwin Williams Company [3]. Ranges of factors were established for filament packing volume fraction, ferrule material coating type, ferrule size

and ferrule shape to be packed into knots and tested using plugs and nylon synthetic filaments. Each knot combination was packed for low, medium and high volume packing fractions. Knots were assembled using 2” wide oval shape ferrules of stainless steel, copper and brass material type in 9/16” thickness. Square shaped stainless steel ferrules of 2”, 1.5” and 1” width and 9/16”, 7/16”, 5/16” thickness respectively were also used to vary the factors of ferrule size. An additional stainless steel ferrule and wooden plug were fabricated for a circular knot for sake of comparing the resulting force distribution between oval, square and circular shape ferrule housings. An in-house fabricated experimental setup was used to hold the ferrule housing, grip and displace the filament bundle, at which time the force required to overcome friction was recorded along with the displacement value. From the testing performed, it was established that magnitude of static friction force for ferrule housings used in knot manufacturing was a function of the filament bundle displacement. Due to the bead geometry on the ferrule, the maximum pulling force to overcome friction occurs at the location of the bead. Gathered results were processed using ANOVA, Tukey-Kramer and Student-t statistical analyses to establish two particular notions. First, it shows that for low, medium and high volume packing fractions, the means of the static friction force are statistically different ($p<<0.5$) for the knots tested. Second, it was also established that the force required to displace filaments from the ferrule housings was dependent on the factors of ferrule housing material coating type, ferrule size and ferrule shape. With ($p<<0.5$), it was shown that the highest means of friction forces for low, medium and high volume packing fractions were achieved using brass coated ferrule, and the lowest forces were observed for the copper coated ferrule housing. For the sizes of 2”, 1.5” and 1” wide ferrule housings, 2” square ferrule of stainless steel material type required

the highest pulling force, 1.5” ferrule the second highest and lowest for 1” ferrule. The analysis performed with respect to the shape of the ferrule housing also displayed that a significant difference between their required pulling forces was present. With tests performed for individual ferrule housings of circular, oval and square shapes, all were found to be statistically different between each other ($p<<0.5$). The square form was found to generate the highest force necessary to displace the filament bundle. From the testing performed, the maximum force required to displace the filaments was 29.75 Newtons, which was established as a design parameter to assist in component selection of pneumatic actuator to displace the filament bundles of the full scale physical prototype of angle trim forming.

Prototype Detail Design. Collected design parameters were used to design and fabricate physical prototypes for the angle trim forming and filament straightening subsystems, and to evaluate the performance of the top chosen proof-of-concept models. Prototypes were developed through a combination of hand sketch design and hand calculations, with solid modeling and analysis also performed through 3D CAD Pro-Engineer software. A catalog design approach was used to create fairly complex, low cost, precise and efficient semi-automated prototype subsystems. Appropriate component selection was performed to meet the DFX criteria for manufacture, assembly, maintenance and cost. Modular subsystem architecture and knot interface was established to offer minimal subsystem footprint while satisfying all specified target specifications and functional requirements.

Pneumatic components, linear and rotational motion hardware, custom fabricated components, structural support components, electronic control and programming were

used to mechanize and automate actions necessary to satisfy the prototype functional requirements. Components were purchased and used directly, purchased and altered or custom fabricated using manual or CNC machining to match the design specifications as well as provide the necessary static and dynamic performance demonstrated by the analysis performed through solid modeling. After stages of prototype detail design were completed, the documentation for manufacture, such as engineering and assembly drawings, was generated to highlight the essential dimensions, tolerances and other specifications required for fabrication and assembly.

Prototype Testing. Prototype models for angle trim forming and filament straightening were assembled and tested in a semi-automated fashion using a combination of LabView-Lego NXT programming modules and electronic controlled pneumatic solenoid valves. Testing was performed in the order of knot processing, where twenty knots of two distinct knot recipes delivered from the factory were settled using a vibration table and then processed to create the angle trim and straighten filaments. The knots tested were of oval ferrule shape and angle trim type, with a nominal size of 2" width and thickness of 9/16" consisting of silver-tip nylon filaments, and size of 2.5" width of 5/8" thickness consisting of nylon and white pig hair natural filament blend. For each size brush, ten knots where processed by hand to create the angle trim form and straighten filaments, and then ten were processed using the prototypes developed.

Angle Trim Forming Results. A significant improvement in the knot quality was established using the two subsystem physical prototypes over hand operation. Specifications of the angle trim forming were to displace filament bundle to a specified

length-out while also forming an angle trim filament profile of 15° within ±1° tolerance. Results from testing were recorded using a rank scale of 0 to 5, with 5 being the best.

For both types of knots tested, a profile of 15° was achieved within ±1° tolerance using the prototype, receiving a rank of 5, where angle trim forming through hand operation received a $\mu = 3.40$; 95% CI: {2.72, 4.08} and $\mu = 3.20$; 95% CI: {2.16,4.24} for 2" knot and 2.5" knot, respectively. As expected, precision of the length-out value was also significantly different between hand and prototype operation. Specifications of length-out for 2" and 2.5" size knots were 2.85" and 2.6875" respectively. For the 2" prototype formed knot, $\mu = 2.86$; 95% CI: {2.84, 2.86}, where hand forming was only $\mu = 2.79$; 95% CI: {2.69, 2.89}. Statistical difference ($p<<0.5$) was also achieved for the 2.5" formed knot when $\mu = 2.66$; 95% CI: {2.64, 2.68} using the prototype and $\mu = 2.60$; 95% CI: {2.57,2.62} with hand forming.

Additional testing criteria were linearity of angle trim distribution, dragback present, time, knot integrity and stability of plug. Both types of brushes received a mean rank of 5 (on rank scale of 0 to 5, with 5 being the best) for linearity of angle trim using the prototype with no dragback present. However, trim forming using hand operation of the 2" knot received $\mu = 2.60$; 95% CI: {1.92, 3.28} and 2.5" knot of $\mu = 1.80$; 95% CI: {1.24, 2.35} with presence of dragback. A significant improvement in the time to gauge the knot was also established as both types of knots received $\mu = 2.02$; 95% CI: {1.87,2.18} and $\mu = 2.03$; 95% CI: {1.93,2.14} for time required by the prototype, and $\mu = 3.52$; 95% CI: {3.35,3.70} and $\mu = 3.65$; 95% CI: {3.50, 3.75} for time required by hand gauging for the 2" and 2.5" inch knots, respectively. Angle trim forming through the prototype showed a mean rank of 5 for knot integrity and stability of plug for both types of knots. No statistical difference

was observed in plug stability for both types of knots due with an equal rank of 5 for hand and prototype angle trim forming. However, this demonstrates an example of system reliability, where the stability of the plug was conserved without any support of the gauging block from the bottom during displacement and rotation of filaments to create the angle trim form.

Filament Straightening Results. For both types of knots tested, a significant improvement was also established within the specification of filament straightness alignment tolerance of ±3° from vertical. For each processed knot, the straightness of the filaments was measured in three places on each side of the knot, where a pass or fail ranking of 1 or 0 was given if the straightness was within or outside of tolerance bounds, respectively.

The generated ranks of the filament straightness were then averaged to represent the straightness for the entire knot. A statistically significant improvement in straightness was achieved where a mean rank for filament straightness performed by the prototype was $\mu = 1$ and $\mu = 0.9$; 95% CI: {0.78, 0.98} (on a ranking scale between 0 and 1) for 2" and 2.5" inch knot respectively. Manual straightening, however, displayed the mean values of $\mu = 0.80$; 95% CI: {0.71, 0.89} and $\mu = 0.70$; 95% CI: {0.53, 0.87} for 2" and 2.5" inch knot respectively.

Other criteria tested were time of filament straightening and combing process, knot integrity and plug stability. The time required to perform straightening and combing was dramatically decreased through the use of the prototype; for the 2" and 2.5" knots: mean time for straightening performed by the prototype were $\mu = 4.49$; 95% CI: {4.06, 4.91} and $\mu = 4.58$; 95% CI: {4.25, 4.91} in seconds, and for straightening by hand $\mu = 33.46$; 95% CI:

{30.62, 36.30} and μ = 34.68; 95% CI: {32.68, 36.69} in seconds. The other criteria for both types of knots, stability of plug and knot integrity, did not show a statistically significant difference and had acceptable ranking for both methods.

Prototype Refinement. Established results from prototype testing clearly demonstrate satisfaction of specifications with significant improvement in the knot quality at a fraction of the time when compared to hand operation. Using 3D-CAD solid modeling, designs of prototype models were further refined to accommodate all of the required specifications of knots with satisfaction of DFX criteria to arrive at a finalized subsystem designs. Modifications were made to help eliminate operator error when performing adjustments of system settings and reduce associated system down time. Electronically controlled automated adjustment mechanisms were added for this purpose, quick-replacement modular components such as filament gripper plates, as well as components that offer easy and precise adjustments such as pivot-rod ends. Furthermore, motion analyses as well as stress and deflection analyses were performed through solid modeling to assure that final subsystem design models meet the performance requirements. Upon completion of the subsystem refinement, documentation necessary for manufacturing and operation were prepared to initiate fabrication. In the refined form demonstrated in Chapter 7, the final design models for angle trim forming and filament straightening are able to accept and process all specifications of knots at the level of quality demonstrated by the full scale physical prototype models while meeting the production rate requirement.

8.2 Proposed Design Guidelines

As a part of the design study performed, gripping and handling of filament bundles was examined. Gripper plates to grip filament bundles were introduced as well as the tests designed and conducted to measure the pulling force required to displace filament bundles for a range of knot factors. Such examination was performed because, as to our knowledge, no design guidelines exist to help estimate the force required to displace filaments within paint-brush or equivalent type housings. Likewise, no design guidelines exist on methods to perform sufficient gripping of filaments which is commonly performed today in scientific and manufacturing environments. As a result of the knowledge gained through the design study, the author would like to present a cohesive set of guidelines, (1) to estimate pulling force required to displace a bundle of filaments as a function of housing and bundle parameters, and (2) to develop effective gripper plate end-effectors to grip filament bundles. The guidelines introduced here, were established in hopes to benefit the current industry of knot manufacturing as well as other manufacturing and automation industries possibly involving manufacture of toothbrushes, hair brushes and fiber optic routing.

8.2.1 Guideline to Estimate Filament Bundle Pulling Force

As it was demonstrated in Chapter 4, the pulling force required to displace filament bundles within ferrule housings is a function of multiple factors. Such factors include filament material type, filament packing density, ferrule material type, ferrule shape, ferrule size and plug size. The multitudes of factors create a significant variation in the necessary pulling force between different assemblies of knots. As already established, no design guidelines exist to help estimate the required pulling force based on the characteristics of the knot or equivalent assembly. Thus, in order to create appropriate

component sizing in stages of detail design, testing was performed to characterize the pulling force. As a result, the author would like to present an introductory design guideline in the form of universal curves. Formulation of the design guideline originates from testing factors of knot assemblies seen as the most manufactured type using nylon filaments and metal alloy ferrule housings. However, the approach to design guideline formulation as well as the established functional relationships through dimensional analysis can be used for equivalent filament bundle and ferrule type assemblies. Furthermore, the author expects that this study would be extended further to make it more applicable.

The following sections reiterate the testing performed, describe formulation of non-dimensional Pi-terms and introduce the established design guideline universal curves.

Summary of Testing. To establish a correlation between the varying factors of a knot assembly and the resulting pulling force, testing was performed as previously described in Chapter 4. To reiterate, knots consisting of a ferrule, plug and filaments were assembled and tested to characterize the force required to overcome the friction associated with displacement of filament bundle. Seven different knots were packed with nylon synthetic filaments and tested using low, medium and high volume packing fractions. For the knots packed, three ferrule housings were of oval shape in stainless steel, copper and brass material coatings, three were of different size in square shape stainless steel ferrules, and one was of circular shape, also in stainless steel material type. To help generalize the design guideline, a circular stainless steel ferrule and wooden plug were fabricated in-house. The dimensions of the ferrule and associated plug were made to resemble the volume available for packing of filaments (between plug and inner walls of the ferrule) to approximately match the volume seen in a square and oval shaped stainless steel ferrules.

For testing to occur, all samples were prepared through manual assembly as per specifications of the company sponsoring this research. The volume packing fraction of the samples was calculated using nylon synthetic filament bundles of known length and density. The mass of the filament bundle was recorded along with measurements of ferrule width, ferrule thickness, ferrule wall thickness, plug width, plug thickness and plug height. Using the specified volume packing fraction of filaments, knots were packed into ferrules with the support of the specified plug. To promote accuracy in testing, filaments were checked for uniform density within knots, settled through vibratory table and combed. Assembled knots were tested using an in-house fabricated test setup for each range of volume packing fraction, where ferrule housing was held stationary as the filament bundle was gripped and displaced. The force required to overcome the static and kinetic friction of the filaments against the ferrule were measured incrementally down the length of the ferrule. More detailed aspects of the factors and testing performed are provided in Chapter 4.

Recorded Testing Variables. Tables 8.1-8.3 list the pertinent measured variables that were involved in the testing performed. To recap, throughout experimentation the density and length of the nylon filaments and the velocity of the filament bundle displacement remained constant (Table 8.1). However, the specifications of the ferrule and plug were varied along with the volume packing fraction (Table 8.2).

Table 8.1 Constant Testing Variables.

Testing Variables	Definition
L_F	Filament Length
ρ_F	Filament Density
v	Velocity of Filament Bundle Displacement

Table 8.2 Changing Testing Variables.

Testing Variables	Definition
W_P	Plug Width
H_P	Plug Height
T_P	Plug Thickness
F_W	Ferrule Width
T_F	Ferrule Thickness
t_F	Ferrule Wall Thickness
m_F	Mass of Filament Bundle
V_P	Volume Packing Fraction
R_F	Inner Radius of Circular Ferrule
R_P	Outer Radius of Circular Plug

Figure 8.1 (shown on the following page) pictorially represents the ferrule and plug specifications on a square ferrule. As mentioned in Chapter 4, the volume packing fraction (V_P), is a ratio of filament bundle volume (V_F) to the volume available between the walls of the ferrule housing and the plug (V_A). Equation 8.1 shows the calculation for volume packing fraction in terms of the variables described in Tables 8.1-8.2, where (A) is the cross-sectional area between the ferrule and plug. The determination of this area is described further and is a function of ferrule and plug specifications.

$$V_P(\%) = \frac{V_F}{V_A} \times 100; \quad V_F = \frac{\rho_F}{m_F}; \quad V_A = A(L_F)$$

(Equation 8.1)

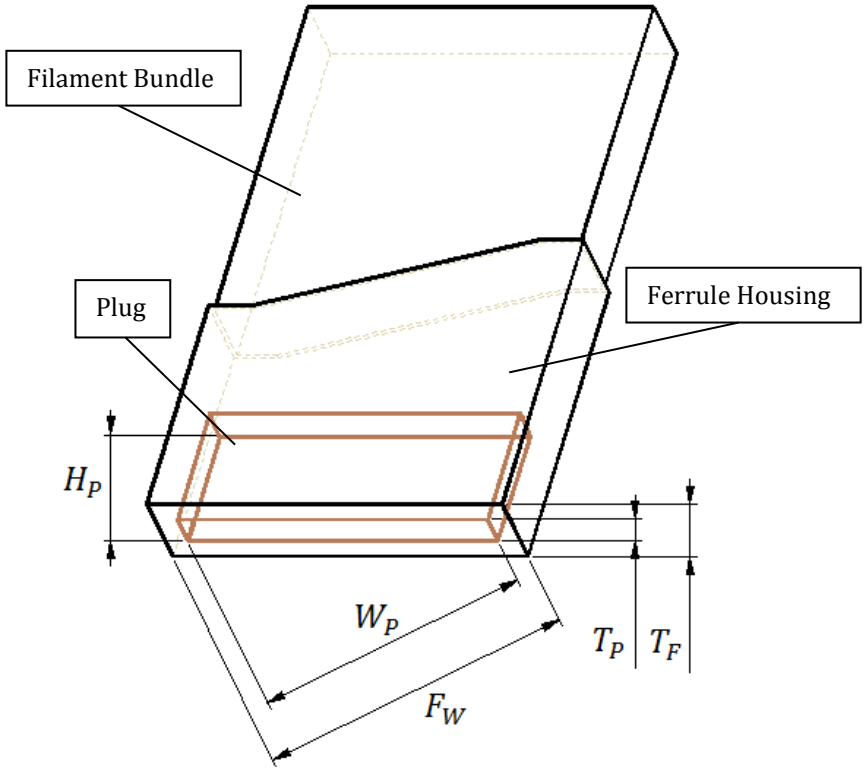

Figure 8.1 Specifications of Ferrule and Plug.

Variables resulting from testing are shown in Table 8.3. For the seven types of knots described, each knot was tested using volume packing fractions of low, medium and high (established from sponsor-specified mass of filament bundle). As a result, the static friction force and kinetic friction force distributions were determined for each combination of ferrule, plug and filament volume packing fraction. Associated mean values of static friction force (F_S) and kinetic friction force (F_K) were calculated.

Table 8.3 Resulting Variables from Testing.

Testing Variables	Definition
F_S	Mean Value of Static Friction Force
F_K	Mean Value of Kinetic Friction Force

Generation of Pi-Terms. With a fairly large number of variables associated with this problem, a non-dimensional analysis approach was taken to create a simple, yet effective design guideline. In the form of master curves, the design guideline would establish the functional relationship achieved through experimentation between variables. To formulate non-dimensional Pi-terms, the variables associated with the problem introduced in Tables 8.1-8.3 were considered and refined to better represent the geometry of the ferrule housing and plug. Further, determination of the necessary Pi-terms was performed by expressing the considered variables in terms of basic dimensions, establishing the required number of Pi-terms, and forming and checking those Pi-terms.

Table 8.4 demonstrates a reduced list of variables chosen to formulate non-dimensional Pi-term products. In comparison to variables in Tables 8.1-8.3, variables that characterize plug and ferrule specifications have been converted to the more universal form of hydraulic diameter (D_{HYD}).

Table 8.4 Variables Used for Dimensional Analysis.

Variable	Definition
F_S	Mean Value of Static Friction Force
F_K	Mean Value of Kinetic Friction Force
m_F	Mass of Filament Bundle
V_F	Volume of Filament Bundle
V_A	Volume Available Between Walls of Ferrule and Plug
V_P	Volume Packing Fraction
D_{HYD}	Hydraulic Diameter of Knot
H_P	Plug Height
L_F	Length of Filament
v	Velocity of Filament Bundle Displacement

As shown in Equation 8.2 below, the hydraulic diameter helps to characterize different forms of ferrule and associated plug combinations. Figure 8.2 visually demonstrates the cross-sectional area between ferrule and plug (A) (red area in Figure 8.2(Left)), and the total perimeter (P) (blue line in Figure 8.2(Right)). Both specifications of (A) and (P) were chosen purposefully to properly establish the functional relationship from experimentation between specifications of the plug and the specifications of the ferrule housing. For this reason, the variables are defined as shown in Figure 8.2, where (P) for example, is not just the perimeter of ferrule housing but a sum of ferrule and plug perimeters. Likewise, the cross-sectional area between ferrule and plug (A) highlights the specifications of both, plug and ferrule housing.

For the sake of simplicity, Figure 8.2 only demonstrates (A) and (P) for a square ferrule, but these specifications can also be found in the same manner for the oval, round and other shape ferrules.

$$D_{HYD} = \frac{4A}{P}$$

(Equation 8.2)

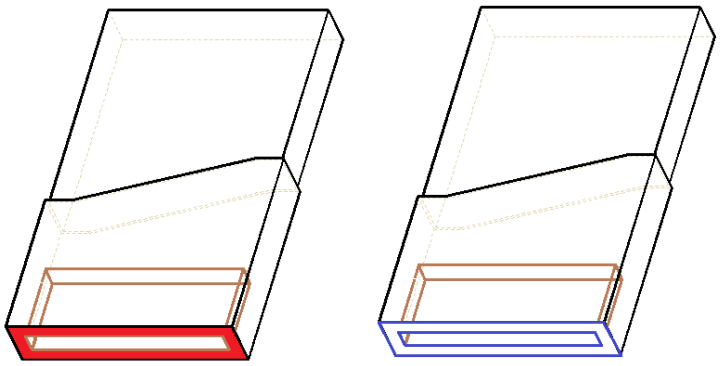

Figure 8.2 Measurement of Variables (A) and (P):
(Left) Cross-sectional Area between Ferrule and Plug (Shown in Red);
(Right) Total Perimeter (Sum of Inner and Outer Perimeters Shown in Blue).

Equations 8.1 - 8.5 introduce five non-dimensional Pi-terms created from combining the variables displayed in Table 8.4. Upon inspection, it can be seen that (π_2) is in fact the volume packing fraction. Additional Pi-terms of (π_3) and (π_5) highlight specifications of the ferrule housing, filament and plug in the form of hydraulic diameter and plug length in relation to filament length. The ratio of the resulting mean static and kinetic friction force can be seen in the form of (π_4), and the aspect of the dynamic displacement of the filament bundle is characterized by (π_1). These terms were used to establish a functional relationship in the form of universal curves, determined through the testing performed. It can be seen that the terms of (π_1) and (π_4) are in-fact a function of (π_2), (π_3) and (π_5) terms (Equations 8.6, 8.7).

$$\pi_1 = \frac{F_K \, L_F}{m_F v^2}$$

(Equation 8. 1)

$$\pi_2 = \frac{V_F}{V_A} = V_P$$

(Equation 8.2)

$$\pi_3 = \frac{D_{HYD}}{L_F}$$

(Equation 8.3)

$$\pi_4 = \frac{F_S}{F_K}$$

(Equation 8.4)

$$\pi_5 = \frac{H_P}{L_F}$$

(Equation 8.5)

$$\pi_1 = \pi_1(\pi_2, \pi_3, \pi_5)$$

(Equation 8.6)

$$\pi_4 = \pi_4(\pi_2, \pi_3, \pi_5)$$

(Equation 8.7)

Resulting Guideline Universal Curves. For the formulation of universal curves, (π_2), (π_3) and (π_5) represent the experimental inputs, while (π_1) and (π_4) signify the outputs. Upon further inspection, it was found that the term of (π_5) did not contribute significantly and was thus eliminated as a weak Pi-term variable. The remaining four Pi-terms were used to establish two distinct plots to serve as the design guideline.

Figures 8.3, 8.4 and 8.5 demonstrate individual plots of (π_3) Vs. (π_2) Vs. (π_1) of resulting universal curves created through a non-linear least square fit for ranges of low, medium and high volume packing fraction (V_P) respectively. As it can be seen, the x-axis of the plots resemble (π_3), the y-axis is (π_1), and curves are fit for constant values of (π_2) achieved through experimentation. The three curves shown here demonstrate a good R^2 value of the data fit.

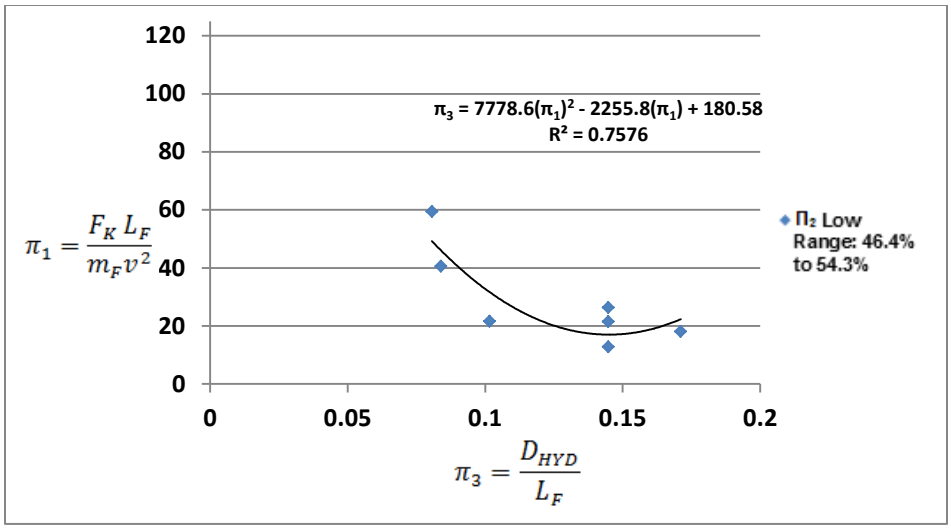

Figure 8.3 Established Universal Curve, (π_3 Vs. π_2 Vs. π_1); Low Volume Packing Fraction Range: 46.4-54.3%.

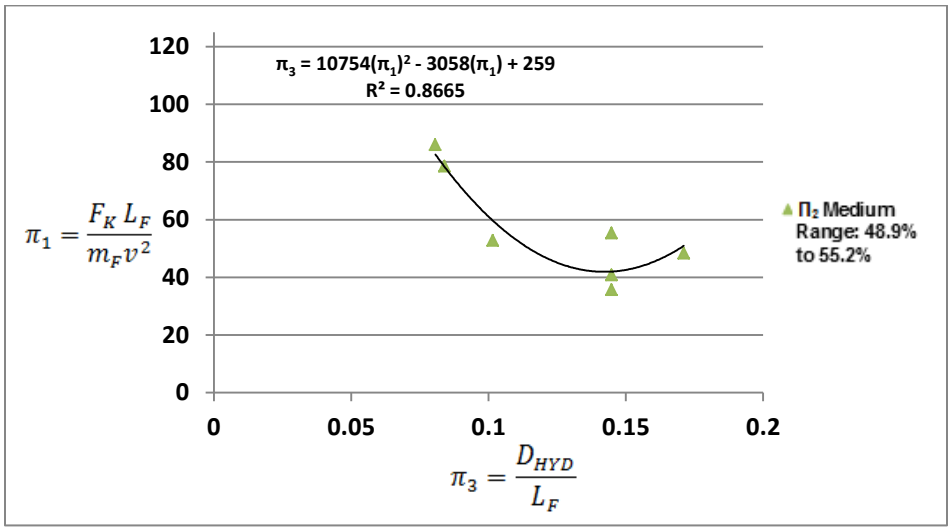

Figure 8.4 Established Universal Curve, (π_3 Vs. π_2 Vs. π_1): Medium Volume Packing Fraction Range: 48.9-55.2%.

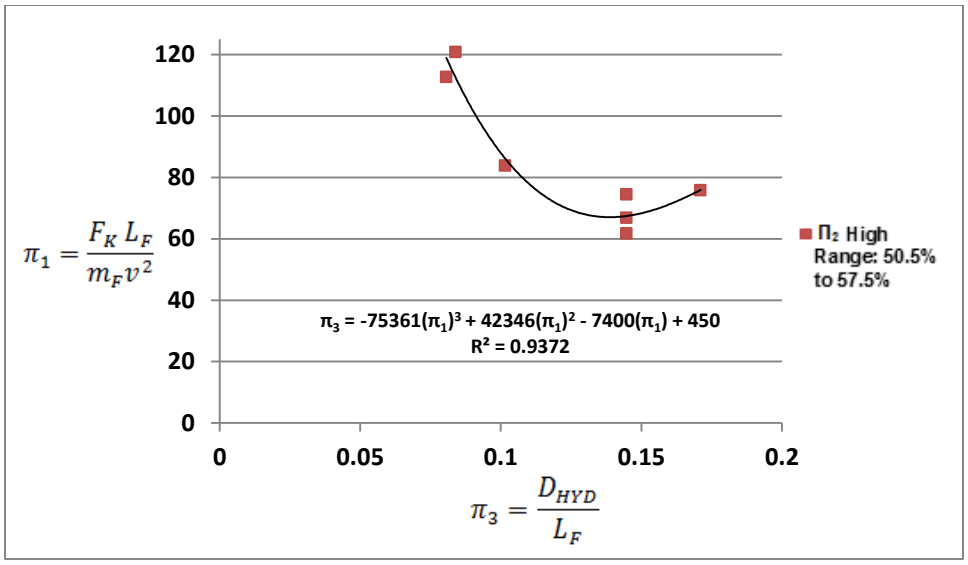

Figure 8.5 Established Universal Curve, (π_3 Vs. π_2 Vs. π_1): High Volume Packing Fraction Range: 50.5-57.5%.

Combination of these curves would further serve as a first plot of the design guideline shown in Figure 8.6 on the following page. The plot shown in Figure 8.7 (also on the following page), is in fact the second plot of the design guideline, where once again (π_3) is the x-axis, with (π_4) plotted on the y-axis. Likewise, a linear least square fit was used for the plot of (π_3) Vs. (π_4). Plots shown in Figure 8.6 and 8.7 demonstrate the proposed design guideline curves. It is expected that through the input of ferrule housing characteristics (π_3) and the desired volume packing fraction (π_2), the value of mean kinetic force within (π_1) would be calculated. Based on the value of mean kinetic force (F_K), mean static force (F_S) necessary to displace the filaments can be found through the plot of (π_3) Vs. (π_4), where the (π_3) term is known.

For Figure 8.6, the ranges for the volume packing fraction for low were 46.4-54.3%, for medium 48.9-55.2% and 50.5-57.5% for high.

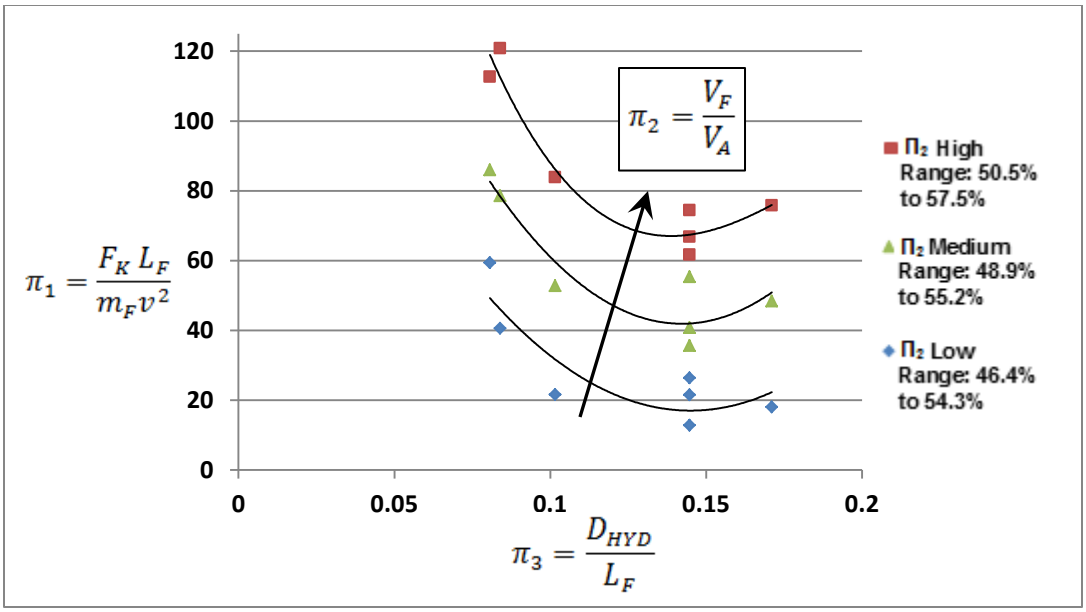

Figure 8.6 Established Universal Curves, (π_3 Vs. π_2 Vs. π_1).

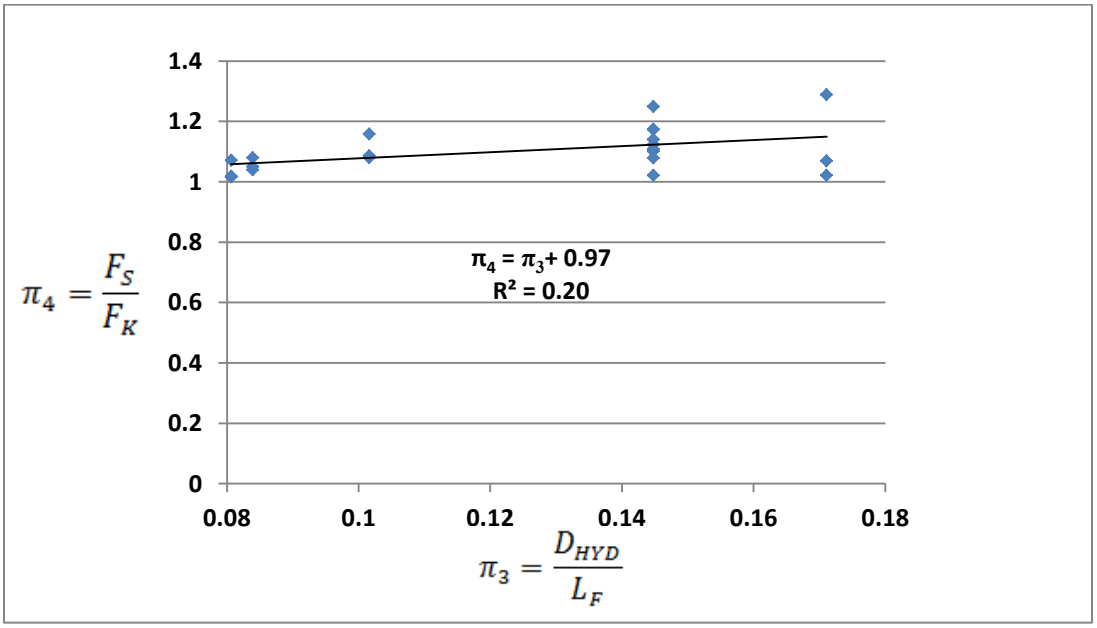

Figure 8.7 Established Universal Curve, (π_3 Vs. π_4).

At this time, it important to discuss the second plot of the design guideline seen in Figure 8.7, where it can be see that R^2 for the universal curve of (π_3) Vs. (π_4) was 0.2. It is recognized that R^2=0.2 demonstrates a data fit, where largest data spread on the plot has an error of 11%. However, it also important to establish that no such guideline currently exists, and in its preliminary form can serve as a useful correlation to create the estimate needed. From the testing performed, it is assumed that possible contributing factor to the error were floating variables associated with the knots tested as an assembly of components. To elaborate, the measurements of static friction were performed separately from the test for kinetic friction. In between, the knot as an assembly was repacked and re-settled. Due to this it is suggested that the location of the plug within filaments were a factor, which contributed to values of mean kinetic force (F_K) and mean static force (F_S) measured, thus resulting in a deviation seen by the ratio of $(\frac{F_S}{F_K})$. As noted previously, this guideline is meant to be preliminary, where it is suggested that further experimentation is performed.

A sample calculation is provided below to demonstrate how to use these universal curves to estimate a value of mean force required to overcome static friction (F_S).

Sample Calculation. The universal curves shown in Figures 8.6 and 8.7 can be used to create an estimate of the mean force required to overcome static friction, or other pertinent variables associated with the functional relationship established. In the case of an application in manufacturing environment, one can perform an estimate through knowledge of basic variables such as the velocity of displacement, filament density and filament length.

The following series of steps demonstrate the process to estimate mean force required to overcome static friction:

Step 1. Calculate the term of $(\boldsymbol{\pi_3})$ ***.***

i) For a combination of ferrule and plug, calculate the cross-sectional area between ferrule and plug (A),

ii) Find the total ferrule and plug perimeter (P).

iii) Specify the filament length (L_F),

iv) Calculate the value of the (π_3) term.

$$\pi_3 = \frac{D_{HYD}}{L_F} = \frac{\frac{4A}{P}}{L_F}$$

Step 2. Estimate Desired Volume Packing Fraction and Calculate $(\boldsymbol{m_F})$***.***

i) Using Figure 8.6 define the desired range of volume packing fraction,

ii) Calculate the mass of filament bundle (m_F) using known values of (A) (calculated in Step 1), filament density (ρ_F), and (L_F).

iii) Estimate a value of volume packing fraction (V_P) desired.

$$V_P = \frac{V_F}{V_A} = \frac{\frac{\rho_F}{m_F}}{A(L_F)}$$

Step 3. Retrieve Value of $(\boldsymbol{\pi_1})$ ***and Calculate*** $(\boldsymbol{F_K})$.

i) Using the correlation provided by the master curve and knowledge of (V_P) and (π_3), retrieve a value of (π_1) using Figure 8.6.

ii) Calculate the mean kinetic friction force (F_K) using known values of (L_F), (m_F) and velocity of filament bundle displacement v.

$$\pi_1 = \frac{F_K \, L_F}{m_F v^2}$$

Step 4. Retrieve $(\boldsymbol{\pi_4})$ ***and Calculate*** $(\boldsymbol{F_S})$.

i) With (π_3) as a previously established value, use the correlation provided by Figure 8.7 to retrieve a value for (π_4).

ii) With (F_K) calculated from the previous step, solve for the value of mean force required to overcome static friction (F_S).

$$\pi_4 = \frac{F_S}{F_K}$$

8.2.2 Guideline for Design of Gripper Plates

As described within the study, an innovative approach to angle trim forming has been accomplished, where in order to create the angle trim form, filaments were gripped, displaced and rotated. Although gripping of filament bundles or equivalent structures is common within the industrial and scientific communities, to our knowledge no guidelines exist to efficiently grip such bundle assemblies. As a result, multiple notions for gripping were examined within this study, where the focus was further placed on modular gripper plates that would serve as an interface between the gripper jaw mechanism and the filament bundle as was shown for angle trim forming subsystem. Well-designed grippers can increase throughput, improve system reliability, compensate for machine inaccuracy, and perform value-added functions to the assembly [7]. The work introduced in this section builds on lessons from the design study performed. Assuming symmetric or "parallel" motion of gripping, the author would like to propose a set of design guidelines that can be used to develop effective gripper plates. A design of gripper plates satisfying the design guideline is introduced, where the gripper designed was for a flat filament bundle type associated with knot manufacturing.

Motivation for establishing the design guidelines builds on the absence of such design guidelines with hopes of benefiting manufacturing and automation industries as well as scientific communities. More importantly, the author would like to further contribute to improvement of the current knot assembly automated process lacking reliability, precision and efficiency. This further results in higher knot production time, decreased knot quality and extended cost due to scrap.

Design Guidelines. The following guidelines have been formed through examination performed in this design study. It is important to note that examination was performed using bundles of hair-like filaments associated with manufacturing of paint brush knots. However, the guidelines introduced here can also be used for gripping applications of other filament bundle types. The study assumes symmetrical or parallel clamping action of filament bundle performed by a gripper mechanism, where especially designed plates for gripping are used as a form of modular end-effector interface. Examples of gripper plates modeled as well as fabricated are provided to demonstrate satisfaction of the design guidelines for gripping of flat-oval shaped filament bundles. Eight proposed design guideline criteria are as follows:

1) Create Symmetrical Design: Establish a filament gripper plate design, such that duplication of a single plate (Figure 8.8(a)) will yield a pair of gripper plates required to symmetrically grip the filament bundle (Figure 8.8(b)). This will yield shorter manufacturing time and lower manufacturing cost as well as resulting in symmetrical gripping action of filament bundle.

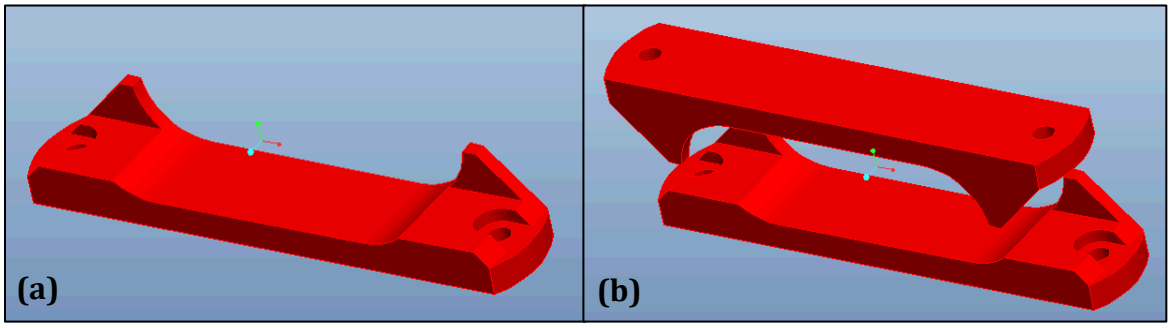

Figure 8.8 Example of Symmetrical Gripper Plate Design:
(a) Single Gripper Plate;
(b) Arrangement of a Pair of Gripper Plates, Simulating Gripping of Filament Bundle.

2) Minimize Filament Gripper Footprint: Depending on the application, the best case is to optimize the size of the gripper plates such that the overall foot print is minimized. Smaller gripper plate design can yield a higher through-put of the system with more clearance for motion as well as ease of gripper mechanism design and lower manufacturing cost.

3) Maximize Contact Patch Area: Maximizing the area of contact between the gripper plate surface and filament bundle is recommended to achieve higher friction characteristics of filament bundle clamping. Resulting improvement may lead to lower requirement for compression force as well as surface finish characteristics of gripper plates during manufacturing. If possible, design the shape of the gripper plate to compliment the shape of the filament bundle, where a recess can also be created to increase the area of contact as demonstrated by Figure 8.9.

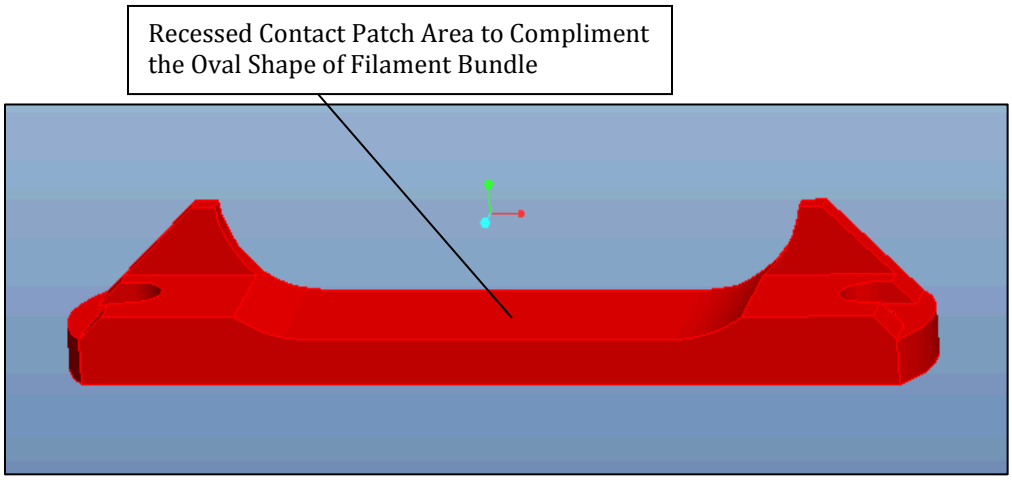

Figure 8.9 Example of Contact Patch Design.

4) Improve Friction of Contact Patch Surface: In most cases, secure filament bundle clamping will require moderate friction between filaments and gripper plates. To improve the friction characteristics of the contact patch surface it is best to add a coating or a layer of foam polymer. For filament bundles in relation to knot manufacturing, EPDM extra-soft Type polymer (Hardness: Shore-A 40-90) was found to work the best. Figure 8.10 demonstrates a gripper plate fabricated and coated with EPDM extra-soft polymer. When gripped, the additional polymer layer due to its high elasticity compresses and allows better encompassing the porous walls of filament bundle. Use of the polymer also creates a soft buffer interface, which helps to eliminate possible filament damage due to compression. Figure 8.10 shows an example of a gripper plate fabricated through rapid prototyping using ABS plastic.

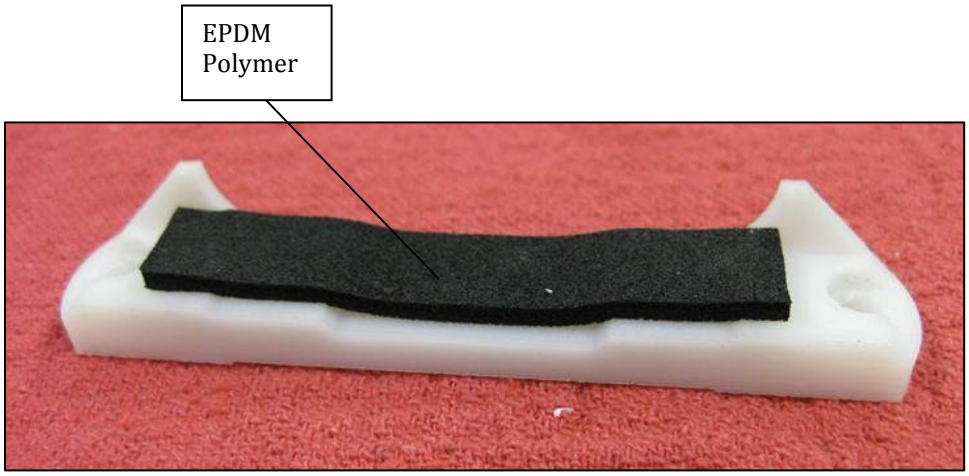

Figure 8.10 Fabricated Gripper Plate Design Coated with EPDM Polymer.

5) Prevent Filament Flaring under Compression: During compression of a filament bundle, flaring of filaments is common as the compression force drives the filaments to escape along the edges of the gripper plates (Figure 8.11(a)). Due to flaring, density of filament bundle is decreased with possibility of non-uniform distribution of compression force. Possible damage to filaments may also occur due to filament escaping. To prevent flaring, adding side-walls is recommended to constrain the filament bundle to its existing cross sectional shape when compressed (Figure 8.11(b)). Figure 8.12 shows an example of a clamped bundle using the gripper plate design shown in Figure 8.11(b) without flaring.

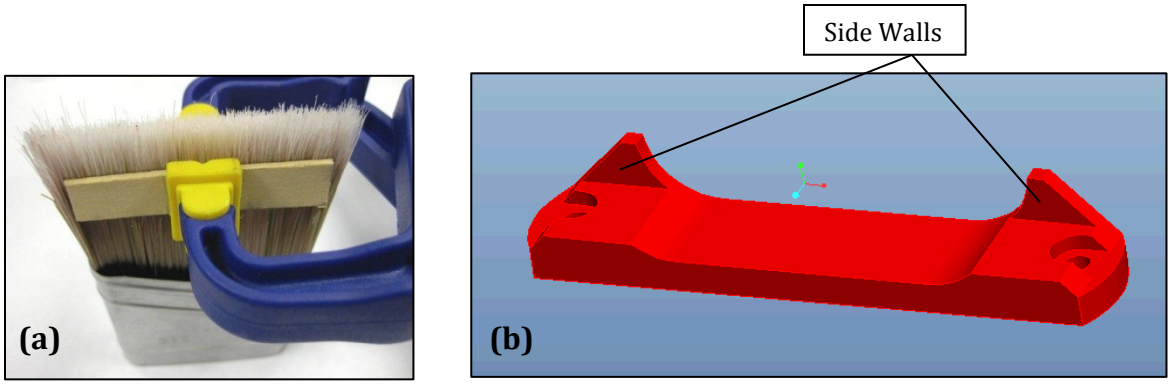

Figure 8.11 (a) Example of Filament Bundle Flaring Under Compression; (b) Concept of Side-walls to Prevent Flaring.

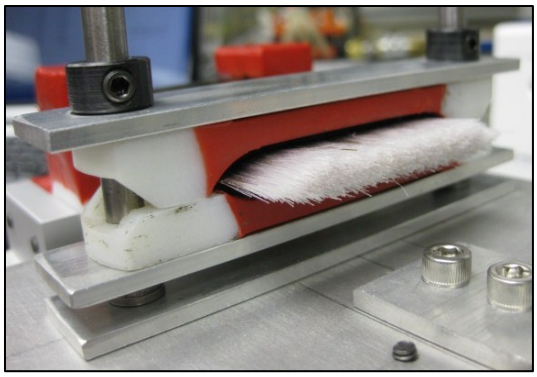

Figure 8.12 Example of Filament Bundle Clamping without Flaring.

6) Optimize Side Wall Design: Create side walls on side of the gripper plate to allow the gripper plate combination to be offset (Figure 8.13(a)) to fully constrain the filament bundle shape depending on the filament bundle thickness. Optimize height of sidewalls to minimize the stroke of clamping action without collision during filament bundle insertion; make sure enough height is present to constrain all of filaments. Minimize side wall thickness, which will minimize the offset distance between two gripper plates (Figure 8.13(b)). To help guide filament into the desired form during compression and to maintain the filament bundle shape, chamfer or round the edges of the side walls.

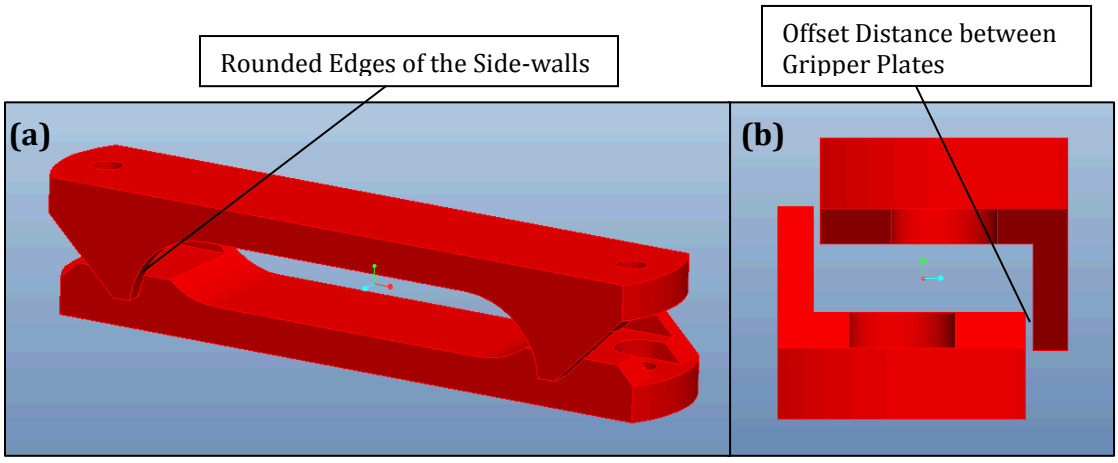

Figure 8.13 Offset Alignment of Gripper Plates:
(a) Pair of Grippers Offset as Shown in Isometric View;
(b) Pair of Grippers Offset as Shown from Side-View.

7) Flat Type Mounting: Ensure that the mounting surface of the gripper plate to the gripper mechanism is flat (Figure 8.14) to distribute the force of compression uniformly through-out the width of the filament gripper plate. Uniform compression force will promote the reliability of holding the filament bundle without slipping.

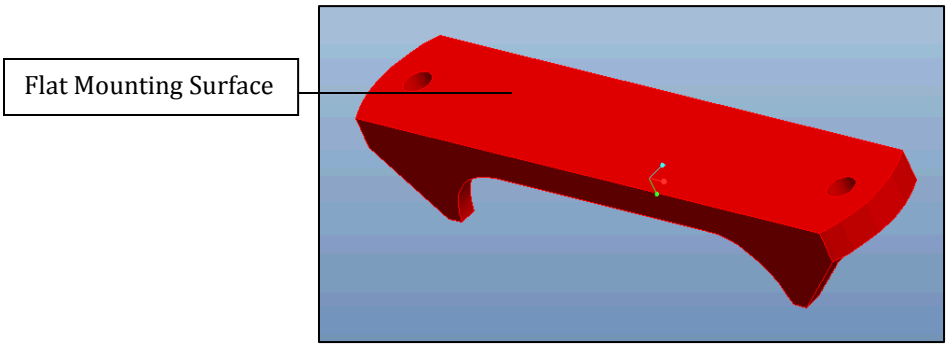

Figure 8.14 Flat Mounting of Gripper Plate.

8) Ease of Mounting: Incorporate mounting hardware to minimize the number of fasteners. In most cases, two fasteners on the outmost edges of the gripper plate located at the center of the gripper are all that may be needed (Figure 8.15). To optimize the size of filament gripper plate, create recessed pockets for mounting hardware. If different modular designs of grippers were designed to be interchanged, quick-release pin (or snap fits) mechanisms are recommended for fastening.

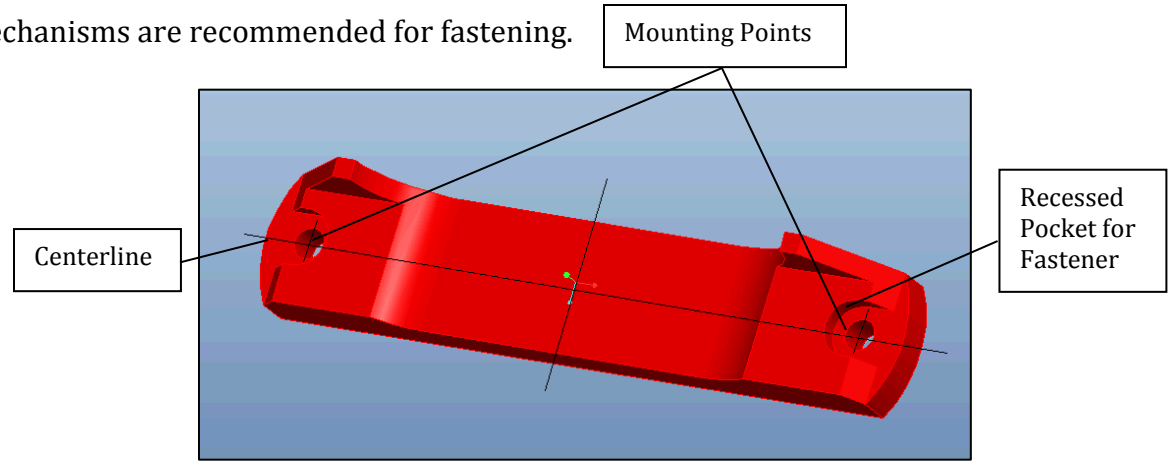

Figure 8.15 Location of Fastener Mounting Points.

8.3 Additional Work Accomplished

To complete the knot assembly process discussed in the functional decomposition (Figure 3.1) of Chapter 3, subsystems of filament density assessment, knot input, knot transfer, filament vibration tip-profile forming and knot output have also been developed through the process introduced in this study. The subsystems were taken from conceptualization stages to detail design to finalized subsystem design models. Based on final design models generated, subsystems were integrated together to simulate process assembly using 3D CAD solid modeling, and troubleshoot if necessary. After the design showed to be successful, documentation necessary for component purchase, component manufacture, assembly and operation of the system was prepared as demonstrated previously. Resulting documentation was then handed over to the sponsor for system manufacturing.

Figure 8.16 shows the design of the developed "Automated System for Knot Processing" in its final form.

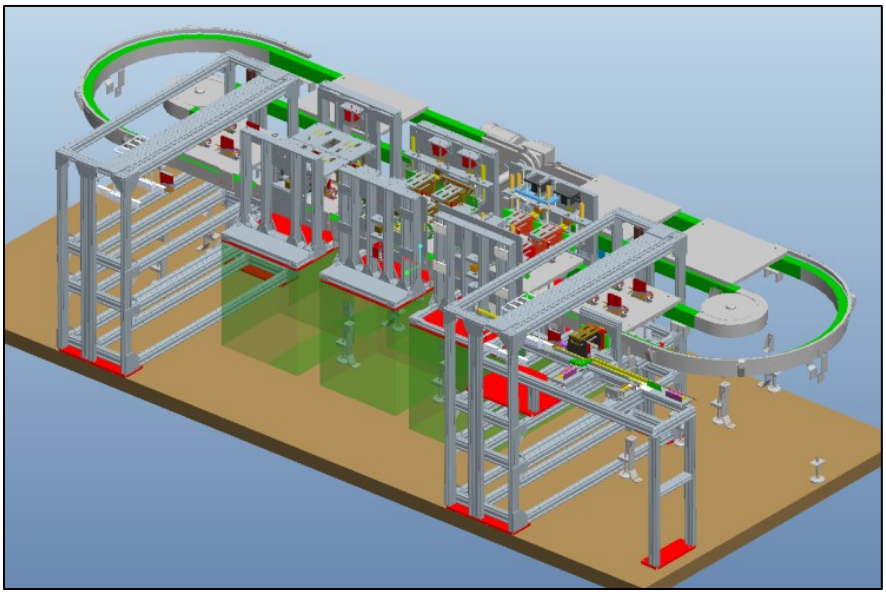

Figure 8.16 Automated System for Knot Processing.

The system offers the capability of processing both, angle and flat trim brushes. In the form shown in Figure 8.16, six subsystems were integrated together to produce an assembly system of 14 feet in length and 6 feet in width at a working table height of 2 feet and 5 inches to satisfy all of the required target specifications specified in Chapter 2.

To meet the required production rate with sufficient time for knot input, transfer, processing and output, the system structure was established where four knots are processed at one time, resulting at a production rate of four knots every eight seconds or 30 knots/min. In order to satisfy this requirement, a design of a transfer subsystem was developed by closely working with FlexLink Conveyor Systems Inc. Figure 8.17 shows the transfer subsystem , where a working surface or a "pallet" is used to hold and transfer four knots between individual subsystem processes. The architecture of the transfer subsystem is in an oval shape as seen in Figure 8.17 to offer processing of knots loaded on pallets on one straight leg of the oval shape (five pallets in the figure depict a station for each subsystem process) and recirculation of empty pallets on the other straight leg of the oval subsystem.

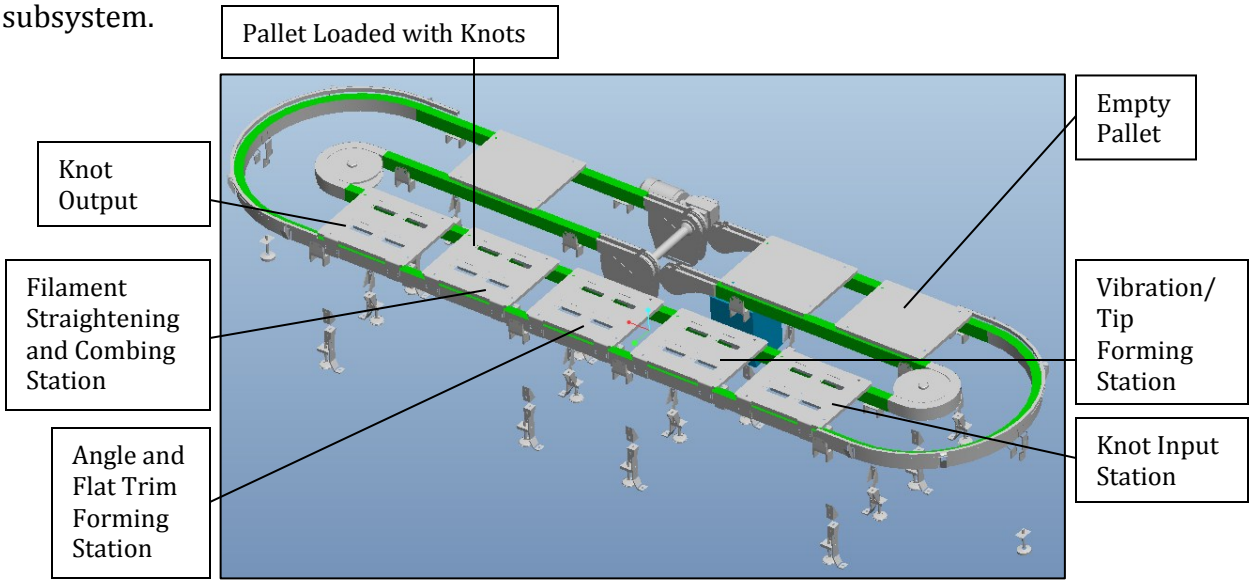

Figure 8.17 FlexLink XTQ52 Model Transfer Subsystem as Modeled in Pro-Engineer.

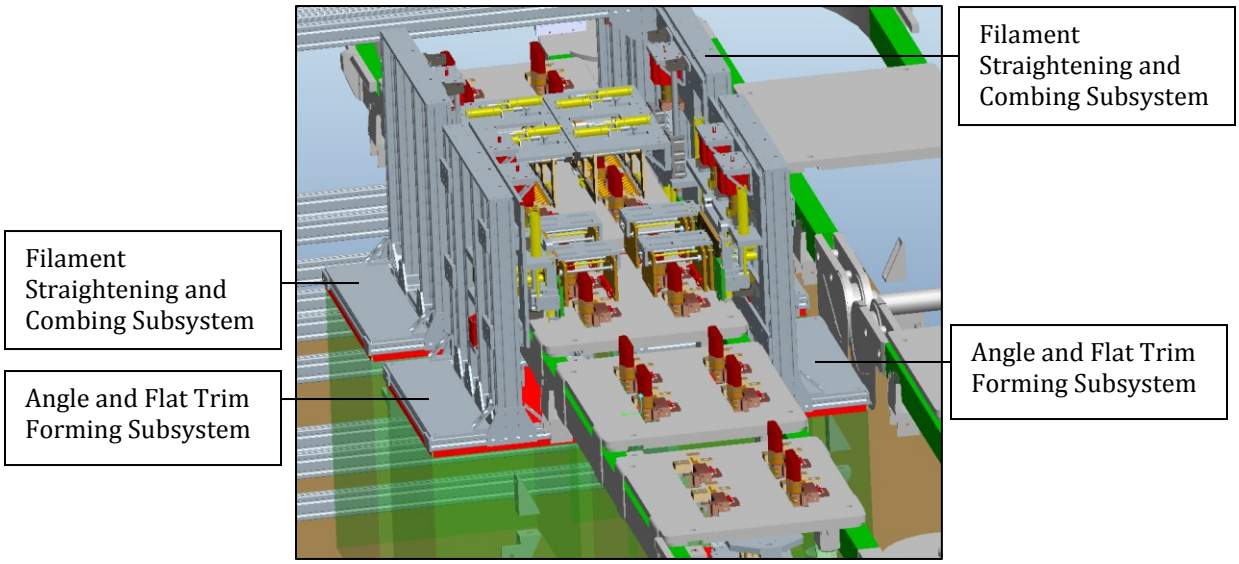

Figure 8.18 Subsystem Integration and Alignment for Knot Processing; (Also shown in Figure is the Vertical Alignment of Knots on the Pallet).

For each subsystem process, the pallet is able to precisely translate, stop and lock in X, Y and Z degrees of freedom at each subsystem station shown in Figure 8.17. Figure 8.18 demonstrates a pair of pallets arriving at the angle trim and filament straightening process stations. As it can be seen, final design models of core subsystems were duplicated to integrate within the transfer subsystem to process a pair of knots on each side of the pallet, resulting in simultaneous production of 4 knots per subsystem process. Additional subsystems not shown are filament density assessment, input, filament vibration and tip forming, and output subsystems. The following section further describes the established design for such subsystems and supplementary subsystems needed to complete the automated method of knot processing.

Process Description. In order to undergo automated knot processing, it is expected that knots from the knot making machine (already in the factory) would be loaded manually in multiples into the automated knot processing system. Loading of knots would occur in the first subsystem of filament density assessment, where individual knots would be assessed for density of filaments. If the density is satisfactory, the knots are picked up by an input subsystem and loaded onto an empty pallet of the transfer subsystem. As shown in Figure 8.17, the transfer system design was performed to accommodate a separate station for phases of knot input and output. At the phase of knot input onto the pallet, knots are placed on the pallet and locked in place. After the knots are secured on the pallet, the pallet would translate through individual subsystem processes of filament vibration and tip forming, angle and flat trim forming, and filament straightening. To process the knot at each subsystem, the pallet would stop with precise location relative to the subsystem and lock in X, Y and Z degrees of freedom. At this time, processing would occur around the stationary location of the knot. When the processing is complete, pallets would proceed to the knot output station, at which time knots would be released and moved from the pallet to a (epoxy filling machine) conveyor by an output subsystem. To repeat the process, the empty pallet would then recirculate back to the input subsystem.

Prior to processing, the system would be pre-adjusted by an operator, where individual settings of subsystems would be adjusted based on the recipe of the knot in production. After the adjustments have been made, loading of knots would occur at the first subsystem of filament density assessment shown in Figure 8.19 (on the following page). With reference to the figure, it is expected that knots would be manually inserted in

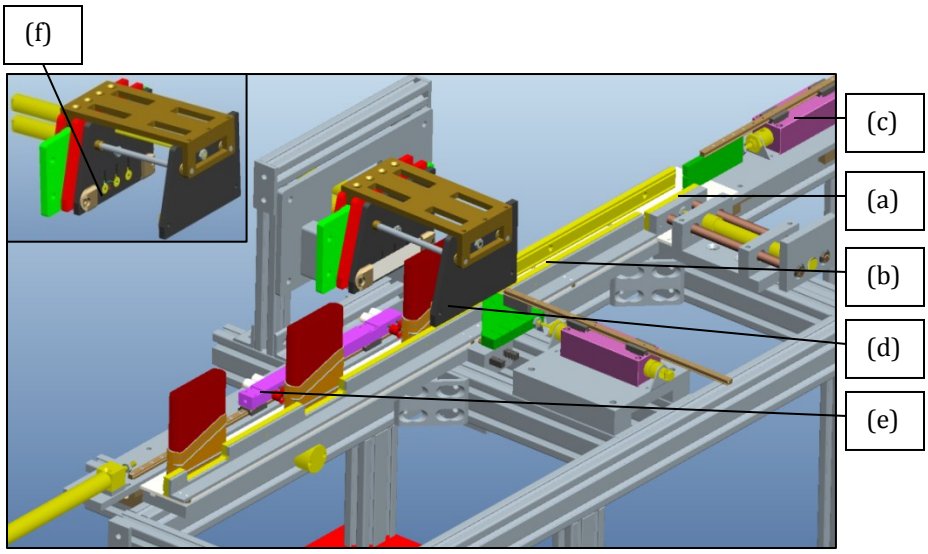

Figure 8.19 Filament Assessment Subsystem:
(a) Spring Actuated Loading Table;
(b) Feeding Tunnel;
(c) Indexing Actuator;
(d) Filament Density Assembly;
(e) Suction Cup Dog Mechanism;
(f) Load Cells.

multiples into a spring-actuated loading table (Figure 8.19(a)). From the loading table, one by one, the knots are fed through the feeding tunnel (Figure 8.19(b)) using an indexing actuator (Figure 8.19(c)) to a filament density assessment assembly (Figure 8.19(d)). Using a jaw subassembly, individual knots are assessed for filament density, where calibrated load cells (Figure 8.19(f)) within jaw plates are used to measure the spring force associated with squeezing of filament bundle upon clamping of bundle. From comparison to a calibrated value based on the required density, the knot is accepted or rejected with a visual warning to an overlooking operator. If accepted, the knot is translated by a suction cup dog mechanism (Figure 8.19(e)), where through proper timing, knots are accumulated to be picked up in two separate pairs and inserted by the input subsystem onto an empty pallet.

Figure 8.20 on the next page shows the concept of the input subsystem, where by using suction cups (Figure 8.20(a)), two separate pairs of knots (Figure 8.20(b)) are picked up, raised vertically and translated over to an awaiting empty pallet of the transfer

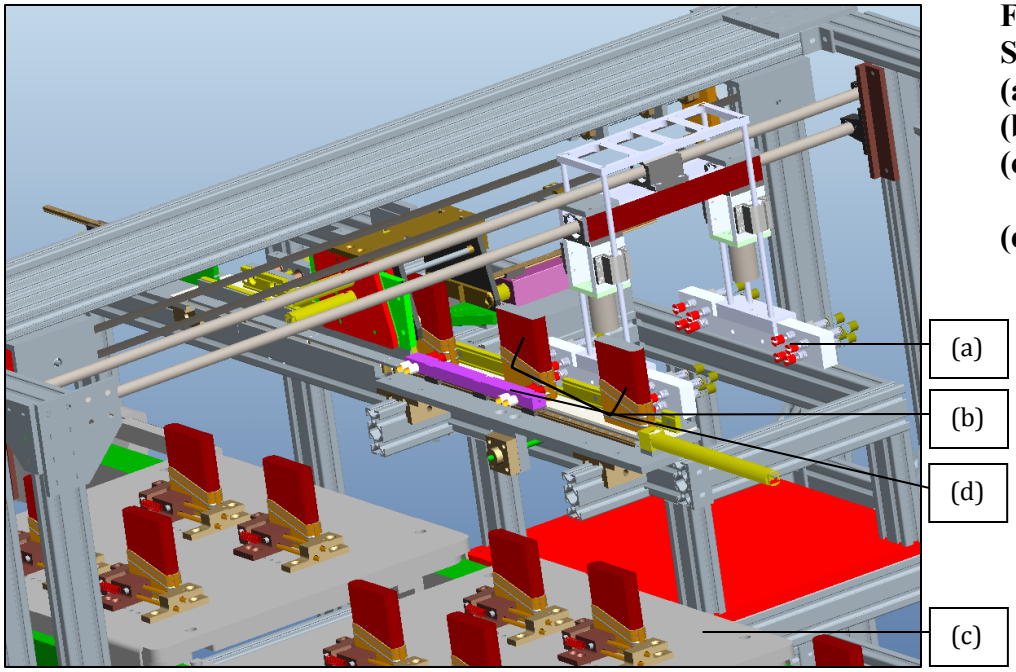

Figure 8.20 Input Subsystem:
(a) Suction Cups;
(b) Pair of Knots;
(c) Loaded Pallet With Knots;
(d) Suction Cup Dog Mechanism.

subsystem. The pallets of the transfer subsystem have been modified to accommodate processing of the knots. Arrangement of the knots on the pallet can been in Figure 8.20(c), where four knots are input by a transfer system in a vertical alignment. To hold knots securely and to allow filament tip profile forming through vibration, pallets were modified with cavities (Figure 8.21(Left-a)) and mounting holes to accommodate modular knot holding mechanisms shown in Figure 8.21(Right).

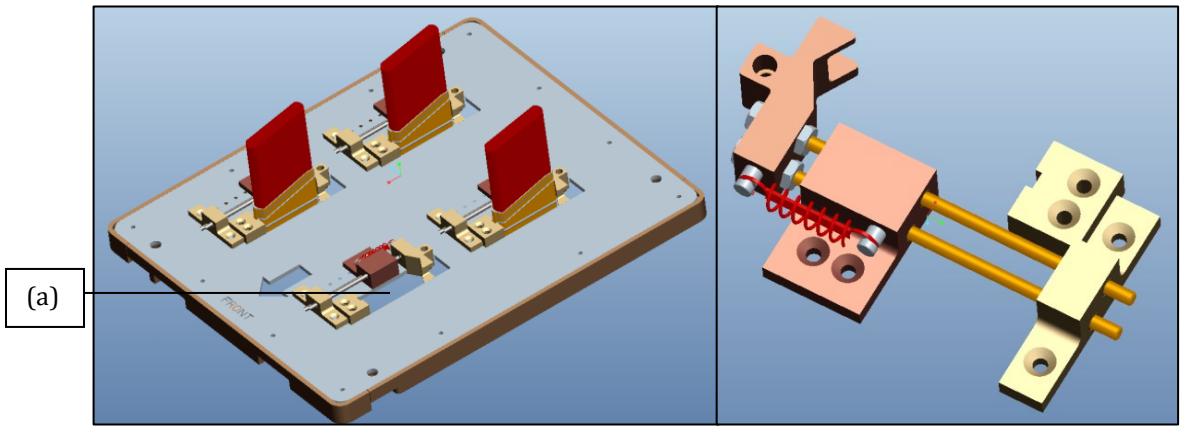

Figure 8.21 (Left) Pallet with Locked in Place Knots:
(Right) Knot Holding Mechanism;
(a) Cavity for Vibration/Filament Tip Forming from Bottom.

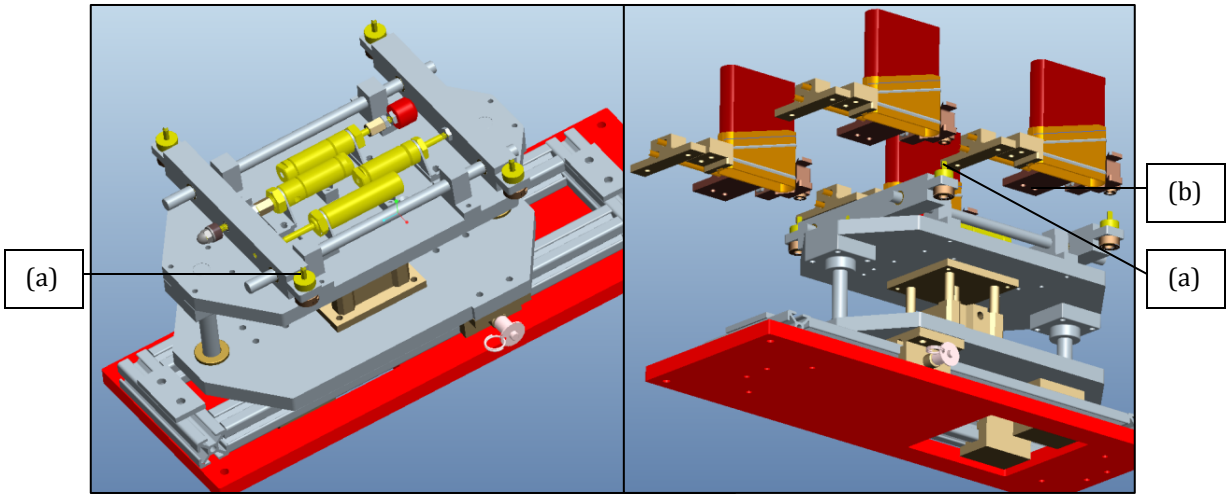

Figure 8.22 Knot Lock and Release Subsystem:
(Left) As shown from Top; (Right) As shown from Bottom of Pallet (Pallet Hidden);
(a) Locating Pin; (b) Knot Holding Mechanism.

The mechanisms were designed to hold the knots through a spring loaded device (Figure 8.21(Right)), regardless of ferrule shape or thickness. In order to open or close the mechanisms, an additional knot release subsystem was designed as shown in Figure 8.22. The subsystem is placed underneath the pallet at the input and output phases of knots. Upon input of knots onto the pallet, the knot holding mechanisms are opened by the knot release subsystem, where locating pins (Figure 8.22(a)) are inserted into the knot holding mechanisms (Figure 8.22(b)) on the pallet, and translated to open the mechanism.

When the knot holding mechanisms are open, the knot is lowered by the input system into the cavity and then locked in place by the release of the spring. When four knots are input and locked in place, the pallet transfers the knots to a vibration and filament tip forming subsystem. Shown in Figure 8.23 are two vibrating filament tip forming subsystems mirrored across to process a pair of knots on each side of the pallet (pallet and transfer subsystem hidden). Supporting vibration table subassemblies (Figure 8.23(a)) have been designed as see in the figure.

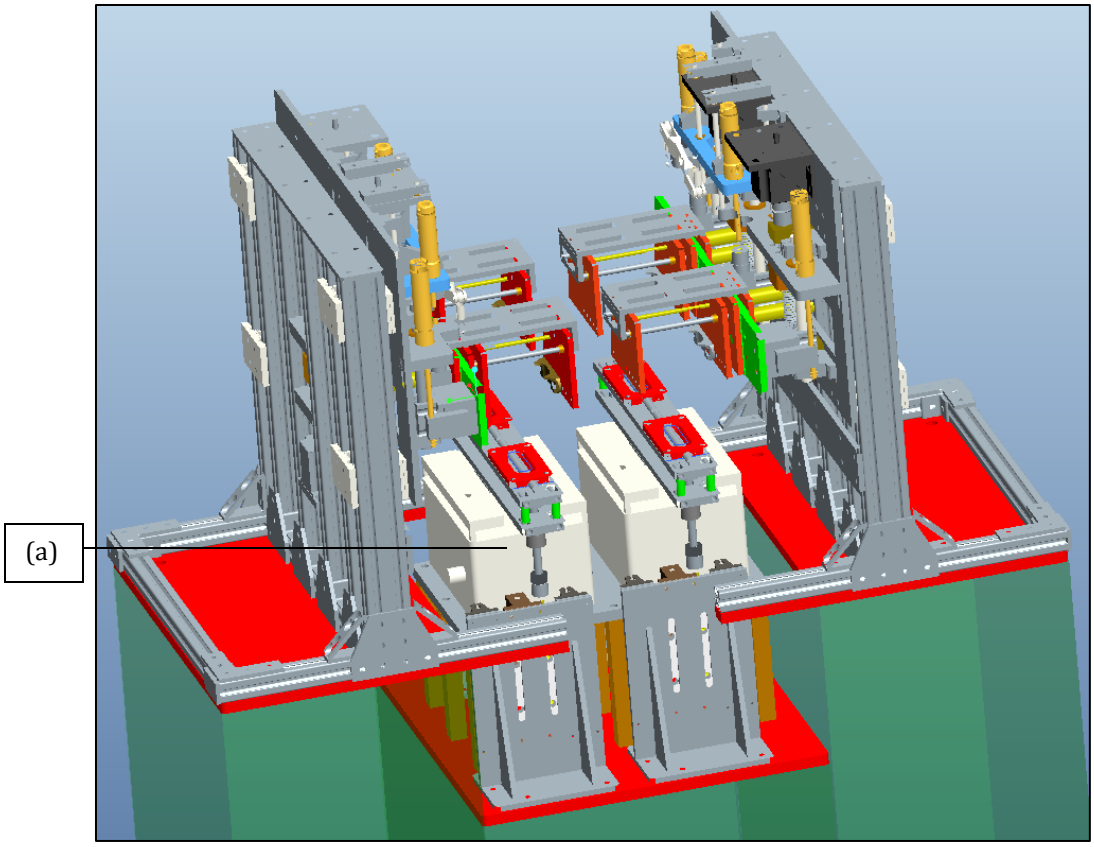

Figure 8.23 Vibration and Filament Tip Forming Subsystems:
(a) Vibration Table Subassembly.

To create a chiseled or a flat trim, a pallet loaded with knots would arrive, stop and lock in place. During the tip forming process performed by the subsystems, the filaments are (1) gripped, (2) translated down from the ferrule (through the cavity in the pallet) onto the vibration table below, (3) filaments are released and settled through vibration, and (4) the filaments are gripped and translated up into the ferrule. The filament tip forming process is complete as the pallet is released and transferred over to angle and flat trim forming subsystem and filament straightening subsystem. Likewise, for each process, the pallet is stopped and locked in place as the knots are processed for the type of trim desired and straightness necessary to meet the specifications.

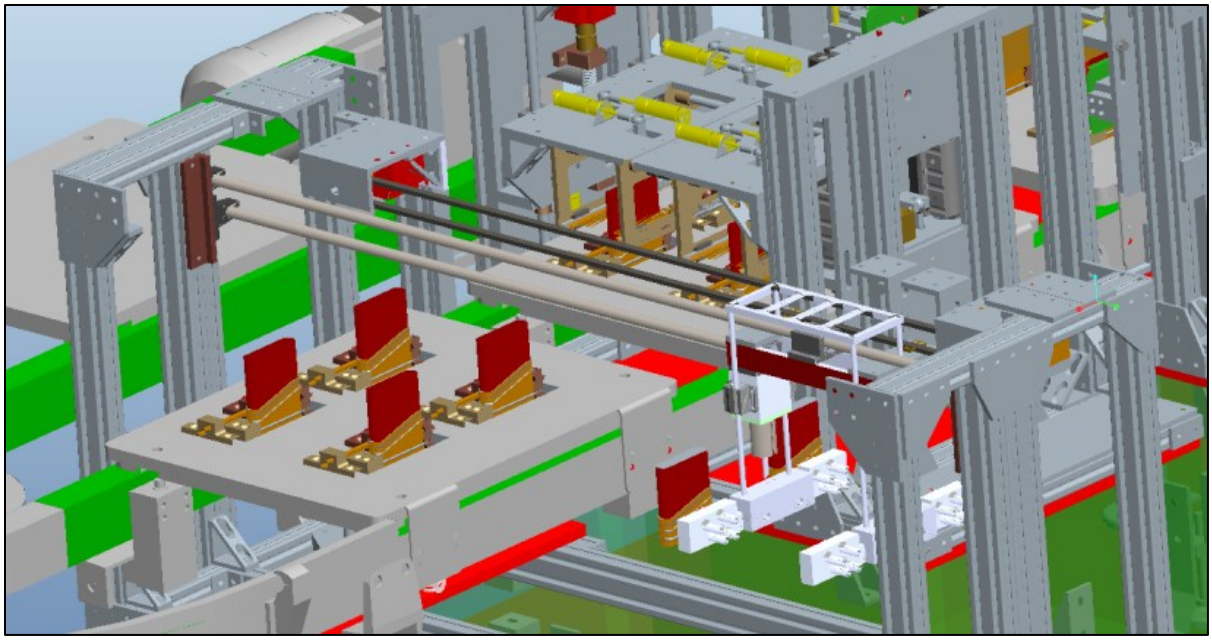

Figure 8.24 Output Subsystem.
(Epoxy Filling and Curing System Conveyor not Shown)

After angle or flat trim forming and filament straightening has been performed, the pallet arrives at the output subsystem shown in Figure 8.24. Much like the input subsystem, the knots are picked up through suction cups. The knot holding mechanism of the pallet is released (by the knot release subsystem) as the knot is transferred from the pallet to an awaiting conveyor (Figure 8.24) as a part of epoxy filling and curing system. This completes the automated knot processing.

In Figure 8.25 (on the next page), the complete system design can be seen again to perform the order of knot processing as just described.

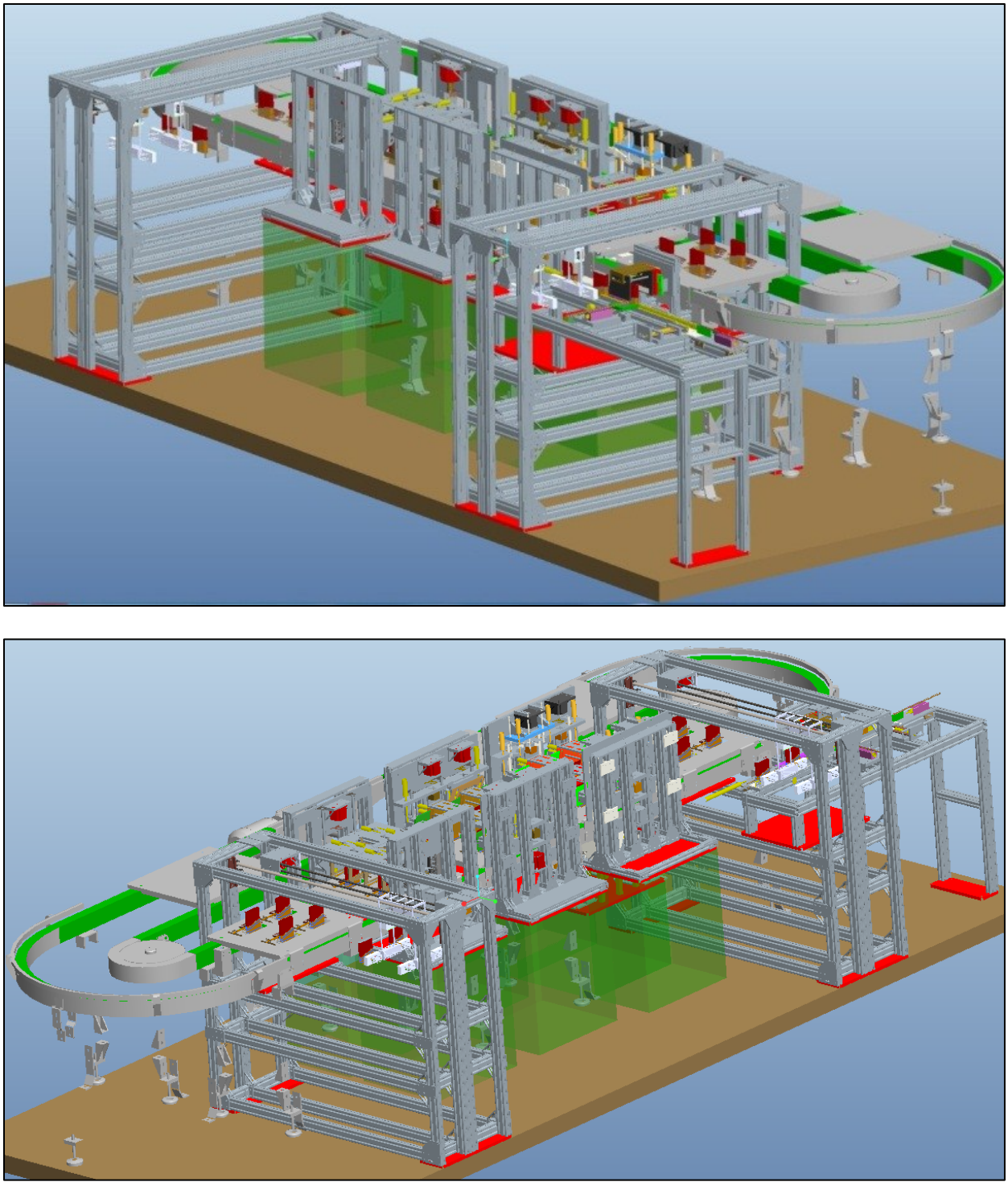

Figure 8.25 System Design for Automated Knot Processing: Isometric View 1; Isometric View 2.

Chapter 9: Conclusion and On-going Work

Conclusion. In forgoing sections, the development process for automated assembly system to process paint-brush knots has been described. Focus was placed on a design study of core subsystems of angle trim forming and filament straightening. For individual subsystems, steps of formulating system needs and specifications, functional decomposition and concept development, testing for design parameters, system detail design, prototype fabrication and testing, and subsystem refinement were introduced. Fabricated physical prototypes for both subsystems were developed and tested, where results from testing demonstrated that the design developed for each subsystem can achieve quality much higher than the traditional hand-made brushes with nearly doubled productivity.

As a result of the design study, the need for automation of angle trim forming process was satisfied. As to our knowledge, no prior automated method for angle trim forming has been accomplished, with worldwide assembly of angle trim knots occurring only through manual operation, resulting in poor product quality and production rate. Significant improvement of angle trim quality was demonstrated as a result of an innovative design established within this study. A distinctive method to angle trim forming was found through pure actions of gripping filaments, pulling to achieve required displacement and rotating to create the angle trim. With no dragback present, this method eliminates the need for a gauging block and the associated cost of gauging block manufacturing. Furthermore, the design eliminates effects of ferrule manufacturing tolerance issues on knot quality.

Additional design guidelines developed as a part of the study were presented for the purpose of global application to better benefit the scientific and industrial communities. Likewise, no design guidelines currently exist for methods of gripping filament bundles or estimating the pulling force required to displace such bundles. From experience gained through the development process as well as testing conducted, guidelines for design of gripper plates to properly grip filament bundles as well as preliminary characterization of the pulling force required to cause displacement of nylon synthetic filaments within varying housings were established. Gripper plates designed using the stated guidelines have been constructed and are being successfully used in subsystems developed in this study. Design guidelines performed through extended testing are expected to benefit manufacturing automation industries, involving manufacture of toothbrushes, hair brushes and other products. For a range of filament packing densities, developed design guideline master curves can be used to estimate the pulling force required to displace nylon filament bundles within a ferrule housing based on the known factors of the housing geometry.

To accommodate knot processing in an automated fashion, full system design was also established and introduced. Development process demonstrated in this design study was performed for other subsystems to complete such assembly system design. The established design approach demonstrates that the system would increase product quality, and improve the production rate while satisfying provided target specifications.

On-going Work. To effectively run the assembly system, logic and system electronic control design through Allen Bradley and SMC Pneumatics Inc. has been initiated and is expected to be completed in the upcoming term to finalize project development.

Manufacturing and assembly of final subsystem design models (Figure 9.1) has also been initiated and would require full execution further performed by the sponsor. Upon full completion of manufacturing, assembly and electronic control, the sponsor is responsible for installation of the completed system onto the factory floor to initiate the automated knot processing.

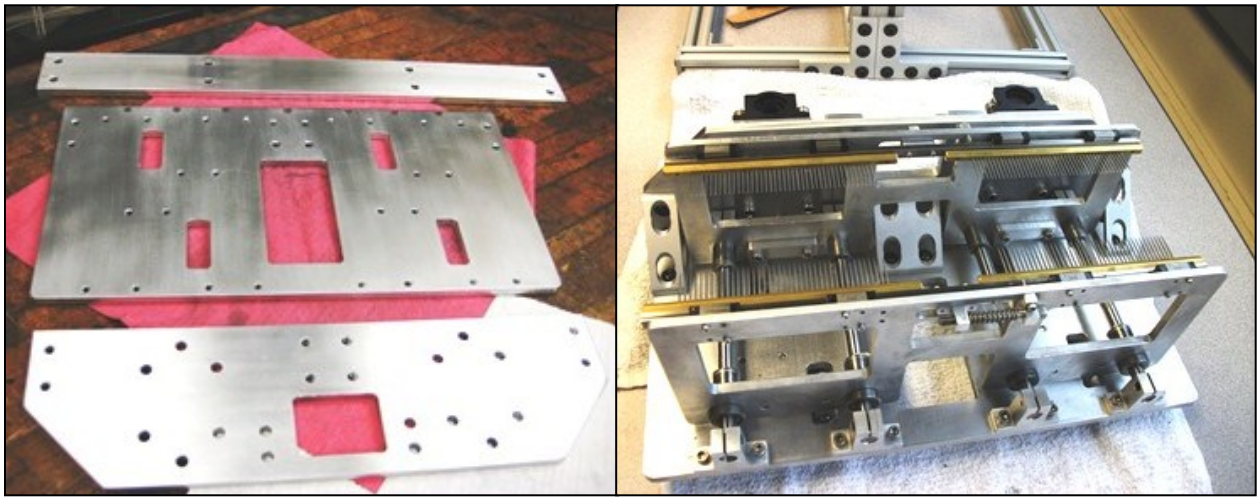

Figure 9.1 Assembly of Filament Straightening and Combing Final Design Subsystem: (Left) Manufactured L-frame Plates for Combing Head Assembly; (Right) Assembled Combing Head Assembly.

Professional Acknowledgements

The author would like to gratefully acknowledge the funding provided by the Maryland Industrial Partnerships (MIPS) program, Maryland Technology Development Corporation (TEDCO), Maryland Technology Extension Service (MTES), and Rubberset/Sherwin Williams Company to support this research.

A big thank you must also go out to Ronnie Giest as a MIPS coordinator, Fadi Khalifeh and Steve King as overlooking engineers from Rubberset/Sherwin Williams Company, along with Bill O'Donnell from FlexLink Conveyor Systems.

Last but not least, the author would like to acknowledge with his outmost deepest appreciation the hard work that has performed by students assisting with this project to make it possible. Those students are: Chris Bunai, James Kromer, Esteban Echeveria, David Chang, Erik Levin, Babak Eslami, Andy Oles, and Azhar Bahrainwala.

Appendix A

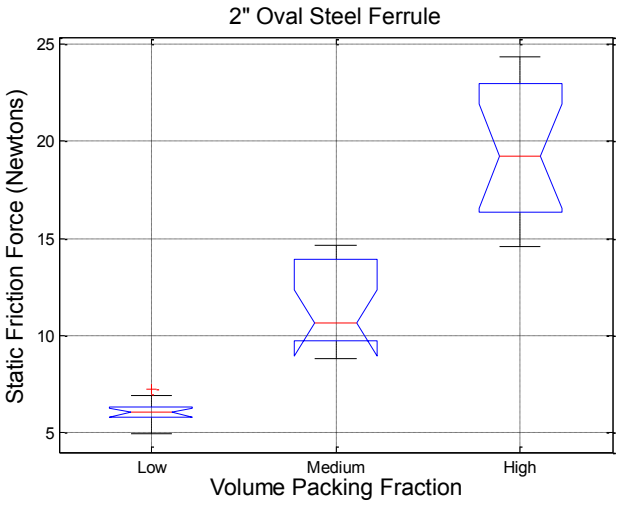

a)

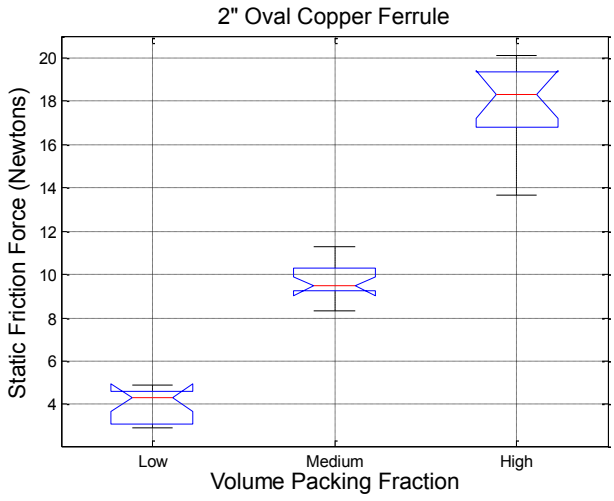

b)

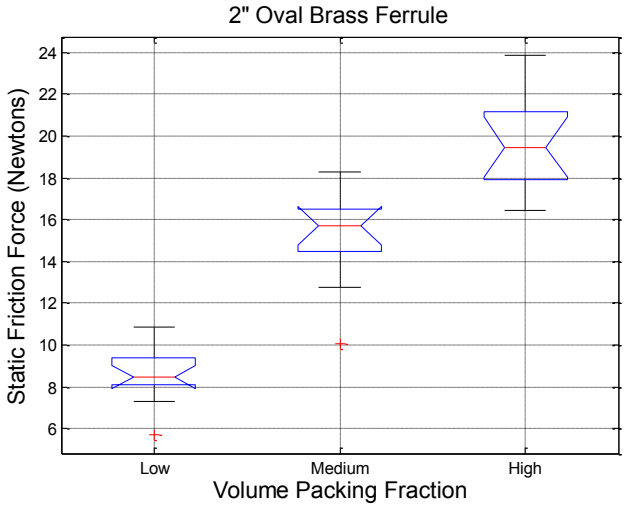

c)

Comparison of Means Achieved Using Different Volume Packing Fractions for Ferrule Material Types of:

a) Stainless Steel;
b) Copper;
c) Brass;

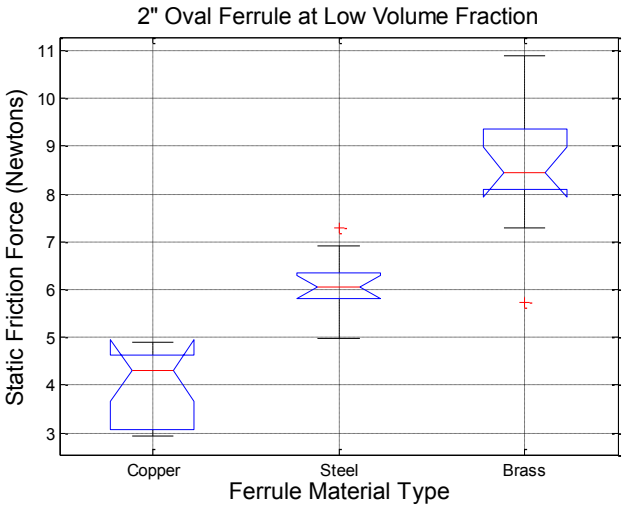

a)

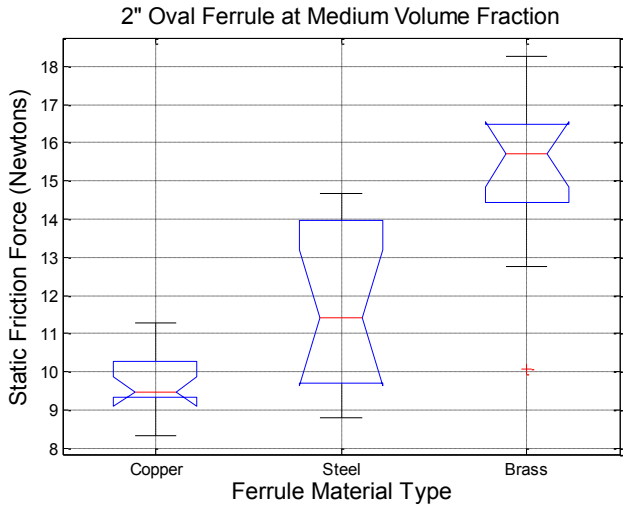

b)

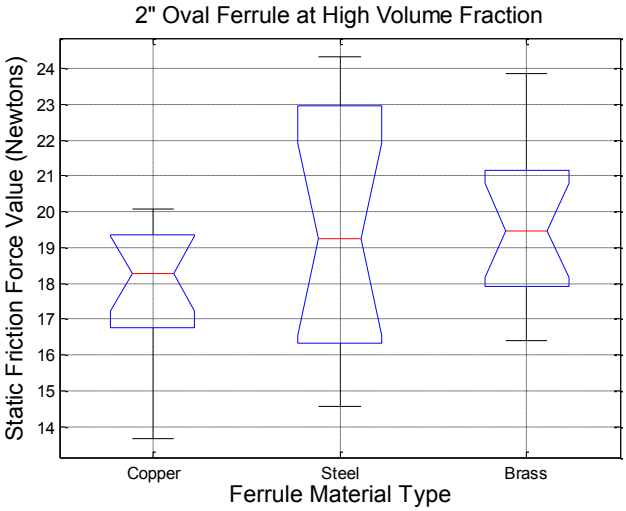

c)

Comparison of Means Achieved Using Different Ferrule Material Type for Volume Packing Fractions of:

a) Low;
b) Medium;
c) High;

Appendix B

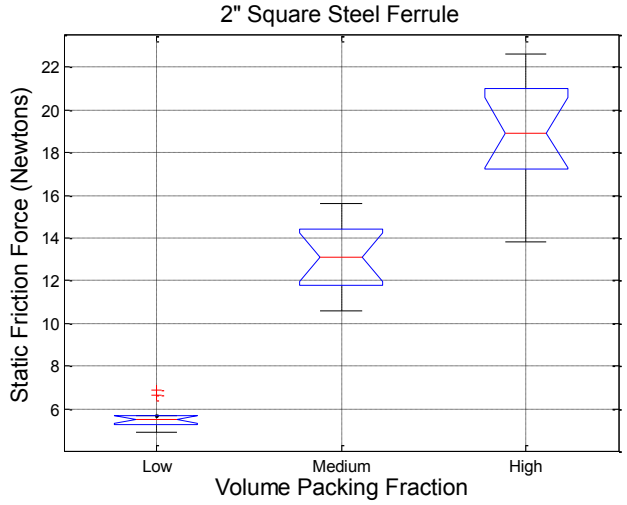

a)

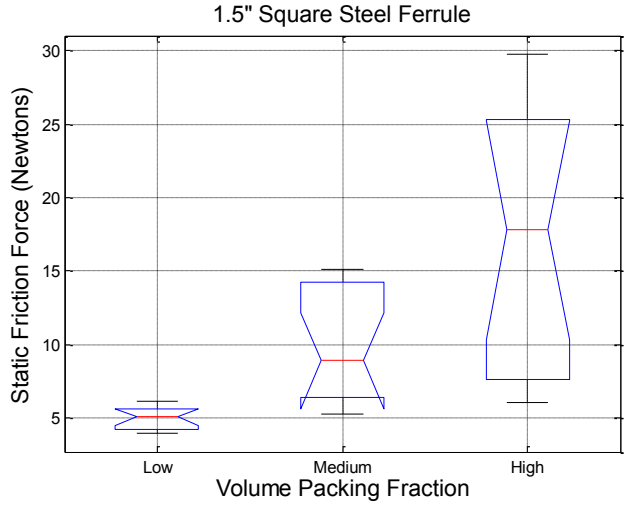

b)

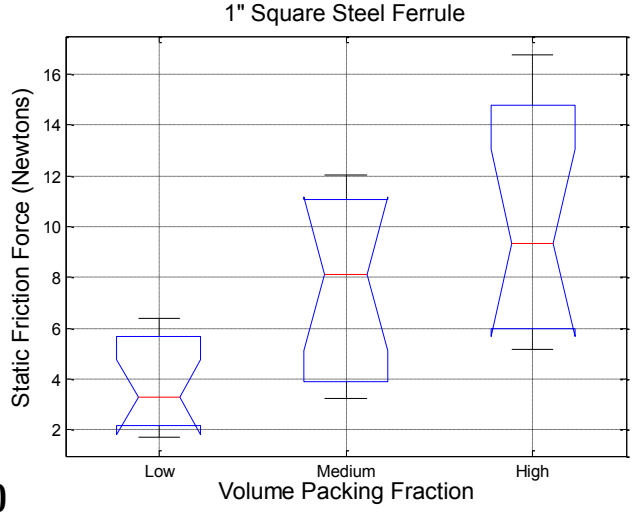

c)

Comparison of Means Achieved Using Different Volume Packing Fractions for Size of:

a) 2” Square Steel Ferrule;
b) 1.5” Square Steel Ferrule;
c) 1” Square Steel Ferrule;

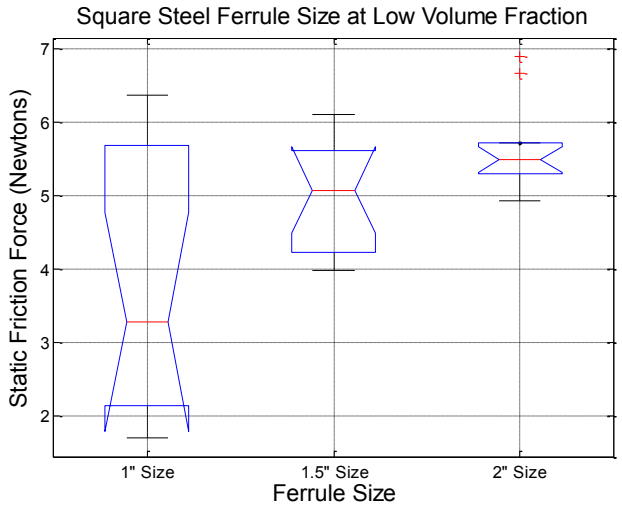

a)

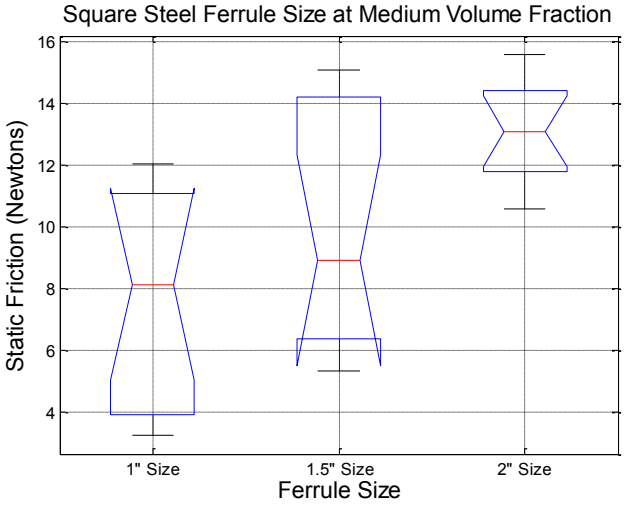

b)

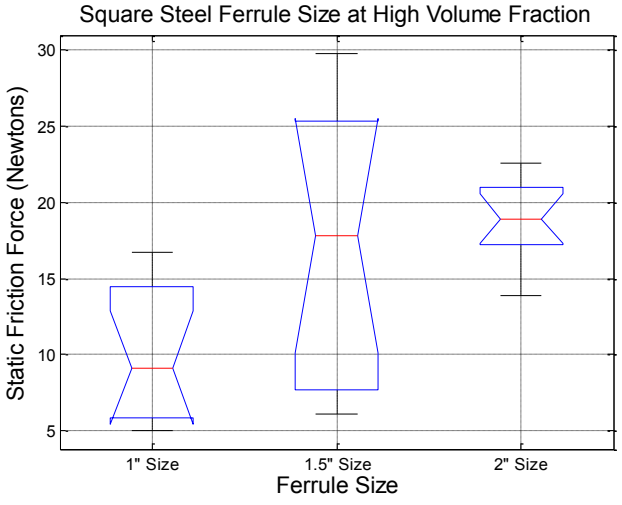

c)

Comparison of Means Achieved Using Different Sizes of Stainless Steel Square Ferrules for Volume Packing Fractions of:

a) Low;
b) Medium;
c) High;

Appendix C

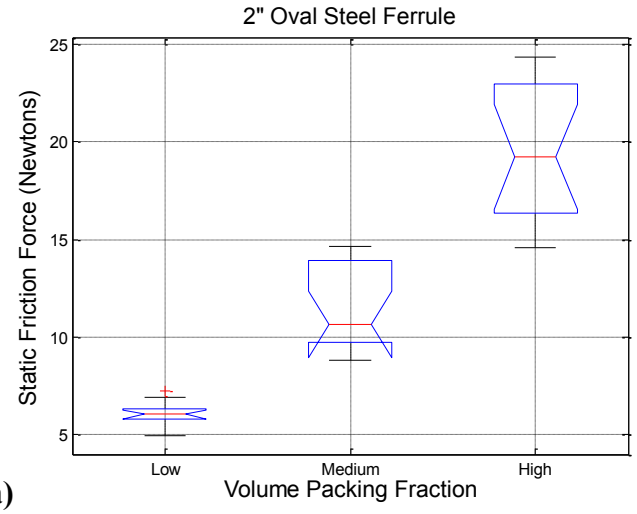

a)

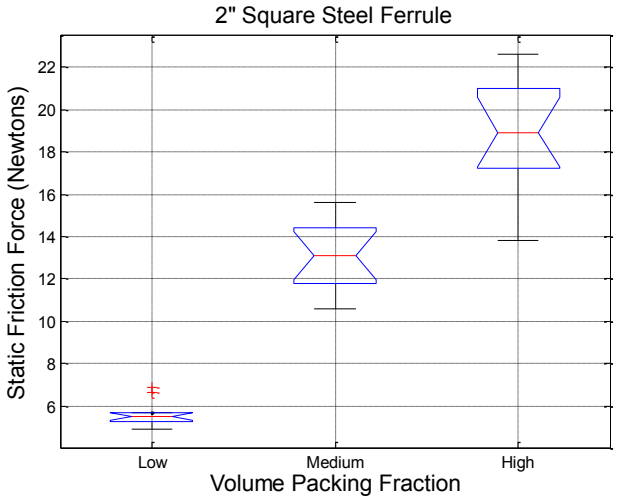

b)

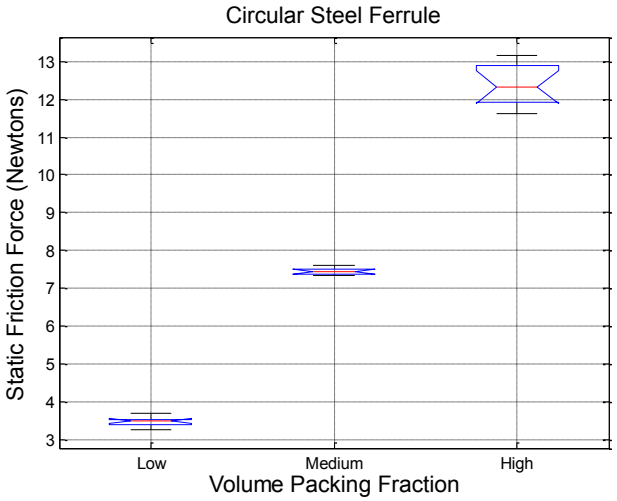

c)

Comparison of Means Achieved Using Different Volume Packing Fractions for Ferrules of:

a) 2" Oval Steel Ferrule;
b) 2" Square Steel Ferrule;
c) Circular Steel Ferrule;

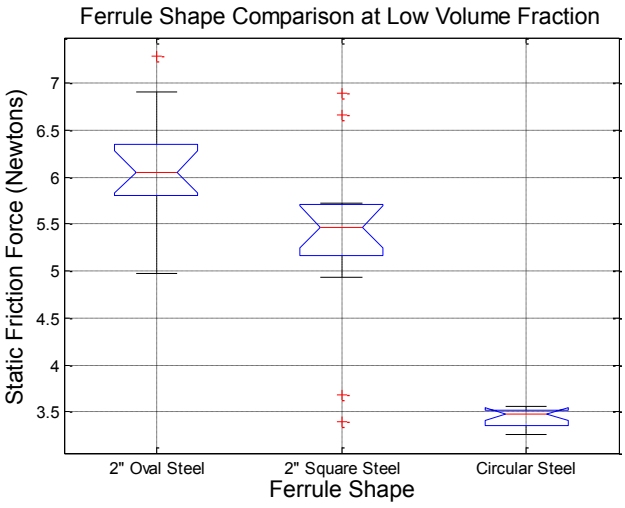

a)

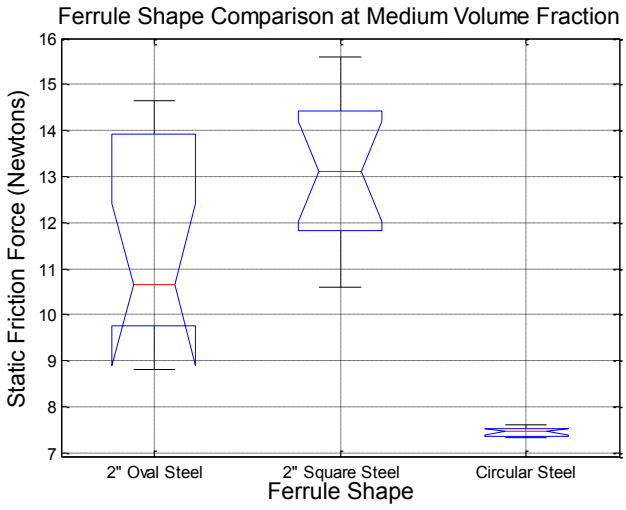

b)

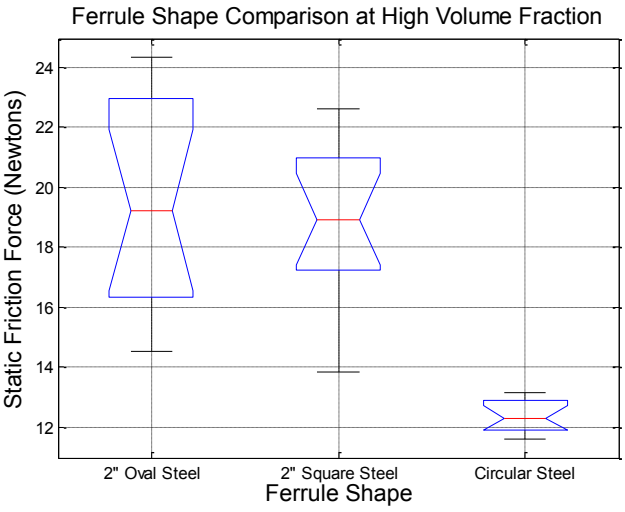

c)

Comparison of Means Achieved Using Different Shape Type Ferrules for Volume Packing Fractions of:

a) Low;
b) Medium;
c) High;

Appendix D

Part Information						Ordering Information						
Item #	Part Name	Drawing #	Type	Need Quantity	Used For	Description	Supplier	Supplier Part Number	Order QTY	Price (Ea.)	Price Total	Comments
						Hard Ware Components						
41	G_41	-	StandOff Collar	3	Grove Guides	18-8 Stainless Steel Threaded Round Standoffs 1/4" OD, 7/16" Length, 8-32	McMaster Carr	91125A623	3	$ 1.29	$ 3.87	-
47	G_47	-	CB Shafts	2	Shafts through plates	Hardened Precision Steel Shaft 1/4" OD, 5" Length	McMaster Carr	6061K413	2	$ 4.15	$ 8.30	-
48	-	-	Screw	8	Mounting CB Shaft	25 Pack - 18-8 SS Self-Lock Flat Head Socket Cap Screw 10-32 Thread, 3/4" Length	McMaster Carr	92805A266	1	$ 8.27	$ 8.27	-
49	-	-	Screw	24	Connecting Grove Guides	50 Pack - Alloy Stl Torx Drive Flat Head Sckt Cap Screw 8-32 Thread, 3/8" Length	McMaster Carr	94414A192	1	$ 7.84	$ 7.84	-
51	G_51	-	Drill Bushing	4	Press fit into plates	Steel Press-Fit Drill Bushing with Head 0.25" (1/4") ID, 1/2" OD, 1/2" Length	McMaster Carr	8492A174	4	$ 5.49	$ 21.96	-
53	-	-	Screw	16	Screws for Bristle Grippers	Stainless Steel Low Head Sckt Cap Screw 10-32 Thread, 3/8" Length, packs of 25	McMaster Carr	93615A370	1	$ 12.24	$ 12.24	-
55	-	-	Nut	8	Nut for Screw 53	Titanium Hex Nut 10-32 Thread Size, 3/8" Width, 1/8" Height	McMaster Carr	90545A111	1	$ 2.48	$ 2.48	-
58	-	-	Screw	16	Securing G_57 to G_56	50 Pack - Alloy Stl Torx Drive Flat Head Sckt Cap Screw 10-32 Thread, 5/8" Length	McMaster Carr	94414A265	1	$ 9.30	$ 9.30	-
60	-	-	Screw	12	Securing G_59 to G_57	25 Pack - Self-Locking 18-8 SS Socket Head Cap Screw 8-32 Thread, 5/8" Length	McMaster Carr	93705A201	1	$ 4.54	$ 4.54	-
64	-	-	Screw	24	Securing G_61 to G_39, G_62 to G_39, G_63 to G_39	25 Pack - Self-Locking 18-8 SS Socket Head Cap Screw 1/4"-20 Thread, 3/4" Length	McMaster Carr	93705A540	2	$ 7.71	$ 15.42	-
68	-	-	Screw	12	Assemble G_56 to G_59 and G_42 to G_46	5 Pack - 18-8 SS Socket Head Cap Screw W/Lock Washer 10-32 Thread, 1" Length	McMaster Carr	94912A345	1	$ 4.81	$ 4.81	-

Item #	Part Name	Drawing #	Type	Need Quantity	Used For	Description	Supplier	Part Number	Order QTY	Price (Ea.)	Price Total	
						PNEUMATIC COMPONENTS						
44	G_44A	G_44A_13	Actuator	4	Parallel Jaw Closing and Opening	Custom Order	Clippard Minimatic Inc.	N/A	4	Per Quote	Per Quote	Custom Order Per Drawing
45	G_45B	G_45B_14	Actuator	4	Parallel Jaw Closing and Opening	Custom Order	Clippard Minimatic Inc.	N/A	4	Per Quote	Per Quote	Custom Order Per Drawing
-	G_44FIT	-	Elbow Fitting	4	Actuator Fitting for Part# G_44	SMC Elbow Fitting	SMC	KQ2L07-32	4	-	-	-
-	G_45FIT	-	Elbow Fitting	4	Actuator Fitting for Part# G_45	SMC Elbow Fitting	SMC	KQ2L07-32	4	-	-	-
-	G_44SF	-	Straight Fitting	4	Straight Line Fitting for Connection to G_44	SMC Fitting Straight (Thin)	SMC	KQ2S07-32	4			-
-	G_45SF	-	Straight Fitting	4	Straight Line Fitting for Connection to G_45	SMC Fitting Straight (Thin)	SMC	KQ2S07-32	4	-	-	-
-	G_44FCLI	-	Inline Flow Control	4	Regulating Speed of Actuators G_44	Omega Inline Flow Speed Control Valve	Omega.com	OM-AIR-C20GE0400	4	-	-	-
-	G_45FCLI	-	Inline Flow Control	4	Regulating Speed of Actuators G_45	Omega Inline Flow Speed Control Valve	Omega.com	OM-AIR-C20GE0400	4	-	-	-
-	G_44YU	-	Y-Union	4	Flow Separation (Extended, Compressed)	SMC Y Union Joint	SMC	KQ2U07-00	4	-	-	-
-	G_45YU	-	Y-Union	4	Flow Separation (Extended, Compressed)	SMC Y Union Joint	SMC	KQ2U07-00	4	-	-	-
-	G_44_45H	-	Pressure Tubing	-	Pressure Line Distribution	Ester Polyurethane Tubing	Mc Master Carr	5108K43	-	$0.57	Cost Per Foot	-

Item #	Part Name	Drawing #	Type	Need Quantity	Used For	Description	Supplier	Part Number	Order QTY	Price (Ea.)	Price Total	
						ELECTRONIC COMPONENTS						
-	-	-	-	-	-	N/A	-	-	-	-	-	-

Appendix E

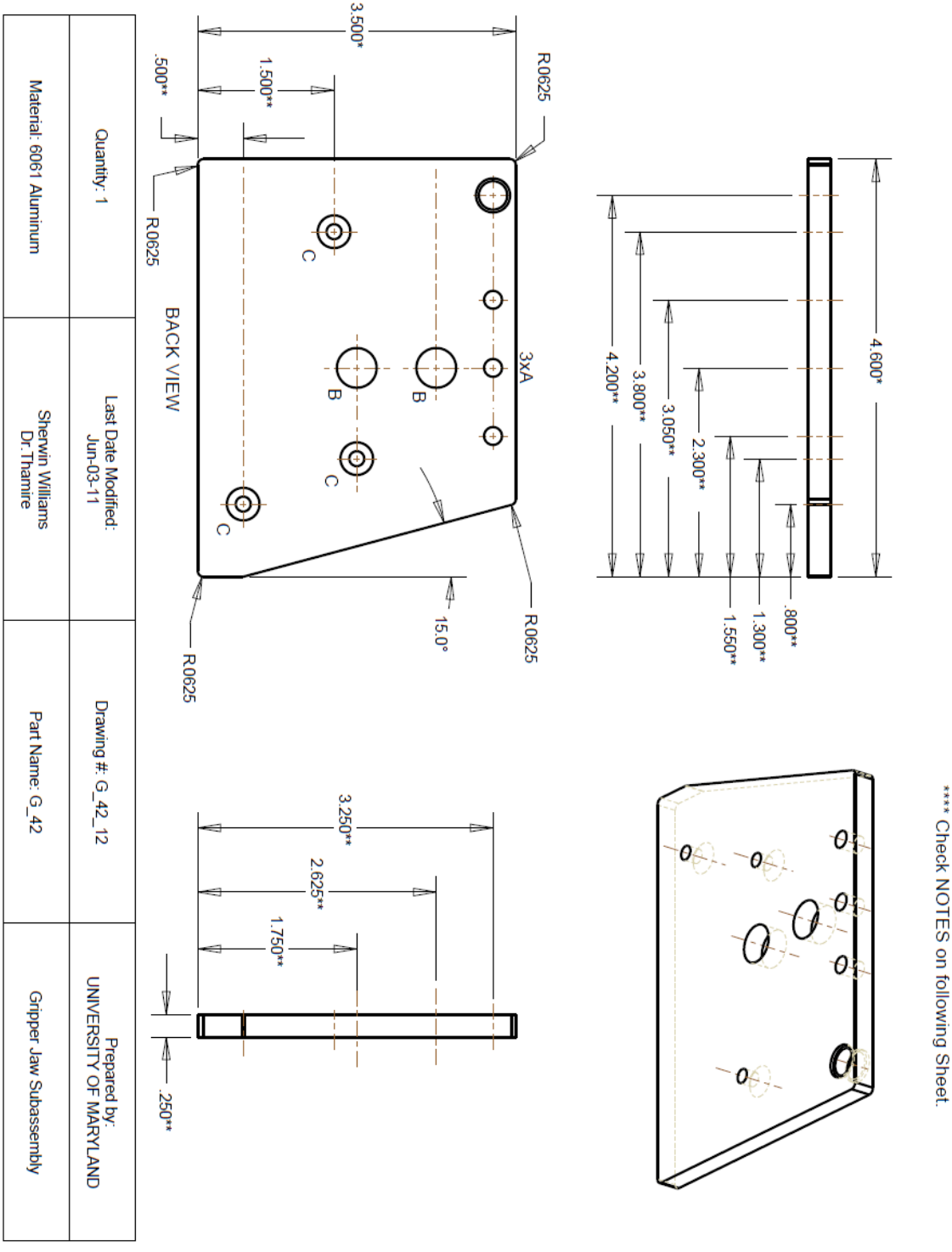
**** Check NOTES on following Sheet.
4.600*
.800**
1.300**
1.550**
2.300**
3.050**
3.800**
4.200**
3.500*
1.500**
.500**
R.0625
R.0625
3xA
BACK VIEW
B
B
C
C
C
15.0°
R.0625
R.0625
3.250**
2.625**
1.750**
.250**
Quantity: 1
Last Date Modified: Jun-03-11
Drawing #: G_42_12
Prepared by: UNIVERSITY OF MARYLAND
Material: 6061 Aluminum
Sherwin Williams Dr.Thamire
Part Name: G_42
Gripper Jaw Subassembly

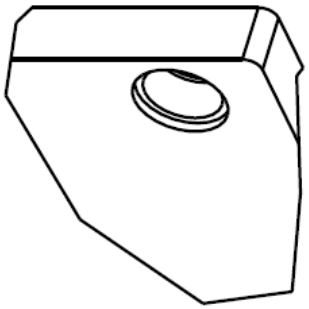

DETAIL B
SCALE 1.750

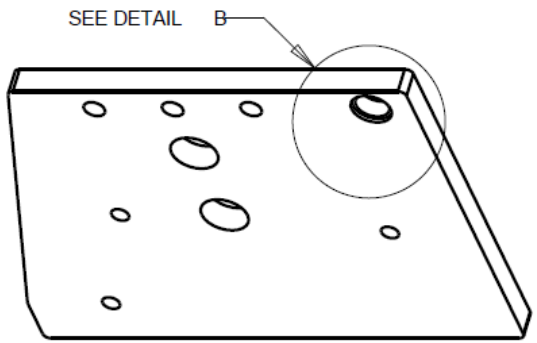

NOTE:

1. Holes "A" are:
Clearence Hole Close Fit
for 10-32 Screw (0.196" ∅)

2. Holes "B" are:
Tapped Through For 7/16"-20
Mounting Thread

3. Holes "C" are:
Clearence Hole Close Fit
for 8-32. In BACK VIEW,
82° ⌵ (Chamfer)
MMCarr PRT#:94414A192

4. Hole "D" is
Press Fit for Bearing:
MacMaster Carr
(MMC-Use as reference)
PRT# 4262T12
∅0.3125
Max. 0.3121
Min. 0.3113

Detail B Highlights the recess
for bearing flange in FRONT and BACK
(NOTE: Same for ROTATION PLATE B)

5. Tolerances:
*: (± 0.010)
**: (± 0.005)
Otherwise: OPEN

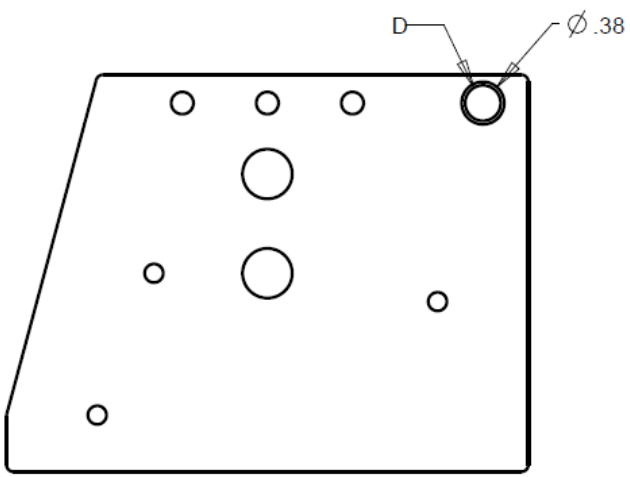

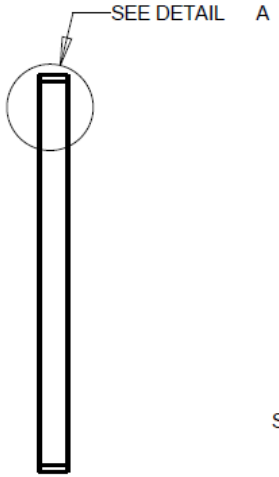

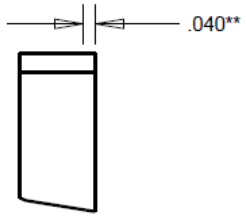

DETAIL A
SCALE 2.000

Tolerances:
*: (± 0.010 inches)
**: (± 0.005 inches)
Otherwise: OPEN

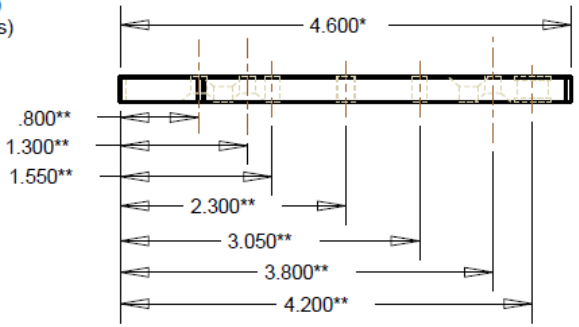

**** Check NOTES on following Sheet.

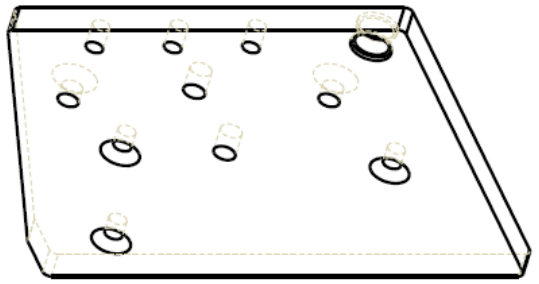

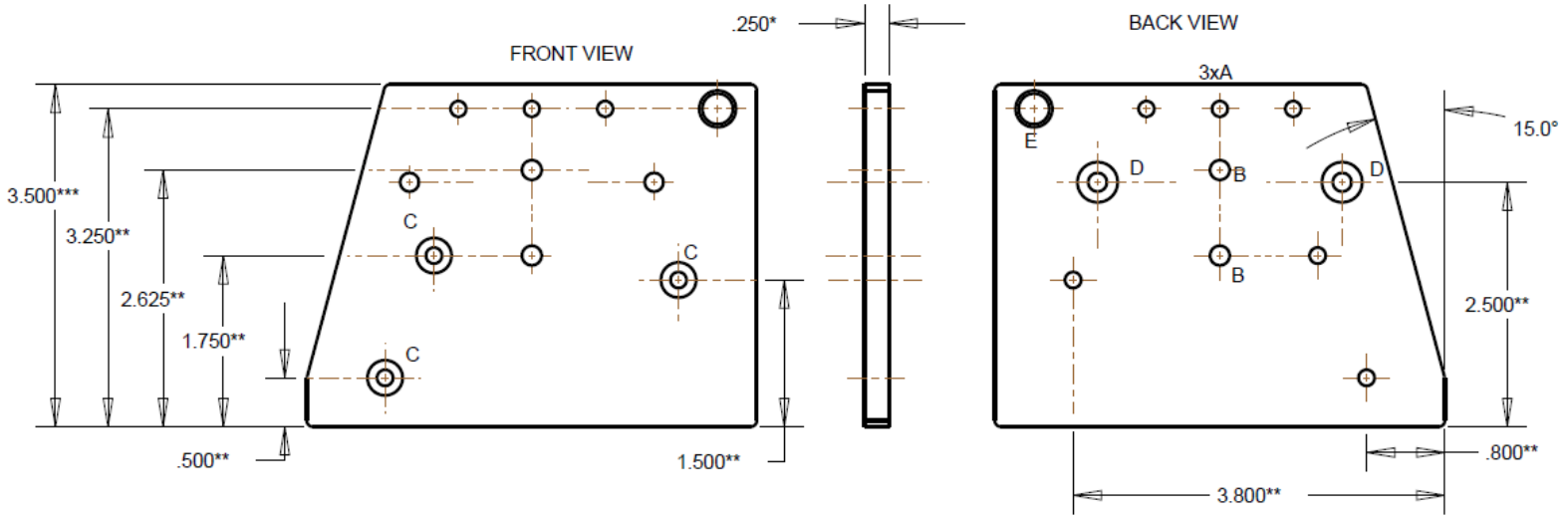

Quantity: 1	Last Date Modified: May-31-11	Drawing #: G_46_15	Prepared by: UNIVERSITY OF MARYLAND
Material: 6061 Aluminum	Sherwin Williams Dr.Thamire	Part Name: G_46	Gripper Jaw Subassembly

NOTE:

1. Holes "A" are:
Drill Through, Drill #21 (∅0.159)
Tapped Through for 10-32

2. Holes "B" are:
0.2" ∅ Through
Open Tolerance

3. Holes "C" are:
Drill Through, Drill #18 (∅0.1695)
Close Fit Clearance Hole
for 8-32. In FRONT VIEW,
Chamfer Angle: 82°
Chamfer Diameter: 0.34 ∅
MMCarr PRT#: 94414A192

4. Holes "D" are:
Clearence Hole Close Fit
for 10-32. In BACK VIEW,
Chamfer Angle: 82°
Chamfer Diameter: 0.40 ∅
MMCarr PRT#: 94414A265

5. Hole "E" is:
Press Fit for Bearing:
MMCarr PRT# 4262T12
Use: 0.3125 ∅
Max: 0.3125
Min: 0.3115

Same as ROTATION PLATE A

6. Tolerances:
*: (± 0.010 inches)
**: (± 0.005 inches)
Otherwise: OPEN

FRONT VIEW

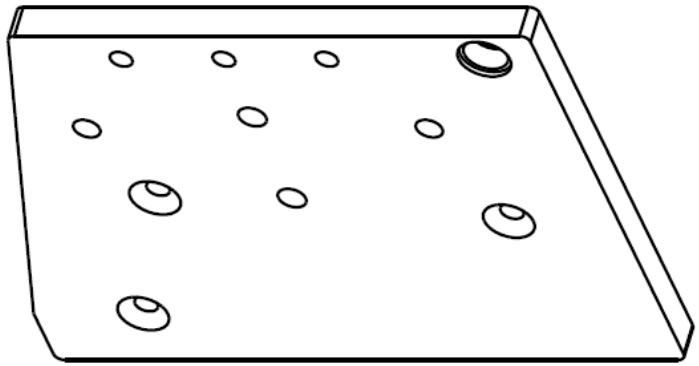

BACK VIEW

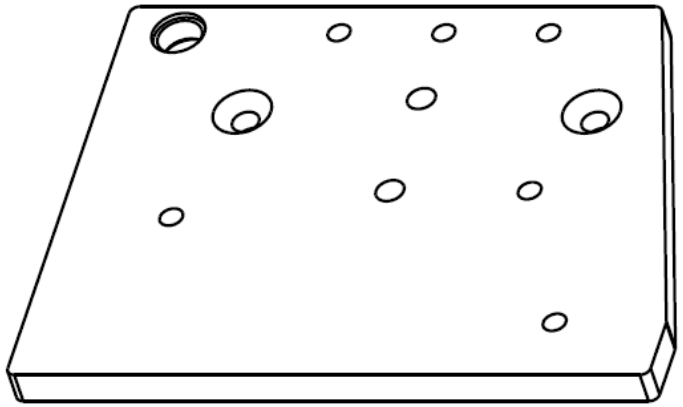

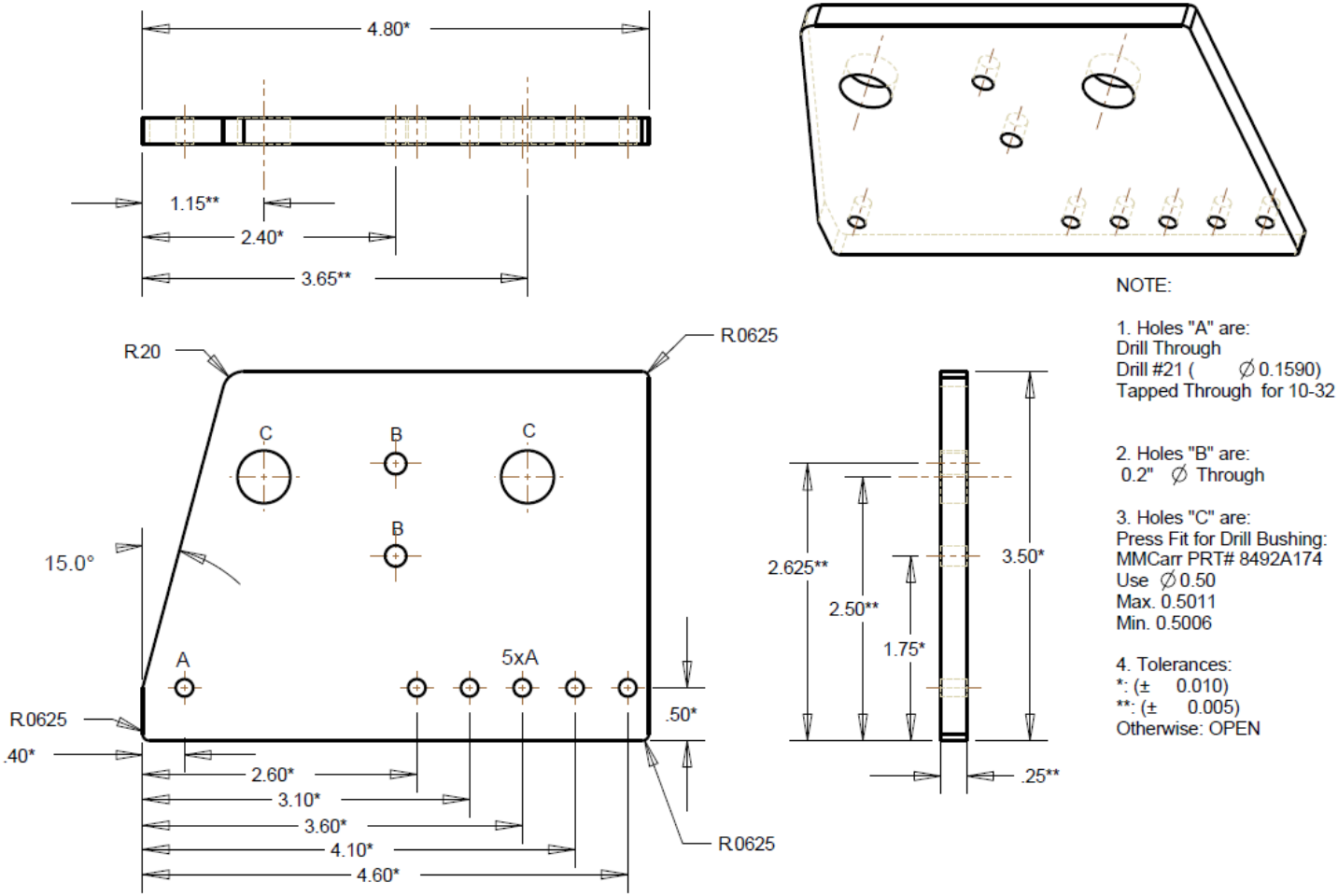

NOTE:

1. Holes "A" are:
Drill Through
Drill #21 (∅0.1590)
Tapped Through for 10-32

2. Holes "B" are:
0.2" ∅ Through

3. Holes "C" are:
Press Fit for Drill Bushing:
MMCarr PRT# 8492A174
Use ∅0.50
Max. 0.5011
Min. 0.5006

4. Tolerances:
*: (± 0.010)
**: (± 0.005)
Otherwise: OPEN

Quantity: 1	Last Date Modified: May-31-11	Drawing #: G_50_16	Prepared by: UNIVERSITY OF MARYLAND
Material: 6061 Aluminum	Sherwin Williams Dr.Thamire	Part Name: G_50	Gripper Jaw Subassembly

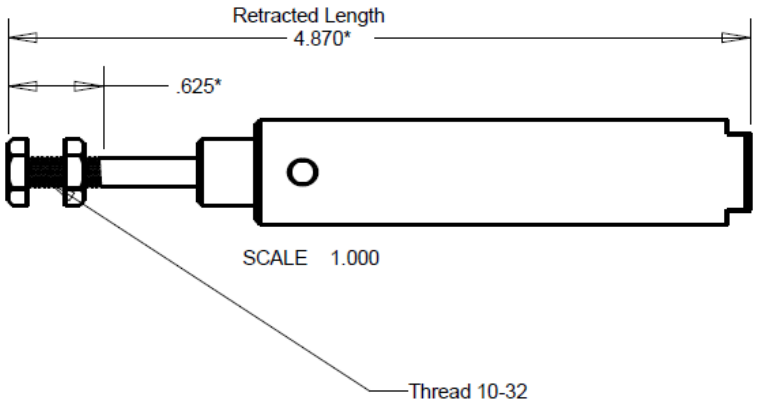

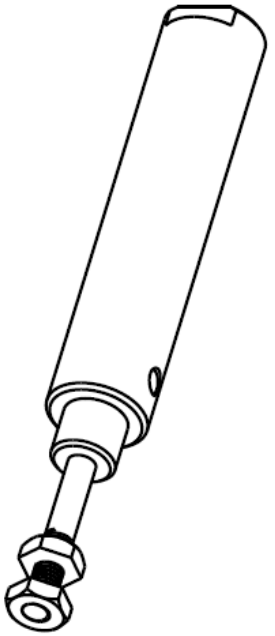

Quantity: 1	Last Date Modified: Jun-21-11	Drawing #: G_44A_13	Prepared by: UNIVERSITY OF MARYLAND
Material: Stainless Steel	Sherwin Williams Dr.Thamire	Part Name: G_44A	Gripper Jaw Subassembly

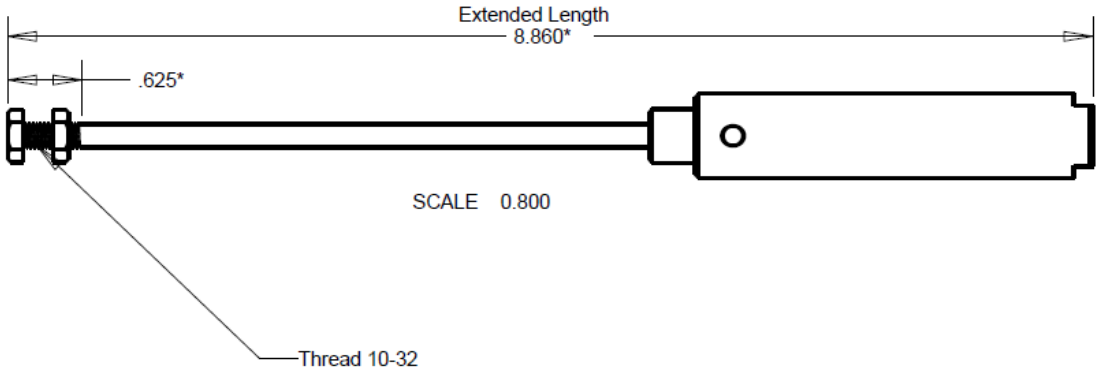

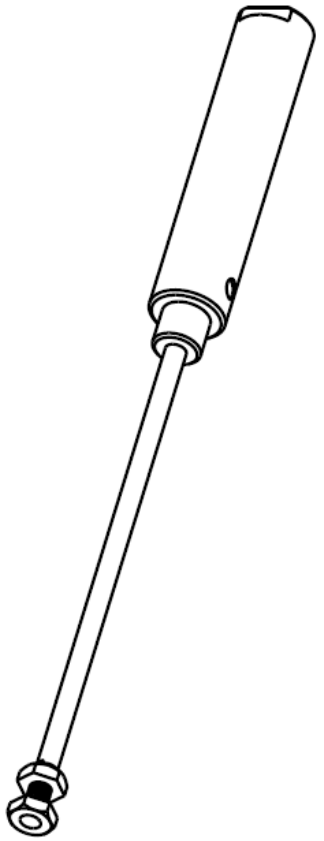

SCALE 0.750

Quantity: 1	Last Date Modified: Jun-21-11	Drawing #: G_45B_14	Prepared by: UNIVERSITY OF MARYLAND
Material: Stainless Steel	Sherwin Williams Dr.Thamire	Part Name: G_45B	Gripper Jaw Subassembly

NOTE:

** THIS PART IS USED TO GRAB
FILAMENT AND SHOULD BE MANUFACTURED
USING CNC MACHINING**

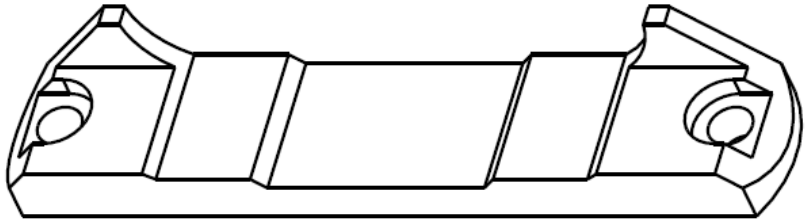

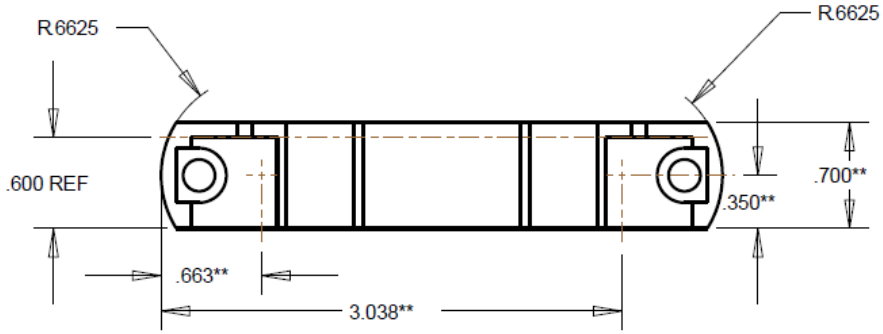

TOLERANCES:
* : (± 0.010 Inches)
**: (± 0.005 Inches)
OTHERWISE: OPEN

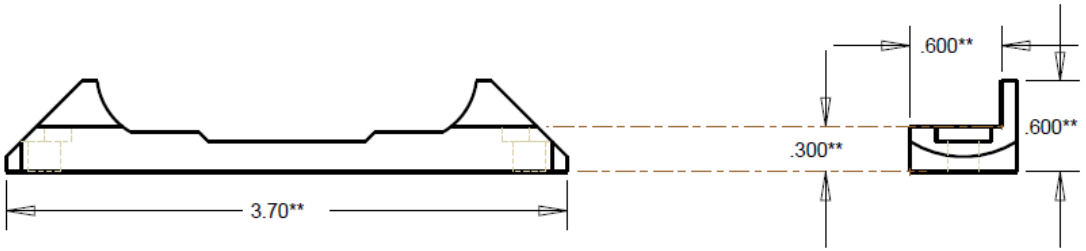

Quantity: 2	Last Date Modified: Jun-01-11	Drawing #: G_52C	Prepared by: UNIVERSITY OF MARYLAND
Material: 6061 ALUMINUM OR 303 STAINLESS STEEL	Sherwin Williams Dr.Thamire	Part Name: G_52C	Gripper Jaw Subassembly

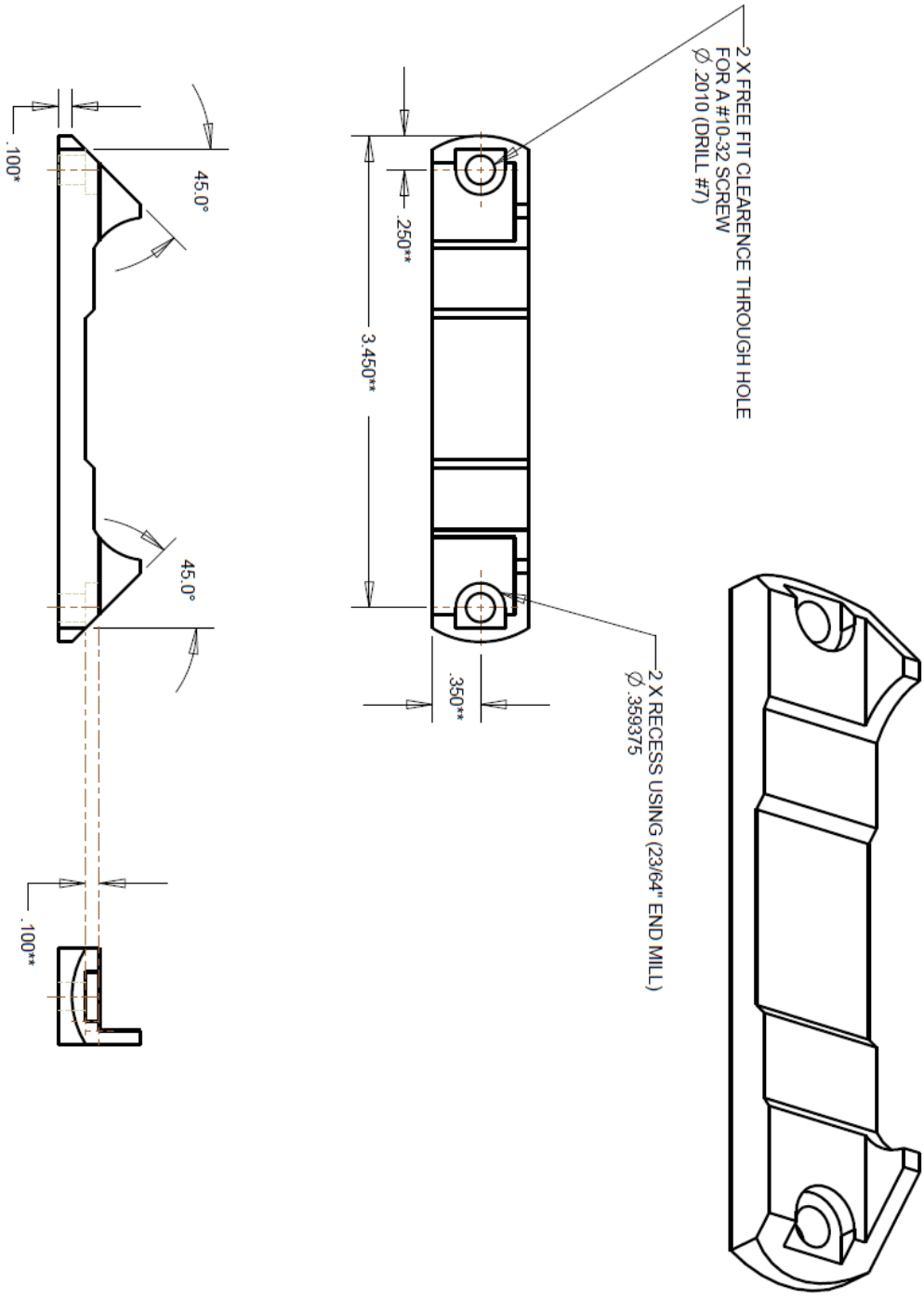
2 X FREE FIT CLEARENCE THROUGH HOLE
FOR A #10-32 SCREW
Ø .2010 (DRILL #7)
2 X RECESS USING (23/64" END MILL)
Ø .359375
.250**
3.450**
.350**
.100*
45.0°
45.0°
.100**

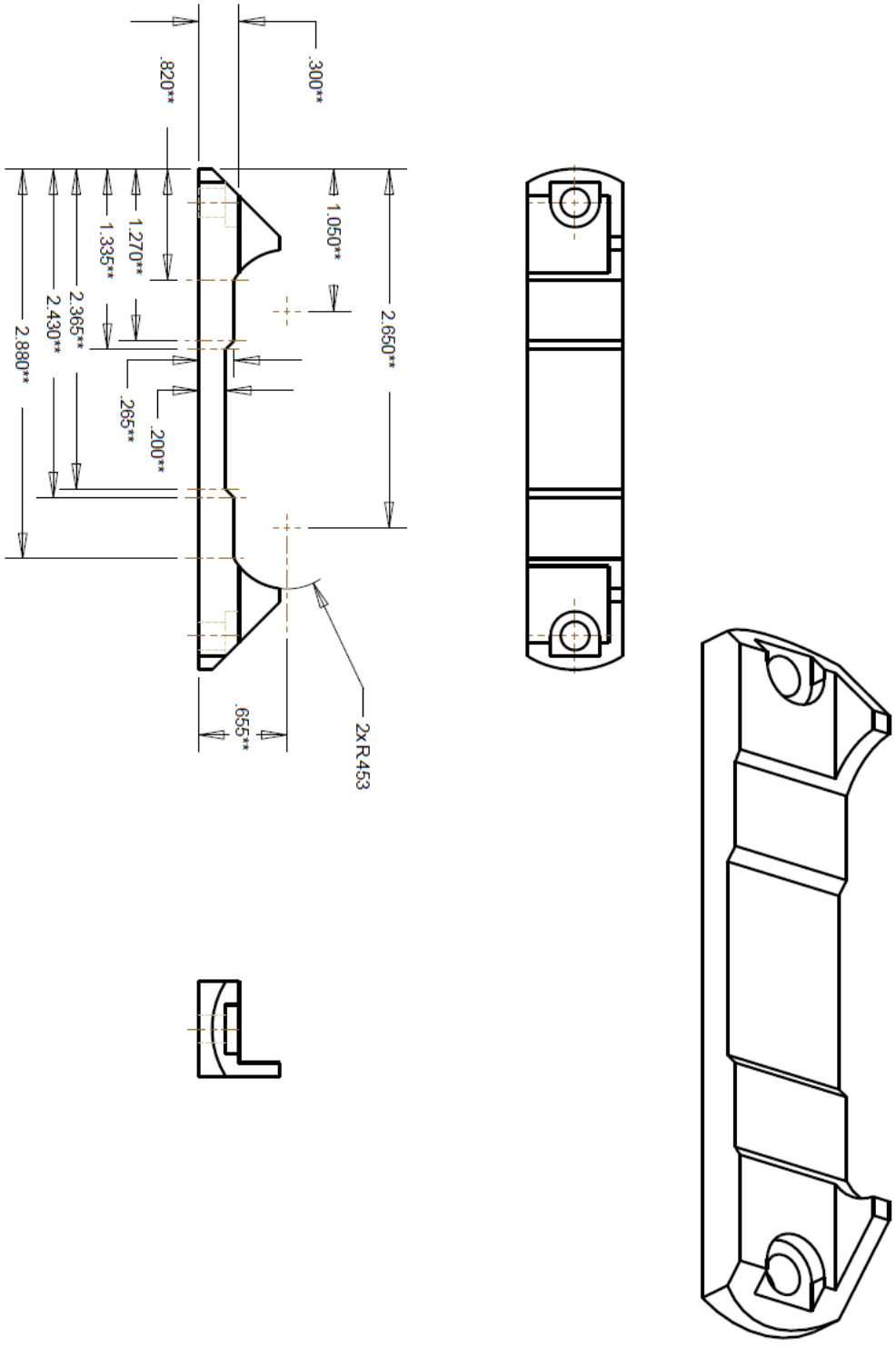
.820**
.300**
1.050**
2.650**
1.335**
1.270**
2.365**
2.430**
2.880**
.265**
.200**
.655**
2xR453

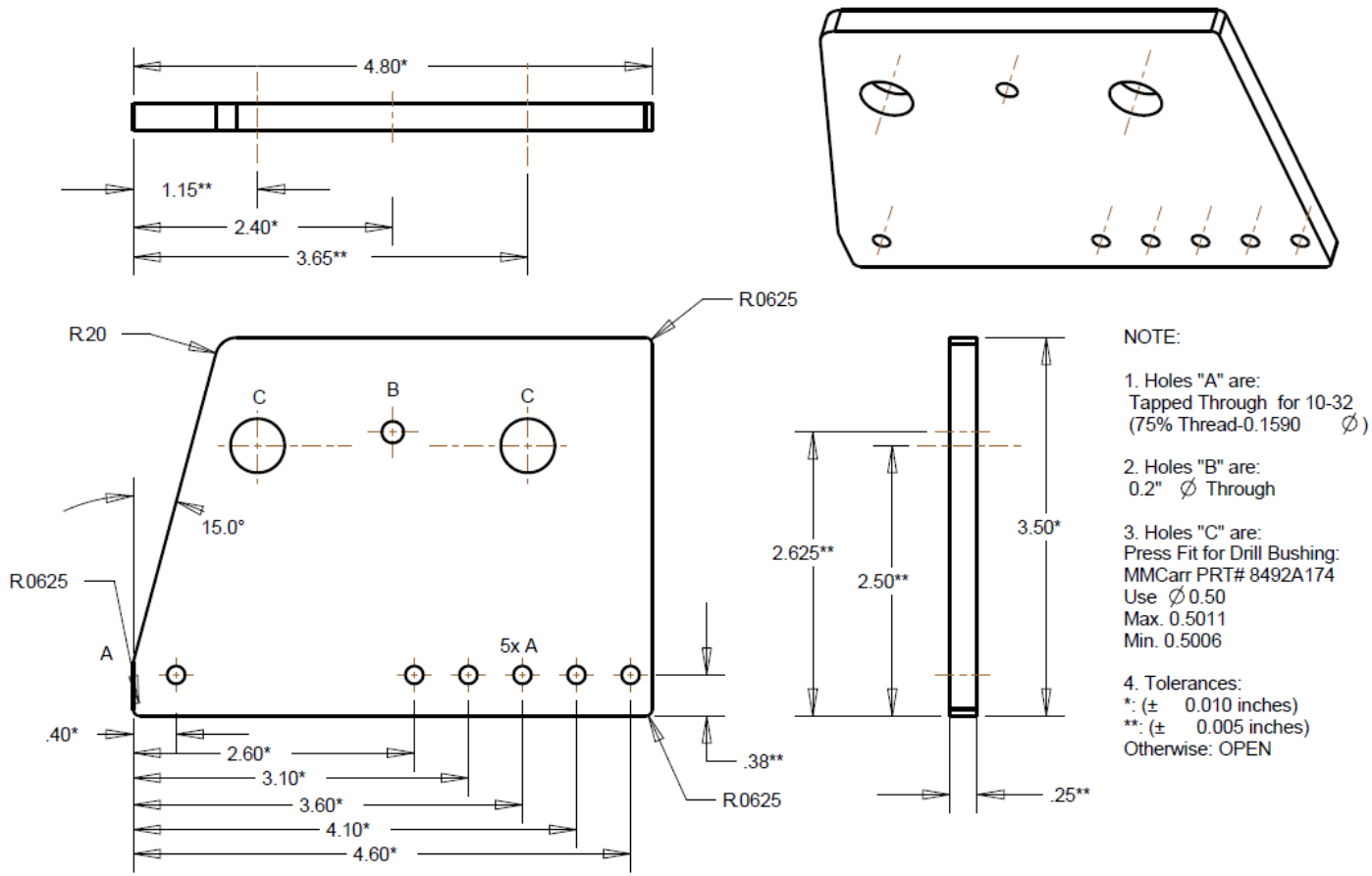

NOTE:

1. Holes "A" are:
Tapped Through for 10-32
(75% Thread-0.1590 ∅)

2. Holes "B" are:
0.2" ∅ Through

3. Holes "C" are:
Press Fit for Drill Bushing:
MMCarr PRT# 8492A174
Use ∅0.50
Max. 0.5011
Min. 0.5006

4. Tolerances:
*: (± 0.010 inches)
**: (± 0.005 inches)
Otherwise: OPEN

Quantity: 1	Last Date Modified: Jun-01-11	Drawing #: G_54_18	Prepared by: University of Maryland
Material: Aluminum	Sherwin Williams Dr.Thamire	Part Name: G_54	Gripper Jaw Subassembly

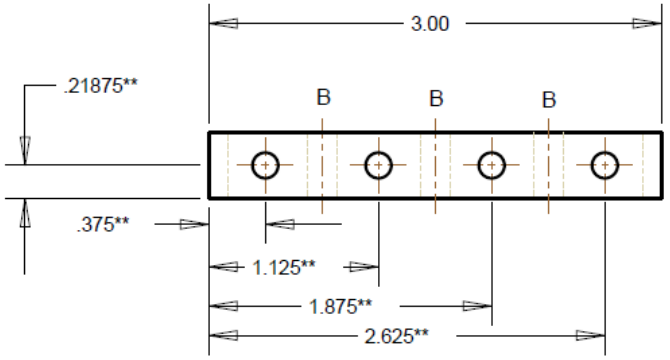

NOTE:

1. Holes "A" are:
Drill to Depth, Drill #18 (Ø 0.1695)
Tapped to Depth 0.375
for 10-32 Screw

2. Holes "B" are:
Drill Through, Drill #9 (Ø 0.1960)
Close Fit Clearance Hole
for 10-32 Screw

3. Tolerances:
*: (± 0.010)
**: (± 0.005)
Otherwise: OPEN

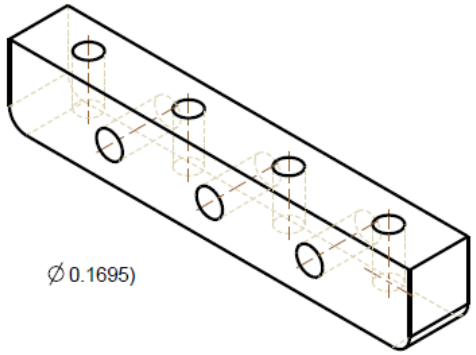

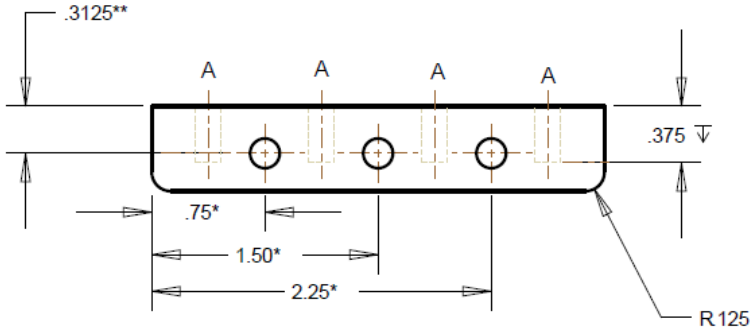

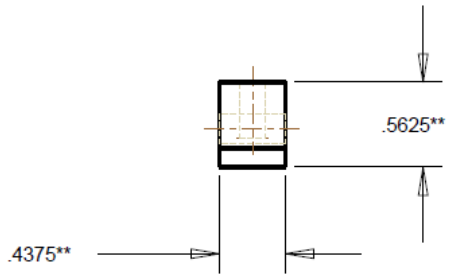

Quantity: 1	Last Date Modified: Jun-01-11	Drawing #: G_56_19	Prepared by: UNIVERSITY OF MARYLAND
Material: 304 Stainless Steel	Sherwin Williams Dr.Thamire	Part Name: G_56	Gripper Jaw Subassembly

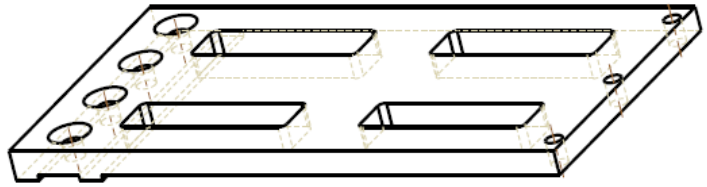

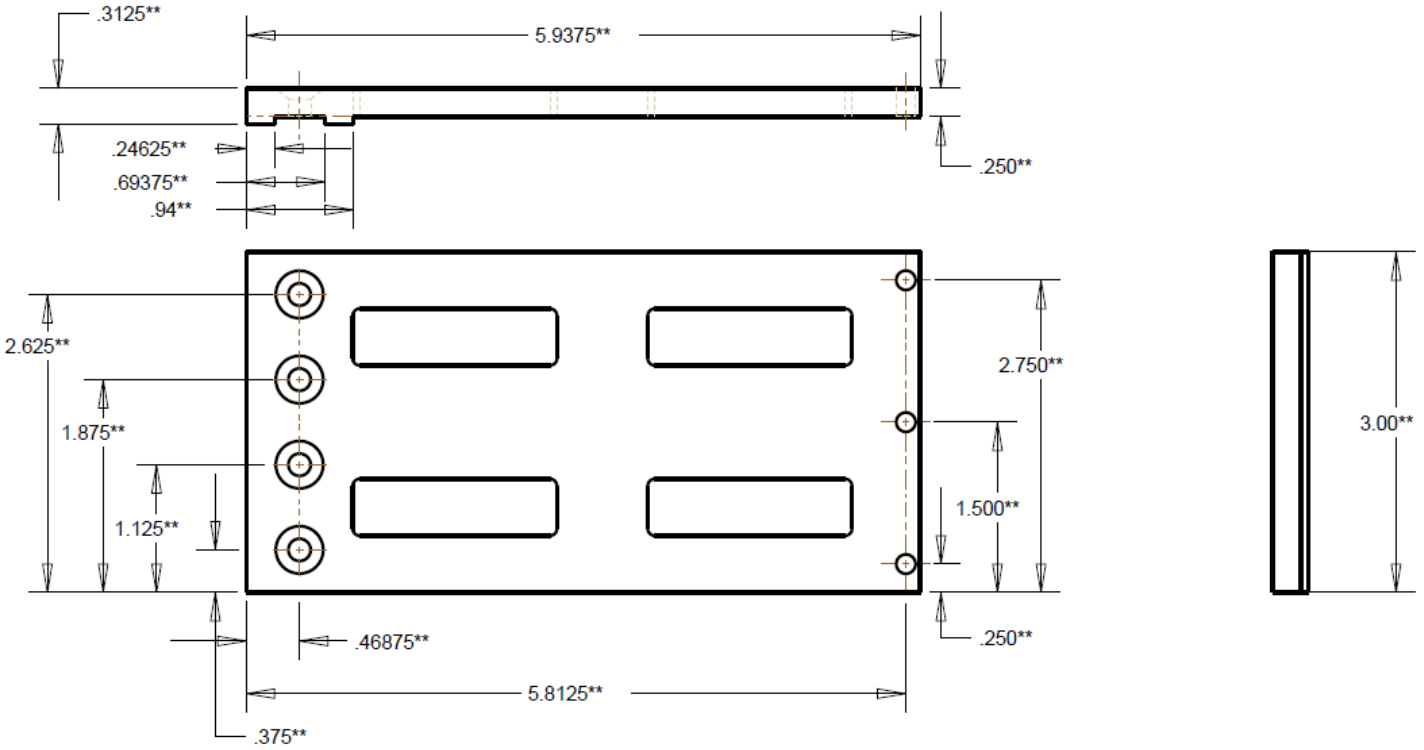

Quantity: 1	Last Date Modified: Jun-01-11	Drawing #: G_57_20	Prepared by: UNIVERSITY OF MARYLAND
Material: 304 Stainless Steel	Sherwin Williams Dr.Thamire	Part Name: G_57	Gripper Jaw Subassembly

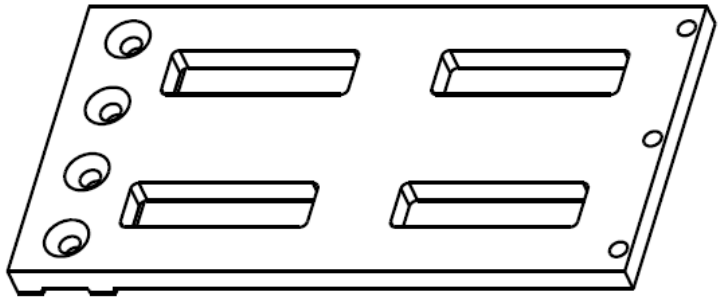

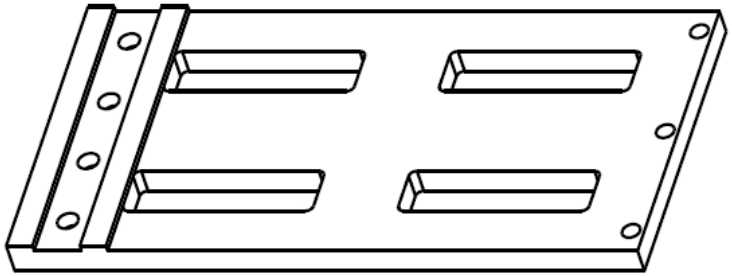

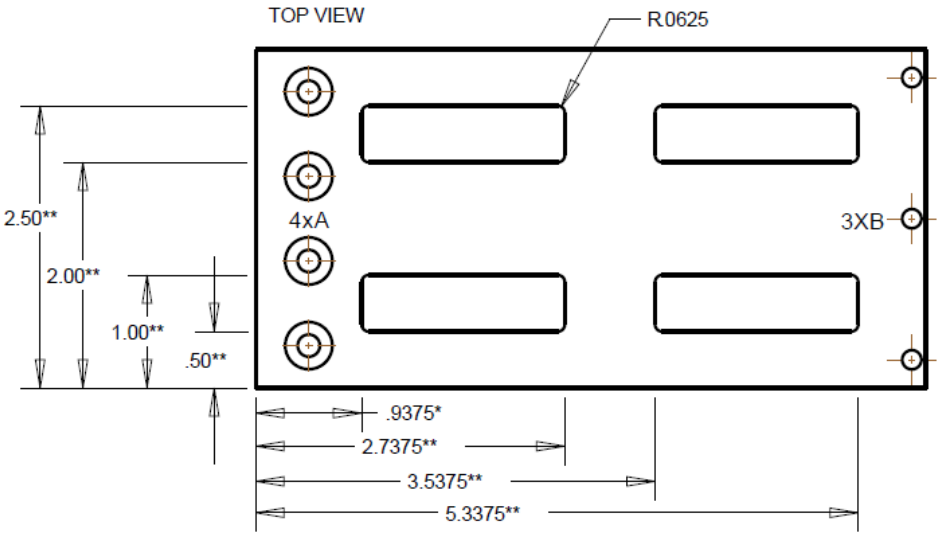

NOTE:

1. Holes "A" are:
Clearence Hole Close Fit
for 10-32. In TOP VIEW,
Chamfer Angle: 82°
Chamfer Diameter: ∅0.42
For Referance:
MMCarr PRT#:94414A265

2. Holes "B" are:
Drill Through, Drill #18 (∅0.1695)
Close Fit Clearence Hole
for 8-32 Screw

3. Tolerances:
*: (± 0.010 inches)
**: (± 0.005 inches)
Otherwise: OPEN

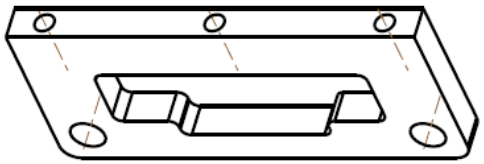

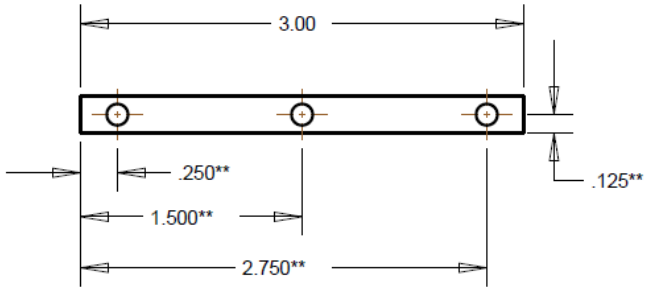

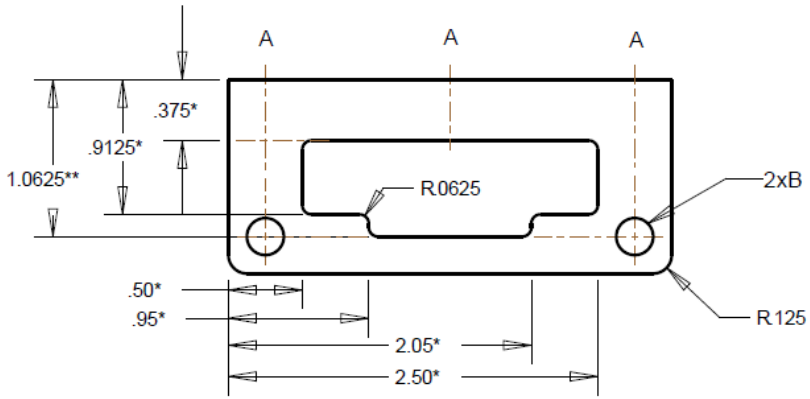

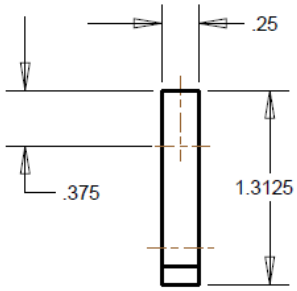

NOTE:

1. Holes "A" are:
Drill to Depth, Drill #27 (∅0.144)
Tapped to Depth (0.375 ↧)
for 8-32 Screw

2. Holes "B" are:
Running Fit for a
0.25 ∅ Precision Shaft
MMCarr PRT#: 6061K413
Max: 0.2575
Min: 0.2497

3. Tolerances:
*: (± 0.010 inches)
**: (± 0.005 inches)
Otherwise: OPEN

Quantity: 1	Last Date Modified: Jun-01-11	Drawing #: G_59_21	Prepared by: UNIVERSITY OF MARYLAND
Material: 304 Stainless Steel	Sherwin Williams Dr.Thamire	Part Name: G_59	Gripper Jaw Subassembly

Appendix F

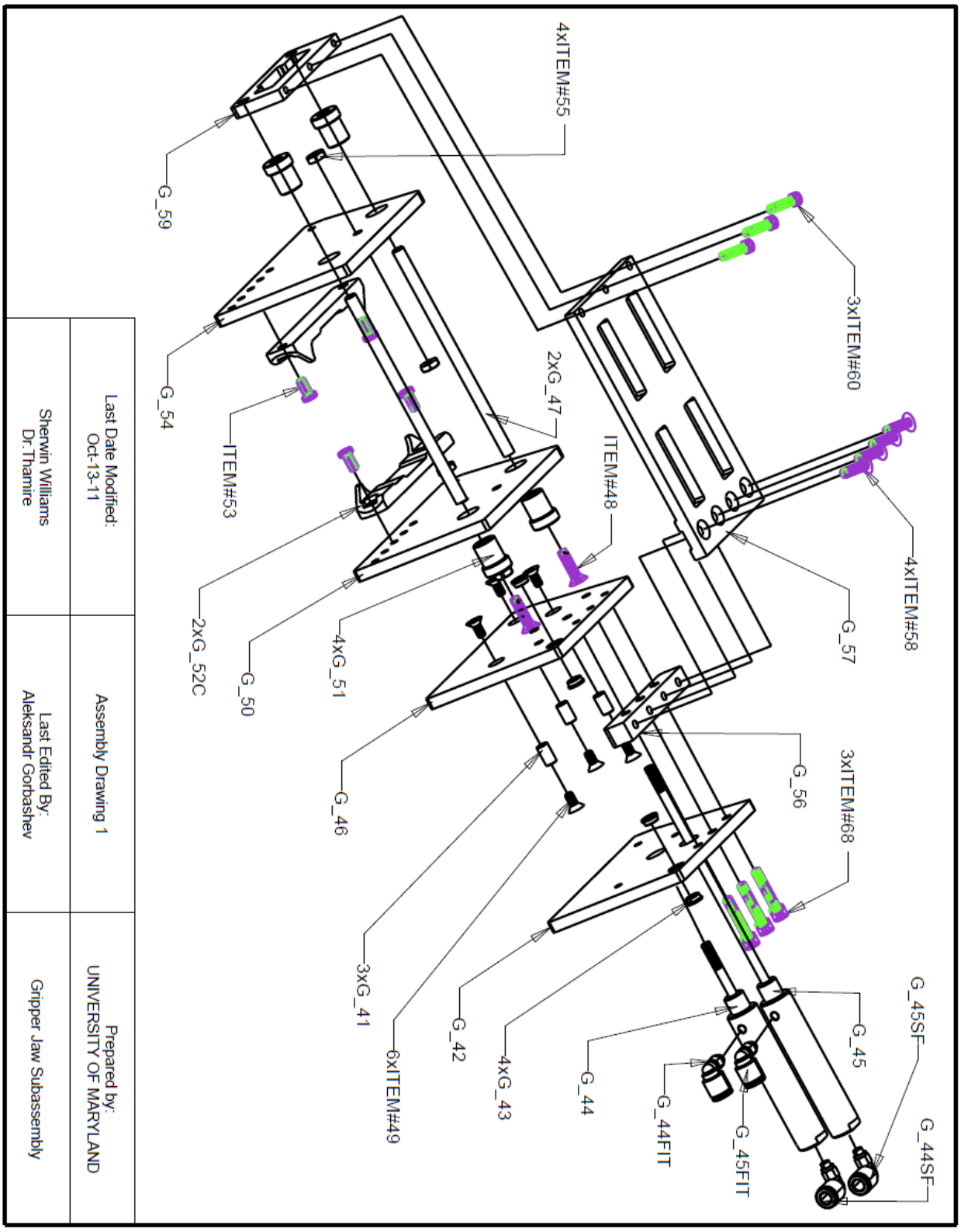
4xITEM#55
G_59
3xITEM#60
G_54
2xG_47
ITEM#53
ITEM#48
4xITEM#58
G_57
2xG_52C
G_50
4xG_51
G_56
3xITEM#68
G_46
3xG_41
G_42
6xITEM#49
4xG_43
G_44
G_45SF
G_45
G_44SF
G_44FIT
G_45FIT
Last Date Modified:
Oct-13-11
Assembly Drawing 1
Prepared by:
UNIVERSITY OF MARYLAND
Sherwin Williams
Dr.Thamire
Last Edited By:
Aleksandr Gorbashev
Gripper Jaw Subassembly

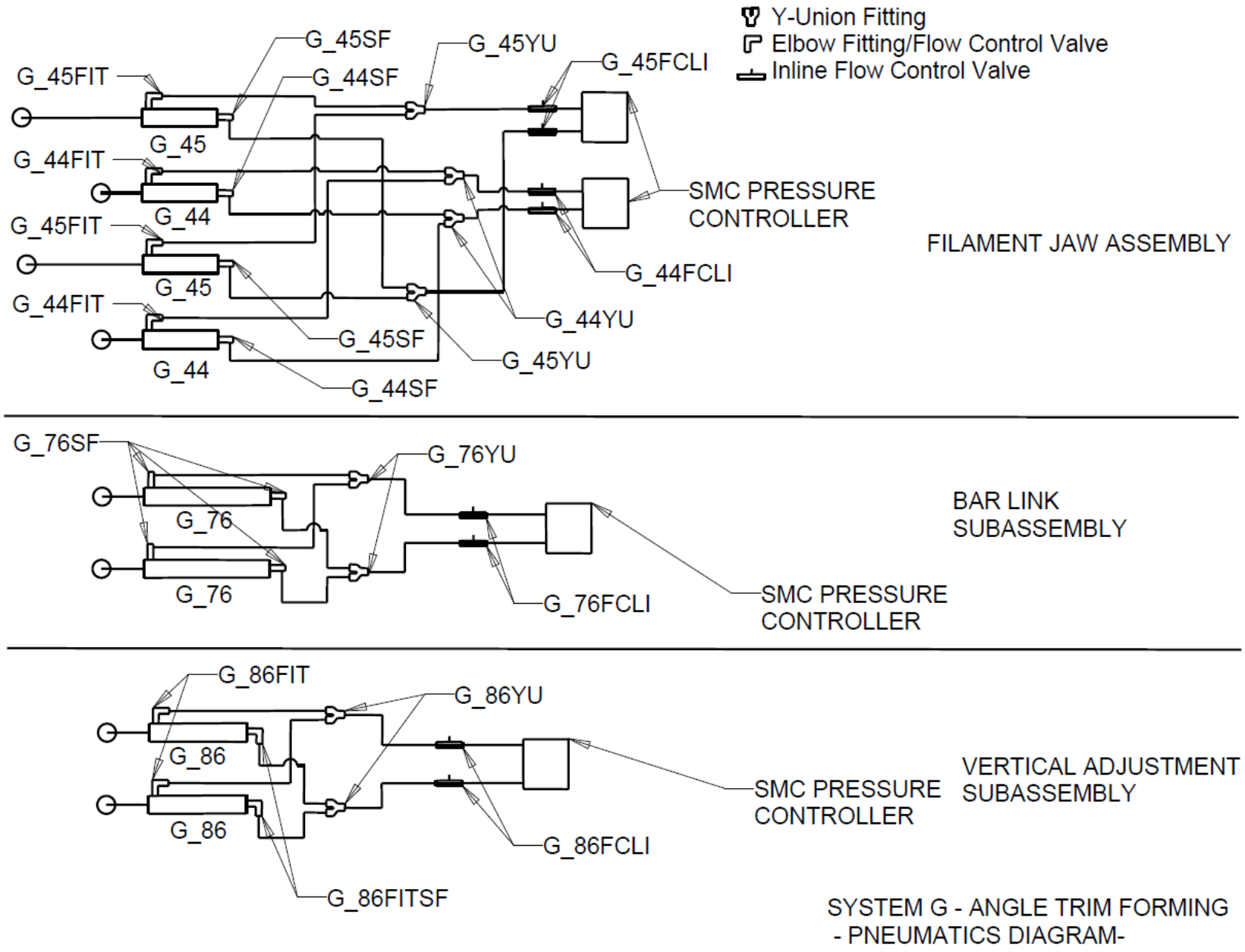

SYSTEM G - ANGLE TRIM FORMING
- PNEUMATICS DIAGRAM-

References

[1] **Gottlieb, Leonard.** *Factory Made: How things are Manufactured.* Boston : Houghton Mufflin Co., 1978.

[2] **Boothroyd, G, Poli, C and Murch, L E.** *Automatic Assembly.* New York : Marcel and Decker, 1982. pp. 271-223.

[3] *Personal Communication with Fadi Khalifeh, Rubberset Co.* 2010-2011.

[4] **Hoss, Gabriel.** *How It is Made: Paint Brushes.* Productions MAJ, 2007.

[5] **Magrab, E. B.** *Integrated Product and Process Design and Development.* New York : CRC Press, 1997.

[6] **Eppinger, Ulrich and.** *Product Design and Development.* New York : McGraw Hill, 1995.

[7] **Causey, Greg C. and Quinn, Roger D.** *Gripper Design Guidelines for Modular Manufacturing.* Clevelend : CWRU, 1998.

[8] **Schmidt, L, et al.** *Product Engineering and Manufacturing .* Knoxville : College House Enterprises, LLC.

[9] **Dieter, G.** *Engineering Design.* 3rd Ed. s.l. : McGraw-Hill Book Co., 2000.